

**University of Alberta**

**Lipid modification of polymeric nanocarriers for  
drug and siRNA delivery**

by

Arash Falamarzian

A thesis submitted to the Faculty of Graduate Studies and Research  
in partial fulfillment of the requirement for the degree of

Doctor of Philosophy

In

Pharmaceutical Sciences

Faculty of Pharmacy and Pharmaceutical Sciences

© Arash Falamarzian

Fall 2013

Edmonton, Alberta

Permission is hereby granted to the University of Alberta Libraries to reproduce single copies of this thesis and to lend or sell such copies for private, scholarly or scientific research purposes only. Where the thesis is converted to, or otherwise made available in digital form, the University of Alberta will advise potential users of the thesis of these terms.

The author reserves all other publication and other rights in association with the copyright in the thesis and, except as herein before provided, neither the thesis nor any substantial portion thereof may be printed or otherwise reproduced in any material form whatsoever without the author's prior written permission.

## **DEDICATION**

I dedicate this thesis to my beloved parents, Dr. Mahmood Falamarzian and Mrs. Jaleh Shirani, for their love, endless support and prayers throughout every stage of my life; to my loving and caring wife, Mrs. Maryam Yazdanshenas, for her unconditional love, support, encouragement and patience. I also dedicate this thesis to my mentor and supervisor Dr. Afsaneh Lavasanifar for her strong guidance, support and belief in my abilities to pursue my studies during the Ph.D. program. I doubt that I will ever be able to convey my appreciation fully, but I dedicate to them all the success I will have in my future career life.

## ABSTRACT

The use of nanotechnology in pharmaceutical development has progressed significantly in recent decades. This rapid advancement is driven by crucial need for improving the performance of present diagnostic and therapeutic modalities, as well as development of a new class of delivery systems for complex entities such as genes and proteins. Nanocarriers currently in use for the delivery of drugs and genetic materials can be generally divided to two categories: those made from lipids and those made from synthetic or natural polymers. Although lipid-based carriers are generally regarded to be safe and efficient, they do not possess sufficient chemical flexibility to fit individual requirements in delivery. In this thesis, we have explored lipid-substitution of three different polymer-based nanocarriers as means to develop optimum structures for drug as well as siRNA delivery. For the delivery of a potent amphiphilic antifungal drug, amphotericin B (AmB), lipid modification (particularly cholesteryl modification) of the core structure in poly(ethylene oxide)-poly(caprolactone) micelles was proved to be efficient in enhancing the solubility while reducing the hemolytic activity of encapsulated AmB. On the other hand, lipid modification of low molecular weight (2 kDa) polyethyleneimine (PEI2) has enhanced the properties of the nanocarriers in the delivery of STAT3-siRNA in wild type and resistant breast cancer cell models leading to an improved anti-cancer efficacy in combination with chemotherapeutic drugs, i.e. DOX and PTX. Finally, cholesteryl modification of poly(ethylene oxide)-poly(caprolactone-g-spermine) enhanced the properties of these nanocarriers for *in vivo* delivery of siRNA. This modification enhanced the stability, safety and cellular uptake of complexed siRNA

leading to better silencing activity at the mRNA level. Overall, our results pointed to the positive impact of lipid modification in enhancing the properties of polymeric nanocarriers leading to viable formulations for effective delivery of AmB and siRNA therapeutics.

## **ACKNOWLEDGEMENTS**

First, I would like to sincerely thank my supervisor Dr. Afsaneh Lavasanifar for accepting me in her research group and providing me with guidance, financial and academic support during the Ph.D. program. Over the past five years she has not only taught me about the field of drug delivery, but taught me how to develop valuable skills which will help me in my future carrier. I will never forget her limitless support during difficult times I faced in my Ph.D. program.

I sincerely thank my co-supervisor Dr. Hasan Uludag for his kindness, advice, endless support as well as providing me with the materials and expertise to develop siRNA formulations.

I thank my supervisory committee member Dr. Kamaljit Kaur for her valuable advice and for providing me with peptides to develop targeted siRNA formulations; as well as Dr. Raymond Lai for giving me access to his lab to do western blot experiments.

I thank my colleagues Dr. Hamidreza Montazeri Aliabadi, Dr. Meysam Abbasi Dr. Mohammad Reza Vakili, Dr. Xiao-Bing Xiong, Dr. Ommoleila Molavi, Dr. Mostafa Shahin and Mr. Abdulraheem Alshareef for their help during my studies.

I thank my parents inlaw, Dr. Afsaneh Lavasanifar and Mr. Mohammadreza Yazdanshenas for their words of encouragement and push for persistence; also my sisters Mrs. Anahita Falamarzian and Mrs. Avid Falamarzian, brothers inlaw Dr. Saeed Jortani

and Mr. Payam Behnam, and sister inlaw Ms. Leila Yazdanshenas for their advice and encouragement throughout my studies.

Last, but not least, thanks to Alberta Cancer Research Institute (ACRI) and Faculty of Pharmacy and Pharmaceutical Sciences for providing me with my scholarships. The studies in this thesis were financially supported by operating grants from the Canadian Institutes of Health Research (CIHR), and Natural Sciences and Engineering Research Council of Canada (NSERC).

## TABLE OF CONTENTS:

<b>Chapter 1. Introduction.....</b>	<b>1</b>
<b>1.1. Nanotechnology for drug delivery: Promises and challenges.....</b>	<b>2</b>
<b>1.2. Commonly used nano-drug delivery systems.....</b>	<b>4</b>
<b>1.2.1. Liposomes.....</b>	<b>4</b>
<b>1.2.2. Polymeric micelles.....</b>	<b>7</b>
<b>1.3. Amphotericin B and its delivery systems.....</b>	<b>20</b>
<b>1.3.1. Clinical significance and applications of Amphotericin B (AmB)..</b>	<b>20</b>
<b>1.3.2. Mechanism of action and toxicity.....</b>	<b>20</b>
<b>1.3.3. Commercial and investigational formulations.....</b>	<b>22</b>
<b>1.4. Use of siRNA as a therapeutic entity: Promises and challenges.....</b>	<b>26</b>
<b>1.4.1. Polymer based strategies for siRNA Delivery.....</b>	<b>32</b>
<b>1.4.2. siRNA therapeutics in clinical trials.....</b>	<b>52</b>
<b>1.5. Signal Transducer and activator of transcription 3 (STAT3) as a target in     oncogene silencing: the relevance to cancer therapy.....</b>	<b>58</b>
<b>1.6. Research proposal.....</b>	<b>71</b>
<b>1.7. References.....</b>	<b>75</b>
<b>Chapter 2. Chemical modification of hydrophobic block in poly(ethylene oxide)- poly(caprolactone) based nanocarriers: effect on the solubilization and hemolytic activity of Amphotericin B</b>	
<b>2.1. Introduction.....</b>	<b>93</b>
<b>2.2. Materials and methods.....</b>	<b>95</b>
<b>2.3. Results.....</b>	<b>102</b>
<b>2.4. Discussion.....</b>	<b>113</b>

2.5. Conclusion.....	117
2.6. References.....	118

**Chapter 3. Optimization of the hydrophobic domain in poly(ethylene oxide)-poly( $\epsilon$ -caprolactone) based nanocarriers for the solubilization and delivery of Amphotericin B**

3.1. Introduction.....	122
3.2. Materials and methods.....	125
3.3. Results.....	131
3.4. Discussion.....	146
3.5. Conclusion.....	149
3.6. References.....	151

**Chapter 4. Lipid-substituted polyethyleneimine polyplexes of STAT3 siRNA for sensitization of breast tumor cells to conventional chemotherapy**

4.1. Introduction.....	155
4.2. Experimental Section.....	158
4.3. Results.....	167
4.4. Discussion.....	186
4.5. Conclusion.....	191
4.6. References.....	192

**Chapter 5. Lipid modification of the core in poly(ethylene oxide)-*block*-poly( $\epsilon$ -caprolactone-grafted spermine) micelles for efficient siRNA delivery to cancer cells: Toward development of systemic siRNA delivery systems**

5.1. Introduction.....	197
5.2. Experimental Section.....	198
5.3. Results.....	210
5.4. Discussion.....	222

5.5. Conclusion.....	225
5.6. References.....	226

**Chapter 6. Optimization of hydrophobic domain in poly(ethylene oxide)-*block*-poly( $\epsilon$ -caprolactone-grafted spermine) for efficient siRNA delivery**

6.1. Introduction.....	229
6.2. Experimental Section.....	230
6.3. Results.....	244
6.4. Discussion.....	263
6.5. Conclusion.....	268
6.6. References.....	269

**Chapter 7. Towards development of peptide modified polymeric micelles for tumor targeted siRNA delivery**

7.1. Introduction.....	271
7.2. Experimental Section.....	272
7.3. Results.....	279
7.4. Discussion.....	287
7.5. Conclusion.....	289
7.6. References.....	290

**Chapter 8. General discussion, conclusions and future direction**

8.1. General discussion.....	293
8.2. Conclusions.....	301
8.3. Future directions.....	303
8.4. References.....	306

## LIST OF TABLES:

1.1. Liposomal drugs approved for clinical application or undergoing clinical evaluation.....	6
1.2. Polymeric micelle-based formulations in clinical trials.....	8
1.3. Characteristics of different marketed AmB formulations.....	25
1.4. Polymeric micelles containing PEG-siRNA.....	39
1.5. Polymeric micelles based on PEG-PEI or PEG-PLL complexed siRNA.....	44
1.6. Polymeric micelles based on other polycationic copolymers for siRNA complexation.....	50
1.7. Clinical trials for RNAi therapy.....	54
1.8. Role of STAT3 in biological functions.....	61
1.9. Agents used for STAT3 targeting.....	69
1.10. STAT3 inhibitors in clinical trials.....	70
1.11. Studies using siRNA for STAT3 inhibition.....	70
2.1. Characteristics of synthesized block copolymers.....	103
2.2. Characteristics of empty nanocarriers.....	107
2.3. Characteristic of AmB-loaded nanocarriers.....	110
3.1. Characteristics of synthesized block copolymers.....	133
3.2. Characteristics of empty nanocarriers.....	138
3.3. Characteristic of AmB-loaded block copolymer nanocarriers.....	141

<b>4.1.</b> Lipid-substituted PEI 2K library.....	168
<b>5.1.</b> Characteristics of empty micelles (n=3).....	212
<b>6.1.</b> Characteristics of prepared copolymers and empty micelles (n=3).....	245
<b>7.1.</b> Preparation of mixed micelles.....	277

## LIST OF FIGURES:

1.1. Examples of nanocarriers used for application in nano-medicine.....	3
1.2. PEO-P(CL-polyamine) micelles for siRNA delivery.....	13
1.3. Polymeric micelles with dual targeting ligands engineered micellar shell and polycationic core to mimic a viral vector for siRNA delivery.....	19
1.4. Chemical structure of Amphotericin B.....	21
1.5. Problems associated with the in vivo use of siRNA and their possible solutions.....	27
1.6. Proposed model for the cellular interaction of ideal polymeric micellar systems for siRNA delivery.....	31
1.7. Chemical structure of linear PEI, branched PEI.....	34
1.8. Models of different polymeric micellar structures for siRNA delivery.....	35
1.9. Chemical structure of Poly-L-lysine (PLL).....	46
1.10. Signaling pathways that converge on STATs.....	60
2.1. Synthetic scheme for the preparation of MePEO- <i>b</i> -PStCL.....	104
2.2. <sup>1</sup> H NMR spectra of MePEO- <i>b</i> -PStCL in CDCl <sub>3</sub> and peak assignments.....	105
2.3. TEM picture of nanocarriers prepared from MePEO- <i>b</i> -PStCL block copolymer...	108
2.4. AFM height images of thin deposits prepared by drop-casting of 0.02 mg/mL MePEO- <i>b</i> -PStCL nanocarrier solution on mica.....	109
2.5. Hemolytic activity of <b>A</b> ) Synthesized MePEO- <i>b</i> -poly(ester)s; <b>B</b> ) Nanoparticle formulations of AmB and its commercial formulation (Fungizone <sup>®</sup> ) against rat red blood cells.....	112

<b>3.1.</b> Chemical structure MePEO- <i>b</i> -poly(ester)s polymers used in this study.....	124
<b>3.2.</b> Synthetic scheme for the preparation of $\alpha$ -palmitoyl $\epsilon$ -caprolactone.....	134
<b>3.3.</b> $^1\text{H}$ NMR spectra of $\alpha$ -palmitoyl $\epsilon$ -caprolactone (substituted monomer) in $\text{CDCl}_3$ and peak assignments.....	134
<b>3.4.</b> Synthetic scheme for the preparation of MePEO- <i>b</i> -PPaCL.....	135
<b>3.5.</b> $^1\text{H}$ NMR spectra of MePEO- <i>b</i> -PPaCL in $\text{CDCl}_3$ and peak assignments.....	136
<b>3.6.</b> TEM picture of nano-carriers prepared from MePEO- <i>b</i> -PPaCL block copolymer (magnification 36000). The bar on the images represents 500 nm.....	139
<b>3.7.</b> Hemolytic activity of synthesized MePEO- <i>b</i> -poly(esters).....	143
<b>3.8.</b> Hemolytic activity of AmB (4 mg initial amount) nanocarrier formulations in comparison to its commercial formulation (Fungizone <sup>®</sup> ) against rat red blood cells.....	144
<b>3.9.</b> Hemolytic activity of AmB (10 mg initial amount) nanocarrier formulations in comparison to its commercial formulation (Fungizone <sup>®</sup> ) against rat red blood cells...	145
<b>4.1.</b> Cellular uptake of siRNA polyplexes by flow cytometry.....	171
<b>4.2.</b> Cellular distribution of selected siRNA polyplexes by fluorescence microscopy...	173
<b>4.3.</b> Cytotoxicity of STAT3-siRNA versus scrambled siRNA polyplexes.....	175
<b>4.4.</b> PEI-LA polymer efficiency.....	177
<b>4.5.</b> siRNA dose response with PEI-LA2.1 polymer.....	179
<b>4.6.</b> Silencing activity of STAT3-siRNA polyplexes by RT-PCR.....	181
<b>4.7.</b> Silencing activity of STAT3-siRNA polyplexes by Western blot.....	182
<b>4.8.</b> Effect of STAT3-siRNA/PEI-LA pre-treatment on the cytotoxicity of Doxorubicin and Paclitaxel in WT and resistant breast cancer cells.....	185

<b>5.1.A.</b> Synthetic scheme for the preparation of MePEO- <i>b</i> -P(CL-g-SP-STA).....	204
<b>5.1.B.</b> Synthetic scheme for the preparation of MePEO- <i>b</i> -P(CL-g-SP-Chol).....	205
<b>5.2.A.</b> <sup>1</sup> H NMR spectra of MePEO- <i>b</i> -P(CL-g-SP) in D <sub>2</sub> O and peak assignments.....	213
<b>5.2.B.</b> <sup>1</sup> H NMR spectra of MePEO- <i>b</i> -P(CL-g-SP-STA) in CDCl <sub>3</sub> and peak assignments.....	214
<b>5.2.C.</b> <sup>1</sup> H NMR spectra of MePEO- <i>b</i> -P(CL-g-SP-Chol) in CDCl <sub>3</sub> and peak assignments.....	215
<b>5.3.</b> TEM picture of micelles prepared from A) MePEO- <i>b</i> -P(CL-g-SP), B) MePEO- <i>b</i> -P(CL-g-SP-STA) and C) MePEO- <i>b</i> -P(CL-g-SP-Chol) block copolymers (magnification 140000). The bar on the images represents 50 nm.....	216
<b>5.4.</b> Electrophoretic retardation analysis of siRNA binding by different polymers.....	218
<b>5.5.</b> Cellular uptake of polymer/siRNA micelles by flow cytometry.....	220
<b>5.6.</b> Confocal microscopy images of cells after treatment with FAM-siRNA formulated in (A) siRNA alone, (B) SP, (C) SP-STA 50%, (D) SP-Chol 25% (E) SP-Chol 50% and (F) Trifectin <sup>®</sup> .....	221
<b>6.1.</b> Synthetic scheme for the preparation of MePEO- <i>b</i> -P(CL-g-SP-Chol).....	234
<b>6.2.A.</b> <sup>1</sup> H NMR spectra of MePEO- <i>b</i> -P(CL-g-SP) in D <sub>2</sub> O and peak assignments.....	246
<b>6.2.B</b> <sup>1</sup> H NMR spectrum of MePEO- <i>b</i> -P(CL-g-SP-Chol) in CDCl <sub>3</sub> and peak assignments.....	247
<b>6.3.</b> The binding affinity of different polymers to scrambled siRNA. Percentage of siRNA binding versus polymer:siRNA weight ratios is shown (n=2).....	248

<b>6.4.</b> siRNA release from different micelles by heparin competition. Scrambled siRNA was complexed with various polymers at 32:1 polymer:siRNA ratio (w/w) and with PEI25K at 1:1 ratio (w/w).....	249
<b>6.5.</b> Cellular uptake of polymer/FAM-siRNA complexes by MDA-MB-435/WT cells.....	251
<b>6.6.</b> Cellular distribution of polymer/siRNA micelles by confocal microscopy.....	252
<b>6.7.</b> Cytotoxicity of the synthesized block copolymers/scrambled siRNA complexes against MDA-MB-435/WT cells.....	253
<b>6.8.</b> Silencing activity of STAT3-siRNA micelles by RT-PCR.....	256
<b>6.9.</b> Silencing activity of STAT3-siRNA micelles by Western blot.....	258
<b>6.10.</b> Cytotoxicity of STAT3-siRNA versus scrambled siRNA micelles.....	260
<b>6.11.</b> Silencing activity of MCL-1siRNA micelles by RT-PCR.....	261
<b>6.12.</b> Cytotoxicity of MCL-1siRNA versus scrambled siRNA micelles.....	262
<b>7.1.</b> Chemical structure PEO- <i>b</i> -poly(ester) polymers used in this study.....	275
<b>7.2.</b> Model for the preparation of RGDfK and P160-decorated PEO- <i>b</i> -PCL micelles.....	281
<b>7.3.</b> Electrophoretic retardation analysis of siRNA binding by different mixed polymeric micelles.....	283
<b>7.4.</b> Cellular uptake of core modified mixed micelles/siRNA by MDA-MB-435/WT cells.....	285
<b>7.5.</b> Cellular uptake of peptide decorated mixed micelles/siRNA by flowcytometry by MDA-MB-435/WT cells.....	286

## LIST OF ABBREVIATIONS:

ABC; Amphiphilic block copolymers

AmB; Amphotericin B

Acetal-PEO-*b*-PBCL; Acetal-PEO-poly-( $\alpha$ -benzyl carboxylate- $\epsilon$ -caprolactone)

Acetal-PEO-*b*-PCCL; Acetal-PEO-poly( $\alpha$ -carboxyl- $\epsilon$ -caprolactone)

ASGP; Asialoglycoprotein

AFM; Atomic force microscopy

APOB; Apolipoprotein B

BCRP; Breast Cancer Resistance Protein

BCL-2; B-cell CLL/lymphoma 2

bFGF; basic fibroblast growth factor

Cu I; Cucurbitacin I

Cu B; Cucurbitacin B

CMC; Critical micelle concentration

CCCs; Cationic comb-type copolymers

CAC; Critical aggregation concentration

cRGDfK; cyc(Arg-Gly-Asp-d-Phe-Lys)

CCR5, C-C chemokine receptor type 5

CL; Caprolactone

DP; N,N-dimethyldipropylenetriamine

DOX; Doxorubicin

dsRNA; double stranded RNA

DMMAAn; Dimethylmaleic anhydride

DC; Dendritic cells

DLS; Dynamic light scattering

EGFP; Enhanced green fluorescence protein

EGF; Epidermal growth factor

FA; Folic acid

FGF; fibroblast growth factor

FAM; 5-carboxyfluorescein

GSH; Glutathione

GFP; Green fluorescence protein

GAPDH; Glyceraldehydes phosphate dehydrogenase

GPC; Gel permeation chromatography

HTFs; Tenon's capsule fibroblasts

HNSCC; Head and neck squamous cell carcinoma

HGF; Hepatocyte growth factor

IFN; Interferon

IC<sub>50</sub>; 50 % inhibitory concentration

IKK; IκB kinase

IL; Interleukin

IGF; insulin-like growth factor

LHRH; luteinizing hormone releasing hormone

LDL; Low-density lipoprotein

mPEGPDLLA; monomethoxy-PEG-b-poly(d,l-lactide)

MDR; Multi drug resistant

mAbs; Monoclonal antibodies

MAL-PEO-PCL; Maleimide-terminated PEO-PCL

MRI; Magnetic resonance imaging

mRNA; messenger RNA

MCL; Multi cellular layer

MePEO-*b*-PBCL; MePEO-*block*-poly( $\alpha$ -benzylcarboxylate- $\epsilon$ -caprolactone)

MePEO-*b*-PCCL; MePEO-*block*-poly ( $\alpha$ -carboxyl- $\epsilon$ -caprolactone)

MePEO-*b*-PStCL; MePEO-*block*-poly( $\alpha$ -stearlycarboxylate- $\epsilon$ -caprolactone)

MePEO-*b*-PCL; Methoxy PEO-*block*-poly( $\epsilon$ -caprolactone)

MePEO-*b*-PStCL; MePEO-*block*-poly( $\alpha$ -stearlycarboxylate- $\epsilon$ -caprolactone)

MePEO-*b*-PChCL; MePEO-*block*-poly( $\alpha$ -cholesteryl carboxylate- $\epsilon$ -caprolactone)

MePEO-*b*-PPaCL; MePEO-*block*-poly ( $\alpha$ -palmitoyl- $\epsilon$ -caprolactone)

MePEO-*b*-P(CL-g-SP); Methoxy-poly(ethylene oxide)-*block*-poly( $\epsilon$ -caprolactone-g-(spermine))

MePEO-*b*-P(CL-g-SP-STA); Methoxy-poly(ethylene oxide)-*block*-poly( $\epsilon$ -caprolactone-g-N-(spermine)-stearamide)

MePEO-*b*-P(CL-g-SP-Chol); Methoxy-poly(ethylene oxide)-*block*-poly( $\epsilon$ -caprolactone-g-N-(spermine)-cholesteryl carboxylate)

MMP2; Matrix metalloproteinase 2

MCL-1; Myeloid cell leukemia sequence 1

NR; Not reported

N/P; Nitrogen to phosphate

ODN; oligonucleotides

PEG-PE; Phosphatidylethanolamine

PEGP(Asp); PEG-poly(L-aspartic acid)

PLAPEG; Poly(lactic acid)-poly(ethylene glycol)

PEG-P(Glu); Polyethylene glycol poly(L-glutamic acid)

PEO-P(Asp); Poly(ethylene oxide)-poly(L-aspartic acid)

PEG; Poly-(ethylene glycol)

PEO-*b*-PCL; Poly-(ethylene oxide)-poly-( $\epsilon$ -caprolactone)

PCL; Poly ( $\epsilon$ -caprolactone)

PEO-PLA; PEO-poly lactide

PEO-PHSA; Poly-(ethylene oxide)-*block*-poly-(N-hexyl stearate-L-aspartamide)

P-gp; P-glycoprotein

PTX; Paclitaxel

PEO-P(Lys); Poly-(ethylene oxide)-block-poly-(lysine)

PEO-P(Glu); PEO-b-poly(L-glutamine)

PLGA; Poly-(DL-lactide-co-glycolide)

PBPA; Poly-benzylated poly-L-aspartic acid

PEOz-b-PAsp; Poly(2-ethyl-2-oxazoline)-block-poly(aspartic acid)

PAA; Poly(acrylic acid)

PEI; Polyethyleneimine

PLL; Poly-L-lysine

PIC; Polyion complex

PIK1; Polo-like kinase 1

PE; Phosphothioethanol

PCP; Prostate cancer-binding peptide

PDMAEMA-PCL-PDMAEMA; dimethylaminoethyl methacrylate-PCL  
dimethylaminoethyl methacrylate

PEO; Poly(ethylene oxide)

p-STAT3; tyrosine-phosphorylated Stat3

RNAi; RNA interference

RISC; RNA-induced silencing complex

RAFT; Reversible addition-fragmentation chain transfer

RRM2; Ribonucleotide reductase subunit M2

RBC; Red blood cell

RES; resistant

RT PCR; Real-time PCR

SP; spermine

siRNA; small interfering RNA

shRNA; short hairpin RNA

STA; Stearic acid

sCLU; Secretory clusterin

STAT; Signal transducers and activators of transcription

SOCS; Suppressors of cytokine signaling

TNF- $\alpha$ ; tumor necrosis factor  $\alpha$

TP; Tetraethylenepentamine

THF; Tetrahydrofuran

TEM; Transmission electron microscopy

TLC; Thin-layer chromatography

TNBC; Triple negative human breast cancer

VEGF; Vascular endothelial growth factor

WT; Wild type

# **CHAPTER ONE**

## **INTRODUCTION**

Parts of this chapter has been published in

**Journal of Controlled Release, 2011; 155, 247-261**

**and**

**Journal of Drug Delivery Science and Technology, 2012; 22-1, 43-54**

## 1.1. Nanotechnology for drug delivery: promises and challenges

Nanotechnology has been the focus of much attention in medicine and the pharmaceutical industry in recent years [1, 2]. The use of nanotechnology in drug delivery is bound to alter the pharmaceutical industry forever. Major applications of nanotechnology in medicine include: (1) enhancing the delivery of water-insoluble drugs; (2) achievement of cell or tissue specific targeted delivery; (3) delivery of macromolecular drugs to intracellular sites of action, (4) and development of more effective combinational therapy [3]. Research in nanomedicine is generally focused into two translational fields nowadays: (1) improving the properties of present diagnostic and therapeutic modalities and (2) development of a new class of biomedical entities such as those involved in RNA interference pathway [4].

The nanotechnology application in drug delivery dates back few decades, when liposomal delivery systems were introduced in 1965 [5]. Sustained release polymeric systems were described later in 1976 for delivery of macromolecules [6] and biodegradable long-circulating polymeric nanospheres were first introduced in 1994 [7]. Various nanotechnology modalities available today include polymeric nanoparticles, polymer conjugates, lipid-based carriers such liposomes, dendrimers and carbon nanotubes (**Figure 1.1**) [8]. Among different nanoparticles available, lipid-based carriers such as liposomes and polymeric systems have received the most attention and exhibited vast amount of promise for clinical translation and are discussed further.

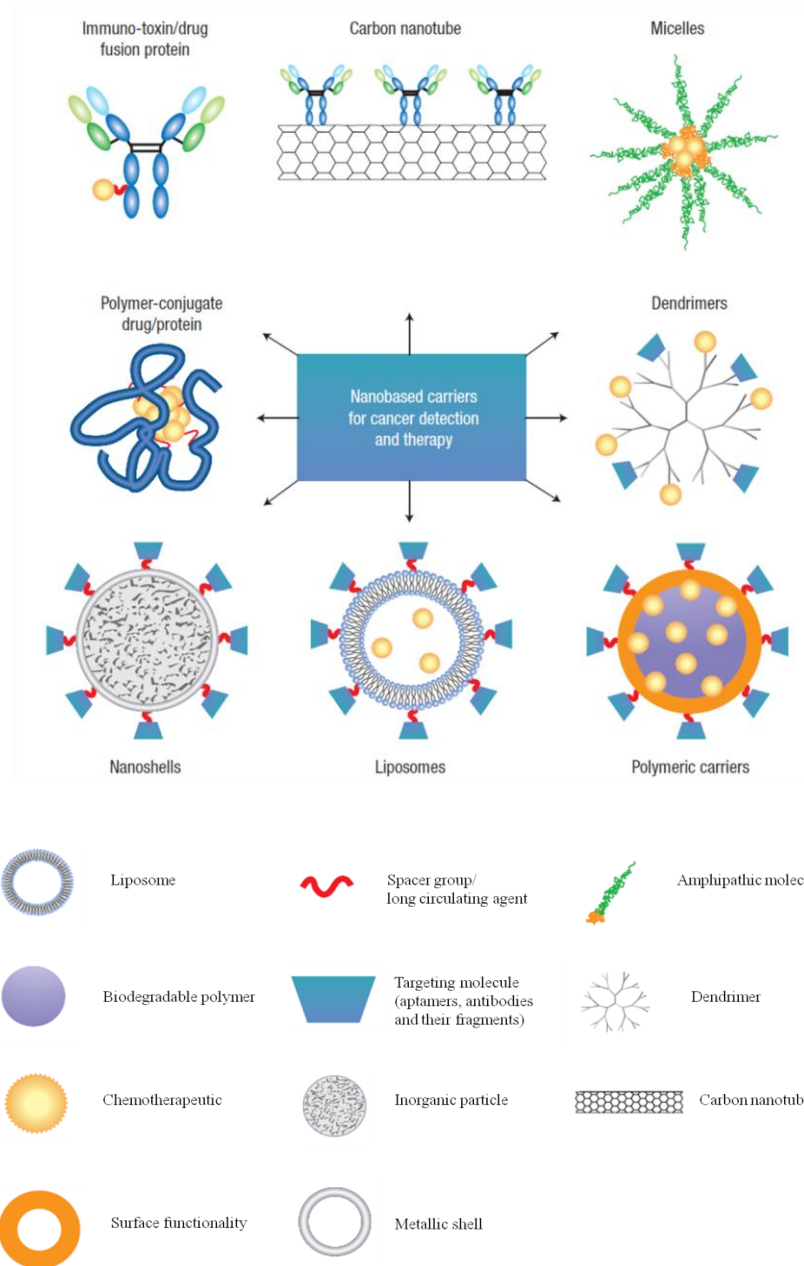


**Figure 1.1.** Examples of nanocarriers used for application in nano-medicine. Adopted from reference [8] with permission. A whole range of delivery agents are possible but the main components typically include a nanocarrier, a targeting moiety conjugated to the nanocarrier, and a cargo (such as the desired chemotherapeutic drugs).

## **1.2. Commonly used nano-drug delivery systems**

### **1.2.1. Liposomes**

Lipid-based nanocarriers offer several striking biochemical properties, including biodegradability, biocompatibility, protection of drug cargo from surrounding environment, and the capability to encapsulate both hydrophobic and hydrophilic drugs. New applications such as gene therapy have made these nanocarriers even more attractive [9]. Among different lipid-based delivery systems, liposomes are in the front line of development, with several formulations in the market. Liposomes are spherical structures made of natural or synthetic lipid bilayers with an aqueous core. They are able to entrap hydrophilic drugs in their aqueous core and hydrophobic drugs into their membrane. There are a number of different type of liposomes classified according to their lamellarity (uni-, oligo-, and multi-lamellar vesicles), size (small, intermediate, or large) and preparation method [10]. Conventional liposomes were readily captured by reticuloendothelial system, primarily in the liver and have short blood residence circulations [11]. As a result, researchers came up with second generation of liposomes, also called stealth liposomes which contain PEG on the surface that increases their blood circulation time, while reducing uptake by reticuloendothelial system. Klivanov et al. incorporated dioleoyl N-(monomethoxy polyethyleneglycol succinyl) phosphatidylethanolamine (PEG-PE) into large unilamellar liposomes. These liposomes showed a significant increase in the blood circulation half-life compared to liposomes without the PEG section [12]. Furthermore, by attachment of monoclonal antibodies or

targeting ligands to terminal PEG molecule, it is possible to enhance the accumulation of liposomes in specific target tissue [10]. Anti-HER2 (ErbB2) immunoliposomes have been developed to target HER2-overexpressing xenograft models. These immunoliposomes loaded with doxorubicin (DOX) exhibited significant tumor inhibition and regression compared to non-targeted liposomes [13]. Folate-receptor targeted liposomal DOX exhibited significant tumor growth inhibition and a 30% increase in animal lifespan compared to non-targeted liposomal DOX, when delivered into a murine tumor xenograft model [14]. Numerous other liposomal formulations are being investigated in detail both *in vitro* and *in vivo*, and are approved for clinical application or undergoing clinical evaluation (**Table 1.1**).

**Table 1.1.** Liposomal drugs approved for clinical application or undergoing clinical evaluation (adopted from reference [15] with permission).

<b>Active drug</b>	<b>Product name</b>	<b>Indication</b>
Daunorubicin	DaunoXome	Kaposi's sarcoma
Doxorubicin	Mycet	Combinational therapy of recurrent breast cancer
Doxorubicin in PEG-liposomes	Doxil/Caelyx	Refractory Kaposi's sarcoma; ovarian cancer; recurrent breast cancer
Amphotericin B	AmBisome	Fungal infections
Cytarabine	DepoCyt	Lymphomatous meningitis
Vincristine	Oncotop	Non-Hodgkin's lymphoma
Lurtotecan	NX211	Ovarian cancer
Nystatin	Nyotran	Topical antifungal agent
All-trans retinoic acid	Altragen	Acute promyelocytic leukaemia; non-Hodgkin's lymphoma; renal cell carcinoma; Kaposi's sarcoma
Platinum compounds	Platar	Solid tumours
Annamycin		Doxorubicin-resistant tumours
E1A gene		Various tumours
DNA plasmid encoding HLA-B7 and $\alpha 2$ microglobulin	Allovectin-7	Metastatic melanoma

### 1.2.2. Polymeric micelles

The use of amphiphilic block copolymers (ABC) in pharmaceutical science and industry has a long history and is experiencing rapid development [16-18]. The rapid development of application for ABC is primarily due to several degrees of freedom in their chemistry that makes design of specific carriers for specific drug delivery applications possible. ABC based nanodelivery systems include, but are not limited to, polymeric micelles, nanoparticles, polymersomes and nano-gels. Among these structures, polymeric micelles have attracted much interest [19, 20]. Polymeric micelles have a nanoscopic, usually spherical core/shell structure, in which the hydrophobic core acts as a nano-depot for accommodation of hydrophobic drugs, proteins or nucleic acid therapeutics (DNA, siRNA or oligonucleotides (ODNS)), and the hydrophilic shell interfaces the biological media. Chemical flexibility of the ABCs allows engineering of polymeric micellar structures for the development of custom-made drug delivery systems with respect to the physicochemical properties of the incorporated drug, pathophysiology of the disease, site of drug action and proposed route of administration. The entry of several polymeric micellar formulations with physically encapsulated or chemically conjugated drugs into clinical trials has established them as credible and promising options for nanomedicine development (**Table 1.2**) [21]. Despite several potential advantages, the advancement of polymeric micellar drug formulations from bench to clinic has been challenging. The major hurdles include low drug loading efficiency, poor blood stability after injection, and difficulty in transport through the cell membrane [22]. In this regard, efforts have been directed towards engineering of the micellar core to

increase drug loading capacity, enhance micelle stability, achieve controlled drug release and encapsulating nucleic acid based therapeutics. The micelle shell has been engineered to achieve active drug targeting, enhanced cellular uptake or stimuli-responsive drug release. Finally, simultaneous engineering of the core and shell have led to the development of multifunctional polymeric micelles which integrate several functions in one nanoformulation entity, providing an infinite control over spatial and temporal drug/gene delivery.

**Table 1.2.** Polymeric micelle-based formulations in clinical trials (adopted from reference [23] with permission).

<b>Formulation</b>	<b>Drug</b>	<b>Polymer</b>	<b>Phase</b>	<b>Indication</b>	<b>Company</b>
Genexol- PM	Paclitaxel	mPEGPDLLA	III, IV	Metastatic breast cancer	Samyang
NK105	Paclitaxel	PEGP(Asp)	II, III	Solid tumors	Nanocarrier/ Nippon Kayaku
SP1049C	Doxorubicin	Pluronic L61, F127	III	Advanced cancer	Suprateck
DTXLTNP	Docetaxel	PLAPEG, PLA-PEG-ACUPA	I	Solid tumors	BIND Biosciences
NC6004	Cisplatin	PEG-P(Glu)-Cisplatin	I, II	Solid tumors	Nanocarrier
NK012	SN- 38	PEG-P(Glu)-SN38	II	Solid tumors	Nippon Kayaku
NK911	Doxorubicin	PEG-P(Asp)-Dox	II	Solid tumors	Nippon Kayaku

mPEGPDLLA, monomethoxy-PEG-b-poly(d,l-lactide); PEGP(Asp), PEG-poly(aspartic acid); PLAPEG, poly(lactic acid)-poly(ethylene glycol); PEG-P(Glu), polyethylene glycol poly(glutamic acid).

### **1.2.2.1. Engineering of the micellar core**

#### **1.2.2.1.1. Increasing drug loading capacity**

Drug loading capacity of polymeric micelles is a bottle-neck issue for the successful development of micellar formulations for clinical use. The goal is to develop polymeric micellar formulations that can achieve therapeutic drug levels upon systemic administration. The miscibility between polymers and drugs plays an important role in drug loading efficiency of polymeric micelles. Increasing the miscibility between the drugs and polymers, as represented by a decrease in the Flory-Huggins interaction parameter ( $\chi_{\text{drug/polymer}}$ ), is shown to lead to increased physical drug loading in polymeric micelles [24]. It is assumed that the level of drug encapsulation in the micellar core is mainly defined by the extent of hydrophobic interaction between drug and the micellar core. The results of recent molecular simulation studies, supported by empirical data, suggest a significant role for polar interactions and hydrogen bonds between the drug molecules (containing hydrogen-bond forming groups in their structure) and the micellar core in defining the degree of drug solubilization by polymeric micelles [25]. In practice, the length of the hydrophobic block and the type and level of substituent on this block are shown to affect the loading efficiency of specific drugs in polymeric micelles [26, 27]. For instance, the core of poly(ethylene oxide)-poly(L-aspartic acid) (PEO-P(Asp)) micelles has been modified by attaching fatty acid side groups on p(Asp) to encapsulate amphotericin B (AmB) [28]. The resulting micelles demonstrated 13 times higher AmB encapsulation as compared to the PEO-P(Asp) micelles containing benzyl core structures.

Poly(ethylene oxide)-poly-( $\epsilon$ -caprolactone) (PEO-*b*-PCL) micelles with benzyl carboxylate substituted core were also used for the solubilization of poorly-water soluble cucurbitacin I (Cu I) and cucurbitacin B (Cu B) [29]. Solubilization was enhanced with PEO-*b*-PCL micelles containing benzyl group in their core by 1.7 times for Cu I and 3 times for Cu B compared to the original PEO-*b*-PCL micelles. Attachment of pendant cholesteryl carboxylate groups to PCL was also found to enhance the Cu I loading level even further than what was achieved with a benzyl substituted PCL core [30].

#### **1.2.2.1.2. Enhancing micelle stability**

Micelle instability upon administration is another main obstacle against development of effective nano-drug carriers. If the micellar structure can stay intact and retain the drug, the normal biodistribution of the encapsulated drug becomes similar to that of the carrier. Existence of a hydrophilic PEO brush on polymeric micelles can introduce steric effects and avoid interaction of polymeric micelles with opsonins preventing early micellar elimination by the reticuloendothelial system. The size of polymeric micelles is large enough to avoid removal by kidneys. The critical micelle concentration (CMC), which is largely dependent on the hydrophobicity of the block copolymer, reflects micellar thermodynamic stability. Micelles with low CMC will have a better chance of staying in a micellar form under diluting conditions of the blood circulation. To reduce CMC, the most common strategy is to increase the hydrophobicity of the block copolymer. For example, attachment of various fatty acids to the core of PEO-P(Asp) micelles was shown to decrease their CMCs [31]. Kinetic stability of

micelles on the other hand reflects their resistance against dissociation at concentrations below CMC. Introduction of stereo regular structures or cross-linking of the hydrophobic core have been attained by various strategies to enhance the kinetic stability of polymeric micelles [32, 33].

#### **1.2.2.1.3. Achieving controlled drug release**

To achieve controlled drug release from micellar nano-containers (i.e., polymeric micelles used for physical encapsulation of drugs) engineering efforts have focused on achieving polymeric cores that can interact strongly with a specific drug. For example, micelles of poly-(ethylene oxide)-block-poly-(N-hexyl stearate-L-aspartamide) (PEO-PHSA) having aliphatic structures in their core were prepared and used for the solubilization of AmB. In this study, the increase in the level of aliphatic chain substitution was found to enhance the encapsulation efficiency while reducing the release of AmB [34].

#### **1.2.2.1.4. Attaining polycationic core for efficient gene delivery**

Block copolymers composed of a polycationic segments have attracted increasing attention as non-viral gene vectors. In this case, neutralization of the positive charge on the polycation by the negatively charged DNA will lead to micelle formation. Poly-(ethylene oxide)-block-poly-(lysine) (PEO-P(Lys)) has been extensively used for this purpose [35-37]. To increase the stability of PEO-P(Lys) micelles against dissociation and at the same to maintain their ability to bind DNA, certain fractions of the lysine residues in the core were replaced by thiol groups that can readily form disulfide cross-

links with other sulfide substituted PEO-P(Lys) and develop a network in the micelle core after DNA complexation. The cross-linked core of the micelles are cleavable inside the cell due to the increased level of glutathione (GSH), but not in blood [38]. To achieve a 'proton sponge effect' which can result in endosomal disruption and gene release [39], PEO-P(Asp) block copolymer containing dipropylene triamine in their side chain was synthesized. The primary amine group located at the distal end of the side chain was used for complexation with phosphate groups of siRNA (small interfering RNA) or DNA, while the secondary amine, which was located closer to the polymeric backbone and had a lower pKa, provided buffering capacity for proton sponge effect [40-42]. Copolymers of PEO-*b*-PCL with grafted polyamine (e.g., spermine (SP), and tetraethylenepentamine (TP)) in the PCL block were synthesized in our lab for siRNA delivery (**Figure 1.2**) [43]. These amphiphilic polycationic copolymers can effectively bind siRNA, self-assemble into micelles and protect siRNA from degradation by nuclease in serum. We also showed that PEO-*b*-P(CL-g-SP) and PEO-*b*-P(CL-g-TP) micelles can efficiently deliver siRNA into cytoplasm by endocytosis and show endosomal escape after cellular uptake. MDR1- (Multi drug resistant-1) targeted siRNA formulated in PEO-*b*-P(CL-g-SP) and PEO-*b*-P(CL-g-TP) exhibited efficient silencing of MDR-1 gene expression leading to down-regulation of P-glycoprotein (P-gp).

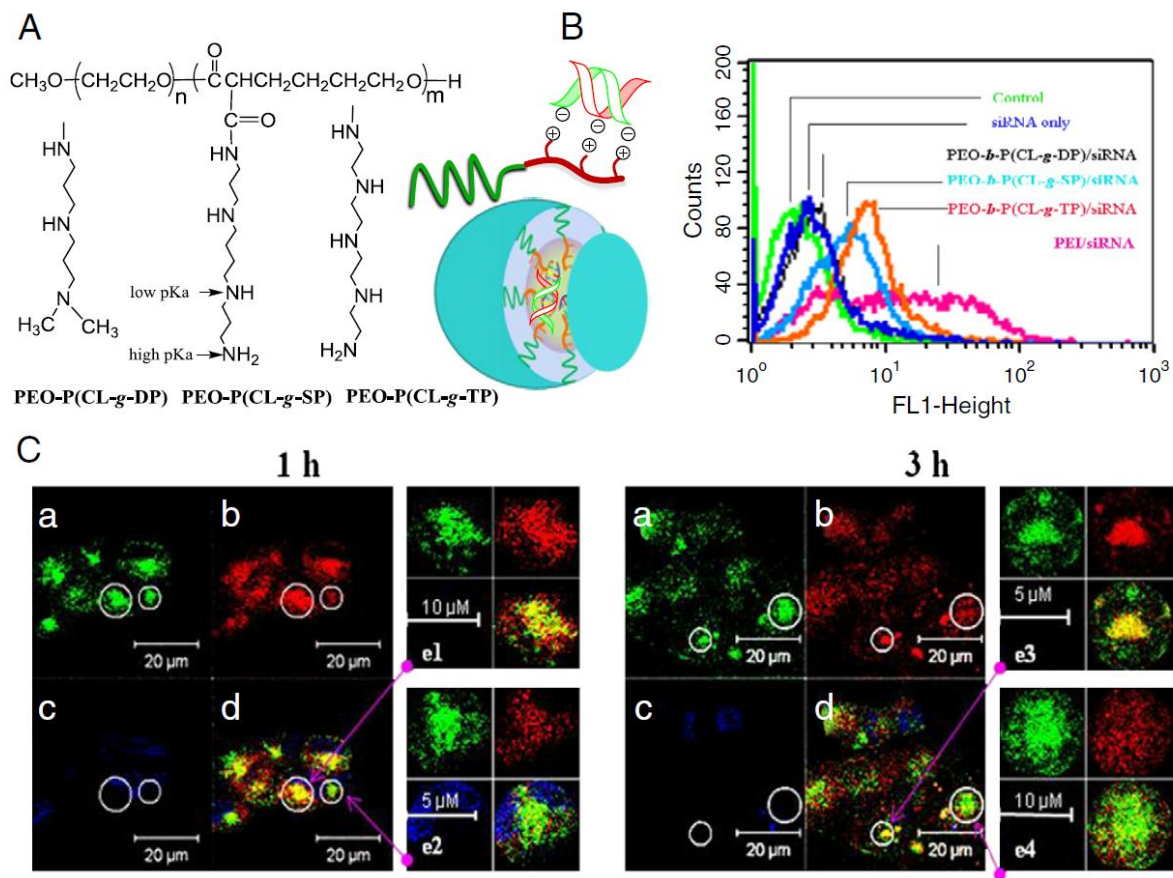


**Figure 1.2.** PEO-P(CL-polyamine) micelles for siRNA delivery. Adopted from reference [43] with permission. A) Schematic structures of PEO-P(CL-polyamines) and siRNA complexed micelles. B) Cellular uptake of FAM-siRNA from different PIC micelles or from PEI/siRNA PICs by MDA435/LCC6 cells. C) Endosome escape of siRNA formulated PEO-P(CL-g-TP) micelles after endocytosis upon 1 and 3 h incubation by confocal microscopy. SP: spermine; TP: tetraethylenepentamine; DP: N,N-dimethyldipropylenetriamine.

## **1.2.2.2. Engineering of the micellar shell**

### **1.2.2.2.1. Active targeting**

Introduction of targeting ligands to the surface of polymeric micelle can provide a mechanism to cross the cell membrane barrier for drug delivery. The micellar shell can be extensively engineered with various ligands to promote binding to cancer cells. The ligands are usually antibodies, small organic molecules, carbohydrates, peptides or aptamers. Conjugation of monoclonal antibodies (mAbs) or their Fab fragments to the micellar shell has led to the development of immunomicelles. One of the early studies on immunomicelles by Kabanov et al., described Pluronic P-85 micelles conjugated to a murine polyclonal antibody against  $\alpha_2$  glycoprotein ( $\alpha_2$ -GP) to deliver the neuroleptic agent haloperidol to the brain [44]. Antibody C225 against epidermal growth factor receptors was coupled to the terminus of a DOX-bound PEO-*b*-poly(L-glutamine) (PEO-P(Glu)) and showed enhanced cytotoxicity on A431 cells compared to free DOX [45].

Peptides containing the RGD sequence can recognize integrins that are overexpressed on the tumor cells or the angiogenic endothelial cells of the tumor vasculature. Nasongkla et al. developed polymeric micelles to selectively deliver hydrophobic drugs to angiogenic tumor endothelial cells which overexpress  $\alpha v \beta 3$  integrins [46]. To couple the cyclic pentapeptide cyc(Arg-Gly-Asp-d-Phe-Lys) (cRGDfK) which contains a thiol group, they synthesized maleimide-terminated PEO-PCL (MAL-PEO-PCL). After micellization, cRGDfK was coupled onto the micelle surface by electrophilic addition to form a thioether bond between the thiol group on the

peptide and the ethylenic bond on the maleimide. The cRGDfK-PEO-PCL micelle, with 76% (molar ratio) peptide density, was used for DOX delivery to angiogenic tumor endothelial cells. Confocal laser scanning microscopy showed 30 times greater accumulation of DOX-loaded cRGDfK-modified micelles compared to unmodified micelles into human Kaposi sarcoma tumor endothelial SLK cells compared to unmodified micelles. This system has recently been used for the co-delivery of DOX and superparamagnetic iron oxide as a contrast agent for magnetic resonance imaging (MRI) [47]. Our group has synthesized acetal-terminated PEO-PCL through anionic ring opening polymerization of  $\epsilon$ -CL by acetal-PEO [48]. After formation of micelles, the acetal group was converted to an aldehyde at acidic pH and used for the conjugation of peptide GRGDS to the micellar surface by Schiff base reaction. Fluorescent spectroscopy and microscopy analysis have shown 4.5 times higher uptake of GRGDS micelles compared to unmodified micelles after 3 h incubation by mouse melanoma B16-F10 cells. To extend the research, an acetal-PEO-poly-( $\alpha$ -benzyl carboxylate- $\epsilon$ -caprolactone) (acetal-PEO-*b*-PBCL) block copolymer was synthesized and then reduced to produce acetal-PEO-poly( $\alpha$ -carboxyl- $\epsilon$ -caprolactone) (acetal-PEO-*b*-PCCL). The anticancer drug DOX was then covalently conjugated to the free side carboxyl groups on the PCCL block by an amide bond to form acetal-PEO-*b*-P(CL-Ami-DOX). After conversion of the acetal group into aldehyde, RGD containing peptides such as GRGDS were attached to the surface of aldehyde-PEO-*b*-P(CL-Ami-DOX) micelles. The RGD-modified micelles bearing conjugated DOX demonstrated higher cytotoxicity against B16-F10 cells than the conjugates without peptide [49].

Human transferrin is a relatively large serum glycoprotein (80 kDa). Transferrin receptors are elevated 2-10 times on various types of cancer cells. The level of elevation in transferrin receptor correlates with the proliferative ability of the tumor cells. Vinogradov et al. proposed transferrin receptor-mediated delivery of phosphorothioate ODNs by using polyion complex micelles formed with transferrin-conjugated PEO-PEI [50]. Transferrin was attached to the PEO corona using an avidin/biotin construct. Compared to unmodified micelles, fluorescent-labeled transferrin-micelles showed a significantly higher accumulation in resistant human oral epidermoid carcinoma (KBv) cells. Delivery of antisense ODNs against the expression of P-gp human MDR1-mRNA by transferrin modified PEO-PEI nanocarriers resulted in a significantly higher inhibition of P-gp efflux in MCF-7/ADR cells that over-expresses P-gp compared to cells treated with unmodified micelles. Transferrin was conjugated to the PEO end of PEO-PEI by various procedures [51]. Complexes were generated by mixing of plasmid DNA, linear PEI (PEI<sub>22</sub>, 22 kDa) as the main DNA condensing agent, PEO-PEI for surface shielding, and transferrin-PEO-PEI to provide a ligand for receptor-mediated cell uptake. The systemic application of freeze thawed complexes exhibited *in vivo* tumor targeted expression; for complexes containing the luciferase reporter gene the highest expression was found in tumor tissue of mice. The optimum formulation for *in vivo* application, i.e., PEI<sub>22</sub>/transferrin-PEO-PEI/PEI<sub>22</sub>-PEO<sub>5</sub>, containing plasmid DNA encoding for the tumor necrosis factor  $\alpha$  (TNF- $\alpha$ ), inhibited tumor growth in three different murine tumor models.

### **1.2.2.3. Simultaneous engineering of core and shell**

The unique structure of polymeric micelles allows for the integration of multiple functional components in a single structure. Multifunctional polymeric micelles can combine tumor targeting and stimulus triggered drug release. Multifunctional polymeric micelles based on PEO-*b*-PCL for DOX delivery were developed in our lab [52]. DOX was chemically conjugated to the micellar core by amide or hydrazone linkages, while the RGD4C specifically homing to integrin  $\alpha v\beta 3$  receptors expressed on cancer cells (e.g. MDA435/LCC6 sensitive and resistant cells) was used to functionalize the micellar shell. These targeted micelles showed markedly increased uptake of DOX in cancer cells. The RGD4C-PEO-P(CL-Hyd-DOX) conjugated micelles showed pH-triggered drug release of intact DOX, leading to preferential accumulation of DOX in the nucleus of sensitive cells and showed a better activity against these cells when compared to free DOX. Micelles containing amide-linked DOX, on the other hand, showed insignificant release of free DOX, but very slow release of DOX-6-hexanoic acid at acidic pH, and led to preferential accumulation of DOX in the mitochondria of sensitive and resistant cancer cells. These micelles showed equal activity to that of free DOX in sensitive cells but a significantly higher cytotoxicity to that of free DOX in resistant cells. The IC<sub>50</sub> of DOX as part of the latter formulation was 10 times lower than that of free DOX in sensitive cells, pointing to the hyper-sensitization of resistant cells to DOX, perhaps through a mitochondrial related mechanism of cytotoxicity. In animal studies, treatment with RGD4C-PEO-*b*-PCL-DOX conjugates with hydrazone and amide links showed not only better activity than free DOX, but also led to longer survival of SCID mice bearing sensitive and resistant MDA-MB-435 tumors, respectively.

The core and shell of PEO-*b*-PCL based micelles were also engineered for effective siRNA delivery (**Figure 1.3**) [53]. The micellar shell was decorated with virus-related peptides such as RGD4C and/or cell penetrating peptide (TAT), while the micellar core was modified with a polycation (spermine) for siRNA binding, protection and endosome disruption. The peptide-functionalized micelles especially those with dual functionality (RGD/TAT-micelles) demonstrated increased cellular uptake and effective endosomal escape of siRNA compared to unmodified micelles (NON-micelles) when tested in MDA435/LCC6 resistant cells. Transfection of these cells with MDR-1 siRNA formulated in peptide-modified micelles led to P-gp down regulation both at the mRNA and protein level, and increased DOX accumulation in the cytoplasm and nucleus of the cells. Compared to RGD- or TAT micelles, RGD/TAT-micellar siRNA complexes produced improved cellular uptake, P-gp silencing, DOX cellular accumulation, DOX nuclear localization and DOX-induced cytotoxicity in MDA435/LCC6 cells, pointing to the potential of RGD/TAT-functionalized virus-like micelles for efficient siRNA delivery.

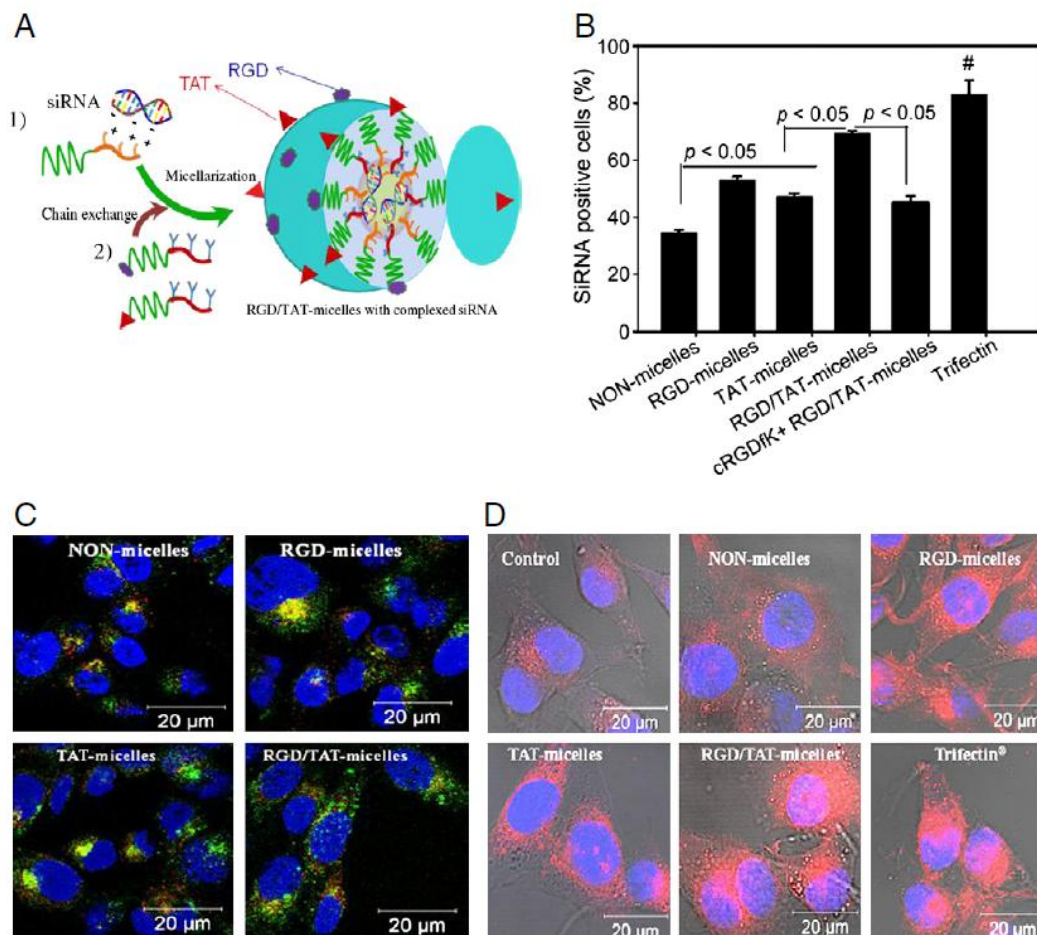


**Figure 1.3.** Polymeric micelles with dual targeting ligands engineered micellar shell and polycationic core to mimic a viral vector for siRNA delivery. Adopted from reference [54] with permission. A) Schematic illustration of RGD/TAT micelles with complexed siRNA. B) Percentage of FAM-siRNA positive cells treated with various siRNA formulations. C) Intracellular distribution of the FAM-siRNA (green) formulated micelles in MDA435/LCC6 resistant cells after 4 h incubation. The endosomes/lysosomes and nucleus were then stained with LysoTracker® (red) and DAPI (blue), respectively. D) DOX (red) distribution MDA435/LCC6 resistant cells after treatment with *mdr1*-targeted siRNA formulations.

### **1.3. Amphotericin B and its delivery systems**

#### **1.3.1. Clinical significance and applications of Amphotericin B (AmB)**

For over 50 years, AmB has played a significant role in the treatment of systemic fungal infections. AmB is isolated as a byproduct by a fermentation process from *Streptomyces nodosus*, a soil actinomycete [55]. AmB is a member of polyene antibiotics and has broad spectrum activity against a wide range of progressive and potential fatal fungal infections such as disseminated blastomycosis, cryptococcosis, coccidioidomycosis, histoplasmosis, mucormycosis, sporotrichosis and aspergillosis disseminated candidiasis [56]. Invasive fungal infections are a significant cause of morbidity and mortality in patients undergoing immunosuppressive therapy such as transplant recipients, tumor and immune deficient patients, and because of that AmB is extensively utilized in clinical practice. The important therapeutic value of AmB is linked to its advantageous biological characteristics such as broad antimicrobial spectrum, high fungicidal activity, reluctance to induce a secondary resistance and activity against multidrug-resistant strains [57, 58]. For instance, since the introduction of AmB treatment, cures are reported in over 50% of cases of cryptococcal meningitis which is the most common and fatal form of fungal meningitis [59].

#### **1.3.2. Mechanism of action and toxicity**

AmB is yellow/orange colored drug with two characteristic physiochemical properties: amphoteric character due to the presence of ionisable carboxyl and amine groups and amphipilic character due to the apolar and polar sides of the lactone ring

**(Figure 1.4).** It is poorly soluble in water (less than 1 mg/mL) and many organic solvents and has a tendency for formation of aggregates in water above a threshold concentration of  $\sim 0.2 \mu\text{g/mL}$  [60].

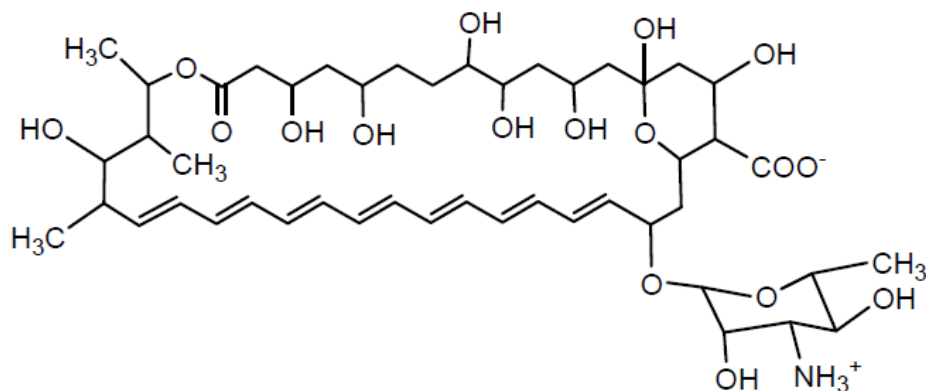


**Figure 1.4.** Chemical structure of Amphotericin B

These aggregates are formed by interaction between neighboring polyene chains [61]. As a result, AmB forms a combination of water soluble monomers and oligomers with insoluble aggregates in water. Depending on the aggregation state, AmB reacts with membrane sterols in various ways to provoke structural changes in the cell membrane. It produces membrane disruptions in the target cells causing subsequent leakage of ions and small molecules that can kill or damage the cells. In fungal cells which have ergosterol containing membranes, AmB reacts with the membrane in its monomeric state at low concentrations. On the other hand, it has been reported that AmB causes leakage of  $\text{K}^+$

through the mammalian cholesterol containing membranes in its aggregation state [62-64]. The adverse-effects of AmB therapy are substantial and may be divided into acute (fever, vomiting, headache) and sub-acute (kidney and liver toxicity). AmB exerts its nephrotoxic effects by altering membrane permeability and probably as a consequence, causing tubular transport defects and vasoconstriction [65]. These may lead to potentially fatal disorders in the electrolyte equilibrium and a loss of cytoplasmic adenosine triphosphate. AmB is also thought to cause hepatic and bile disorders as well as blood disorders such as normochrome anemia, thrombocytopenia, and agranulocytosis [66].

### **1.3.3. Commercial and investigational formulations**

For intravenous administration, two types of AmB formulations have been introduced into the market. First, Fungizone<sup>®</sup> which is a sodium deoxycholate micellar dispersion of AmB (**Table 1.3**). This formulation is still the most common formulation used in AmB therapy. Unfortunately, Fungizone<sup>®</sup> causes extensive nephrotoxicity. Newer lipid AmB formulations have been introduced into the market in the 1990s (**Table 1.3**) with the purpose of reducing AmB nephrotoxicity. Ambisome<sup>®</sup> is AmB inserted into unilamellar liposomes consists of hydrogenated soy bean lecithine, phosphocholine, cholesterol, and sucrose for an isotonic milieu, with  $\alpha$ -tocopherol and disodium succinate hydrate. In a randomized, multi-center, clinical study with 66 participants, comparing the nephrotoxicity and efficacy of Ambisome<sup>®</sup> with that of Fungizone<sup>®</sup>, only 14.2% of the patients treated with Ambisome<sup>®</sup> developed renal complications, compared with 42.3% of the patients treated with Fungizone<sup>®</sup>. Furthermore, the mortality rate of the first group

was three-fold lower [67]. Ambisome<sup>®</sup> has a superior bioavailability profile and fewer side effects compared to other formulations, however it is the most expensive among all formulations. Abelcet<sup>®</sup> consists of AmB with dimyristoylphosphatidylcholine and dimyristoylphosphatidyl- glycerol. Abelcet<sup>®</sup> has a better therapeutic index and a lower risk of causing renal disorders compared to Fungizone<sup>®</sup>. However, one setback of Abelcet<sup>®</sup> is quick clearance from circulation by mononuclear phagocyte system, possibly causing hepatic disorders. Amphotec<sup>®</sup> is an AmB formulation with cholesterol sulfate in equimolar concentrations. It has similar antifungal activity to Fungizone<sup>®</sup>, while showing less hemolytic activity. Significant side-effects and signs of nephrotoxicity appear at a daily dose of >1.5 mg/kg/day for Amphotec<sup>®</sup>, compared with 0.5-0.75 mg/kg/day for Fungizone<sup>®</sup>, perhaps due to the affinity of AmB to the cholesterol present in the formulation which decreases the amount of free AmB in the circulation [68]. Despite clear superiority of the above mentioned lipid AmB formulations to Fungizone<sup>®</sup>, possible disadvantages such as unpredictable pharmacokinetics, toxic effects at higher AmB doses, emergence of infusion related reactions and high cost, have limited their benefit in clinical settings.

Alternative formulation strategies that can potentially correct one or several of the mentioned shortcomings have been examined for AmB delivery in recent years. Some of these investigational delivery systems include pegylated liposomes [69], microemulsions [70], polymeric nano-formulations [28], multi-lamellar cylindrical micelles (cochleates) [71], complexes with polyvinylpyrrolidone [72], albumin and PLGA microspheres [73], nanosuspensions [74], lipid and poly-( $\epsilon$ -caprolactone) nanospheres [75].

Among the above mentioned formulations, polymeric nanoformulations that exhibit controlled drug release have been the focus of much interest. MePEO-*b*-poly-(L-amino acid) micelles with stearyl modified core structure were tried for AmB delivery. Substitution of stearyl groups in the core of MePEO-*b*-poly(L-amino acid) micelles has shown to increase the solubility of AmB in its micellar carrier and reduce the hemolytic activity of encapsulated AmB [28, 76]. In another study, Bang et al. prepared AmB-encapsulated polymeric micelle of poly-(DL-lactide-co-glycolide) (PLGA) grafted-dextran (DexLG) copolymer. These AmB carriers exhibited reduced hemolytic activity compared to AmB alone while maintaining similar antifungal activity [77]. Yoo et al. reported on preparation of nanoparticulate AmB micelles using benzylated poly-L-aspartic acid (PBPA) polymer. The resultant AmB micelles demonstrated significantly less toxicity on proximal tubular cells of male rats due to the alteration of self-aggregation behavior of AmB [78]. In another study a block copolymer poly(2-ethyl-2-oxazoline)-block-poly(aspartic acid) (PEOz-*b*-PAsp) was synthesized and investigated as the carrier for AmB. These carriers increased the solubility of AmB, prolonged its release from micelles while effectively inhibiting the growth of *Candida albicans* even after three days of administration compared to Fungizone<sup>®</sup> [79]. Adams et al. reported on preparation of AmB encapsulated micelles made up of methoxypoly(ethylene oxide)-*b*-poly(L-aspartate) (PEO-*b*-p(L-Asp)), which were derivatized to incorporate stearate side chains. These carriers exhibited potent *in vivo* activity in neutropenic murine model of disseminated candidiasis [80].

**Table 1.3.** Characteristics of different marketed AmB formulations (adopted from reference [60] with permission).

	Fungizone <sup>®</sup>	Ambisome <sup>®</sup>	Abelcet <sup>®</sup>	Amphotec <sup>®</sup>
Class	Colloidal system	Unilamellar liposome	Lipid complex	Colloidal lipid dispersion
Particle diameter (nm)	80–100	60–80	1600–6000	120–140
Approved indication	Treatment of invasive potentially life-threatening fungal infections and also for treatment of leishmaniasis although not as primary therapy	Empirical therapy for presumed fungal infections in febrile, neutropenic patients; treatment of cryptococcal meningitis in HIV-infected patients; treatment of patients with <i>Aspergillus</i> , <i>Candida</i> , and/or <i>Cryptococcus</i> infections	Treatment of invasive fungal infections in patients who are refractory to or intolerant of conventional AmB therapy	Treatment of invasive aspergillosis in patients whom renal impairment or unacceptable toxicity precludes the use of Fungizone in effective doses, and in patients with aspergillosis for whom previous Fungizone therapy has failed
Recommended dose (mg/kg/day)	0.6–1	3–5	5	3–4
Average Wholesale Price	\$12 per 50 mg	\$188 per 50 mg	\$135 per 50 mg, \$230 per 100 mg	\$93 per 50 mg, \$160 per 100 mg
Est. cost/day/70 kg	\$10–\$17	\$790–\$1316	\$805	\$336–\$448

#### **1.4. Use of siRNA as a therapeutic entity: Promises and challenges**

RNA interference (RNAi) is a sequence specific, evolutionary mechanism where double stranded RNA (dsRNA) is used for regulation of gene expression. In this post-transcriptional gene silencing mechanism, which was discovered by A. Fire and C. Mello in *Caenorhabditis elegans* [81, 82], sequence specific double-stranded small interfering RNA (siRNA) selectively degrades complementary messenger RNAs (mRNA) [83, 84]. Degradation of mRNA occurs when the antisense or guide strand of the siRNA directs the RNA-induced silencing complex (RISC) to cleave the target mRNA [85, 86]. siRNA can be produced either synthetically or from vectors expressing short hairpin RNA (shRNA) that are cytoplasmically cleaved to siRNA. The synthetic siRNA acts similar to natural microRNAs that are used by the cells to regulate many protein-coding genes [87].

siRNA has created much interest as research tool with high degree of specificity for temporary silencing of the gene of interest to identify their biological function. Therapeutically, RNAi can be employed to silence any specific gene at will, rendering it more advantageous than typical drugs that may cause widespread toxicity as a result of activity on undesired molecular targets. However, the development of this technology as a ground-breaking therapy with high degree of specificity for disease related genes has been relatively slow, as compared to its role as a research tool. The slow progress in therapeutic use of siRNA has been mainly due to problems associated with its safe and effective delivery in a clinical setting (**Figure 1.5**) [88].

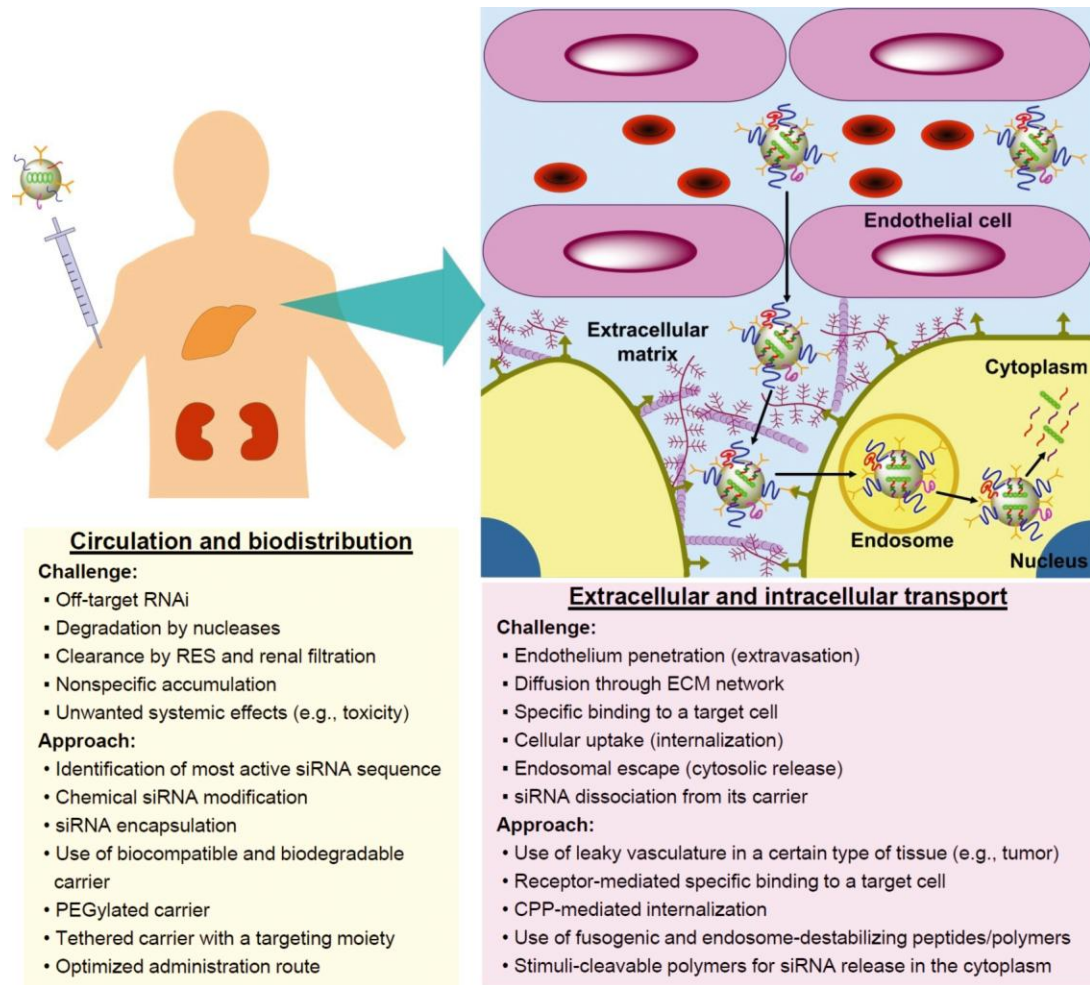


**Figure 1.5.** Problems associated with the *in vivo* use of siRNA and their possible solutions. Adopted from reference [86] with permission.

The objective of RNAi-based therapeutics is to selectively stimulate targeted mRNA cleavage for effective gene silencing. With the shRNA approach, an oligonucleotide containing the siRNA sequence followed by a 9 nucleotide loop and a reverse complement of the siRNA sequence is cloned into expression vectors to endogenously express hairpin loops with the desired sequence, which is subsequently

processed by the dicer enzyme into the desired siRNA [89]. Viral vectors are the most effective shRNA delivery systems due to their innate ability to protect the genetic information in the extracellular environment and to bind and cross plasma membranes in order to deliver their genetic cargo efficiently. The common viral delivery systems used for this purpose include adenoviruses, adeno-Associated Viruses, lentiviruses and retroviruses. The attractive aspect of viral delivery is their good ability to transfect clinically-relevant primary cells and mediation of repeatable, long-term protein knockdown [86]. However, high immunogenicity, potential of saturating the endogenous microRNA pathways, difficulty in constructing selective and effective hairpin RNAs and a negative view on the safety of viral vectors, limit application of these vehicles in clinical settings [90-92].

Synthetic siRNAs are less likely to interfere with endogenous microRNA pathway and are less prone to non-specific off-target effects if used at reasonable quantities. They have been successfully used to knockdown targets in different malignancies such as ovarian carcinoma [93], bone tumors [94] and prostate cancer [95]. However, significant hurdles remain with siRNA for its effective employment as a therapeutic agent (**Figure 1.5**). Potential off-target effects, instability in serum and the potential for activation of innate immune response by siRNA duplex are major obstacles [96, 97]. Furthermore, siRNA delivery to the site of action represents a major challenge in the development of RNAi therapeutics [89]. siRNA has a large molecular weight (~13 kDa; ~50 times larger than small molecule drugs [89]) and a very short half-life owing to degradation by nucleases, uptake by reticuloendothelial system and rapid renal excretion, all of which

can lead to early elimination of the siRNA [98]. The polyanionic nature of siRNA makes it impossible to cross the cell membrane for access to intracellular targets [43]. In order to address these problems, chemical modifications on siRNA molecule and/or development of lipid as well as polymer based carriers of siRNA have been examined.

Chemical modifications on the sugars, backbone or bases of the oligoribonucleotides have been employed to alleviate problems associated with siRNA stability and immunogenicity [99-105]. An important approach to enhance the accessibility of siRNA to its cellular or intracellular targets include conjugation of a variety of small molecules to siRNA [106]. Some of these molecules include cholesterol [107],  $\alpha$ -tocopherol [108], lipid [109], TAT [110], penetratin [111], PEG [112], and antibodies [113]. For instance, Lorenz et al. prepared lithocholic acid or lauric acid linked siRNAs. Lipid modified siRNAs exhibited promising results in inhibition of  $\beta$ -galactosidase expression in human hepatoma cell line Huh-7 compared to unmodified siRNA [107]. Wolfrum et al. used cholesterol conjugated siRNAs for targeting apolipoprotein B *in vivo*. When cholesterol-siRNA were preassembled with high density lipoprotein, they have shown 8 to 15 times more affectivity compared to cholesterol-siRNA alone [109]. These modifications are intended to improve the pharmacokinetic behaviour, cellular uptake or increase the protein binding of siRNA [114].

The more common approach has been to employ nanocarriers made from lipids or polymers for siRNA delivery. Most lipid-based siRNA delivery systems make use of cationic lipids to form complexes with negatively charged siRNA by electrostatic

interactions [115]. Cationic lipids are composed of three domains: a positively charged head group, a hydrophobic chain and a linker which connects polar and non-polar groups [116]. Solid lipid nanoparticles [117], liposomes [118-120] and lipoplexes [121, 122] are some of configurations of lipid-based nanoparticles used in siRNA delivery.

Cationic polymers can also be used to electrostatically bind and entrap siRNA in nanoparticles. Polymeric systems are advantageous compared to their lipid counterparts since their structure can be easily changed and modified in order to obtain desirable physiochemical properties [123]. Natural cationic polymers used for siRNA delivery include chitosan [124, 125], atelocollagen [94, 126] and cationic polypeptides [127]; the synthetic ones consist of branched or linear PEI [128-130], poly-L-lysine (PLL) [131] and cyclodextrin [132, 133]. Introducing molecules such as PEG stabilizes these nanoparticles and usually improves their pharmacokinetic profile (i.e., prolongs their circulation time). Introduction of targeting ligands such as RGD peptide or folate to these nanoparticles, makes them more effective in targeting cells expressing specific receptors.

In recent years, significant progress has been made in the design of polymeric siRNA carriers mimicking structural aspects of viruses. An ideal carrier for systemic siRNA administration should have the following properties: *a)* be non-toxic and non-immunogenic for systemic human administration; *b)* condense siRNA efficiently; *c)* maintain integrity of its content before reaching the target site and avoid rapid elimination from blood circulation; *d)* reach diseased tissue and specifically interact and get internalized by target cells; and finally *e)* dissociate in intracellular compartments of the

target cell to release the entrapped siRNA, making it accessible to mRNA. Polymeric micelles are one of those carriers, which have a nanoscopic size, are easy to prepare, have the ability to deliver their siRNA cargo to cytoplasm and are versatile enough to be equipped with targeting ligands on the surface and/or fusogenic molecules for enhanced siRNA delivery in selective cell populations (**Figure 1.6**).

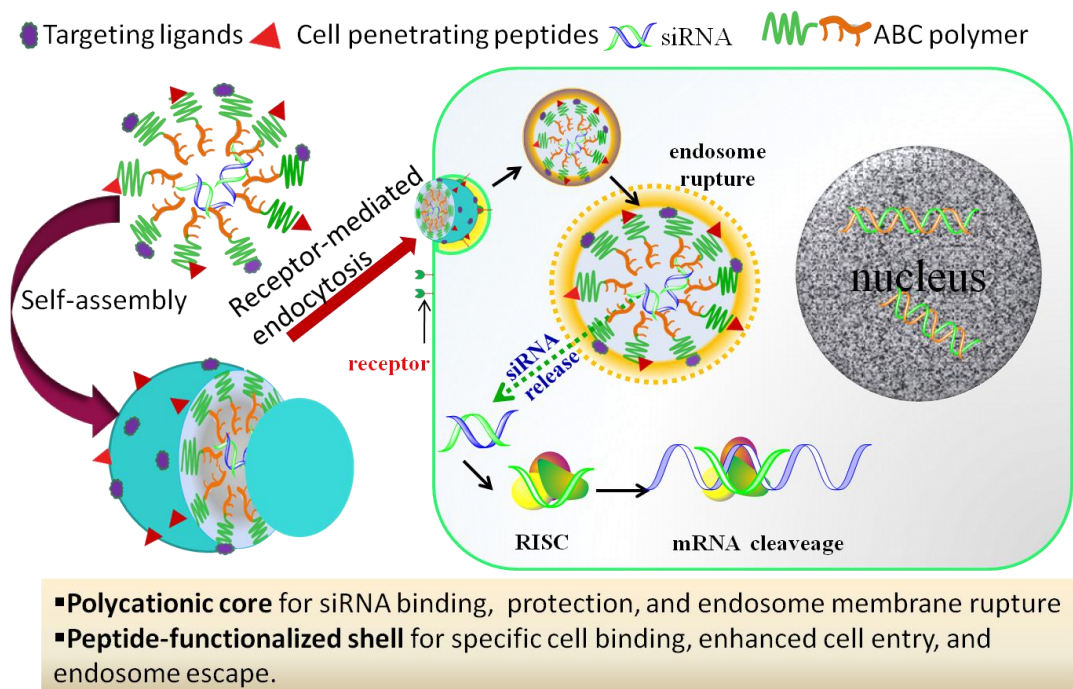


**Figure 1.6.** Proposed model for the cellular interaction of ideal polymeric micellar systems for siRNA delivery.

## 1.4.1. Polymer based strategies for siRNA Delivery

### 1.4.1.1. Polyethylenimines for siRNA delivery

PEI is a cationic polyamine polymer that comes in two forms: linear and branched and are available in molecular weights ranging from <1 kDa to >1000 kDa (**Figure 1.7**) [134, 135]. It is considered one of the most efficient carriers in gene delivery due to its capability to condense nucleic acids via electrostatic interaction between the anionic phosphate in the nucleic acid backbone and the cationic primary, secondary, and tertiary amines of the polymer. Furthermore, every third atom of PEI is a protonable amino nitrogen atom, which makes the polymeric network an effective "proton sponge" at virtually any pH [136, 137]. Due to proton sponge effect, there is influx of protons and water into endosomes where the particles are located. As a result, endosomes will eventually burst, releasing the complexes to the cytoplasm. High molecular weight PEI (>25 KDa) have been shown to serve as an effective siRNA delivery agent [138] and its efficacy in transfecting and properly delivering siRNA has been evaluated both *in vitro* and *in vivo* [128, 139]. For instance, Werth et al. exhibited that the non-covalent complexation of siRNA and a commercially available Jet-PEI, led to enhanced siRNA stabilization and delivery efficacy. They also showed that lyophilized PEI/siRNA complexes reserved the activity and the stability to serve as a ready-to-use reagent for specific and efficient silencing of genes [140]. In another study, intraperitoneal administration of complexed siRNA containing linear PEI and HER-2 siRNA resulted in a marked decrease of tumor growth in ovarian carcinoma xenografts [128]. PEI 25 KDa

modified with stearic acid (STA) was utilized for STAT3 siRNA delivery into B16 melanoma tumor cells. This has led to a significant regression in tumor growth after multi-dose treatments both *in vitro* and *in vivo* (upon intra-tumoral administration) [141]. However, cytotoxicity and limited biodegradability of high molecular weight PEI has hampered its clinical use [142]. Lower molecular weight PEIs might be more suitable due to better safety profiles, but these polymers have shown low transfection efficiency [143]. Hydrophobic modifications of low MW PEIs have been tried in order to develop more effective delivery systems for siRNA. These hydrophobic moieties are expected to increase the interaction of polymers with lipophilic membrane of cells and ease the uptake of complexed siRNA [144]. In previous studies, aliphatic lipid-substituted 2 kDa PEIs with an array of fatty acids with different chain lengths (from C8 to C18) have been explored for plasmid DNA delivery. An equivalent transfection ability to that of 25 kDa PEI was observed for lipid-substituted 2 kDa PEIs, without the toxic effect associated with the former polymer [143]. In separate studies, the lipid-substituted 2 kDa PEIs have been utilized for siRNA delivery and shown to improve the cellular uptake of siRNA compared to unmodified 2 kDa PEIs while demonstrating negligible toxicity. Effective silencing of target P-gp and Breast Cancer Resistance Protein (BCRP) by relevant siRNAs complexes of lipid modified PEI 2 kDa in P-gp transfected MDA-MB-435/MDR cells and BCRP-transfected MDCK cells have also been demonstrated, respectively [144, 145]. BCRP silencing caused a reversal in resistance to an anticancer agent, mitoxantrone, and a 14-fold reduction of its IC<sub>50</sub> value in drug resistant cells.

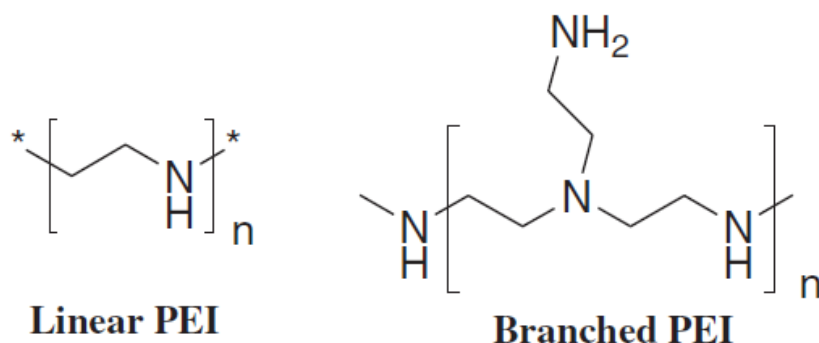


**Figure 1.7.** Chemical structure of linear PEI, branched PEI [146].

#### 1.4.1.2. Polymeric micelles for siRNA delivery

Polymeric micelles of siRNA developed to date can be classified under two categories based on their structure: A) Polymeric micelles formed through direct conjugation of PEG via degradable or non-degradable linkages to siRNA and further condensation of PEG-siRNA with an siRNA condensing agent (e.g., polycations) to micellar structure (**Figure 1.8**); B) Polymeric micelles formed by complexation of an amphiphilic block copolymer containing a polycation (and/or lipid) segment with siRNA followed by micellization of block copolymer/siRNA complex (**Figure 1.8**). Incorporation of targeting ligands on the surface of carriers and/or fusogenic peptides under each category has also been tried.

##### 1.4.1.2.1. Polymeric micelles based on PEG-siRNA conjugates

Several micelle-like structures that use polymer-siRNA conjugates and siRNA condensing agents have been reported in the literature (**Table 1.4**). In most cases, conjugation of PEG to siRNA is accomplished via disulfide linkages. The use of PEG is expected to reduce the adsorption of proteins (including nucleases) to siRNA *in vivo* and provide means for its stabilization. Disulfide linkages ensure *in vivo* degradability of the siRNA-polymer conjugate inside cells where reducing enzymes cleave the linkage leading to intracellular siRNA release.

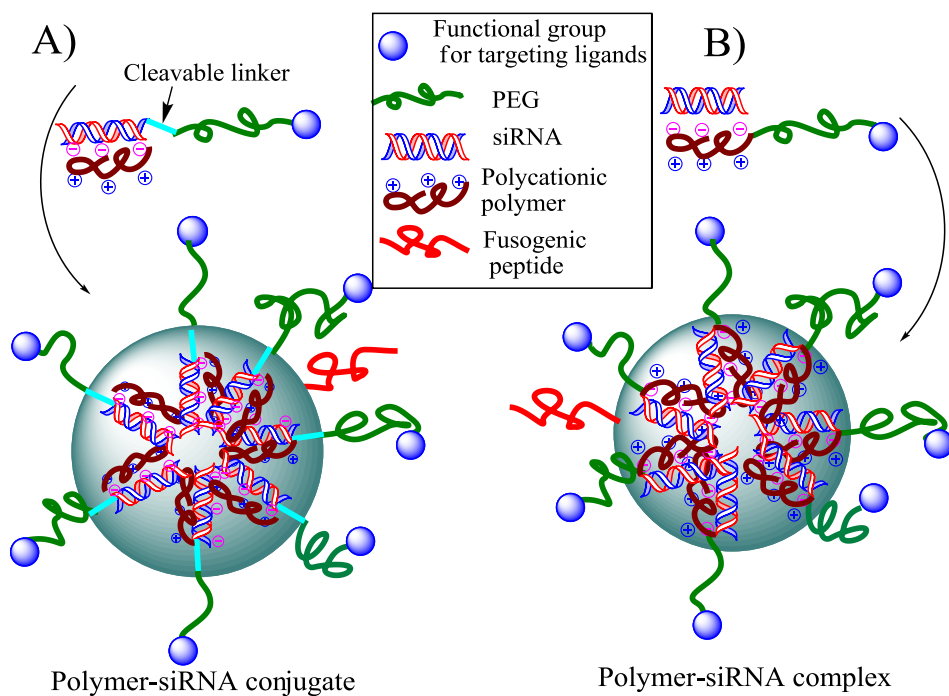


**Figure 1.8.** Models of different polymeric micellar structures for siRNA delivery. A) Block copolymers complexed with siRNA. B) Polymer-siRNA conjugates complexed with polycations.

Kim et al. conjugated vascular endothelial growth factor (VEGF) siRNA to PEG (5 kDa) via a disulfide linkage and interacted these conjugates with PEI (25 kDa), as the siRNA condensing agent, to form polyion complex (PIC) micelles. VEGF is established as a key regulator of angiogenesis, an important stage in the process of tumor growth and metastasis [147, 148]. A maximum of 96% inhibition in the expression of VEGF was shown in prostate carcinoma cells (PC-3) at 100 nM of VEGF siRNA [112]. Upon intratumoral administration, the siRNA-SS-PEG/PEI PIC micelles inhibited the expression of VEGF protein by 75% compared to no treatment control. This formulation was shown to inhibit the formation of intratumoral microvessles effectively, leading to a significant reduction in tumor size compared to no treatment group (13 % of the size of the tumor in the no treatment group 36 day after treatment). Systemic administration of the PIC micelles that used much higher doses of siRNA resulted in a significant suppression of VEGF protein (up to 86%) compared to no treatment control. An inhibition of 78% for microvessel formation was reported for this formulation compared to no treatment control. Tumor volume at 36 days after intravenous treatment with PEG-SS-siRNA PIC micelles was reduced to 25% of tumor volume in non-treatment control group. Minor antitumor effects were observed for scrambled and naked siRNA. No detectable IFN- $\alpha$  response for the PIC micelle was observed both *in vitro* and *in vivo*, indicating a lack of siRNA mediated immune-stimulation. The results suggested a potential for siRNA-SS-PEG/PEI PIC micelles for suppression of VEGF expression in anti-angiogenic cancer therapy, although off-target effects might be also important in the observed responses [130].

The authors continued this work and generated targeted siRNA PIC micelles through conjugation of luteinizing hormone releasing hormone (LHRH) peptide analogue as a targeting moiety to the PEG end of siRNA-SS-PEG (PEG, 3400 Da) conjugate, followed by mixing this conjugate with PEI (25 kDa). LHRH- modified PIC micelles containing 50 nM siRNA reduced VEGF expression by 63%, significantly better than unmodified siRNA-PEG/PEI that reduced VEGF expression by 50% at similar dose. In contrast, in SK-OV3 cells that are LHRH receptor negative, the same level of VEGF expression was observed after treatment with LHRH modified and unmodified PIC micelles containing VEGF siRNA [149].

The same group prepared PIC micelles by conjugating siRNA to PEG via disulfide linkage and further condensing it with cationic fusogenic peptide (KALA). KALA is an amphipathic 30 amino acid peptide undergoing conformational change from pH 5.0 to 7.5, resulting in endosomal membrane disruption [150]. siRNA-PEG/KALA micelles were used for down-regulation of VEGF in PC-3 cells making comparisons with siRNA-PEG micelles that used PEI or PLL as siRNA condensing agents. Overall, at optimum N/P (nitrogen to phosphate) ratios, siRNA-PEG/PEI micelles exhibited better VEGF down-regulation compared to siRNA-PEG/KALA and siRNA-PEG/PLL micelles, but were also more toxic than the latter two delivery systems. The authors suggested the use of KALA (instead of PEI used in a previous paper, ref [130]) as a less toxic and effective fusogenic peptide for siRNA condensation and delivery [151].

In general, PEG-siRNA micelles prepared through condensation of PEG-siRNA conjugates with a polycation (e.g., PLL, PEI or KALA) were shown to be more effective siRNA delivery agents than PEG-siRNA conjugates alone. It is, however, unclear whether this increase in siRNA transfection by PIC micelles is merely due to better uptake of siRNA by cells and/or better protection of siRNA by the micellar carrier compared to the PEG-siRNA conjugates against degradation. The following issues; however, may reduce the enthusiasm over application of PEG-siRNA conjugates for effective *in vivo* gene silencing activity. First, effective down-regulation of targeted proteins by PIC micelles, has generally been achieved at relatively high siRNA concentrations (~100 nM). This may enhance the chance of off-target effects by siRNA. Although, incorporation of cell targeting ligands as well as fusogenic peptides is shown to partially compensate for this shortcoming. Second, the use of this approach for siRNA delivery necessitates the synthesis of PEG-siRNA for individual siRNAs targeting expression of specific genes. This can restrict the usefulness of the project in large scale applications. Despite extensive *in vitro* studies reflecting a potential for polymeric micellar delivery systems based on PEG-siRNA conjugates, reported data on their *in vivo* efficiency is still limited.

**Table 1.4.** Polymeric micelles containing PEG-siRNA.

Carrier composition	Targeted gene	Down-regulation of gene compared to control	Dose of siRNA	Efficacy following <i>in vivo</i> study	Reference
PEG-SS-siRNA/PEI	VEGF	~96%	100 nM	NR	Kim et al.[112]
PEG-SS-siRNA/PEI	VEGF	~75% after intratumoral inj., ~86% after intravenous inj.	Multiple Intratumoral inj. 500 pmol/ Multiple intravenous inj.1.5 nmol	Significant inhibition of tumor growth compared to no treatment	Kim et al.[130]
LHRH-PEG-SS-siRNA/PEI	VEGF	~63%	50 nM	NR	Kim et al.[149]
PEG-SS-siRNA/PEI/KALA	VEGF	~90%	200 pmol/ml	NR	Lee et al.[151]
PEG-SS-siRNA/PEI	VEGF	~50%	200 pmol	NR	Al-Abd et al.[152]
6PEG-siRNA-Hph1/KALA	GFP	~69%	75 pmol	NR	Choi et al.[153]
Lactose-PEG-siRNA/PLL	luciferase	~70% ~60%	100 nM 10nM	NR	Oishi et al.[154]

PEG, Polyethylene glycol; PEI, Polyethyleneimine; VEGF, vascular endothelial growth factor; LHRH, luteinizing hormone-releasing hormone; GFP, Green fluorescent protein; 6PEG-siRNA-Hph1, siRNA conjugated to a six-arm polyethylene, glycol (PEG) functionalized with a cell penetrating peptide, Hph1; PLL, poly-L-lysine; Inj., Injection; NR, not reported

#### **1.4.1.2.2. Polymeric micelles based on block copolymer/siRNA complexes**

Among polycationic polymers, PEI and PLL have been extensively used in siRNA delivery formulations *in vitro* and *in vivo* [155][156]. The toxicity caused by nonspecific interactions attributed to the cationic charges has been a hurdle for their clinical use. To prevent non-specific interactions, PEGylation of PLL and PEI has been widely investigated (**Table 1.5**) [157-160]. Chemical modifications of PEI and PLL with cell/tissue-specific ligands were also explored to increase specificity and efficacy for *in vivo* delivery [161].

##### **1.4.1.2.2.1. PEG-PEI**

PEG-PEI copolymers at different PEG chain length and PEG density have been tried in several studies for siRNA delivery [162-164]. In general PEG substitution on PEI (at relatively higher PEG lengths and low density) is a worthwhile strategy to improve the stability of complexes against siRNA degradation [159, 162]. Lower liver uptake for PEGylated PEI upon systemic intravenous administration has also been observed [165] .

Lipid modification of PEG-PEI for complexation of siRNA has been pursued by Beyerle et al. who investigated the *in vivo* efficacy and lung toxicity of lipid modified PEG-PEI complexes for siRNA in mice after intratracheal administration. Their test group consisted of low molecular weight PEI (8.3 kDa) with a fatty acid modification, i.e., a mixture of palmityl (C16)/stearyl (C18) modified with 1.4 kDa PEG [PEI8.3(C16-C18-EO25)1.4]. The control polymer was composed of 25 kDa PEI grafted with hydrophilic 2 kDa PEG (1:1 ratio). The hydrophilic PEG modification reduced the

cytotoxicity but increased the immune response and caused pro-inflammatory effects. Increased levels of IgM in broncho-alveolar fluid (BALF) have been observed with PEG-PEI. The PEI<sub>8.3</sub>(C16-C18-EO<sub>25</sub>)<sub>1.4</sub> exhibited acute proinflammatory effects as well. Although an EGFP knockdown of 75, 66 and 69 % was achieved for PEG-PEI, 8.3kDa PEI and PEI<sub>8.3</sub>(C16-C18-EO<sub>25</sub>)<sub>1.4</sub>, respectively, these polyplexes also caused a non-specific knockdown of EGFP with non-specific siRNA against luciferase (GL3) [166].

Second generation of PEG-PEI polyplexes containing targeting ligands on the PEG end has also been developed and studied for siRNA delivery. In this context, prostate cancer-binding peptide (PCP) was conjugated to PEI via a PEG linker (PEI-PEG-PCP) for VEGF gene silencing in PC3 cells. In the absence of serum, the highest VEGF silencing effect was achieved by siRNA/PEI polyplexes, exhibiting 83% down-regulation. PEI-PEG-PCP/siRNA and PEI-PEG/siRNA exhibited 79 and 60% down-regulation under serum free condition, respectively. In the presence of serum, the highest down-regulation of VEGF was achieved with PEI-PEG-PCP/siRNA showing 68% silencing followed by PEI/siRNA and PEI-PEG/siRNA with 51 and 48% gene silencing, respectively [167].

Using a PEI-graft-PEG-folate (PEI-PEG-FOL) polymer, Kim et al. compared the silencing abilities of an ODN, siRNA, and siRNA expressing plasmid. Target specific inhibition of GFP expression was measured for the complexes in folate receptor overexpressing KB cells. At a siRNA dose of 0.5 µg, PEI-PEG-FOL complexes of siRNA exhibited highest level of GFP down-regulation (75% down-regulation at an N/P

ratio of 16). PEI-PEG-FOL complexes with 2  $\mu\text{g}$  ODN and 2  $\mu\text{g}$  plasmid siRNA reduced GFP expression by 69% and 59%, respectively. These results indicated the superiority of PEI-PEG-FOL over PEI complexes. However, mechanistic studies as well as comparisons between targeted and non-targeted PEI-PEG siRNA complexes that can shed light on the reason behind this observation were missing [168].

In general, different studies points to a positive impact for PEGylation of PEI in siRNA delivery. The final outcome; however, will extremely be dependent on the density and length of conjugated PEG as well as PEI architecture and N/P ratio in the PEG-PEI/siRNA complex. The protective effect of PEG-PEI seems to compensate for the negative impact of PEG on the condensation of siRNA and its cellular uptake by PEI complexes. Systematic studies are required to achieve optimized PEG/PEI based delivery systems of siRNA for maximum effect as well as minimum toxicity for *in vivo* use.

#### **1.4.1.2.2.2. PEG-PLL**

Similar to PEI, PLL have been the subject of extensive studies for siRNA delivery (**Figure 1.9**). PLL based carriers may be advantageous over PEI because of better biocompatibility and biodegradability profile. Similar to observations with PEI, PEGylation of PLL have produced positive impact on transfection efficiency of complexed siRNA perhaps by providing a better siRNA protection [169].

Sato et al. synthesized a series of cationic comb-type copolymers (CCCs) with a PLL backbone and PEG side chains at different densities. Cationic comb-type copolymers with higher density of PEG chains exhibited stronger interaction with siRNA

than the one with lower density. *In vivo* stability for CCC/siRNA complexes was evaluated in mice as well. Both naked siRNA and jet PEI/siRNA injected to mice disappeared at 5 min after injection. In contrast, CCC/siRNA complex with long cationic backbone and higher PEG content retained the siRNA in bloodstream by  $\geq 100$ -fold [170]. Interestingly, the half-life of siRNA upon preinjection of CCC was increased by more than 60 fold compared to siRNA alone, but this increase did not reach the level achieved by CCC/siRNA complexes.

PIC micelles were prepared from iminothiolane-modified PEG-*b*-PLL [PEG-*b*-(PLL-IM)] where the mercaptopropyl groups were used to prepare disulfide cross-linked micelles. The presence of both disulfide cross-links and amidine groups was suggested to increase the stability of the micelles. These PIC micelles exhibited good stability at physiological salt conditions contributing to the protection of micellar structure compared to PEG-*b*-PLL/siRNA system. Dose dependent siRNA transfection efficiencies were evaluated in Huh7 cells; at a dose of 100 nM siRNA concentration, PIC micelles exhibited 80% down-regulation of luciferase while the non-cross-linked PIC assemblies with PEG-*b*-PLL exhibited 20% silencing [171]. The superior transfection efficiency of PIC micelles was attributed to the efficient protection of incorporated siRNA by the cross linked micellar structure.

**Table 1.5.** Polymeric micelles based on PEG-PEI or PEG-PLL complexed siRNA.

Carrier composition	Targeted gene	Down-regulation of gene compared to control	Dose of siRNA	<i>In vivo</i> study	References
PEI-PEG	$\beta$ -galactosidase	~70%	50 pmol	NR	Mao et al.[162]
PEG-PEI	EGFP	~42% ( <i>in vivo</i> )	50 $\mu$ g	intratracheal instillation	Merkel et al.[159]
PEI-g-PEG	sCLU	~60%	400 pmol	NR	Sutton et al.[163]
PEG-PEI	CD44v6	~60%	20 pM	NR	Wu et al.[164]
PEG-PEI	EGFP	~75% ( <i>in vivo</i> )	35 $\mu$ g	Intratracheal instillation	Beyerle et al.[166]
PEI8.3(C16-C18-EO25)1.4	EGFP	~69% ( <i>in vivo</i> )	35 $\mu$ g	Intratracheal instillation	Beyerle et al.[166]
CS-g-(PEI- <i>b</i> -mPEG)	IKK $\beta$	~40%	50 nM	NR	Duan et al.[172]
PEG-PEI	VEGF	68%	50 nM	NR	Kim et al.[167]
PEI-PEG-PCP	VEGF	79%	50 nM	NR	Kim et al.[167]

Carrier composition	Targeted gene	Down-regulation of gene compared to control	Dose of siRNA	<i>In vivo</i> study	References
PEI-PEG-FOL	GFP	~75%	0.5 µg	NR	Kim et al.[168]
PLL/PEG/DMMAn-Mel/	Luciferase	~90%	500 ng	NR	Meyer et al.[169]
PEI/PEG/DMMAn-Mel	Luciferase	~60%	500 ng	NR	Meyer et al.[169]
PLL-g-PEG	NR	NR	NR	Increase in siRNA half life upon Intravenous inj.	Sato et al.[170]
PEG- <i>b</i> -(PLL-IM)	Pp-Luc	~80%	100 nM	NR	Matsumoto et al.[171]

PEI-PEG-FOL, PEI-poly(ethylene glycol)-folate; GFP, Green fluorescent protein; EGFP, Enhanced green fluorescent protein; PEI8.3(C16-C18-EO25)1.4, low molecular weight PEI 8.3 kDa with a fatty acid modification, namely palmityl-stearyl-(C16-C18-) modified hydrophobic PEG; CS-g-(PEI-*b*-mPEG), linear poly(ethyleneimine) blocked with polyethylene glycol and grafted onto a chitosan; IKK $\beta$ , I $\kappa$ B kinase subunit  $\beta$ ; PEI-PEG-PCP, Prostate cancer-binding peptide (PCP) conjugated with polyethylenimine (PEI) via a poly(ethylene glycol); VEGF, vascular endothelial growth factor; sCLU, signalling peptide of secretory clusterin; PLL, Polylysine; DMMAn, dimethylmaleic anhydride; Mel, melittin; PLL-g-PEG, poly(L-lysine)-graft-poly(ethylene glycol); PEG-*b*-(PLL-IM), iminothiolane-modified poly(ethylene glycol)-*block*-poly(L-lysine); Pp-Luc, Photinus pyralis luciferase; NR, not reported.

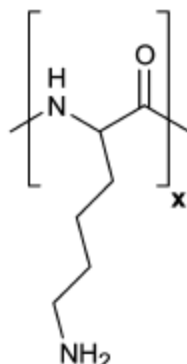


**Figure 1.9.** Chemical structure of Poly-L-lysine (PLL).

#### **1.4.1.2.2.3. Polymeric micelles based on other polycationic copolymers for siRNA complexation**

Despite development of several systems based on PEG modified PEI and PLL, the non-specific toxicity, immunogenicity, long term biocompatibility and safety of these transfection agents for *in vivo* use, is still under question. Development of siRNA transfecting agents with degradable backbone can't only enhance the safety of these agents but may help release of siRNA from the polymer upon entry to endosomal compartment. This can in turn facilitate the delivery of siRNA to its intracellular site of action, i.e., cytoplasm.

In this context, Sun et al. synthesized an amphiphilic triblock copolymer consisting of monomethoxy PEG, PCL and poly(2-aminoethyl ethylene phosphate) denoted as mPEG-*b*-PCL-*b*-PPEEA and used it for siRNA delivery. The micellar structures exhibited prolonged stability when incubated with bovine serum albumin due

to PEG segment preventing particle aggregation. Fluorescent microscope images indicated partial internalization of micelles, followed by the dissociation of internalized micelles in the cytoplasm and release of siRNA. This was attributed to the deprotonation polyphosphoester block in cytoplasm leading to siRNA release. Delivery of siRNA at 150 nM and N/P ratio of 50:1 significantly inhibited GFP expression (by 70%) in HEK293 cells. This level of gene silencing was similar to that by Lipofectamine 2000™ delivery at 20 nM siRNA. Interestingly, the micelles at N/P ratio of 100:1 exhibited  $\geq 90\%$  silencing that surpassed what observed with Lipofectamine 2000™. The advantage of this triblock copolymer based delivery system was its superior cytocompatibility compared to lipofectamine 2000™ rendering it useful for siRNA delivery [173].

Zhu et al. prepared cationic micelles from dimethylaminoethyl methacrylate-PCL-dimethylaminoethyl methacrylate (PDMAEMA-PCL-PDMAEMA) triblock copolymers for simultaneous delivery of siRNA and paclitaxel. PDMAEMA-PCL-PDMAEMA micelles, particularly those with lower PDMAEMA molecular weights, exhibited lower toxicity compared to PEI 25 kDa. Micelles containing the shortest PDMAEMA chains (2.7 kDa), showed the highest transfection efficiency reducing GFP expression up to 70% at siRNA dose of 0.5  $\mu\text{g/mL}$ , compared to PEI which only inhibited GFP expression by 40%. PDMAEMA homopolymer did not show any silencing efficiency. Co-delivery of VEGF siRNA and PTX in PC-3 cells caused 85% silencing efficiency. This level of silencing was higher than that of micelle/VEGF siRNA alone which reduced the gene silencing by 70%. The effect of combination therapy on the *in vitro/in vivo* cell viability

was not reported. Nevertheless the results showed a potential in combination cancer therapy with siRNA and chemotherapeutic drug [174].

Our research group derivatized the biodegradable PEG-*b*-PCL with polyamine side chains spermine (SP), tetraethylenepentamine (TP) and N,N-dimethyldipropylenetriamine (DP) for siRNA delivery (**Figure 1.2**). These polymers were able to effectively bind siRNA, self-assemble into micelles, protect siRNA from degradation by nuclease and release complexed siRNA efficiently in the presence of low concentrations of anionic heparin. siRNA formulated in PEO-*b*-P(CL-g-SP) and PEO-*b*-P(CL-g-TP) micelles showed efficient cellular uptake through endocytosis by drug resistant MDA435/LCC6/MDR cells which over-express *mdr-1* gene encoding for P-gp. P-gp is most abundant protein pump involved in ATP dependent efflux of chemotherapeutic drugs in cancer [175, 176]. PEO-*b*-P(CL-g-TP) and PEO-*b*-P(CL-g-SP)/MDR-1 siRNA complex micelles were able to down-regulate the P-gp expression up to 60 and 50 %, respectively, at a dose of 300 nM. This is a relatively high dose, consistent with the intended use of these micelles (i.e., systemic application) [43].

In continuation of this study, PEO-*b*-PCL micelles containing polyamines in their core were decorated with integrin  $\alpha\beta3$  targeting peptide (RGD4C) and/or cell penetrating peptide (TAT) on the PEO shell. An increase in cellular uptake and effective endosomal escape of delivered siRNA has been observed with RGD/TAT micelles compared to unmodified micelles in MDA435/LCC6/MDR cells. RGD/TAT micelles caused a 70% decrease in MDR-1 mRNA expression and a 55% reduction of P-gp

protein levels at a dose of 100 nM siRNA. A 3-fold lower dose of siRNA was required by the RGD/TAT modified micelles compared to unmodified ones to cause similar level of P-gp down-regulation. As a result of P-gp down-regulation by RGD/TAT micelles delivering MDR-1 siRNA, a 2-fold increase in the intracellular levels of DOX in MDA435/LCC6/MDR cells has been observed compared to unmodified micelles. Assessment of the effect of P-gp silencing on cytotoxicity of DOX showed a 3-fold increase in the cytotoxicity to DOX obtained with RGD/TAT micelles delivering MDR-1 siRNA compared to unmodified micelles [53].

More recently, micelles were prepared from PEO-*b*-P(CL-SP) and a PEO-*b*-PCL block copolymer with pendent DOX attached on PCL backbone through pH sensitive hydrazone linkages PEO-*b*-P(CL-DOX) [177]. The PEO-*b*-P(CL-SP) and PEO-*b*-P(CL-DOX) were partially modified with TAT and RGD4C peptides on the PEO end. The prepared micelles had a versatile core that could stably complex siRNA and conjugate DOX via a pH sensitive linkage, and a virus-like shell for cell specific recognition and efficient cellular uptake. The peptide-functionalized micelles demonstrated significant cellular uptake, pH-triggered DOX release, improved DOX penetration into nuclei and enhanced DOX cytotoxicity in the DOX resistant MDA-MB-435/MDR cells when compared to unmodified micelles. Incorporation of fluorescent probes in the micellar core through covalent linkages, allowed for *in vivo* tracking of micelles providing evidence for tumor targeted delivery of RGD decorated micelles and incorporated siRNA in animal models following intravenous administration of this system.

**Table 1.6.** Polymeric micelles based on other polycationic copolymers for siRNA complexation.

Carrier composition	Targeted gene	Down-regulation of gene compared to control	Dose of siRNA	<i>In vivo</i> study	References
FA-PEG-PGA/PEI-PCL	BCL-2	~90%	20 nM	NR	Cao et al.[178]
mPEG-b-PCL-b-PPEEA	GFP	~70%	150 nmol/L	NR	Sun et al.[173]
PDMAEMA-PCL-PDMAEMA	GFP, VEGF	~70% for GFP and ~85% VEGF	0.5 µg/mL	NR	Zhu et al.[174]
PEO-b-PCL-SP	P-gp	~50%	300 nM	NR	Xiong et al.[43]
RGD4C/TAT decorated PEO-b-PCL-SP	P-gp	~55%	100 nM	NR	Xiong et al.[53]
pDMAEMA-b- pDbB/pSMA	Plk1	~60%	50 nM	NR	Benoit et al.[179]
PAMAM/PEG-b-P(PrMA-co-MAA)	BCL-2	60%	25 nM	NR	Elsabahy et al.[180]
PEG-b-P(PrMA-co-MAA)/PAMAM	BCL-2	~60%	50 nM	NR	Felber et al.[181]
PMAA-b-PEG/PLL	EGFP	Qualitative down-regulation was observed	2.5 nM	NR	Boudier et al.[182]

Carrier composition	Targeted gene	Down-regulation of gene compared to control	Dose of siRNA	<i>In vivo</i> study	References
poly[(DMAEMA)- <i>b</i> -(BMA)- <i>co</i> -(DMAEMA)- <i>co</i> -(PAA)]	GAPDH	~90%	100 nM	NR	Convertine et al.[183]
PAsp(-SS-siRNA)/ PAsp(DET)	Luciferase	~80%	100 nM	NR	Takemoto et al.[184]
siRNA-SS-PE/ PEG-PE	GFP	~28%	84 nM	NR	Musacchio et al.[185]

FA-PEG-PGA, Folic acid-poly(ethylene glycol)-block-poly(glutamic acid); PEI-PCL, poly( $\epsilon$ -caprolactone) (PCL) and linear poly(ethylene imine); mPEG-b-PCL-b-PPEEA, Monomethoxy poly(ethylene glycol)-b-poly( $\epsilon$ -caprolactone) and poly(2-aminoethyl ethylene phosphate); PDMAEMA-PCL-PDMAEMA, 2-(N,N-dimethylaminoethyl) methacrylate-poly caprolactone-2-(N,N-dimethylaminoethyl) methacrylate; P-gp, P-glycoprotein; PEO-b-PCL, poly(ethylene oxide)-block-poly( $\epsilon$ -caprolactone); SP, spermine; TP, tetraethylenepentamine; DP, N,N-dimethyldipropylenetriamine; PIC, polyion complex; pDMAEMA, dimethylaminoethyl methacrylate; pDbB, butyl methacrylate; pSMA, poly(styrene-*alt*-maleic anhydride); plk1, polo-like kinase 1; PEG-b-P(PrMA-co-MAA), Poly(ethylene glycol)-b-poly(propyl methacrylate-co-methacrylic acid); PAMAM, poly(amido amine); PMAA-b-POE, polymethacrylic acid-*b*-polyethylene oxide; polyDMAEMA, poly(*N,N*-dimethylaminoethyl methacrylate); BMA, butyl methacrylate; PAA, propylacrylic acid; GADPH, glyceraldehydes phosphate dehydrogenase; PAsp, poly(aspartic acid); PAsp(DET), poly(aspartamide) having 1,2-diaminoethane side chains; PE, Phosphothioethanol; NR, not reported.

#### **1.4.2. siRNA therapeutics in clinical trials**

Although the clinical usage of RNAi has not yet been realized, several clinical trials are under way which may provide prospects for success. Administrations of most siRNAs in clinical trials are by local delivery such as intravitreal or intranasal routes, although several ongoing trials involve the use of delivery agents. siRNA therapeutics have been examined in a variety of diseases including in retinal degeneration, dominantly inherited brain and skin diseases, viral infections, respiratory disorders, cancer and metabolic diseases (**Table 1.7**). Silence Therapeutics has developed Atu027 siRNA delivery system which is derived from a cationic, a neutral and a PEGylated lipid, where a siRNA against protein kinase N3 was incorporated onto the liposome shell by ionic interaction [118]. A Phase I study evaluated the safety, tolerability and pharmacokinetics of Atu027 in patients with colorectal cancer metastasizing to the liver reported preliminary data that showed disease stabilization and other indications of potential efficacy in cancer patients with advanced solid tumors. In another study, Calando Pharmaceuticals developed the first targeted delivery system for siRNA. It consists of four components: a double-stranded siRNA, a cyclodextrin-containing polycation, a PEG-based stabilizing agent, and transferrin capable of binding to transferrin receptor of tumor cells. CALAA-01 was used to deliver siRNA against ribonucleotide reductase subunit M2 (RRM2) in Phase I clinical trials. It was shown that the supramolecular siRNA complexes decreased the target gene expression and provided transient inhibition of tumor growth [133, 186, 187]. The National Cancer Institute conducted a study to test the safety and effectiveness of TKM-080301 for cancer in the liver. They used lipid

nanoparticles containing siRNA against the Polo-like kinase 1 gene. The study results have not been posted yet [188, 189]. In summary, the area of RNA therapeutics has made significant progress in potent and specific silencing of broad range of genetic targets. However, delivery remains the most significant hurdle in advancement of RNAi therapeutics for use in clinical settings. Therefore, future work must focus on development of safe and effective delivery vehicles needed to guarantee broad application of this ground-breaking technology.

**Table 1.7.** Clinical trials for RNAi therapy (Adopted from reference [190] with permission and updated from www.clinicaltrial.gov).

<b>Clinical setting</b>	<b>Drug</b>	<b>Indication(s)</b>	<b>Target(s)</b>	<b>Sponsor</b>	<b>Status</b>
Ocular and retinal disorder	TD101	Pachyonychia congenita	Keratin 6A N171K mutant	Pachyonychia Congenita Project	Completed, Phase I
	QPI-1007	Non-arteritic anterior ischaemic optic neuropathy	Caspase 2	Quark Pharm., Inc.	Active, Phase I
	AGN211745	Age-related macular degeneration; choroidal neovascularization	VEGFR1	Sirna Therapeutics, Inc.	Completed, Phase I, II
	PF-655	Diabetic macular oedema (DME); age-related macular degeneration (AMD)	RTP801	Quark Pharm., Inc.	Active, Phase I
	SYL040012	Glaucoma	$\beta$ 2 adrenergic receptor	Sylentis	Active, Phase I, II
	Bevasiranib	Diabetic macular oedema	VEGF	Opko Health, Inc.	Completed, Phase II

	<b>Drug</b>	<b>Indication(s)</b>	<b>Target(s)</b>	<b>Sponsor</b>	<b>Status</b>
Ocular and retinal disorder	Bevasiranib	Macular degeneration	VEGF	Opko Health, Inc.	Completed, Phase II
Cancer	siRNA-EphA2-DOPC	Advanced, recurrent cancer	EphA2	M.D. Anderson Cancer Center	Active, Phase I
	siG12D LODER	Adenocarcinoma of the pancreas	-	Silenseed Ltd	Active, Phase I
	TKM 080301	Colorectal, Pancreas, Gastric, Breast, Ovarian and Esophageal Cancers	PLK1	<u>National Cancer Institute (NCI)</u>	Completed, Phase I
	CEQ508	Familial adenomatous polyposis	$\beta$ -catenin	MDRNA, Inc.	Active, Phase I
	ALN-PLK1	Liver tumours	PLK1	Alnyam Pharm	Active, Phase I
	FANG	Solid tumours	Furin	Gradalis, Inc.	Active, Phase II
	SPC2996	Chronic myeloid leukemia	BCL-2	Santaris Pharm.	Ongoing, Phase I, II

	<b>Drug</b>	<b>Indication(s)</b>	<b>Target(s)</b>	<b>Sponsor</b>	<b>Status</b>
Cancer	ALN-VSP02	Solid tumours	VEGF, kinesin	Alnylam Pharm.	Active, Phase I
	NCT00672542	Metastatic melanoma	LMP2, LMP7, and MECL1	Duke University	Active, Phase I
	Atu027	Advanced, recurrent or metastatic solid malignancies	PKN3	Silence Therapeutics	Active, Phase I
Kidney disorders	QPI-1002/I5NP	Acute kidney injury	p53	Quark Pharm., Inc.	Terminated, Phase I
	QPI-1002/I5NP	Delayed graft function kidney transplant	p53	Quark Pharm., Inc.	Active, Phase I, II
	QPI-1002/I5NP	Kidney injury acute renal failure	p53	Quark Pharm., Inc.	Completed, Phase I
LDL lowering	TKM-ApoB	Hypercholesterolaemia	APOB	Tekmira Pharm. Corp.	Terminated, Phase I
	PRO-040,201	Hypercholesterolaemia	APOB	Tekmira Pharm. Corp.	Terminated, Phase I
Antiviral	SPC3649	Hepatitis C virus	miR-122	Santaris Pharm	Active, Phase II

	<b>Drug</b>	<b>Indication(s)</b>	<b>Target(s)</b>	<b>Sponsor</b>	<b>Status</b>
Antiviral	pHIV7-shI-TAR-CR5RZ	HIV	HIV Tat protein, HIV TAR RNA	City of Hope Medical Center/Benitec	Active, Phase 0
	ALN-RSV01	RSV in volunteers	RSV nucleocapsid	Alnylam Pharm.	Completed, Phase II
	ALN-RSV01	RSV in lung transplant patients	RSV nucleocapsid	Alnylam Pharm.	Completed, Phase I
	ALN-RSV01	RSV in lung transplant patients	RSV nucleocapsid	Alnylam Pharm.	Active, Phase II

APOB, apolipoprotein B; BCL-2, B-cell CLL/lymphoma 2; CCR5, C-C chemokine receptor type 5; LDL, low-density lipoprotein; LMP2, also known as proteasome subunit beta type 9 (PSMB9); LMP7, also known as proteasome subunit beta type 8 (PSMB8); MECL1, also known as proteasome subunit beta type 10 (PSMB10); Pharm., Pharmaceuticals; PKN3, protein kinase N3; PLK1, polo-like kinase 1; RRM2, ribonucleoside-diphosphate reductase subunit M2; RSV, respiratory syncytial virus; RTP801, also known as DNA damage-inducible transcript 4 protein (DDIT4); VEGF, vascular endothelial growth factor.

### **1.5. Signal transducer and activator of transcription 3 (STAT3) as a target in oncogene silencing: the relevance to cancer therapy**

STAT proteins have dual role as signal transducers and activators of transcription. They are activated by phosphorylation in response to extracellular signaling proteins (e.g. cytokines, growth factors and hormones) that bind to specific cell surface receptors [191]. The activated STATs dimerize, accumulate in the nucleus in which they interact with consensus promoter sequences and bind DNA to drive transcription (**Figure 1.10**) [192, 193]. STAT proteins were initially identified by studies on induction of transcription by interferon signaling molecules [194]. Following this discovery, seven mammalian STAT genes have been identified in three chromosomal clusters, STAT1 to STAT4, closely related STAT5a and STAT5b and STAT6 [195]. STATs 1, 3, 4, 5a are between 750 and 795 amino acids long, whereas STATs 2 and 6 are about 850 amino acids long. All members of STAT family have distinct structural domains, including the N-terminal, coiled-coil, DNA binding, SH2 and a carboxyl terminus transactivation domains (TAD) [196]. There are four-stranded helical coiled coil regions of STAT proteins presenting opportunities for protein-protein interactions [192]. The DNA-binding fold located between residues 320 and 490 can bind to both major and minor grooves of DNA. The SH2 domain extends between residues 580 to 680 and functions in binding phosphotyrosine, having a role in associating with receptor-kinase complex [197]. It is followed by a tyrosine residue in the region of residue 700 which becomes phosphorylated upon activation [198]. The amino-terminal region of the STAT family is highly conserved and is involved in dimer-dimer interactions leading to DNA binding

[199]. Formation of tetramer greatly induces STAT-DNA interaction [200]. The physiological function of individual STAT proteins has been investigated using anti-sense molecules or dominant negative STAT protein encoding constructs, performed in cell lines or knockout mice lacking specific STATs [201]. These studies indicate that STAT3 plays an important role in a variety of biological functions including cell cycle progression, suppression and induction of apoptosis and cell motility in different tissues (**Table 1.8**) [202]. STAT3 has a potential role in involution as well. However, its function has been complex to identify from knockout mice studies because of embryonic lethality prior to gastrulation [203].

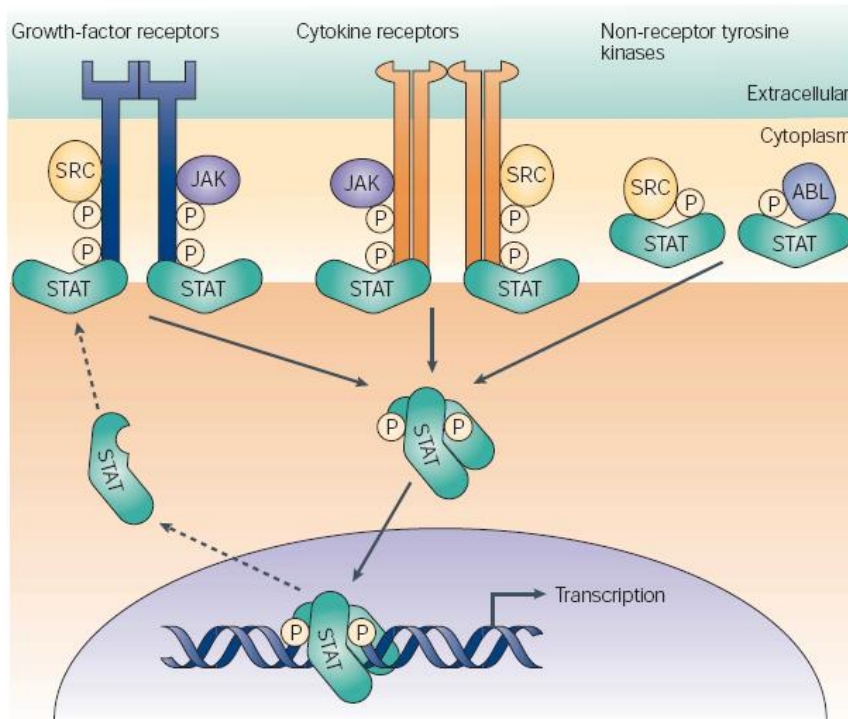


**Figure 1.10.** Signaling pathways that converge on STATs (adopted from reference [201] with permission). STATs are an important point of convergence for many signaling pathways. Binding of growth factors or cytokines to their receptors result in the activation of intrinsic receptor tyrosine kinase activity or of receptor-associated kinases, such as the Janus kinase (JAK) or SRC tyrosine kinases. These tyrosine kinases subsequently phosphorylate the cytoplasmic tails of the receptor to provide docking sites for the recruitment of monomeric STATs. Once they have been recruited, STATs themselves become substrates for tyrosine phosphorylation. Non-receptor tyrosine kinases, such as the oncoproteins SRC and BCR–ABL (a fusion of the breakpoint-cluster region (BCR) and Abelson leukemia (ABL) proteins), can phosphorylate STATs independently of receptor engagement. Phosphorylated STATs dimerize and translocate to the nucleus, where the dimers directly regulate gene expression. Dashed arrows indicate the ‘recycling’ of STAT proteins from the nucleus to the cytoplasm.

**Table 1.8.** Role of STAT3 in biological functions.

<b>Target tissue</b>	<b>Role of STAT3</b>	<b>Cells/animal model studied</b>	<b>Upstream signaling</b>	<b>Downstream signaling</b>	<b>Ref.</b>
Mammary epithelium	Apoptosis and involution	STAT3 null mice, BLG-Cre transgenic mice	N/D	IGFBP-5, p53, p21	[204]
Mammary gland	Apoptosis and involution	LIF Null mice, KIM-2 mammary epithelial cells	LIF	ERK1/2 IGFBP-5, p53, p21	[205]
Mammary epithelium	involution	STAT3 null mice, WAP-Cre transgenic mice	N/D	proteases	[206]
T-Cell	Prevention of apoptosis	STAT3 null mice, T-cell specific	IL-6	N/D	[207]
Macrophages and neutrophils	Suppression of activity	STAT3 null mice, macrophage and neutrophils specific	IL-10	TNF $\alpha$ , IL-1, IL-6 and IL-12	[208]
Heart	Cardiomyogenesis, expression of cardiac specific genes	Murine embryonic stem cells	JAK2	NKx2.5, DHP and cardiac actin	[209]
Heart	Regulation of inflammatory response	STAT3 null mice, cardiac restricted	gp130	TNF $\alpha$	[210]

<b>Target tissue</b>	<b>Role of STAT3</b>	<b>Cells/animal model studied</b>	<b>Upstream signaling</b>	<b>Downstream signaling</b>	<b>Ref.</b>
Skin	Migration and wound healing	STAT3 null mice, keratinocyte specific	EGF, HGF and IL-6	p130 <sup>cas</sup>	[211]
Liver	Acute phase response	STAT3 null mice, Cre mediated deletion	IL-6	Acute phase genes	[212]

### **1.5.1. STAT3 as an oncoprotein**

STAT3 is constitutively activated in variety of cancers including breast, head and neck, melanoma, ovarian, lung, pancreatic, prostate cancers as well as hematologic tumors [201]. Overactive kinases, dysfunctional receptors, loss of proteins that negatively regulate STAT3 (PIAS) and loss of suppressors of cytokine signaling (SOCS) are the major reasons of STAT3 over-activation in tumor cells [213]. As discussed previously, STAT3 is involved in controlling variety of fundamental biological processes; including cell proliferation, apoptosis, angiogenesis and immune regulation; hence its persistence activation in tumor cells should have an intense biological effect.

### **1.5.2. Tumor cell proliferation and apoptosis**

Different studies linked constitutive activation of STAT3 to proliferation of tumor cells. Alterations in a number of STAT3 target genes including those encoding for cyclin D1 and c-Myc are identified and are known to be up-regulated during tumor cell proliferation [214, 215]. Possible connection between STAT3 and cyclin D1 over-expression has been established both in rodent fibroblast cell line [216], and human ovarian carcinoma cell line [217]. Masuda et al. examined the effect of STAT3 on cyclin D1 expression and cell proliferation in YCU-H891 head and neck squamous cell carcinoma (HNSCC) cell line that display constitutive activation of STAT3. They concluded that over-expression of cyclin D1 contributes to malignancy through activation of EGFR-STAT3 pathway [218]. Kiuchi et al. showed that activation of c-Myc gene in murine proB cell line upon stimulation of IL-6 receptor or gp130 is mediated through STAT3. STAT3 activated the

c-Myc gene promoter by binding to a site overlapping with c-Myc E2F site [219]. Bowman et al. investigated the function of STAT3 in c-Myc expression in NIH3T3 fibroblast cells transformed by v-Src or stimulated with PDGF. They concluded that STAT3 participated in c-Myc induction and it is required for cell cycle progression from G1 to S phase [220].

Evidence indicates that constitutive STAT3 activation contributes to oncogenesis by preventing apoptosis. STAT3 signaling supplies malignancy by preventing apoptosis through increased expression of BCL-X<sub>L</sub>, a member of BCL-2 family [221]. Grandis et al. inhibited STAT3 activation by intratumoral injection of STAT3 antisense plasmid. They observed an increased tumor cell apoptosis and decreased BCL-X<sub>L</sub> expression in a head and neck xenograft model [222]. Niu et al. showed that disrupting STAT3 signaling with either tyrosine kinase inhibitors or dominant negative STAT3 proteins resulted in down-regulating the expression of both BCL-X<sub>L</sub> and MCL-1 leading to apoptosis in melanoma cell lines. They concluded that STAT3 signaling has a critical role in melanoma survival and malignant progression. By targeting constitutively active STAT3 in melanoma cell line, they could induce growth inhibition and apoptosis.[223] Aoki et al. found that STAT3 inhibition increased a selective down-regulation of expression of survivin, another member of BCL-2 family, in AIDS-defining primary effusion lymphoma (PEL) cells [224]. These results suggest that by inhibition of apoptosis, constitutively active STAT3 can cause massive cell survival and contribute to tumorigenesis.

### **1.5.3. Tumor angiogenesis**

Most tumors are not able to maintain their growth unless they are supplied with oxygen and nutrients [201]. Constitutive activation of STAT3 contributes to tumorigenesis by up-regulating VEGF expression. This in turn increases angiogenesis in tumors [225]. Niu et al. showed that constitutively active STAT3 is capable of activating VEGF expression and angiogenesis stimulation. Activated mutant STAT3 (STAT3C) induced VEGF up-regulation, was inhibited when STAT3 binding site in the VEGF promoter was mutated. These results provided evidence that VEGF is a direct target gene of STAT3. Furthermore dominant-negative STAT3 protein or STAT3 antisense oligonucleotide blocked STAT3 signaling and caused down-regulation of VEGF expression in tumor cells under study [226]. Chen et al. showed that VEGF could activate endothelial cell p-STAT3 in K1735 tumors. Their results identified STAT3 as a mediator of VEGF-VEGFR2 signaling in angiogenic tumor endothelium [227]. Masuda et al. studied the role of constitutively active STAT3 in HNSCC, on VEGF production and tumor angiogenesis both *in vitro* and clinical samples. They exhibited that STAT3 plays a critical role in VEGF production in HNSCC and at least partially is responsible for tumor invasiveness [228]. Blocking of STAT3 signaling pathway with dominant negative mutant STAT3 has shown to inhibit IL-6 induced up-regulation of VEGF mRNA expression in human cervical cancer cells as well [229].

### **1.5.4. Immune regulation by STAT3 in tumor cells**

In cancer, activated STAT3 has been suggested to be a mediator of inflammation [230]. STAT3 signaling is a major intrinsic pathway in cancer inflammation. It is activated by many inflammatory mediators such as cytokines, chemokines, IL-6 and TNF $\alpha$  that are critical in inducing and maintaining a cancer promoting inflammatory environment [231]. Inflammatory mediators can serve as mitogens and survival factors in tumorigenesis. They also can contribute to the induction of angiogenesis [232]. Groblewska et al. showed an increase in serum levels of IL-6 in colorectal cancer patients, suggesting its role in local inflammation which may lead to colorectal carcinogenesis via adenomatous polyps [233]. Using a mouse model of gastric cancer which carries a mutated gp130 cytokine receptor, Ernst et al. characterized a hyperactivation of STAT3 signaling leading to chronic gastric inflammation and associated tumorigenesis [234]. STAT3 signaling pathway is also crucial in inflammatory conditions caused by repetitive injury and infections which could cause chronic inflammatory response leading to cancer. Bronte-Tinkew et al. showed that persistence infection with *Helicobacter pylori* may lead to development of gastric cancer through activation of STAT3 [235]. Choudhari et al. exhibited that hepatitis B virus can cause hepatocellular carcinoma by activating STAT3 pathway through phosphoinositide-3-kinase and cyclooxygenase-2 [236]. Lipopolysaccharide and live bacteria are also capable of causing inflammation induced cancer through STAT3 activation and production of IL-1 $\beta$  and IL-6 [237].

#### **1.5.5. STAT3 as a target for cancer therapy: an update on development of STAT3 inhibitors**

As discussed above, STAT3 as an oncogene is a crucial player in human cancer development and its direct or indirect inhibition represents a legitimate target for anticancer drug design [238]. It was shown that ablation of STAT3 in multiple hematopoietic elements resulted in immune cell-mediated anticancer response. Inhibiting the STAT3 signal with a small molecule drug induced T-Cell and NK-cell dependent growth inhibition of tumors [239]. Direct targeting of the STAT3 is possible through several strategies including SH2 domain inhibitors [240, 241], dimerization inhibitors [242], DNA binding domain inhibitors [243] and the N-terminal domain inhibitors [244]. Indirectly, it is also possible to target the upstream receptors for STAT3 activation [238]. **Table 1.9** lists some of the agents that are used to target STAT3. However, limitations including stability and permeability have limited the usage of these agents *in vivo*. **Table 1.10** lists some of the STAT3 inhibitors currently in clinical trials.

A more selective and specific approach is to inhibit the STAT3 gene expression using antisense RNA, small interfering RNA (siRNA) and decoy ODN [230]. Huang et al. used plasmid vectors expressing shRNA against STAT3 and studied the effect STAT3 knock-down in CAOV3 ovarian cancer cells. BCL-X<sub>L</sub>, cyclin D1 and c-Myc were down-regulated, whereas cleaved caspase 3 was up-regulated. Decreased tumor cell growth was observed both *in vitro* and *in vivo* [245]. Another study used decoy oligonucleotide to selectively abolish activated STAT3. Leong et al. showed that treatment of head and neck cancer cell with STAT3 decoy inhibited their proliferation and STAT3-mediated gene expression [246]. Liu et al. targeted STAT3 with STAT3 siRNA, a small STAT3 molecule inhibitor LLL12. They demonstrated that targeting of STAT3 signaling could

abolish anti-apoptotic function of IL-6 in human liver cancer cells [247]. Alshamsan et al. used siRNA specific STAT3 for STAT3 knock-down in B16 tumor cells both *in vitro* and *in vivo*. They demonstrated an increase in IL-6 level and caspase 3 activity, accompanied by a decrease in VEGF level and STAT3 activity in tumor cells. The results showed a regression of tumor growth and tumor weight *in vivo* after treatment [141]. **Table 1.11** lists some of the studies which used siRNA for STAT3 inhibition.

**Table 1.9.** Agents used for STAT3 targeting.

<b>Agent</b>	<b>Target site</b>	<b>Mode of STAT3 inhibition</b>	<b>Cell line</b>	<b>Ref.</b>
ISS 610	STAT3 SH2	Dimerziation	NIH3T3/vSrc, MDA-MB-231, MDA-MB-435	[241]
S31-201	STAT3 SH2	Dimerziation	NIH3T3/vSrc, MDA-MB-231, MDA-MB-435	[248]
Stattic	STAT3 SH2	Phosphorylation	MDA-MB-231, MDA-MB-435, HepG2	[249]
CPA-1, CPA-7	STAT3 DBD	DNA binding	NIH3T3/vSrc, MDA-MB-231, MDA-MB-435, CT26	[250]
Peptides	STAT3 ND	Transcriptional activity	MDA-MB-231, MDA-MB-435, MCF-7	[244]
JSI-124	JAK	Phosphotyrosine STAT3 level	NIH3T3/vSrc, MDA-MB-468, NIH3T3/Ras	[251]
STAT3 decoy ODN	STAT3 gene	STAT3 expression	A549	[252]
siRNA	STAT3 mRNA	STAT3 expression	B16	[141]

DBD, DNA binding domain; ND, N-terminal domain; ODN, Decoy oligodeoxynucleotide.

**Table 1.10.** STAT3 inhibitors in clinical trials.

<b>Agent</b>	<b>Trial phase</b>	<b>Indication</b>	<b>Ref.</b>
STA-21	Phase I/II	Psoriasis	[253]
Pyrimethamine	Phase I/II	Chronic lymphocytic leukemia/ small lymphocytic lymphoma	[254]
OPB-31121	Phase I	Advanced solid tumor	[255]
CDDO-Me, RTA 402	Phase I/II Phase II	Pancreatic cancer/ Solid tumors and lymphoid malignancies	[256, 257]

**Table 1.11.** Studies using siRNA for STAT3 inhibition.

<b>Target</b>	<b>Cell line/Animal</b>	<b>Effect</b>	<b>Ref.</b>
STAT3	MDA-MB-231/mice	↓ Bcl-xL, ↓ survivin, Fas mediated intrinsic apoptosis, ↓ tumor growth	[258]
STAT3	Hep2	↓ Bcl-2, ↑ apoptosis	[259]
STAT3	PC3 and LNCaP	Growth suppression and induction of apoptosis	[260]
STAT3	Dendritic cells	DC maturation, ↑ TNF- $\alpha$ secretion, allogenic T cell proliferation	[261]
STAT3	Cutaneous T-cell lymphomas (Hut78)	↑ apoptosis, ↓ Bcl2	[262]
STAT3	B16/Mice	↑ IL-6, ↓ VEGF, ↑ Caspase 3 activity, ↓ Cell viability, ↓ tumor growth	[141]

## **1.6. Research proposal**

### **1.6.1. Rationale**

In previous sections, we provided evidence from literature on the potential of polymeric micellar carriers as means to enhance the delivery of their drug and/or siRNA cargo. However, several difficulties including low drug/siRNA loading efficiency, poor blood stability after injection, and difficulty in transport through the cell membrane have limited the progress of these carriers. In order to circumvent such limitations, efforts have been directed towards engineering of the micellar core to increase drug/siRNA loading capacity, enhance micelle stability and achieve controlled drug/siRNA release. Evidence from literature has provided a strong case for lipid modification of nanocarriers as a successful tool in enhancing their properties in drug/gene delivery. In this context, development of lipid-modified polymeric nanocarriers may improve drug/siRNA encapsulation efficiency, increase nanocarrier stability, effectively enhance the detainment of the therapeutic cargo within the carrier and/or enhance the interaction of such carriers with cell membrane providing increased access of encapsulated drug/siRNA to intracellular space. Lipid modification of three different polymeric nanocarrier systems as means to enhance their properties in drug and siRNA delivery was explored here.

In the first section of this thesis (Chapter 2 and 3), we report on the development of novel hydrolytically degradable polymeric nanoparticles modified in their core with different lipid, i.e., palmitoyl, stearyl and cholesteryl substituents. We then explored the success of this strategy and the effect of lipid substituent structure on the solubilisation

and controlled delivery of an amphiphilic drug, amphotericin B (AmB). Commercial formulation of anti-fungal drug AmB, Fungizone<sup>®</sup> causes substantial acute (fever, vomiting, headache) and sub-acute (kidney and liver toxicity) side effects. Despite development of several alternative AmB commercial formulations, possible disadvantages such as unpredictable pharmacokinetics, toxic effects at higher AmB doses, emergence of infusion related reactions and high cost, have limited the benefits of such formulations in clinical settings. Here, we developed a novel family of lipid modified MePEO-*b*-PCL and tested the capability of such carriers for AmB encapsulation as well as reduction of its hemolytic activity. Lipid modified polymeric micelles may act as artificial lipoproteins binding hydrophobic as well as amphiphilic drugs and governing their biological fate. The advantage of a synthetic biocompatible polymeric nanocarrier over natural lipoproteins is the feasibility for their mass production and safety of administration. The second part of this thesis, we explored development of lipid modified nanocarriers for local or systemic delivery of STAT3-siRNA as means for sensitization of breast tumor cells to chemotherapy. STAT3 has been established to participate in many features of oncogenesis including cell proliferation, survival, angiogenesis, invasion, and tumor induced immune-suppression. In this context, polymeric nanocarriers for siRNA delivery to MDA-MB-435 human breast cancer cell line were designed. First, lipid substituted low molecular weight (2 kDa) PEI was tested to provide proof of principle for the efficacy of STAT3 silencing as means to enhance the effect of chemotherapy in breast cancer (Chapter 4). Then, a novel family of amphiphilic lipid-substituted MePEO-*b*-

P(CL-g-SP) has been developed with potential for *in vivo* delivery of STAT3-siRNA to tumor environment (Chapter 5-7).

### **1.6.2. Hypothesis**

1) Chemical modification of MePEO-*b*-PCL block copolymers through substitution of lipids will lead to development of nanocarriers which are capable of increasing solubility of AmB and reducing its hemolytic activity (as a measure of AmB toxicity).

2) Among different lipid substituents, incorporation of cholesteryl groups in the core of MePEO-*b*-PCL will provide a better means for AmB incorporation leading to maximum level of loaded drug in micellar carrier and minimum hemolytic activity for encapsulated AmB.

3) Lipid modified PEI2K can effectively deliver STAT3-siRNA to MDA-MB-435 human breast tumor cells increasing the sensitivity of wild type and resistant breast tumor cells to the effect of conventional cancer chemotherapy.

4) Chemical modification of MePEO-*b*-P(CL-polyamine) side chains through substitution of lipids will improve the properties of these nanocarriers for systemic delivery of STAT3-siRNA and lead to effective siRNA delivery and gene silencing activity in MDA-MB-435 human breast cancer cells.

5) Modification of PEO-*b*-PCL-polyamine micellar shell with breast cancer cell targeting ligands will enhance the transfection of siRNA in breast tumor cells.

### **1.6.3. Objective**

- 1) To synthesize a family of amphiphilic MePEO-*b*-PCL polymeric nanocarriers bearing different substituents on the PCL block and assess the efficacy of nanocarriers on the solubilization and hemolytic activity of AmB against rat red blood cell.
- 2) To optimize the structure of the lipid substituted core in polymeric micelles based MePEO-*b*-PCL for AmB delivery.
- 3) To investigate downregulation of STAT3 by STAT3 siRNA/lipid modified PEI PEI2K complexes as means to enhance the efficacy of conventional chemotherapy in a triple negative breast tumor cell line, i.e, MDA-MB-435.
- 3) To develop lipid-modified MePEO-*b*-P(CL-spermine) polymeric nanocarriers and evaluate their properties in siRNA delivery.
- 4) To optimize the structure of the core in lipid-modified MePEO-*b*-P(CL-spermine) polymeric nanocarriers for enhanced properties in siRNA delivery.
- 5) To conduct preliminary studies assessing the effect of a novel breast cancer cell targeting peptide on the shell of PEO-*b*-PCL-polyamine micellar surface in enhancing the properties of the carrier in siRNA delivery.

## 1.7. References

- [1] Balzani V. Nanoscience and nanotechnology: a personal view of a chemist. *Small* 2005;1:278-83.
- [2] Dosch H. Some general aspects of confinement in nanomaterials. *Appl Surf Sci* 2001;182:192-5.
- [3] Farokhzad OC, Langer R. Impact of Nanotechnology on Drug Delivery. *ACS Nano* 2009;3:16-20.
- [4] Farokhzad OC, Langer R. Nanomedicine: Developing smarter therapeutic and diagnostic modalities. *Adv Drug Deliver Rev* 2006;58:1456-9.
- [5] Bangham AD, Standish MM, Watkins JC. Diffusion of Univalent Ions across Lamellae of Swollen Phospholipids. *J Mol Biol* 1965;13:238-&.
- [6] Langer R, Folkman J. Polymers for the sustained release of proteins and other macromolecules. *Nature* 1976;263:797-800.
- [7] Gref R, Minamitake Y, Peracchia MT, Trubetskoy V, Torchilin V, Langer R. Biodegradable long-circulating polymeric nanospheres. *Science* 1994;263:1600-3.
- [8] Peer D, Karp JM, Hong S, Farokhzad OC, Margalit R, Langer R. Nanocarriers as an emerging platform for cancer therapy. *Nat Nanotechnol* 2007;2:751-60.
- [9] Zasadzinski JA. Novel approaches to lipid based drug delivery. *Curr Opin Solid St M* 1997;2:345-9.
- [10] Immordino ML, Dosio F, Cattel L. Stealth liposomes: review of the basic science, rationale, and clinical applications, existing and potential. *Int J Nanomedicine* 2006;1:297-315.
- [11] Scherphof GL, Dijkstra J, Spanjer HH, Derksen JT, Roerdink FH. Uptake and intracellular processing of targeted and nontargeted liposomes by rat Kupffer cells in vivo and in vitro. *Ann N Y Acad Sci* 1985;446:368-84.
- [12] Klibanov AL, Maruyama K, Torchilin VP, Huang L. Amphipathic polyethyleneglycols effectively prolong the circulation time of liposomes. *FEBS Lett* 1990;268:235-7.
- [13] Park JW, Kirpotin DB, Hong K, Shalaby R, Shao Y, Nielsen UB, et al. Tumor targeting using anti-her2 immunoliposomes. *J Control Release* 2001;74:95-113.
- [14] Pan XQ, Wang H, Lee RJ. Antitumor activity of folate receptor-targeted liposomal doxorubicin in a KB oral carcinoma murine xenograft model. *Pharm Res* 2003;20:417-22.
- [15] Torchilin VP. Recent advances with liposomes as pharmaceutical carriers. *Nat Rev Drug Discov* 2005;4:145-60.
- [16] Adams ML, Lavasanifar A, Kwon GS. Amphiphilic block copolymers for drug delivery. *J Pharm Sci* 2003;92:1343-55.
- [17] Kataoka K, Harada A, Nagasaki Y. Block copolymer micelles for drug delivery: design, characterization and biological significance. *Adv Drug Deliv Rev* 2001;47:113-31.

- [18] Letchford K, Burt H. A review of the formation and classification of amphiphilic block copolymer nanoparticulate structures: micelles, nanospheres, nanocapsules and polymersomes. *Eur J Pharm Biopharm* 2007;65:259-69.
- [19] Aliabadi HM, Lavasanifar A. Polymeric micelles for drug delivery. *Expert Opin Drug Deliv* 2006;3:139-62.
- [20] Mahmud A, Xiong XB, Aliabadi HM, Lavasanifar A. Polymeric micelles for drug targeting. *J Drug Target* 2007;15:553-84.
- [21] Matsumura Y, Kataoka K. Preclinical and clinical studies of anticancer agent-incorporating polymer micelles. *Cancer Sci* 2009;100:572-9.
- [22] Kim S, Shi Y, Kim JY, Park K, Cheng JX. Overcoming the barriers in micellar drug delivery: loading efficiency, in vivo stability, and micelle-cell interaction. *Expert Opin Drug Deliv* 2010;7:49-62.
- [23] Lu Y, Park K. Polymeric micelles and alternative nanonized delivery vehicles for poorly soluble drugs. *Int J Pharm* 2012.
- [24] Nagarajan R, Barry M, Ruckenstein E. Unusual Selectivity in Solubilization by Block Copolymer Micelles. *Langmuir* 1986;2:210-5.
- [25] Patel SK, Lavasanifar A, Choi P. Roles of nonpolar and polar intermolecular interactions in the improvement of the drug loading capacity of PEO-b-PCL with increasing PCL content for two hydrophobic Cucurbitacin drugs. *Biomacromolecules* 2009;10:2584-91.
- [26] Jette KK, Law D, Schmitt EA, Kwon GS. Preparation and drug loading of poly(ethylene glycol)-block-poly(epsilon-caprolactone) micelles through the evaporation of a cosolvent azeotrope. *Pharm Res* 2004;21:1184-91.
- [27] Shuai XT, Ai H, Nasongkla N, Kim S, Gao JM. Micellar carriers based on block copolymers of poly(epsilon-caprolactone) and poly(ethylene glycol) for doxorubicin delivery. *J Control Release* 2004;98:415-26.
- [28] Lavasanifar A, Samuel J, Sattari S, Kwon GS. Block copolymer micelles for the encapsulation and delivery of amphotericin B. *Pharm Res* 2002;19:418-22.
- [29] Molavi O, Ma Z, Mahmud A, Alshamsan A, Samuel J, Lai R, et al. Polymeric micelles for the solubilization and delivery of STAT3 inhibitor cucurbitacins in solid tumors. *Int J Pharm* 2008;347:118-27.
- [30] Mahmud A, Patel S, Molavi O, Choi P, Samuel J, Lavasanifar A. Self-associating poly(ethylene oxide)-b-poly(alpha-cholesteryl carboxylate-epsilon-caprolactone) block copolymer for the solubilization of STAT-3 inhibitor cucurbitacin I. *Biomacromolecules* 2009;10:471-8.
- [31] Lavasanifar A, Samuel J, Kwon GS. The effect of alkyl core structure on micellar properties of poly(ethylene oxide)-block-poly(L-aspartamide) derivatives. *Colloids Surf B Biointerfaces* 2001;22:115-26.
- [32] Shuai XT, Merdan T, Schaper AK, Xi F, Kissel T. Core-cross-linked polymeric micelles as paclitaxel carriers. *Bioconjugate Chem* 2004;15:441-8.
- [33] Tao J, Liu GJ. Polystyrene-block-poly(2-cinnamoyl ethyl methacrylate) tadpole molecules. *Macromolecules* 1997;30:2408-11.

- [34] Lavasanifar A, Samuel J, Kwon GS. The effect of fatty acid substitution on the in vitro release of amphotericin B from micelles composed of poly(ethylene oxide)-block-poly(N-hexyl stearate-L-aspartamide). *J Control Release* 2002;79:165-72.
- [35] Kakizawa Y, Harada A, Kataoka K. Glutathione-sensitive stabilization of block copolymer micelles composed of antisense DNA and thiolated poly(ethylene glycol)-block-poly(L-lysine): a potential carrier for systemic delivery of antisense DNA. *Biomacromolecules* 2001;2:491-7.
- [36] Harada A, Togawa H, Kataoka K. Physicochemical properties and nuclease resistance of antisense-oligodeoxynucleotides entrapped in the core of polyion complex micelles composed of poly(ethylene glycol)-poly(L-lysine) block copolymers. *Eur J Pharm Sci* 2001;13:35-42.
- [37] Miyata K, Kakizawa Y, Nishiyama N, Harada A, Yamasaki Y, Koyama H, et al. Block catiomer polyplexes with regulated densities of charge and disulfide cross-linking directed to enhance gene expression. *J Am Chem Soc* 2004;126:2355-61.
- [38] Meister A, Anderson ME. Glutathione. *Annu Rev Biochem* 1983;52:711-60.
- [39] Behr JP. The proton sponge: A trick to enter cells the viruses did not exploit. *Chimia* 1997;51:34-6.
- [40] Kanayama N, Fukushima S, Nishiyama N, Itaka K, Jang WD, Miyata K, et al. A PEG-based biocompatible block catiomer with high buffering capacity for the construction of polyplex micelles showing efficient gene transfer toward primary cells. *ChemMedChem* 2006;1:439-44.
- [41] Itaka K, Kanayama N, Nishiyama N, Jang WD, Yamasaki Y, Nakamura K, et al. Supramolecular nanocarrier of siRNA from PEG-based block catiomer carrying diamine side chain with distinctive pKa directed to enhance intracellular gene silencing. *J Am Chem Soc* 2004;126:13612-3.
- [42] La SB, Okano T, Kataoka K. Preparation and characterization of the micelle-forming polymeric drug indomethacin-incorporated poly(ethylene oxide)-poly(beta-benzyl L-aspartate) block copolymer micelles. *J Pharm Sci* 1996;85:85-90.
- [43] Xiong XB, Uludag H, Lavasanifar A. Biodegradable amphiphilic poly(ethylene oxide)-block-polyesters with grafted polyamines as supramolecular nanocarriers for efficient siRNA delivery. *Biomaterials* 2009;30:242-53.
- [44] Kabanov A, Zhu J, Alakhov V. Pluronic block copolymers for gene delivery. *Adv Genet* 2005;53:231-61.
- [45] Vega J, Ke S, Fan Z, Wallace S, Charsangavej C, Li C. Targeting doxorubicin to epidermal growth factor receptors by site-specific conjugation of C225 to poly(L-glutamic acid) through a polyethylene glycol spacer. *Pharm Res* 2003;20:826-32.
- [46] Nasongkla N, Shuai X, Ai H, Weinberg BD, Pink J, Boothman DA, et al. cRGD-functionalized polymer micelles for targeted doxorubicin delivery. *Angew Chem Int Ed Engl* 2004;43:6323-7.
- [47] Nasongkla N, Bey E, Ren JM, Ai H, Khemtong C, Guthi JS, et al. Multifunctional polymeric micelles as cancer-targeted, MRI-ultrasensitive drug delivery systems. *Nano Lett* 2006;6:2427-30.
- [48] Xiong XB, Mahmud A, Uludag H, Lavasanifar A. Conjugation of arginine-glycine-aspartic acid peptides to poly(ethylene oxide)-b-poly(epsilon-caprolactone) micelles for

enhanced intracellular drug delivery to metastatic tumor cells. *Biomacromolecules* 2007;8:874-84.

[49] Xiong XB, Mahmud A, Uludag H, Lavasanifar A. Multifunctional polymeric micelles for enhanced intracellular delivery of doxorubicin to metastatic cancer cells. *Pharm Res* 2008;25:2555-66.

[50] Vinogradov S, Batrakova E, Li S, Kabanov A. Polyion complex micelles with protein-modified corona for receptor-mediated delivery of oligonucleotides into cells. *Bioconjugate Chem* 1999;10:851-60.

[51] Kursa M, Walker GF, Roessler V, Ogris M, Roedl W, Kircheis R, et al. Novel shielded transferrin-polyethylene glycol-polyethylenimine/DNA complexes for systemic tumor-targeted gene transfer. *Bioconjug Chem* 2003;14:222-31.

[52] Xiong XB, Ma Z, Lai R, Lavasanifar A. The therapeutic response to multifunctional polymeric nano-conjugates in the targeted cellular and subcellular delivery of doxorubicin. *Biomaterials* 2010;31:757-68.

[53] Xiong XB, Uludag H, Lavasanifar A. Virus-mimetic polymeric micelles for targeted siRNA delivery. *Biomaterials* 2010;31:5886-93.

[54] Xiong XB, Falamarzian A, Garg SM, Lavasanifar A. Engineering of amphiphilic block copolymers for polymeric micellar drug and gene delivery. *J Control Release* 2011;155:248-61.

[55] Gallis HA, Drew RH, Pickard WW. Amphotericin B: 30 years of clinical experience. *Rev Infect Dis* 1990;12:308-29.

[56] Robinson RF, Nahata MC. A comparative review of conventional and lipid formulations of amphotericin B. *J Clin Pharm Ther* 1999;24:249-57.

[57] Hartsel S, Bolard J. Amphotericin B: new life for an old drug. *Trends Pharmacol Sci* 1996;17:445-9.

[58] Ellis D. Amphotericin B: spectrum and resistance. *J Antimicrob Chemother* 2002;49 Suppl 1:7-10.

[59] Gottfredsson M, Perfect JR. Fungal meningitis. *Semin Neurol* 2000;20:307-22.

[60] Torrado JJ, Espada R, Ballesteros MP, Torrado-Santiago S. Amphotericin B formulations and drug targeting. *J Pharm Sci* 2008;97:2405-25.

[61] Milhaud J, Ponsinet V, Takashi M, Michels B. Interactions of the drug amphotericin B with phospholipid membranes containing or not ergosterol: new insight into the role of ergosterol. *Biochim Biophys Acta* 2002;1558:95-108.

[62] Legrand P, Romero EA, Cohen BE, Bolard J. Effects of aggregation and solvent on the toxicity of amphotericin B to human erythrocytes. *Antimicrob Agents Chemother* 1992;36:2518-22.

[63] Brajtburg J, Elberg S, Kobayashi GS, Bolard J. Amphotericin B incorporated into egg lecithin-bile salt mixed micelles: molecular and cellular aspects relevant to therapeutic efficacy in experimental mycoses. *Antimicrob Agents Chemother* 1994;38:300-6.

[64] Bolard J, Legrand P, Heitz F, Cybulska B. One-sided action of amphotericin B on cholesterol-containing membranes is determined by its self-association in the medium. *Biochemistry-Us* 1991;30:5707-15.

- [65] Sawaya BP, Briggs JP, Schnermann J. Amphotericin B nephrotoxicity: the adverse consequences of altered membrane properties. *J Am Soc Nephrol* 1995;6:154-64.
- [66] Lemke A, Kiderlen AF, Kayser O. Amphotericin B. *Appl Microbiol Biotechnol* 2005;68:151-62.
- [67] Bates DW, Su L, Yu DT, Chertow GM, Seger DL, Gomes DR, et al. Mortality and costs of acute renal failure associated with amphotericin B therapy. *Clin Infect Dis* 2001;32:686-93.
- [68] Gates C, Pinney RJ. Amphotericin B and its delivery by liposomal and lipid formulations. *J Clin Pharm Ther* 1993;18:147-53.
- [69] Moribe K, Maruyama K. Pharmaceutical design of the liposomal antimicrobial agents for infectious disease. *Curr Pharm Des* 2002;8:441-54.
- [70] Moreno MA, Frutos P, Ballesteros MP. Lyophilized lecithin based oil-water microemulsions as a new and low toxic delivery system for amphotericin B. *Pharm Res* 2001;18:344-51.
- [71] Zarif L. Drug delivery by lipid cochleates. *Methods Enzymol* 2005;391:314-29.
- [72] Charvalos E, Tzatzarakis MN, Van Bambeke F, Tulkens PM, Tsatsakis AM, Tzanakakis GN, et al. Water-soluble amphotericin B-polyvinylpyrrolidone complexes with maintained antifungal activity against *Candida* spp. and *Aspergillus* spp. and reduced haemolytic and cytotoxic effects. *J Antimicrob Chemother* 2006;57:236-44.
- [73] Sanchez-Brunete JA, Dea MA, Rama S, Bolas F, Alunda JM, Torrado-Santiago S, et al. Influence of the vehicle on the properties and efficacy of microparticles containing amphotericin B. *J Drug Target* 2005;13:225-33.
- [74] Kayser O, Olbrich C, Yardley V, Kiderlen AF, Croft SL. Formulation of amphotericin B as nanosuspension for oral administration. *Int J Pharm* 2003;254:73-5.
- [75] Schwarz C, Mehnert W. Solid lipid nanoparticles (SLN) for controlled drug delivery. II. Drug incorporation and physicochemical characterization. *J Microencapsul* 1999;16:205-13.
- [76] Adams ML, Kwon GS. Relative aggregation state and hemolytic activity of amphotericin B encapsulated by poly(ethylene oxide)-block-poly(N-hexyl-L-aspartamide)-acyl conjugate micelles: effects of acyl chain length. *J Control Release* 2003;87:23-32.
- [77] Bang JY, Song CE, Kim C, Park WD, Cho KR, Kim PI, et al. Cytotoxicity of amphotericin B-incorporated polymeric micelles composed of poly(DL-lactide-co-glycolide)/dextran graft copolymer. *Arch Pharm Res* 2008;31:1463-9.
- [78] Yoo BK, Jalil Miah MA, Lee ES, Han K. Reduced renal toxicity of nanoparticulate amphotericin B micelles prepared with partially benzylated poly-L-aspartic acid. *Biol Pharm Bull* 2006;29:1700-5.
- [79] Wang CH, Wang WT, Hsiue GH. Development of polyion complex micelles for encapsulating and delivering amphotericin B. *Biomaterials* 2009;30:3352-8.
- [80] Adams ML, Andes DR, Kwon GS. Amphotericin B encapsulated in micelles based on poly(ethylene oxide)-block-poly(L-amino acid) derivatives exerts reduced in vitro hemolysis but maintains potent in vivo antifungal activity. *Biomacromolecules* 2003;4:750-7.

- [81] Fire A, Xu S, Montgomery MK, Kostas SA, Driver SE, Mello CC. Potent and specific genetic interference by double-stranded RNA in *Caenorhabditis elegans*. *Nature* 1998;391:806-11.
- [82] Montgomery MK, Xu S, Fire A. RNA as a target of double-stranded RNA-mediated genetic interference in *Caenorhabditis elegans*. *Proc Natl Acad Sci U S A* 1998;95:15502-7.
- [83] Elbashir SM, Harborth J, Lendeckel W, Yalcin A, Weber K, Tuschl T. Duplexes of 21-nucleotide RNAs mediate RNA interference in cultured mammalian cells. *Nature* 2001;411:494-8.
- [84] Gondi CS, Rao JS. Concepts in in vivo siRNA delivery for cancer therapy. *J Cell Physiol* 2009;220:285-91.
- [85] Tuschl T, Zamore PD, Lehmann R, Bartel DP, Sharp PA. Targeted mRNA degradation by double-stranded RNA in vitro. *Genes Dev* 1999;13:3191-7.
- [86] Dorsett Y, Tuschl T. siRNAs: applications in functional genomics and potential as therapeutics. *Nat Rev Drug Discov* 2004;3:318-29.
- [87] Bartel DP. MicroRNAs: genomics, biogenesis, mechanism, and function. *Cell* 2004;116:281-97.
- [88] Shim MS, Kwon YJ. Efficient and targeted delivery of siRNA in vivo. *The FEBS journal*;277:4814-27.
- [89] Kim SS, Garg H, Joshi A, Manjunath N. Strategies for targeted nonviral delivery of siRNAs in vivo. *Trends Mol Med* 2009;15:491-500.
- [90] Edelstein ML, Abedi MR, Wixon J. Gene therapy clinical trials worldwide to 2007--an update. *J Gene Med* 2007;9:833-42.
- [91] Smaglik P. Merck blocks 'safer' gene therapy trials. *Nature* 2000;403:817.
- [92] Couto LB, High KA. Viral vector-mediated RNA interference. *Curr Opin Pharmacol* 2010;10:534-42.
- [93] Halder J, Kamat AA, Landen CN, Jr., Han LY, Lutgendorf SK, Lin YG, et al. Focal adhesion kinase targeting using in vivo short interfering RNA delivery in neutral liposomes for ovarian carcinoma therapy. *Clin Cancer Res* 2006;12:4916-24.
- [94] Takeshita F, Minakuchi Y, Nagahara S, Honma K, Sasaki H, Hirai K, et al. Efficient delivery of small interfering RNA to bone-metastatic tumors by using atelocollagen in vivo. *Proc Natl Acad Sci U S A* 2005;102:12177-82.
- [95] Wen X, Li X, Liao B, Liu Y, Wu J, Yuan X, et al. Knockdown of p21-activated kinase 6 inhibits prostate cancer growth and enhances chemosensitivity to docetaxel. *Urology* 2009;73:1407-11.
- [96] Marques JT, Williams BR. Activation of the mammalian immune system by siRNAs. *Nat Biotechnol* 2005;23:1399-405.
- [97] Bumcrot D, Manoharan M, Kotliansky V, Sah DW. RNAi therapeutics: a potential new class of pharmaceutical drugs. *Nat Chem Biol* 2006;2:711-9.
- [98] Dykxhoorn DM, Palliser D, Lieberman J. The silent treatment: siRNAs as small molecule drugs. *Gene Ther* 2006;13:541-52.
- [99] Shukla S, Sumaria CS, Pradeepkumar PI. Exploring chemical modifications for siRNA therapeutics: a structural and functional outlook. *ChemMedChem* 2010;5:328-49.

- [100] Behlke MA. Chemical modification of siRNAs for in vivo use. *Oligonucleotides* 2008;18:305-19.
- [101] Hornung V, Guenther-Biller M, Bourquin C, Ablasser A, Schlee M, Uematsu S, et al. Sequence-specific potent induction of IFN-alpha by short interfering RNA in plasmacytoid dendritic cells through TLR7. *Nat Med* 2005;11:263-70.
- [102] Zhang H, Cook J, Nickel J, Yu R, Stecker K, Myers K, et al. Reduction of liver Fas expression by an antisense oligonucleotide protects mice from fulminant hepatitis. *Nat Biotechnol* 2000;18:862-7.
- [103] Elmen J, Thonberg H, Ljungberg K, Frieden M, Westergaard M, Xu Y, et al. Locked nucleic acid (LNA) mediated improvements in siRNA stability and functionality. *Nucleic Acids Res* 2005;33:439-47.
- [104] De Paula D, Bentley MV, Mahato RI. Hydrophobization and bioconjugation for enhanced siRNA delivery and targeting. *RNA* 2007;13:431-56.
- [105] Eckstein F. Developments in RNA chemistry, a personal view. *Biochimie* 2002;84:841-8.
- [106] Jeong JH, Mok H, Oh YK, Park TG. siRNA conjugate delivery systems. *Bioconjug Chem* 2009;20:5-14.
- [107] Lorenz C, Hadwiger P, John M, Vornlocher HP, Unverzagt C. Steroid and lipid conjugates of siRNAs to enhance cellular uptake and gene silencing in liver cells. *Bioorg Med Chem Lett* 2004;14:4975-7.
- [108] Nishina K, Unno T, Uno Y, Kubodera T, Kanouchi T, Mizusawa H, et al. Efficient in vivo delivery of siRNA to the liver by conjugation of alpha-tocopherol. *Mol Ther* 2008;16:734-40.
- [109] Wolfrum C, Shi S, Jayaprakash KN, Jayaraman M, Wang G, Pandey RK, et al. Mechanisms and optimization of in vivo delivery of lipophilic siRNAs. *Nat Biotechnol* 2007;25:1149-57.
- [110] Chiu YL, Ali A, Chu CY, Cao H, Rana TM. Visualizing a correlation between siRNA localization, cellular uptake, and RNAi in living cells. *Chem Biol* 2004;11:1165-75.
- [111] Moschos SA, Jones SW, Perry MM, Williams AE, Erjefalt JS, Turner JJ, et al. Lung delivery studies using siRNA conjugated to TAT(48-60) and penetratin reveal peptide induced reduction in gene expression and induction of innate immunity. *Bioconjug Chem* 2007;18:1450-9.
- [112] Kim SH, Jeong JH, Lee SH, Kim SW, Park TG. PEG conjugated VEGF siRNA for anti-angiogenic gene therapy. *J Control Release* 2006;116:123-9.
- [113] Hicke BJ, Stephens AW. Escort aptamers: a delivery service for diagnosis and therapy. *J Clin Invest* 2000;106:923-8.
- [114] Whitehead KA, Langer R, Anderson DG. Knocking down barriers: advances in siRNA delivery. *Nat Rev Drug Discov* 2009;8:129-38.
- [115] Oh YK, Park TG. siRNA delivery systems for cancer treatment. *Adv Drug Deliv Rev* 2009;61:850-62.
- [116] Gao H, Hui KM. Synthesis of a novel series of cationic lipids that can act as efficient gene delivery vehicles through systematic heterocyclic substitution of cholesterol derivatives. *Gene Ther* 2001;8:855-63.

- [117] Kim HR, Kim IK, Bae KH, Lee SH, Lee Y, Park TG. Cationic solid lipid nanoparticles reconstituted from low density lipoprotein components for delivery of siRNA. *Mol Pharm* 2008;5:622-31.
- [118] Santel A, Aleku M, Keil O, Endruschat J, Esche V, Fisch G, et al. A novel siRNA-lipoplex technology for RNA interference in the mouse vascular endothelium. *Gene Ther* 2006;13:1222-34.
- [119] Kim HK, Davaa E, Myung CS, Park JS. Enhanced siRNA delivery using cationic liposomes with new polyarginine-conjugated PEG-lipid. *Int J Pharm* 2010;392:141-7.
- [120] Palliser D, Chowdhury D, Wang QY, Lee SJ, Bronson RT, Knipe DM, et al. An siRNA-based microbicide protects mice from lethal herpes simplex virus 2 infection. *Nature* 2006;439:89-94.
- [121] Elbashir SM, Harborth J, Weber K, Tuschl T. Analysis of gene function in somatic mammalian cells using small interfering RNAs. *Methods* 2002;26:199-213.
- [122] Verma UN, Surabhi RM, Schmaltieg A, Becerra C, Gaynor RB. Small interfering RNAs directed against beta-catenin inhibit the in vitro and in vivo growth of colon cancer cells. *Clin Cancer Res* 2003;9:1291-300.
- [123] Putnam D. Polymers for gene delivery across length scales. *Nat Mater* 2006;5:439-51.
- [124] Howard KA, Rahbek UL, Liu X, Damgaard CK, Glud SZ, Andersen MO, et al. RNA interference in vitro and in vivo using a novel chitosan/siRNA nanoparticle system. *Mol Ther* 2006;14:476-84.
- [125] Ji AM, Su D, Che O, Li WS, Sun L, Zhang ZY, et al. Functional gene silencing mediated by chitosan/siRNA nanocomplexes. *Nanotechnology* 2009;20:405103.
- [126] Minakuchi Y, Takeshita F, Kosaka N, Sasaki H, Yamamoto Y, Kouno M, et al. Atelocollagen-mediated synthetic small interfering RNA delivery for effective gene silencing in vitro and in vivo. *Nucleic Acids Res* 2004;32:e109.
- [127] Won YW, Yoon SM, Lee KM, Kim YH. Poly(oligo-D-arginine) With Internal Disulfide Linkages as a Cytoplasm-sensitive Carrier for siRNA Delivery. *Mol Ther* 2010.
- [128] Urban-Klein B, Werth S, Abuharbeid S, Czubayko F, Aigner A. RNAi-mediated gene-targeting through systemic application of polyethylenimine (PEI)-complexed siRNA in vivo. *Gene Ther* 2005;12:461-6.
- [129] Grzelinski M, Urban-Klein B, Martens T, Lamszus K, Bakowsky U, Hobel S, et al. RNA interference-mediated gene silencing of pleiotrophin through polyethylenimine-complexed small interfering RNAs in vivo exerts antitumoral effects in glioblastoma xenografts. *Hum Gene Ther* 2006;17:751-66.
- [130] Kim SH, Jeong JH, Lee SH, Kim SW, Park TG. Local and systemic delivery of VEGF siRNA using polyelectrolyte complex micelles for effective treatment of cancer. *J Control Release* 2008;129:107-16.
- [131] Abbasi M, Lavasanifar A, Berthiaume LG, Weinfeld M, Uludag H. Cationic polymer-mediated small interfering RNA delivery for P-glycoprotein down-regulation in tumor cells. *Cancer* 2010;116:5544-54.
- [132] Heidel JD, Yu Z, Liu JY, Rele SM, Liang Y, Zeidan RK, et al. Administration in non-human primates of escalating intravenous doses of targeted nanoparticles containing

- ribonucleotide reductase subunit M2 siRNA. *Proc Natl Acad Sci U S A* 2007;104:5715-21.
- [133] Hu-Lieskovan S, Heidel JD, Bartlett DW, Davis ME, Triche TJ. Sequence-specific knockdown of EWS-FLI1 by targeted, nonviral delivery of small interfering RNA inhibits tumor growth in a murine model of metastatic Ewing's sarcoma. *Cancer Res* 2005;65:8984-92.
- [134] Godbey WT, Wu KK, Mikos AG. Poly(ethylenimine) and its role in gene delivery. *J Control Release* 1999;60:149-60.
- [135] Aigner A. Gene silencing through RNA interference (RNAi) in vivo: strategies based on the direct application of siRNAs. *J Biotechnol* 2006;124:12-25.
- [136] Boussif O, Lezoualc'h F, Zanta MA, Mergny MD, Scherman D, Demeneix B, et al. A versatile vector for gene and oligonucleotide transfer into cells in culture and in vivo: polyethylenimine. *Proc Natl Acad Sci U S A* 1995;92:7297-301.
- [137] Demeneix B, Behr JP. Polyethylenimine (PEI). *Adv Genet* 2005;53PA:215-30.
- [138] Jere D, Jiang HL, Arote R, Kim YK, Choi YJ, Cho MH, et al. Degradable polyethylenimines as DNA and small interfering RNA carriers. *Expert Opin Drug Deliv* 2009;6:827-34.
- [139] Bologna JC, Dorn G, Natt F, Weiler J. Linear polyethylenimine as a tool for comparative studies of antisense and short double-stranded RNA oligonucleotides. *Nucleosides Nucleotides Nucleic Acids* 2003;22:1729-31.
- [140] Werth S, Urban-Klein B, Dai L, Hobel S, Grzelinski M, Bakowsky U, et al. A low molecular weight fraction of polyethylenimine (PEI) displays increased transfection efficiency of DNA and siRNA in fresh or lyophilized complexes. *J Control Release* 2006;112:257-70.
- [141] Alshamsan A, Hamdy S, Samuel J, El-Kadi AO, Lavasanifar A, Uludag H. The induction of tumor apoptosis in B16 melanoma following STAT3 siRNA delivery with a lipid-substituted polyethylenimine. *Biomaterials* 2010;31:1420-8.
- [142] Wightman L, Kircheis R, Rossler V, Carotta S, Ruzicka R, Kurska M, et al. Different behavior of branched and linear polyethylenimine for gene delivery in vitro and in vivo. *J Gene Med* 2001;3:362-72.
- [143] Neamnark A, Suwantong O, Bahadur RK, Hsu CY, Supaphol P, Uludag H. Aliphatic lipid substitution on 2 kDa polyethylenimine improves plasmid delivery and transgene expression. *Mol Pharm* 2009;6:1798-815.
- [144] Aliabadi HM, Landry B, Bahadur RK, Neamnark A, Suwantong O, Uludag H. Impact of lipid substitution on assembly and delivery of siRNA by cationic polymers. *Macromol Biosci* 2011;11:662-72.
- [145] Aliabadi HM, Landry B, Mahdipoor P, Hsu CY, Uludag H. Effective down-regulation of breast cancer resistance protein (BCRP) by siRNA delivery using lipid-substituted aliphatic polymers. *Eur J Pharm Biopharm* 2012;81:33-42.
- [146] Singha K, Namgung R, Kim WJ. *Polymers in Small-Interfering RNA Delivery. Oligonucleotides* 2011.
- [147] Hicklin DJ, Ellis LM. Role of the vascular endothelial growth factor pathway in tumor growth and angiogenesis. *J Clin Oncol* 2005;23:1011-27.

- [148] Ferrara N, Gerber HP, LeCouter J. The biology of VEGF and its receptors. *Nat Med* 2003;9:669-76.
- [149] Kim SH, Jeong JH, Lee SH, Kim SW, Park TG. LHRH receptor-mediated delivery of siRNA using polyelectrolyte complex micelles self-assembled from siRNA-PEG-LHRH conjugate and PEI. *Bioconjug Chem* 2008;19:2156-62.
- [150] Wyman TB, Nicol F, Zelphati O, Scaria PV, Plank C, Szoka FC, Jr. Design, synthesis, and characterization of a cationic peptide that binds to nucleic acids and permeabilizes bilayers. *Biochemistry* 1997;36:3008-17.
- [151] Lee SH, Kim SH, Park TG. Intracellular siRNA delivery system using polyelectrolyte complex micelles prepared from VEGF siRNA-PEG conjugate and cationic fusogenic peptide. *Biochem Biophys Res Commun* 2007;357:511-6.
- [152] Al-Abd AM, Lee SH, Kim SH, Cha JH, Park TG, Lee SJ, et al. Penetration and efficacy of VEGF siRNA using polyelectrolyte complex micelles in a human solid tumor model in-vitro. *J Control Release* 2009;137:130-5.
- [153] Choi SW, Lee SH, Mok H, Park TG. Multifunctional siRNA delivery system: polyelectrolyte complex micelles of six-arm PEG conjugate of siRNA and cell penetrating peptide with crosslinked fusogenic peptide. *Biotechnol Prog* 2010;26:57-63.
- [154] Oishi M, Nagasaki Y, Itaka K, Nishiyama N, Kataoka K. Lactosylated poly(ethylene glycol)-siRNA conjugate through acid-labile beta-thiopropionate linkage to construct pH-sensitive polyion complex micelles achieving enhanced gene silencing in hepatoma cells. *J Am Chem Soc* 2005;127:1624-5.
- [155] Gunther M, Lipka J, Malek A, Gutsch D, Kreyling W, Aigner A. Polyethylenimines for RNAi-mediated gene targeting in vivo and siRNA delivery to the lung. *Eur J Pharm Biopharm*;77:438-49.
- [156] Moriguchi R, Kogure K, Akita H, Futaki S, Miyagishi M, Taira K, et al. A multifunctional envelope-type nano device for novel gene delivery of siRNA plasmids. *Int J Pharm* 2005;301:277-85.
- [157] Kano A, Moriyama K, Yamano T, Nakamura I, Shimada N, Maruyama A. Grafting of poly(ethylene glycol) to poly-lysine augments its lifetime in blood circulation and accumulation in tumors without loss of the ability to associate with siRNA. *J Control Release*;149:2-7.
- [158] Patil ML, Zhang M, Minko T. Multifunctional triblock Nanocarrier (PAMAM-PEG-PLL) for the efficient intracellular siRNA delivery and gene silencing. *ACS Nano* 2011;5:1877-87.
- [159] Merkel OM, Beyerle A, Librizzi D, Pfestroff A, Behr TM, Sproat B, et al. Nonviral siRNA delivery to the lung: investigation of PEG-PEI polyplexes and their in vivo performance. *Mol Pharm* 2009;6:1246-60.
- [160] Malek A, Merkel O, Fink L, Czubayko F, Kissel T, Aigner A. In vivo pharmacokinetics, tissue distribution and underlying mechanisms of various PEI(-PEG)/siRNA complexes. *Toxicol Appl Pharmacol* 2009;236:97-108.
- [161] Biswal BK, Debata NB, Verma RS. Development of a targeted siRNA delivery system using FOL-PEG-PEI conjugate. *Molecular biology reports*;37:2919-26.
- [162] Mao S, Neu M, Germershaus O, Merkel O, Sitterberg J, Bakowsky U, et al. Influence of polyethylene glycol chain length on the physicochemical and biological

- properties of poly(ethylene imine)-graft-poly(ethylene glycol) block copolymer/SiRNA polyplexes. *Bioconjug Chem* 2006;17:1209-18.
- [163] Sutton D, Kim S, Shuai X, Leskov K, Marques JT, Williams BR, et al. Efficient suppression of secretory clusterin levels by polymer-siRNA nanocomplexes enhances ionizing radiation lethality in human MCF-7 breast cancer cells in vitro. *Int J Nanomedicine* 2006;1:155-62.
- [164] Wu Y, Wang W, Chen Y, Huang K, Shuai X, Chen Q, et al. The investigation of polymer-siRNA nanoparticle for gene therapy of gastric cancer in vitro. *Int J Nanomedicine* 2010;5:129-36.
- [165] Merkel OM, Librizzi D, Pfestroff A, Schurrat T, Buyens K, Sanders NN, et al. Stability of siRNA polyplexes from poly(ethylenimine) and poly(ethylenimine)-g-poly(ethylene glycol) under in vivo conditions: effects on pharmacokinetics and biodistribution measured by Fluorescence Fluctuation Spectroscopy and Single Photon Emission Computed Tomography (SPECT) imaging. *J Control Release* 2009;138:148-59.
- [166] Beyerle A, Braun A, Merkel O, Koch F, Stoeger T, Kissel T. Comparative in vivo study of poly(ethylene imine)/siRNA complexes for pulmonary delivery in mice. *J Control Release* 2011.
- [167] Kim SH, Lee SH, Tian H, Chen X, Park TG. Prostate cancer cell-specific VEGF siRNA delivery system using cell targeting peptide conjugated polyplexes. *J Drug Target* 2009;17:311-7.
- [168] Kim SH, Mok H, Jeong JH, Kim SW, Park TG. Comparative evaluation of target-specific GFP gene silencing efficiencies for antisense ODN, synthetic siRNA, and siRNA plasmid complexed with PEI-PEG-FOL conjugate. *Bioconjug Chem* 2006;17:241-4.
- [169] Meyer M, Philipp A, Oskuee R, Schmidt C, Wagner E. Breathing life into polycations: functionalization with pH-responsive endosomolytic peptides and polyethylene glycol enables siRNA delivery. *J Am Chem Soc* 2008;130:3272-3.
- [170] Sato A, Choi SW, Hirai M, Yamayoshi A, Moriyama R, Yamano T, et al. Polymer brush-stabilized polyplex for a siRNA carrier with long circulatory half-life. *J Control Release* 2007;122:209-16.
- [171] Matsumoto S, Christie RJ, Nishiyama N, Miyata K, Ishii A, Oba M, et al. Environment-responsive block copolymer micelles with a disulfide cross-linked core for enhanced siRNA delivery. *Biomacromolecules* 2009;10:119-27.
- [172] Duan Y, Guan X, Ge J, Quan D, Zhuo Y, Ye H, et al. Cationic nano-copolymers mediated IKKbeta targeting siRNA inhibit the proliferation of human Tenon's capsule fibroblasts in vitro. *Mol Vis* 2008;14:2616-28.
- [173] Sun TM, Du JZ, Yan LF, Mao HQ, Wang J. Self-assembled biodegradable micellar nanoparticles of amphiphilic and cationic block copolymer for siRNA delivery. *Biomaterials* 2008;29:4348-55.
- [174] Zhu C, Jung S, Luo S, Meng F, Zhu X, Park TG, et al. Co-delivery of siRNA and paclitaxel into cancer cells by biodegradable cationic micelles based on PDMAEMA-PCL-PDMAEMA triblock copolymers. *Biomaterials* 2010;31:2408-16.
- [175] Eckford PD, Sharom FJ. ABC efflux pump-based resistance to chemotherapy drugs. *Chem Rev* 2009;109:2989-3011.

- [176] Loo TW, Clarke DM. Recent progress in understanding the mechanism of P-glycoprotein-mediated drug efflux. *J Membr Biol* 2005;206:173-85.
- [177] Lavasanifar A, Xiong XB. Traceable Multifunctional Micellar Nanocarriers for Cancer-targeted Co-delivery of MDR-1 siRNA and Doxorubicin. *ACS nano*.
- [178] Cao N, Cheng D, Zou S, Ai H, Gao J, Shuai X. The synergistic effect of hierarchical assemblies of siRNA and chemotherapeutic drugs co-delivered into hepatic cancer cells. *Biomaterials* 2011;32:2222-32.
- [179] Benoit DS, Henry SM, Shubin AD, Hoffman AS, Stayton PS. pH-responsive polymeric siRNA carriers sensitize multidrug resistant ovarian cancer cells to doxorubicin via knockdown of polo-like kinase 1. *Mol Pharm* 2010;7:442-55.
- [180] Elsabahy M, Wazen N, Bayo-Puxan N, Deleavey G, Servant M, Damha MJ, et al. Delivery of Nucleic Acids through the Controlled Disassembly of Multifunctional Nanocomplexes. *Adv Funct Mater* 2009;19:3862-7.
- [181] Felber AE, Castagner B, Elsabahy M, Deleavey GF, Damha MJ, Leroux JC. siRNA nanocarriers based on methacrylic acid copolymers. *J Control Release* 2010.
- [182] Boudier A, Aubert-Pouessel A, Gerardin C, Devoisselle JM, Begu S, Louis-Pence P, et al. Tripartite siRNA micelles as controlled delivery systems for primary dendritic cells. *Drug Dev Ind Pharm* 2009;35:950-8.
- [183] Convertine AJ, Diab C, Prieve M, Paschal A, Hoffman AS, Johnson PH, et al. pH-Responsive Polymeric Micelle Carriers for siRNA Drugs. *Biomacromolecules* 2010.
- [184] Takemoto H, Ishii A, Miyata K, Nakanishi M, Oba M, Ishii T, et al. Polyion complex stability and gene silencing efficiency with a siRNA-grafted polymer delivery system. *Biomaterials* 2010;31:8097-105.
- [185] Musacchio T, Vaze O, D'Souza G, Torchilin VP. Effective stabilization and delivery of siRNA: reversible siRNA-phospholipid conjugate in nanosized mixed polymeric micelles. *Bioconjug Chem* 2010;21:1530-6.
- [186] Wang Y, Li Z, Han Y, Liang LH, Ji A. Nanoparticle-based delivery system for application of siRNA in vivo. *Curr Drug Metab* 2010;11:182-96.
- [187] Heidel JD, Liu JY, Yen Y, Zhou B, Heale BS, Rossi JJ, et al. Potent siRNA inhibitors of ribonucleotide reductase subunit RRM2 reduce cell proliferation in vitro and in vivo. *Clin Cancer Res* 2007;13:2207-15.
- [188] Steegmaier M, Hoffmann M, Baum A, Lenart P, Petronczki M, Krssak M, et al. BI 2536, a potent and selective inhibitor of polo-like kinase 1, inhibits tumor growth in vivo. *Curr Biol* 2007;17:316-22.
- [189] Strebhardt K, Ullrich A. Targeting polo-like kinase 1 for cancer therapy. *Nat Rev Cancer* 2006;6:321-30.
- [190] Davidson BL, McCray PB, Jr. Current prospects for RNA interference-based therapies. *Nat Rev Genet* 2011;12:329-40.
- [191] Darnell JE, Jr., Kerr IM, Stark GR. Jak-STAT pathways and transcriptional activation in response to IFNs and other extracellular signaling proteins. *Science* 1994;264:1415-21.
- [192] Levy DE, Darnell JE, Jr. Stats: transcriptional control and biological impact. *Nat Rev Mol Cell Biol* 2002;3:651-62.

- [193] Wen Z, Zhong Z, Darnell JE, Jr. Maximal activation of transcription by Stat1 and Stat3 requires both tyrosine and serine phosphorylation. *Cell* 1995;82:241-50.
- [194] Darnell JE, Kerr IM, Stark GR. Jak-Stat Pathways and Transcriptional Activation in Response to Ifns and Other Extracellular Signaling Proteins. *Science* 1994;264:1415-21.
- [195] Copeland NG, Gilbert DJ, Schindler C, Zhong Z, Wen Z, Darnell JE, Jr., et al. Distribution of the mammalian Stat gene family in mouse chromosomes. *Genomics* 1995;29:225-8.
- [196] Turkson J. STAT proteins as novel targets for cancer drug discovery. *Expert Opin Ther Targets* 2004;8:409-22.
- [197] Shuai K, Ziemiecki A, Wilks AF, Harpur AG, Sadowski HB, Gilman MZ, et al. Polypeptide signalling to the nucleus through tyrosine phosphorylation of Jak and Stat proteins. *Nature* 1993;366:580-3.
- [198] Schindler C, Darnell JE, Jr. Transcriptional responses to polypeptide ligands: the JAK-STAT pathway. *Annu Rev Biochem* 1995;64:621-51.
- [199] Hoey T, Schindler U. STAT structure and function in signaling. *Curr Opin Genet Dev* 1998;8:582-7.
- [200] Vinkemeier U, Cohen SL, Moarefi I, Chait BT, Kuriyan J, Darnell JE, Jr. DNA binding of in vitro activated Stat1 alpha, Stat1 beta and truncated Stat1: interaction between NH2-terminal domains stabilizes binding of two dimers to tandem DNA sites. *EMBO J* 1996;15:5616-26.
- [201] Yu H, Jove R. The STATs of cancer--new molecular targets come of age. *Nat Rev Cancer* 2004;4:97-105.
- [202] Akira S. Roles of STAT3 defined by tissue-specific gene targeting. *Oncogene* 2000;19:2607-11.
- [203] Takeda K, Noguchi K, Shi W, Tanaka T, Matsumoto M, Yoshida N, et al. Targeted disruption of the mouse Stat3 gene leads to early embryonic lethality. *Proc Natl Acad Sci U S A* 1997;94:3801-4.
- [204] Chapman RS, Lourenco PC, Tonner E, Flint DJ, Selbert S, Takeda K, et al. Suppression of epithelial apoptosis and delayed mammary gland involution in mice with a conditional knockout of Stat3. *Genes Dev* 1999;13:2604-16.
- [205] Kritikou EA, Sharkey A, Abell K, Came PJ, Anderson E, Clarkson RW, et al. A dual, non-redundant, role for LIF as a regulator of development and STAT3-mediated cell death in mammary gland. *Development* 2003;130:3459-68.
- [206] Humphreys RC, Bierie B, Zhao L, Raz R, Levy D, Hennighausen L. Deletion of Stat3 blocks mammary gland involution and extends functional competence of the secretory epithelium in the absence of lactogenic stimuli. *Endocrinology* 2002;143:3641-50.
- [207] Takeda K, Kaisho T, Yoshida N, Takeda J, Kishimoto T, Akira S. Stat3 activation is responsible for IL-6-dependent T cell proliferation through preventing apoptosis: generation and characterization of T cell-specific Stat3-deficient mice. *J Immunol* 1998;161:4652-60.

- [208] Takeda K, Clausen BE, Kaisho T, Tsujimura T, Terada N, Forster I, et al. Enhanced Th1 activity and development of chronic enterocolitis in mice devoid of Stat3 in macrophages and neutrophils. *Immunity* 1999;10:39-49.
- [209] Foshay K, Rodriguez G, Hoel B, Narayan J, Gallicano GI. JAK2/STAT3 directs cardiomyogenesis within murine embryonic stem cells in vitro. *Stem Cells* 2005;23:530-43.
- [210] Jacoby JJ, Kalinowski A, Liu MG, Zhang SS, Gao Q, Chai GX, et al. Cardiomyocyte-restricted knockout of STAT3 results in higher sensitivity to inflammation, cardiac fibrosis, and heart failure with advanced age. *Proc Natl Acad Sci U S A* 2003;100:12929-34.
- [211] Sano S, Chan KS, DiGiovanni J. Impact of Stat3 activation upon skin biology: a dichotomy of its role between homeostasis and diseases. *J Dermatol Sci* 2008;50:1-14.
- [212] Alonzi T, Maritano D, Gorgoni B, Rizzuto G, Libert C, Poli V. Essential role of STAT3 in the control of the acute-phase response as revealed by inducible gene inactivation [correction of activation] in the liver. *Mol Cell Biol* 2001;21:1621-32.
- [213] Darnell JE. Validating Stat3 in cancer therapy. *Nat Med* 2005;11:595-6.
- [214] Bromberg J, Wang TC. Inflammation and cancer: IL-6 and STAT3 complete the link. *Cancer Cell* 2009;15:79-80.
- [215] Dang CV, Resar LM, Emison E, Kim S, Li Q, Prescott JE, et al. Function of the c-Myc oncogenic transcription factor. *Exp Cell Res* 1999;253:63-77.
- [216] Bromberg JF, Wrzeszczynska MH, Devgan G, Zhao Y, Pestell RG, Albanese C, et al. Stat3 as an oncogene. *Cell* 1999;98:295-303.
- [217] Huang M, Page C, Reynolds RK, Lin J. Constitutive activation of stat 3 oncogene product in human ovarian carcinoma cells. *Gynecol Oncol* 2000;79:67-73.
- [218] Masuda M, Suzui M, Yasumatu R, Nakashima T, Kuratomi Y, Azuma K, et al. Constitutive activation of signal transducers and activators of transcription 3 correlates with cyclin D1 overexpression and may provide a novel prognostic marker in head and neck squamous cell carcinoma. *Cancer Res* 2002;62:3351-5.
- [219] Kiuchi N, Nakajima K, Ichiba M, Fukada T, Narimatsu M, Mizuno K, et al. STAT3 is required for the gp130-mediated full activation of the c-myc gene. *J Exp Med* 1999;189:63-73.
- [220] Bowman T, Broome MA, Sinibaldi D, Wharton W, Pledger WJ, Sedivy JM, et al. Stat3-mediated Myc expression is required for Src transformation and PDGF-induced mitogenesis. *Proc Natl Acad Sci U S A* 2001;98:7319-24.
- [221] Grad JM, Zeng XR, Boise LH. Regulation of Bcl-xL: a little bit of this and a little bit of STAT. *Curr Opin Oncol* 2000;12:543-9.
- [222] Grandis JR, Drenning SD, Zeng Q, Watkins SC, Melhem MF, Endo S, et al. Constitutive activation of Stat3 signaling abrogates apoptosis in squamous cell carcinogenesis in vivo. *Proc Natl Acad Sci U S A* 2000;97:4227-32.
- [223] Niu G, Bowman T, Huang M, Shivers S, Reintgen D, Daud A, et al. Roles of activated Src and Stat3 signaling in melanoma tumor cell growth. *Oncogene* 2002;21:7001-10.

- [224] Aoki Y, Feldman GM, Tosato G. Inhibition of STAT3 signaling induces apoptosis and decreases survivin expression in primary effusion lymphoma. *Blood* 2003;101:1535-42.
- [225] Chen Z, Han ZC. STAT3: a critical transcription activator in angiogenesis. *Med Res Rev* 2008;28:185-200.
- [226] Niu G, Wright KL, Huang M, Song L, Haura E, Turkson J, et al. Constitutive Stat3 activity up-regulates VEGF expression and tumor angiogenesis. *Oncogene* 2002;21:2000-8.
- [227] Chen SH, Murphy DA, Lassoued W, Thurston G, Feldman MD, Lee WM. Activated STAT3 is a mediator and biomarker of VEGF endothelial activation. *Cancer Biol Ther* 2008;7:1994-2003.
- [228] Masuda M, Ruan HY, Ito A, Nakashima T, Toh S, Wakasaki T, et al. Signal transducers and activators of transcription 3 up-regulates vascular endothelial growth factor production and tumor angiogenesis in head and neck squamous cell carcinoma. *Oral Oncol* 2007;43:785-90.
- [229] Wei LH, Kuo ML, Chen CA, Chou CH, Lai KB, Lee CN, et al. Interleukin-6 promotes cervical tumor growth by VEGF-dependent angiogenesis via a STAT3 pathway. *Oncogene* 2003;22:1517-27.
- [230] Yu H, Pardoll D, Jove R. STATs in cancer inflammation and immunity: a leading role for STAT3. *Nat Rev Cancer* 2009;9:798-809.
- [231] Grivennikov SI, Karin M. Inflammation and oncogenesis: a vicious connection. *Curr Opin Genet Dev* 2010;20:65-71.
- [232] Zumsteg A, Christofori G. Corrupt policemen: inflammatory cells promote tumor angiogenesis. *Curr Opin Oncol* 2009;21:60-70.
- [233] Groblewska M, Mroczko B, Wereszczynska-Siemiatkowska U, Kedra B, Lukaszewicz M, Baniukiewicz A, et al. Serum interleukin 6 (IL-6) and C-reactive protein (CRP) levels in colorectal adenoma and cancer patients. *Clin Chem Lab Med* 2008;46:1423-8.
- [234] Ernst M, Najdovska M, Grail D, Lundgren-May T, Buchert M, Tye H, et al. STAT3 and STAT1 mediate IL-11-dependent and inflammation-associated gastric tumorigenesis in gp130 receptor mutant mice. *J Clin Invest* 2008;118:1727-38.
- [235] Bronte-Tinkew DM, Terebiznik M, Franco A, Ang M, Ahn D, Mimuro H, et al. *Helicobacter pylori* cytotoxin-associated gene A activates the signal transducer and activator of transcription 3 pathway in vitro and in vivo. *Cancer Res* 2009;69:632-9.
- [236] Choudhari SR, Khan MA, Harris G, Picker D, Jacob GS, Block T, et al. Deactivation of Akt and STAT3 signaling promotes apoptosis, inhibits proliferation, and enhances the sensitivity of hepatocellular carcinoma cells to an anticancer agent, Atiprimod. *Mol Cancer Ther* 2007;6:112-21.
- [237] Samavati L, Rastogi R, Du W, Huttemann M, Fite A, Franchi L. STAT3 tyrosine phosphorylation is critical for interleukin 1 beta and interleukin-6 production in response to lipopolysaccharide and live bacteria. *Mol Immunol* 2009;46:1867-77.
- [238] Al Zaid Siddiquee K, Turkson J. STAT3 as a target for inducing apoptosis in solid and hematological tumors. *Cell Res* 2008;18:254-67.

- [239] Kortylewski M, Kujawski M, Wang T, Wei S, Zhang S, Pilon-Thomas S, et al. Inhibiting Stat3 signaling in the hematopoietic system elicits multicomponent antitumor immunity. *Nat Med* 2005;11:1314-21.
- [240] Turkson J, Ryan D, Kim JS, Zhang Y, Chen Z, Haura E, et al. Phosphotyrosyl peptides block Stat3-mediated DNA binding activity, gene regulation, and cell transformation. *J Biol Chem* 2001;276:45443-55.
- [241] Turkson J, Kim JS, Zhang S, Yuan J, Huang M, Glenn M, et al. Novel peptidomimetic inhibitors of signal transducer and activator of transcription 3 dimerization and biological activity. *Mol Cancer Ther* 2004;3:261-9.
- [242] Buerger C, Nagel-Wolfrum K, Kunz C, Wittig I, Butz K, Hoppe-Seyler F, et al. Sequence-specific peptide aptamers, interacting with the intracellular domain of the epidermal growth factor receptor, interfere with Stat3 activation and inhibit the growth of tumor cells. *J Biol Chem* 2003;278:37610-21.
- [243] Deng J, Grande F, Neamati N. Small molecule inhibitors of Stat3 signaling pathway. *Curr Cancer Drug Targets* 2007;7:91-107.
- [244] Timofeeva OA, Gaponenko V, Lockett SJ, Tarasov SG, Jiang S, Michejda CJ, et al. Rationally designed inhibitors identify STAT3 N-domain as a promising anticancer drug target. *ACS Chem Biol* 2007;2:799-809.
- [245] Huang F, Tong X, Fu L, Zhang R. Knockdown of STAT3 by shRNA inhibits the growth of CAOV3 ovarian cancer cell line in vitro and in vivo. *Acta Biochim Biophys Sin (Shanghai)* 2008;40:519-25.
- [246] Leong PL, Andrews GA, Johnson DE, Dyer KF, Xi S, Mai JC, et al. Targeted inhibition of Stat3 with a decoy oligonucleotide abrogates head and neck cancer cell growth. *Proc Natl Acad Sci U S A* 2003;100:4138-43.
- [247] Liu Y, Li PK, Li C, Lin J. Inhibition of STAT3 signaling blocks the anti-apoptotic activity of IL-6 in human liver cancer cells. *J Biol Chem* 2010;285:27429-39.
- [248] Siddiquee K, Zhang S, Guida WC, Blaskovich MA, Greedy B, Lawrence HR, et al. Selective chemical probe inhibitor of Stat3, identified through structure-based virtual screening, induces antitumor activity. *Proc Natl Acad Sci U S A* 2007;104:7391-6.
- [249] Schust J, Sperl B, Hollis A, Mayer TU, Berg T. Stattic: a small-molecule inhibitor of STAT3 activation and dimerization. *Chem Biol* 2006;13:1235-42.
- [250] Turkson J, Zhang S, Palmer J, Kay H, Stanko J, Mora LB, et al. Inhibition of constitutive signal transducer and activator of transcription 3 activation by novel platinum complexes with potent antitumor activity. *Mol Cancer Ther* 2004;3:1533-42.
- [251] Blaskovich MA, Sun J, Cantor A, Turkson J, Jove R, Sefti SM. Discovery of JSI-124 (cucurbitacin D), a selective Janus kinase/signal transducer and activator of transcription 3 signaling pathway inhibitor with potent antitumor activity against human and murine cancer cells in mice. *Cancer Res* 2003;63:1270-9.
- [252] Zhang X, Zhang J, Wang L, Wei H, Tian Z. Therapeutic effects of STAT3 decoy oligodeoxynucleotide on human lung cancer in xenograft mice. *BMC Cancer* 2007;7:149.
- [253] NCT01047943. Inpatient Comparison Study of Efficacy of STA-21 Ointment on Psoriatic Skin Lesions.
- [254] NCT01066663. A Phase I/II Study of Pyrimethamine, a STAT3 Inhibitor, for the Treatment of Relapsed Chronic Lymphocytic Leukemia/Small Lymphocytic Lymphoma.

- [255] NCT00955812. A Phase I, Open-label, Dose Escalation, Nonrandomized Study To Assess the Pharmacokinetics, Dose Limiting Toxicity, and Maximum Tolerated Dose of OPB-31121 in Subjects with Advanced Solid Tumors.
- [256] NCT00529113. A Randomized Phase I/II Study with Gemcitabine and RTA 402 or Gemcitabine and Placebo for Patients with Unresectable Pancreatic Cancer.
- [257] Hong DSK, R.; Supko, J. G.; Lawrence, D. P.; Wheler, J. J.; Meyer, C. J.; Mier, J. W.; Andreeff, M.; Shapiro, G. I.; Dezube, B. J. Phase I trial with a novel oral NF- $\kappa$ B/STAT3 inhibitor RTA 402 in patients with solid tumors and lymphoid malignancies. *J Clin Oncol* 2008;26:3517.
- [258] Kunigal S, Lakka SS, Sodadasu PK, Estes N, Rao JS. Stat3-siRNA induces Fas-mediated apoptosis in vitro and in vivo in breast cancer. *Int J Oncol* 2009;34:1209-20.
- [259] Gao LF, Xu DQ, Wen LJ, Zhang XY, Shao YT, Zhao XJ. Inhibition of STAT3 expression by siRNA suppresses growth and induces apoptosis in laryngeal cancer cells. *Acta Pharmacol Sin* 2005;26:377-83.
- [260] Gao LF, Xu DQ, Shao YT, Zhao D, Zhao XJ. [Knockdown of STAT3 expression using siRNA inhibits the growth of prostate cancer cell lines]. *Zhonghua Nan Ke Xue* 2005;11:29-33, 7.
- [261] Alshamsan A, Haddadi A, Hamdy S, Samuel J, El-Kadi AO, Uludag H, et al. STAT3 Silencing in Dendritic Cells by siRNA Polyplexes Encapsulated in PLGA Nanoparticles for the Modulation of Anticancer Immune Response. *Mol Pharm* 2010.
- [262] Verma NK, Davies AM, Long A, Kelleher D, Volkov Y. STAT3 knockdown by siRNA induces apoptosis in human cutaneous T-cell lymphoma line Hut78 via downregulation of Bcl-xL. *Cell Mol Biol Lett* 2010;15:342-55.

## CHAPTER TWO

### CHEMICAL MODIFICATION OF HYDROPHOBIC BLOCK IN POLY (ETHYLENE OXIDE)-POLY(CAPROLACTONE) BASED NANOCARRIERS: EFFECT ON THE SOLUBILIZATION AND HEMOLYTIC ACTIVITY OF AMPHOTERICIN B

A version of this chapter has been published in

**Macromolecular Bioscience 2010; 10, 648–656**

**Arash Falamarzian<sup>1</sup>, Afsaneh Lavasanifar<sup>1,2</sup>**

<sup>1</sup>Faculty of Pharmacy and Pharmaceutical Sciences, University of Alberta, Edmonton, Alberta, Canada,

<sup>2</sup>Department of Chemical and Material Engineering, University of Alberta, Edmonton, Alberta, Canada.

## 2.1. Introduction

Amphiphilic block copolymers can self-assemble to nanoscopic, core/shell structures in which the hydrophilic shell interfaces the media and the hydrophobic core acts as a nanoreservoir for the encapsulation and controlled delivery of potent water insoluble drugs [1, 2]. Among different block copolymers designed for drug delivery, those with poly(ethylene oxide) (PEO), as the hydrophilic block, and polyester as the hydrophobic block, are receiving increasing attention because of their biocompatibility and biodegradability. Previously, our research group reported on the introduction of functional side groups, i.e. benzyl and carboxyl, to the polyester segment of methoxy PEO-*b*-poly( $\epsilon$ -caprolactone) (MePEO-*b*-PCL) block copolymers [3]. This has provided additional opportunities for the chemical modification of the poly(ester) structure as means to modify the properties of resulting nano-carrier in terms of drug solubilization, drug release, thermodynamic as well as kinetic stability and biodegradation. In addition biodegradable self-assembling biomaterials that can incorporate chemically conjugated drugs (e.g., DOX) [4] or drug compatible structures (e.g., cholesterol) [5] within the micellar core, have been developed. The present study reports on the synthesis and self-assembly of another member of this family, MePEO-*b*-PCL copolymers with stearyl side groups on the PCL block, and the potential of nanocarriers formed from this structure for the solubilization and delivery of AmB in comparison to original MePEO-*b*-PCL nanocarriers and those with carboxyl groups on the PCL segment, i.e., MePEO-*block*-poly( $\alpha$ -carboxyl- $\epsilon$ -caprolactone) (MePEO-*b*-PCCL).

AmB is one of the most potent, antifungal agents in clinical practice [6]. Poor water solubility and severe side effects, are major drawbacks for AmB application [7]. The severe nephrotoxicity of its water-soluble formulation, Fungizone®, has restricted the clinical application of AmB [8, 9]. Three alternative lipid-base carriers of AmB can overcome the problem of poor water solubility and dose-dependent toxicity of AmB. However, unpredictable pharmacokinetics, toxic effects at higher AmB doses, emergence of infusion related reactions and high cost, have limited their benefit [10-12]. Different alternative formulation strategies that can potentially correct one or several of the mentioned shortcomings have been examined for AmB delivery [9, 13, 14], among which polymeric nano-formulations have been the focus of much interest [15-17]. Owing to nanoscopic dimensions and stealth properties, a PEO-*b*-PCL nano-formulation of AmB can reduce the distribution of AmB to the kidney and reticuloendothelial system upon intravenous administration, leading to reduced nephrotoxic and infusion related reactions against AmB while maintaining effective drug concentrations in blood for prolonged periods. This is facilitated by efficient encapsulation and *in vivo* stability of AmB within its polymeric carrier.

AmB contains several hydrogen bond-forming hydroxyl groups as well as a hydrophobic polyene chain in its structure (**Figure 1.4**). Hydrogen bonds and hydrophobic interactions between AmB and the block copolymer are expected to be major intermolecular forces that determine the extent of AmB encapsulation and stability within its polymeric nanocarrier [18]. The importance of hydrophobic interactions between AmB and polymer structure in enhancing the solubilization and controlling the

release of encapsulated AmB has been documented before [2, 19]. In this chapter, the effect of hydrophobic fatty acid and hydrogen bond-forming carboxyl substituents on the PCL on the solubilization and delivery AmB to rat red blood cell membrane by its polymeric nano-carrier was investigated.

## **2.2. Materials and methods**

### **2.2.1. Materials**

AmB, MePEO (average molecular weight of 5000 g/mol), diisopropylamine (99%), sodium (in kerosin), benzophenone, butyl lithium (Bu-Li) in hexane (2.5 M solution), pyrene, palladium-coated charcoal, stearyl alcohol (1-octadecanol), triton X 100 were purchased from Sigma, St. Louis, MO. Diisopropylamine was dried over calcium hydride at room temperature and freshly distilled before use.  $\epsilon$ -Caprolactone was purchased from Lancaster Synthesis, U.K., dried over calcium hydride for 48 h at room temperature, and freshly distilled before polymerization. Tetrahydrofuran (THF) was refluxed over sodium and benzophenone for several hours and distilled immediately before use. Stannous octoate was purchased from MP Biomedicals Inc., Germany, and used without further purification. Fluorescent probe 1,3-(1,1'-dipyrenyl)propane was purchased from Molecular Probes, U.S.A. 1,2 distearyl-sn-glycero-3-phosphocholine was from Syngena Inc. (Cambridge, MA, USA). Phosphotungstic acid solution 10% v/v was purchased from Sigma- Aldrich (Oakville, ON, Canada). Flogopite mica surface was purchased from Ted Pella Inc., (Redding, CA, USA). All other chemicals were reagent grade and were used as received.

## 2.2.2. Methods

### 2.2.2.1. Synthesis of block copolymers and their characterization

Synthesis of MePEO-*b*-PCL, MePEO-*block*-poly( $\alpha$ -benzylcarboxylate- $\epsilon$ -caprolactone) (MePEO-*b*-PBCL), MePEO-*b*-PCCL have been described in detail in our previous publications [3, 20]. In general, MePEO-*b*-PCL co-polymer was synthesized by ring opening polymerization of  $\epsilon$ -caprolactone using MePEO (molecular weight of 5000 g/mol) as initiator and stannous octoate as catalyst [20]. The molar feed ratio of monomer ( $\epsilon$ -caprolactone) to initiator (MePEO) was set at 44 to achieve MePEO-*b*-PCL block copolymers with PCL average molecular weights of 5000 g/mol.

MePEO-*b*-PBCL was synthesized, first, by preparing benzyl bearing monomer, i.e.,  $\alpha$ -benzyl carboxylate- $\epsilon$ -caprolactone. This procedure was followed by the synthesis of MePEO-*b*-PBCL co-polymer by ring opening polymerization of  $\alpha$ -benzylcarboxylate- $\epsilon$ -caprolactone using MePEO as initiator and stannous octoate as catalyst [3].

Preparation of MePEO-*b*-PCCL was accomplished by catalytic debenzylation of PEO-*b*-PBCL in the presence of charcoal coated with palladium as catalyst and hydrogen gas [3]. The degree of polymerization of the synthesized copolymers was estimated based on peak intensity ratio of the protons from MePEO (-CH<sub>2</sub>CH<sub>2</sub>O-,  $\delta$  3.65 ppm) to that of PCCL (-O-CH<sub>2</sub>-,  $\delta$  4.10 ppm).

MePEO-*b*-poly( $\alpha$ -stearly carboxylate- $\epsilon$ -caprolactone) (MePEO-*b*-PStCL) was synthesized by adding stearyl alcohol (12 eq.), DCC (10 eq.) and DMAP (10 eq.) to a

stirred solution of PEO-*b*-PCCL (63 mg) in dried THF (25 mL) (**Figure 2.1**). The reaction mixture was stirred for 4 days. The solvent was evaporated using nitrogen gas and the precipitate was dissolved in DMSO subsequently. The mixture was dialyzed against DMSO using a dialysis membrane with a MWCO=3500 g/mol for 24 h and later dialyzed against water for 48 h [21]. The resulting mixture was freeze dried and characterized by <sup>1</sup>H-NMR spectroscopy (Bruker 300 AM; Billerica MA) in CDCl<sub>3</sub>. The corresponding proton peaks were observed at  $\delta$  (ppm): 0.86 (m, 3H); 1.3 (s, 32H); 1.6-2 (m, 6H); 3.4 (m, 4H); 3.65 (s, 4H); 4.25 (m, 4H). The number of protons in the parentheses represents the corresponding number of protons in one ethylene oxide versus one stearyl caprolactone unimer in MePEO-*b*-PStCL block copolymer. The polymerization degree of  $\epsilon$ -caprolactone in PStCL block was estimated comparing the peak intensity of protons from caprolactone backbone (-O-CH<sub>2</sub>-,  $\delta$  4.10 ppm) to that of ethylene oxide (O-CH<sub>2</sub>-CH<sub>2</sub>-,  $\delta$  3.65 ppm). The stearic acid substitution level was estimated based on the peak intensity ratio of protons from stearic acid substituent on PStCL (-CH<sub>3</sub>,  $\delta$  0.85 ppm) to that of  $\epsilon$ -caprolactone backbone (-O-CH<sub>2</sub>-,  $\delta$  4.10 ppm).

#### **2.2.2.2. Characterization of block copolymers**

The number average molecular weight (M<sub>n</sub>) of prepared co-polymers were determined from <sup>1</sup>H NMR spectrum comparing the peak intensity of MePEO (-CH<sub>2</sub>CH<sub>2</sub>O-,  $\delta$  3.65 ppm) to that of PCL (-O-CH<sub>2</sub>-,  $\delta$  4.10 ppm), considering a 5000 g/mol molecular weight for MePEO. The M<sub>n</sub> and weight average molecular weight (M<sub>w</sub>) as well as polydispersity (M<sub>w</sub>/M<sub>n</sub>) of the prepared block copolymers were assessed by

gel permeation chromatography (GPC). Briefly, samples (20  $\mu$ L from 10 mg/mL polymer stock solutions in THF) were injected into a 4.6  $\times$  300 mm Waters Styragel HT4 column (Waters Inc., Milford, MA). The elution pattern was detected at 35  $^{\circ}$ C by refractive index (PD2000, Percision Detectors, Inc.)/light scattering detectors (Model 410, Waters Inc.). THF was used as eluent at a flow rate of 1.0 mL/min. The column was calibrated with a series of polystyrene standards of varying molecular weights ( $M_w$ : from 5900 g/mol to 13700 g/mol).

### **2.2.2.3. Assembly of block copolymers and characterization of self assembled structures**

Assembly of prepared block copolymers was achieved by dissolving copolymers (15 mg) in THF (1 mL) and dropwise addition ( $\sim$ 1 drop/15 s) of polymer solution to doubly distilled water (5 mL) under moderate stirring at 25  $^{\circ}$ C for 4 h. The resultant solution was dialyzed against doubly distilled water for 24 h. Average diameter (Z average) and size distribution of prepared particles were estimated by dynamic light scattering (DLS) using a Malvern Zetasizer 3000 at a polymer concentration of 2.5 mg/mL in water at 25  $^{\circ}$ C after centrifuging the nanoparticle solution at 11,600 $\times$ g for 5 min [4]. Morphology of the self-assembled structures was investigated by transmission electron microscopy (TEM) and atomic force microscopy (AFM). For TEM an aqueous droplet of nanoparticulate solution (20  $\mu$ L) with a polymer concentration of 1-1.5 mg/mL was placed on a copper coated grid. The grid was held horizontally for 20 s to allow the colloidal aggregates to settle. A drop of 2% solution of phosphotungstic acid (PTA) in

PBS (pH 7.0) was then added to provide the negative stain. After 1 min, the excess fluid was removed by filter paper. The samples were then air-dried and loaded into a Hitachi H 700 transmission electron microscope. Images were obtained at a magnification of  $\times 140000$  at 75 KV. The diameter of individual particles ( $n=50$ ) from micrographs was measured manually to obtain their average size. For AFM an aliquot (2  $\mu\text{L}$ ) of polymer solution (0.1 mg/mL) which was prepared using a THF/water system as described above was deposited on a freshly cleaved mica surface (flogopite,  $\text{KMg}_3\text{AlSi}_3\text{O}_{10}(\text{OH})_2$ ) and air dried at room temperature. Samples were imaged in air at room temperature and humidity with MFP-3D inverted optical atomic force microscopy (Digital Instruments, Santa Barbara, CA), equipped with a 120  $\mu\text{m}$   $xy$  and 6  $\mu\text{m}$   $z$  scanner for accurate length, height and force measurements. An integral silicon tip cantilevers (OMCL-AC160TS-W2, Olympus Cantilevers) with a spring constant of 10 pN/nm was used. AFM tapping mode imaging was done at scan rates of 1-1.5 Hz/line and set point of 600 mV. All the images were processed with a second-order flattening routine for background correction. A change in the fluorescence excitation spectra of pyrene in the presence of varied concentrations of MePEO-*b*-PStCL block copolymer was used to measure the critical aggregation concentration of block copolymers (CAC) as described before [22]. The viscosity of the hydrophobic domain in the nanoparticulate structure was estimated by measuring excimer to monomer intensity ratio ( $I_e/I_m$ ) from the emission spectra of 1,3-(1,1'-dipyrenyl) propane at 373 and 480 nm, respectively, as described in detail previously [1].

#### **2.2.2.4. Encapsulation of AmB in polymeric nanocarriers**

Encapsulation of AmB in MePEO-*b*-PCL, MePEO-*b*-PCCL, MePEO-*b*-PStCL nanoparticles was achieved by dialysis method. Briefly, prepared block copolymers (15 mg) and AmB (10 mg) were dissolved in THF (0.5 mL) and DMSO (0.5 mL), respectively, and mixed. This solution was added to 5 mL of doubly distilled water in a drop-wise manner. After 4 h stirring at room temperature, the resultant solution was dialyzed against doubly distilled water for 24 h. The aqueous solution of the nanocarrier formulation was then centrifuged at 11, 600 × g for 5 min to remove possible AmB precipitants. The hydrodynamic diameter of AmB loaded nanocarriers in the supernatant was measured by DLS as described above. Samples were frozen in dry ice/acetone and then freeze-dried (Virtis BenchTop Freeze Dryer). AmB loading level and encapsulation efficiency was determined by UV spectroscopy. To determine the level of encapsulated AmB, 100 μL aliquot of the supernatant solution was diluted with 6900 μL of DMSO to disrupt the nano-carrier structure and release the incorporated drug. The level of AmB was determined from its UV absorbance at 415 nm. The amount of polymer (mg) in 1 mL of nanoparticle solution was determined by subtracting the amount of AmB (mg) in 1 mL of solution from the total weight of dry powder in freeze dried sample. AmB loading and encapsulation efficiency were calculated by the following equations:

$$\text{Amphotericin B loading (w/w)(\%)} = \frac{\text{Amount of loaded AmB in mg}}{\text{Amount of copolymer in mg}} \times 100$$

$$\text{Encapsulation efficiency (\%)} = \frac{\text{Amount of loaded AmB in mg}}{\text{Amount of added AmB in mg}} \times 100$$

### **2.2.2.5. Assessing the hemolytic activity of AmB formulations against rat red blood cells (RBCs)**

Blood was collected from Sprague-Dawley rats (250-350 g) by cardiac puncture under anesthesia and centrifuged. Supernatant and buffy coat were removed. RBCs were washed and diluted with isotonic PBS, pH 7.4. The proper dilution factor was estimated from UV/VIS absorbance of hemoglobin at 576 nm in the supernatant after RBCs were lysed by 0.1 % triton X 100. Different empty polymeric nanocarriers, nanocarrier formulations of AmB and commercial formulation of AmB (Fungizone®) were incubated with diluted RBCs at 37 °C for 30 min and placed in ice afterwards to stop hemolysis. The unlysed RBCs were removed by centrifugation (11,600 × g for 30 s), and the supernatant was analyzed for hemoglobin at 576 nm using a microplate reader. The percent of hemolysis was determined using the following equation:

$$\text{Hemolysis (\%)} = \frac{(\text{Abs} - \text{Abs}_0)}{(\text{Abs}_{100} - \text{Abs}_0)} \times 100$$

where Abs, Abs<sub>0</sub>, and Abs<sub>100</sub> are the absorbances for the sample, control with no drug and control in the presence of hemolytic dose of 0.1 % triton X 100, respectively [23, 24].

### **2.2.2.6. Statistical Analysis**

Compiled data were presented as means ± SD. Where feasible, the data were analyzed for statistical significance by unpaired Student's test. The level of significance was set at  $P \leq 0.5$ .

## 2.3. Results

### 2.3.1. Preparation and characterization of block copolymers

The calculated molecular weight of MePEO-*b*-PCL, MePEO-*b*-PCCL block copolymers determined from their <sup>1</sup>H NMR spectra was found to be 10001 and 6779 g/mol, respectively. This corresponds to degrees of polymerization of 44 and 12 for  $\epsilon$ -caprolactone and  $\alpha$ -carboxyl- $\epsilon$ -caprolactone, respectively. The average molecular weight obtained by <sup>1</sup>H NMR spectroscopy was close to their molecular weight determined by GPC (Mn=9874 and 7382 g/mol for MePEO-*b*-PCL, and MePEO-*b*-PCCL, respectively) (**Table 2.1**). The composition of MePEO-*b*-PStCL (**Figure 2.1**) was confirmed by the analysis of its <sup>1</sup>H NMR spectra in CDCl<sub>3</sub> (**Figure 2.2**). The presence of characteristic peaks for stearyl moiety at  $\delta$  4.25 (-O-CH<sub>2</sub> protons),  $\delta$  1.3 (-(CH<sub>2</sub>)<sub>16</sub> protons) and  $\delta$  0.86 ppm (-CH<sub>3</sub> protons) confirmed the presence of pendant stearyl groups in the structure of the block copolymer. The degree of stearyl conjugation onto MePEO-*b*-PCCL was found to be 41 %. The calculated molecular weight of MePEO-*b*-PStCL block copolymer, determined from its <sup>1</sup>H NMR spectrum was found to be 8762 g/mol, which was close to the molecular weight determined by GPC (Mn= 8666) (**Table 2.1**). The resulting MePEO-*b*-PStCL copolymer showed a broader polydispersity ( $M_w/M_n=1.7$ ) compared to the unfunctionalized MePEO-*b*-PCL block copolymer ( $M_w/M_n=1.41$ ).

**Table 2.1.** Characteristics of synthesized block copolymers.

<b>Polymer<sup>a</sup></b>	<b>Side group on PCL</b>	<b>Conjugation level of side group on PCL block (%)</b>	<b>M<sub>n</sub> (g.mol<sup>-1</sup>)<sup>b</sup></b>	<b>M<sub>n</sub> (g.mol<sup>-1</sup>)<sup>c</sup></b>	<b>PDI<sup>d</sup></b>
PEO <sub>114</sub> - <i>b</i> -PCL <sub>44</sub>	-	-	10001	9874	1.41
PEO <sub>114</sub> - <i>b</i> -PCCL <sub>12</sub>	carboxyl	100	6779	7382	1.14
PEO <sub>114</sub> - <i>b</i> -PStCL <sub>12</sub>	stearyl	41	8762	8666	1.70

<sup>a</sup> The number showed as subscript indicates the polymerization degree of each block.

<sup>b</sup> Number average molecular weight of block copolymer measured by <sup>1</sup>H NMR.

<sup>c</sup> Number average molecular weight of block copolymer measured by GPC.

<sup>d</sup> Polydispersity index (*M<sub>w</sub>/M<sub>n</sub>*) measured by GPC.



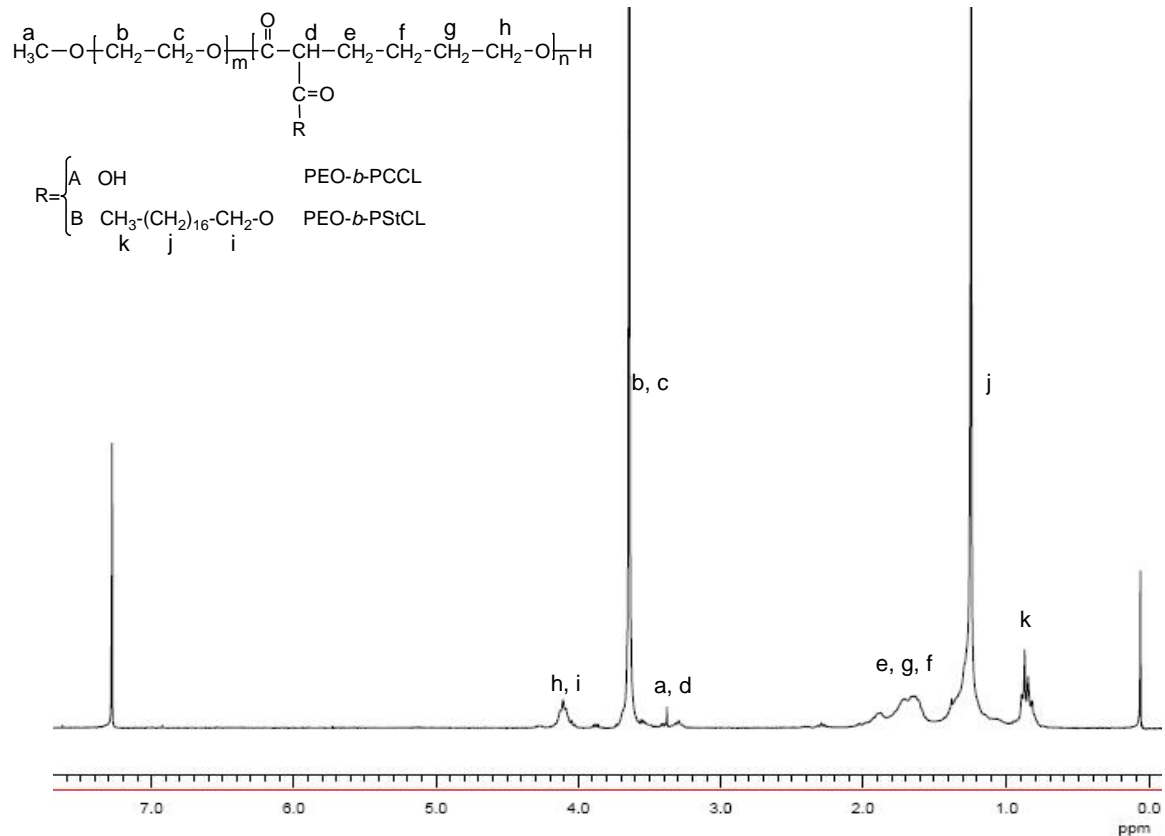


**Figure 2.2.** <sup>1</sup>H NMR spectra of MePEO-*b*-PStCL in CDCl<sub>3</sub> and peak assignments.

### 2.3.2. Assembly of block copolymers and characterization of self-assembled structures

The average diameter of MePEO-*b*-PStCL particles determined by the DLS technique was  $122\pm 7$  nm. On the other hand, particles formed from MePEO-*b*-PCL and MePEO-*b*-PCCL were found to be much smaller showing average diameters of  $43\pm 3$  and  $73\pm 18$  nm, respectively. The TEM picture of MePEO-*b*-PStCL particles showed the formation of true spherical particles having a clear boundary with an average diameter of  $60\pm 16$  nm (**Figure 2.3**), which is much smaller than the size obtained from DLS measurement. A tendency for aggregation was also evident from the TEM pictures. AFM images of MePEO-*b*-PStCL particles are shown in **Figure 2.4**, where the formation of spherical carriers is illustrated very clearly in the 3D images as well as the phase and height images. The CAC of synthesized block copolymer was found to decrease upon attachment of stearyl group. The CAC of MePEO-*b*-PStCL copolymer with a degree of polymerization (DP) of 12 in hydrophobic block was  $0.14\pm 0.01$   $\mu\text{M}$ , which was 1.29 and 80 times lower than that of MePEO-*b*-PCL ( $\epsilon$ -caprolactone DP=44) and MePEO-*b*-PCCL ( $\alpha$ -carboxyl- $\epsilon$ -caprolactone DP=12) nano-carriers, respectively (**Table 2.2**). The lower CAC value for MePEO-*b*-PStCL clearly shows the introduction of hydrophobic stearyl substituents makes the self-association of block copolymers thermodynamically more favorable. The MePEO-*b*-PStCL nanoparticles possessed viscous hydrophobic domains, as evidenced by the low  $I_e/I_m$  ratios ( $0.2\pm 0.03$ ). However, the  $I_e/I_m$  value of MePEO-*b*-PStCL was higher than that of MePEO-*b*-PCL and MePEO-*b*-PCCL particles (**Table 2.2**).

**Table 2.2.** Characteristics of empty nanocarriers (n = 3).

Polymer	Size (nm) $\pm$ SD <sup>b</sup>	PD $\pm$ SD <sup>c</sup>	CAC ( $\mu$ M) $\pm$ SD <sup>d</sup>	Ie/Im $\pm$ SD <sup>e</sup>
PEO <sub>114</sub> - <i>b</i> -PCL <sub>44</sub>	43 $\pm$ 3	0.22 $\pm$ 0.02	0.18 $\pm$ 0.01 <sup>f</sup>	0.08 $\pm$ 0.01
PEO <sub>114</sub> - <i>b</i> -PCCL <sub>12</sub>	73 $\pm$ 18	0.41 $\pm$ 0.11	11.2 $\pm$ 0.42 <sup>f*</sup>	0.09 $\pm$ 0.01
PEO <sub>114</sub> - <i>b</i> -PStCL <sub>12</sub> (41%) <sup>a</sup>	122 $\pm$ 7 <sup>*†</sup>	0.36 $\pm$ 0.01	0.14 $\pm$ 0.01 <sup>*†</sup>	0.20 $\pm$ 0.03 <sup>*†</sup>

<sup>a</sup> The number showed as subscript is the degree of stearyl conjugation calculated based on the <sup>1</sup>H NMR.

<sup>b</sup> Z average mean estimated by DLS technique.

<sup>c</sup> Polydispersity (PD) of size distribution estimated by DLS technique.

<sup>d</sup> Measured from the onset of a rise in the intensity ratio of peaks at 339 nm to peaks at 334 nm in the fluorescence excitation spectra of pyrene plotted versus logarithm of polymer concentration.

<sup>e</sup> Intensity ratio (excimer/monomer) from emission spectrum of 1,3-(1,1' dipyrenyl) propane in presence of polymeric nano-carriers.

<sup>f</sup> data are reproduced from our previous publications for comparison.

<sup>\*</sup>Significantly different from MePEO-*b*-PCL (P<0.05, unpaired student's test).

<sup>†</sup>Significantly different from MePEO-*b*-PCCL (P<0.05, unpaired student's test).

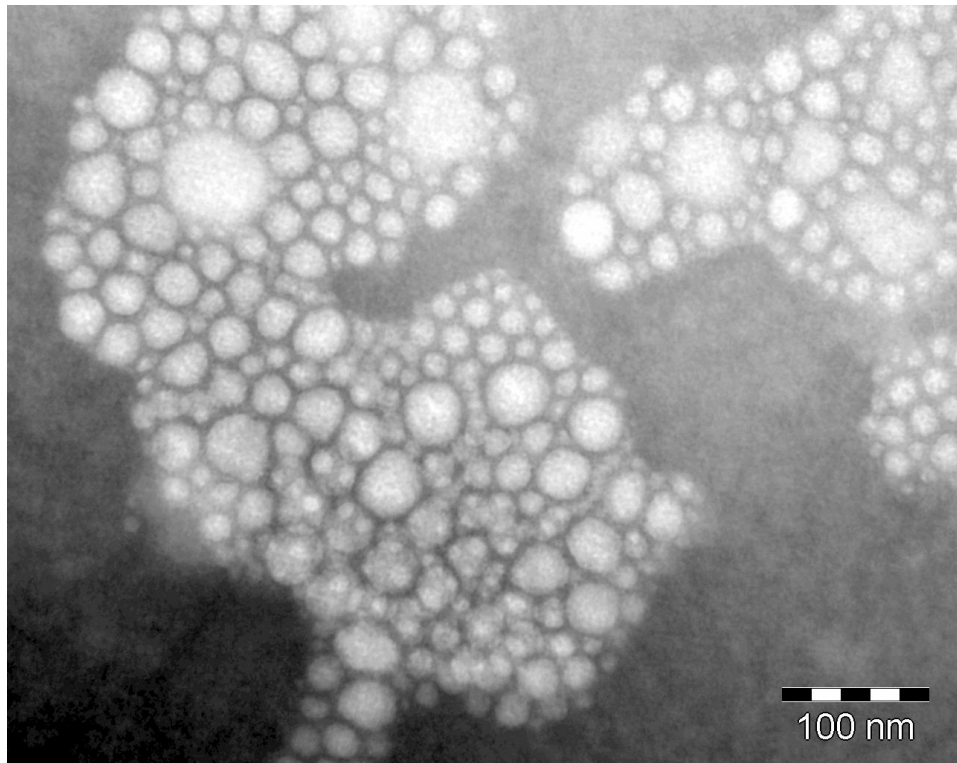


**Figure 2.3.** TEM picture of nanocarriers prepared from MePEO-*b*-PStCL block copolymer (magnification 140000). The bar on the images represents 100 nm.

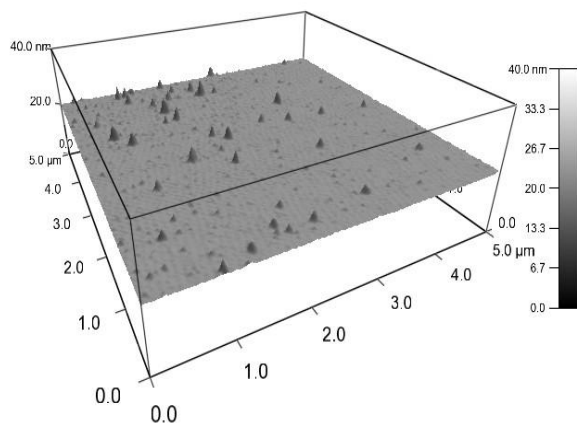
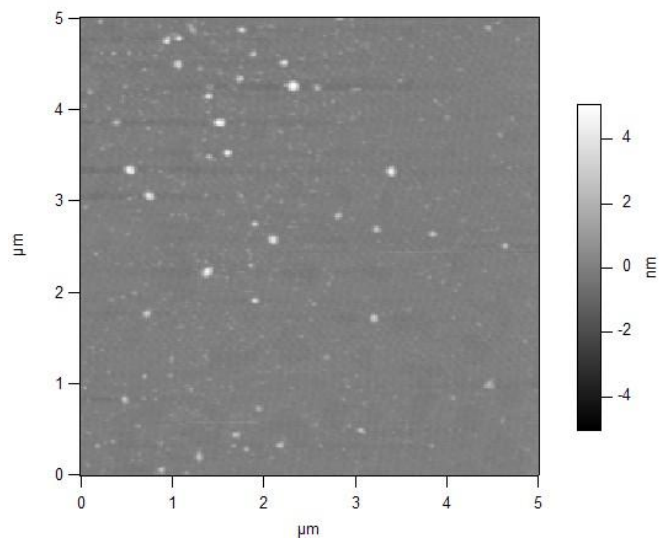


**Figure 2.4.** AFM height images of thin deposits prepared by drop-casting of 0.02 mg/mL MePEO-*b*-PStCL nanocarrier solution on mica.

### 2.3.3. Encapsulation of AmB in polymeric nanocarriers

The calculated AmB loading level (based on the drug to polymer weight percentage) for PCL, PCCL and PStCL core were 10.5, 35.6 and 29 %, respectively (**Table 2.3**). Compared to PCL core, the loading content was increased by 3.4- and 2.8-fold in MePEO-*b*-PCCL and MePEO-*b*-PStCL nano-carriers, respectively. The average size of the AmB-loaded MePEO-*b*-PCL, MePEO-*b*-PCCL nano-carriers measured by DLS technique was 196 and 141 nm, respectively, while the average size of MePEO-*b*-PStCL nano-carriers was found to be 183 nm (**Table 2.3**). A significant difference between the average diameters of unloaded and loaded carriers was observed for all three block copolymers under study ( $P \leq 0.05$ , unpaired student's t test).

**Table 2.3.** Characteristic of AmB-loaded nanocarriers. Polymer concentration used in this study was 2.5 mg/mL.

Polymer	AmB conc. ( $\mu\text{g/mL}$ ) $\pm$ SD	Encapsulation efficiency % $\pm$ SD	Loading level % (w/w) $\pm$ SD	Size (nm) $\pm$ SD <sup>d</sup>	PD $\pm$ SD <sup>e</sup>
PEO <sub>114</sub> - <i>b</i> -PCL <sub>44</sub>	222 $\pm$ 59 <sup>b</sup>	13.9 $\pm$ 3.8 <sup>b</sup>	10.5 $\pm$ 2.9 <sup>b</sup>	196 $\pm$ 10 <sup>b</sup>	0.37 $\pm$ 0.06 <sup>b</sup>
PEO <sub>114</sub> - <i>b</i> -PCCL <sub>12</sub>	543 $\pm$ 91 <sup>c,*</sup>	37.3 $\pm$ 5.5 <sup>c,*</sup>	35.6 $\pm$ 2.1 <sup>c,*</sup>	141 $\pm$ 10 <sup>c,*</sup>	0.26 $\pm$ 0.01 <sup>c</sup>
PEO <sub>114</sub> - <i>b</i> -PStCL <sub>12</sub> (41%) <sup>a</sup>	463 $\pm$ 40 <sup>c,*</sup>	29.7 $\pm$ 2.5 <sup>c,*</sup>	29.0 $\pm$ 3.7 <sup>c,*</sup>	183 $\pm$ 7 <sup>c,†</sup>	0.31 $\pm$ 0.01 <sup>c</sup>

<sup>a</sup>The number showed as subscript is the degree of stearyl conjugation calculated based on the <sup>1</sup>H NMR.

<sup>b</sup> Values are the average of four different measurements.

<sup>c</sup> Values are the average of three different measurements.

<sup>d</sup> Z average mean estimated by DLS technique.

<sup>e</sup> Polydispersity (PD) of size distribution estimated by DLS technique.

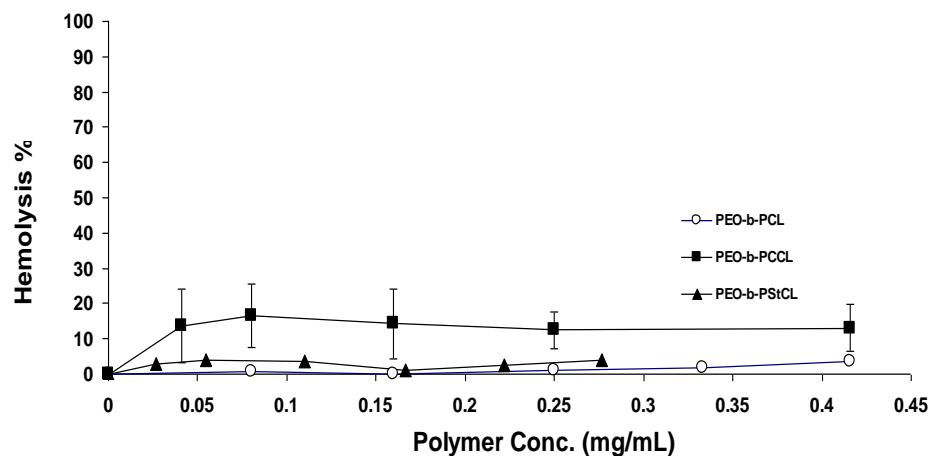
\*Significantly different from MePEO-*b*-PCL ( $P < 0.05$ , unpaired student's t test).

†Significantly different from MePEO-*b*-PCCL ( $P < 0.05$ , unpaired student's t test).

#### 2.3.4. Hemolytic activity of AmB encapsulated nanocarriers

The MePEO-*b*-poly(ester)s under study did not display a significant hemolytic activity at polymer concentration as high as 2.5 mg/mL (**Figure 2.5A**). Only MePEO-*b*-PCCL showed around 15 % hemolysis at 0.05-0.41 mg/mL concentration range. The commercial formulation of AmB, Fungizone® caused >90 % hemolysis against rat RBCs at AmB concentration of 30 µg/mL. At a similar concentration AmB loaded in MePEO-*b*-PCCL nano-carriers showed 66 % hemolysis. MePEO-*b*-PStCL started showing hemolysis at 15 µg/mL AmB concentrations. At 30 µg/mL AmB levels, its hemolysis as part of the latter formulation reached 50 %. The least hemolysis was shown by AmB in MePEO-*b*-PCL nano-carriers which only caused 15 % hemolysis at a similar AmB concentration (**Figure 2.5B**). The equivalent concentration of MePEO-*b*-PCL, MePEO-*b*-PCCL and MePEO-*b*-PStCL block copolymers in the hemolysis study was between 0.04-0.39, 0.02-0.12 and 0.02-0.14 mg/mL, respectively. This level was above the corresponding CACs for MePEO-*b*-PCL and MePEO-*b*-PStCL block copolymers (**Table 2.2**). However, in case of MePEO-*b*-PCCL, the polymer concentration fell below CAC at 0.075 mg/mL (equivalent to 26.7 µg/mL AmB) (**Figure 2.5B**).

A)



B)

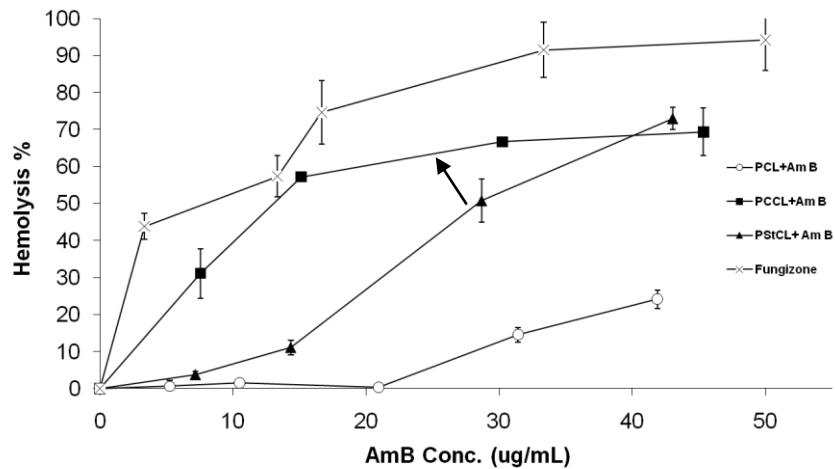


**Figure 2.5.** Hemolytic activity of **A)** Synthesized MePEO-*b*-poly(ester)s; **B)** Nanoparticle formulations of AmB and its commercial formulation (Fungizone®) against rat red blood cells. Each point represents average  $\pm$  standard error ( $n = 3$ ). The arrow indicates MePEO-*b*-PCCL polymer concentration that fell below CAC at 0.075 mg/mL (equivalent to 26.7  $\mu$ g/mL AmB).

## 2.4. Discussion

Our research group has previously reported on the preparation of self-associating MePEO-*b*-PCL block copolymers bearing carboxyl, benzyl and cholesteryl groups on the  $\alpha$ -carbon of caprolactone unit in the PCL block [3, 5]. Nanocarriers formed from self-assembly of MePEO-*b*-PCL bearing pendent benzyl groups on their PCL block have particularly shown superior capacity for the encapsulation and controlling the release of hydrophobic drugs containing aromatic as well as hydrogen bond forming groups in their structure [25]. A new member in this family of block copolymers, i.e, MePEO-*b*-PCL copolymers bearing aliphatic stearyl side groups on the PCL block were synthesized (**Figure 2.1**) and their potential in the solubilization of an aliphatic and amphiphilic drug, AmB, was assessed here. A similar strategy has proven to be successful in the solubilization and controlling the delivery of AmB from MePEO-*b*-poly(L-aspartic acid) based micellar carriers [2, 19].

Attachment of the stearyl moiety to the PCL segment of PEO-*b*-PCL was carried out through replacement of benzylcarboxylate groups in PEO-*b*-PBCL with carboxyl groups, and further esterification of the pendant carboxyl groups with stearyl alcohol, using DCC and DMAP as a coupling reagent and catalyst, respectively. The synthesized MePEO-*b*-PStCL block copolymers self-assembled to spherical nanocarriers with larger average diameter than that of PEO-*b*-PCL or PEO-*b*-PCCL (**Figure 2.3 and 2.4, Table 2.2**).

A decrease in the CAC of MePEO-*b*-PStCL block copolymer compared to MePEO-*b*-PCL despite shorter PCL backbone in MePEO-*b*-PStCL block copolymer was observed reflecting a higher tendency for self-association in MePEO-*b*-PStCL. In contrast, MePEO-*b*-PCCL block copolymers that have hydrophilic COOH groups on their PCL block showed a lower tendency for self-association [26]. The low CACs of polymeric nanocarriers reflect their thermodynamic stability that is important factor determining the stability of resulting nanocarriers in the biological system after dilution in blood upon intravenous administration [3, 27].

Moreover, the MePEO-*b*-PCL particles with no substituent on PCL, but longer PCL chains (DP=44) and MePEO-*b*-PCCL particles with carboxyl substituent on PCL, but shorter PCL chains (DP=12) showed similar viscosity in their hydrophobic domain, which was higher than the viscosity of hydrophobic domain in MePEO-*b*-PStCL (DP of PStCL=12) nanocarriers. The increase in the viscosity of hydrophobic domain in MePEO-*b*-PCCL particles despite shorter length of hydrophobic block compared to MePEO-*b*-PCL may be attributed to the formation of intraparticulate hydrogen bonding between carboxyl groups on PCCL segment. On the other hand, large size of stearyl substituents in PStCL core might have induced steric hindrance restricting the intraparticulate interactions of hydrophobic chains leading to lower viscosities. The rigidity of the hydrophobic domain in polymeric nanocarriers is believed to restrict dissociation of carrier and limit release of encapsulated drug [28].

Among different structures under study, MePEO-*b*-PCCL nanocarriers showed the most efficient solubilization of AmB (**Table 2.3**), perhaps due to formation of hydrogen bonds between the carboxyl groups of PCCL and hydroxyl groups of AmB. AmB is a drug containing both hydrophobic and hydrogen bond forming groups in its structure (**Figure 1.4**). Therefore, both polar and non-polar interactions with the polymer are expected to affect the extent of AmB solubilization as well as release from its polymeric carrier [29]. On the other hand, MePEO-*b*-PStCL copolymer showed higher encapsulation efficiency compared to MePEO-*b*-PCL, despite a shorter PCL backbone. This can be attributed to non-polar interactions between AmB and stearyl groups of the nanocarriers [19] and/or polar interactions between AmB and unconjugated COOH groups or extra carbonyl groups in MePEO-*b*-PStCL (in comparison to MePEO-*b*-PCL)[29][36]. Nonetheless, the presence of free carboxyl groups on PCL block seemed to positively impact AmB solubilization, as block copolymers with > 90% stearyl substitution showed reduced AmB solubilization (data not shown). In general, the extent of AmB solubilization achieved by MePEO-*b*-PCL, MePEO-*b*-PCCL and MePEO-*b*-PStCL nanocarriers at a polymer concentration of 2.5 mg/mL under current study, appears to be higher than AmB water solubility levels achieved by previously reported polymeric nanocarriers [30, 31].

The lowest hemolytic activity for encapsulated AmB was observed for MePEO-*b*-PCL followed by MePEO-*b*-PstCL and then MePEO-*b*-PCCL nanocarriers. Since the equivalent concentrations of MePEO-*b*-PCL and MePEO-*b*-PstCL in the hemolysis study were above their corresponding CACs, the dissociation of nanoparticles in the hemolysis

experiment was unlikely. Therefore, the lower hemolysis observed for AmB as part of MePEO-*b*-PCL nanocarrier, perhaps reflects a better control over the rate of AmB diffusion from these vehicles over MePEO-*b*-PStCL rather than micellar dissociation under experimental condition (**Figure 2.5B**) [7, 28]. The lower viscosity of hydrophobic domain in PStCL structure compared to that of PCL might have contributed to an increased release of encapsulated AmB causing more hemolysis for the PEO-*b*-PStCL compared to PEO-*b*-PCL formulation. However, in case of MePEO-*b*-PCCL, the polymer concentration fell below its CAC at 0.075 mg/mL polymer levels which was equivalent to AmB concentrations of 26.7  $\mu\text{g/mL}$ . Therefore the hemolysis observed for AmB as a part of MePEO-*b*-PCCL nanocarriers, might be a reflection of nano-carrier dissociation at AmB concentrations lower than 26.7  $\mu\text{g/mL}$ .

The argument made in the manuscript on the comparative solubilization and hemolytic profile of AmB from polymeric nanocarriers, is based on the assumption that the majority of AmB is located inside the hydrophobic domain of these nanocarriers. There is possibility for the incorporation of AmB in the core/shell interface or its interaction with PEO that needs to be also taken into account. Nonetheless, the results point to the importance of other factors, such as polar and non-polar polymer/drug as well as polymer/polymer interactions within the particles in defining the solubility and release of AmB from its polymeric carrier.

## 2.5. Conclusion

A new member of the family of functionalized PEO-*b*-PCL block copolymers bearing pendant stearyl groups on the PCL block, i.e., MePEO-*b*-PStCL, was successfully synthesized. A comparison between characteristics of nanoparticles formed from this structure and those from unmodified PEO-*b*-PCL or PEO-*b*-PCCL (bearing carboxyl groups on PCL) on AmB solubilization and delivery to red blood cell membrane was made. The results showed a reduced hemolytic activity for all polymeric nanoformulations of AmB under study over Fungizone®. Among polymeric nanocarriers, MePEO-*b*-PStCL and MePEO-*b*-PCCL showed similarly increased capacity for AmB encapsulation when compared to MePEO-*b*-PCL. However, minimum hemolytic activity was observed for AmB in MePEO-*b*-PCL followed by MePEO-*b*-PStCL and MePEO-*b*-PCCL nanoformulations. Thus, incorporation of hydrogen binding groups (like COOH) although effective in increasing AmB solubility, reduced the thermodynamic stability of micelles and was not effective in reducing AmB delivery to RBC membranes from its polymeric formulation. On the other hand, reaction of free COOH groups with hydrophobic stearyl substitutes at 41 % substitution level maintained the solubilization capacity of PEO-*b*-PCCL carrier, and reduced the hemolytic activity of solubilized AmB.

## 2.6. References

- [1] Lavasanifar A, Samuel J, Kwon GS. Micelles self-assembled from poly(ethylene oxide)-block-poly(N-hexyl stearate L-aspartamide) by a solvent evaporation method: effect on the solubilization and haemolytic activity of amphotericin B. *J Control Release* 2001;77:155-60.
- [2] Lavasanifar A, Samuel J, Sattari S, Kwon GS. Block copolymer micelles for the encapsulation and delivery of amphotericin B. *Pharmaceutical Research* 2002;19:418-22.
- [3] Mahmud A, Xiong XB, Lavasanifar A. Novel self-associating poly(ethylene oxide)-block-poly(epsilon-caprolactone) block copolymers with functional side groups on the polyester block for drug delivery. *Macromolecules* 2006;39:9419-28.
- [4] Mahmud A, Xiong XB, Lavasanifar A. Development of novel polymeric micellar drug conjugates and nano-containers with hydrolyzable core structure for doxorubicin delivery. *European Journal of Pharmaceutics and Biopharmaceutics* 2008;69:923-34.
- [5] Mahmud A, Patel S, Molavi O, Choi P, Samuel J, Lavasanifar A. Self-associating poly(ethylene oxide)-b-poly(alpha-cholesteryl carboxylate-epsilon-caprolactone) block copolymer for the solubilization of STAT-3 inhibitor cucurbitacin I. *Biomacromolecules* 2009;10:471-8.
- [6] Bekersky I, Fielding RM, Buell D, Lawrence I. Lipid-based amphotericin B formulations: from animals to man. *Pharmaceutical Science & Technology Today* 1999;2:230-6.
- [7] Bang JY, Song CE, Kim C, Park WD, Cho KR, Kim PI, et al. Cytotoxicity of Amphotericin B-incorporated Polymeric Micelles Composed of Poly(DL-lactide-co-glycolide)/dextran Graft Copolymer. *Archives of Pharmacal Research* 2008;31:1463-9.
- [8] Aramwit P, Yu BG, Lavasanifar A, Samuel J, Kwon GS. The effect of serum albumin on the aggregation state and toxicity of amphotericin B. *Journal of Pharmaceutical Sciences* 2000;89:1589-93.
- [9] Torrado JJ, Espada R, Ballesteros MP, Torrado-Santiago S. Amphotericin B formulations and drug targeting. *Journal of Pharmaceutical Sciences* 2008;97:2405-25.
- [10] Slain D. Lipid-based amphotericin B for the treatment of fungal infections. *Pharmacotherapy* 1999;19:306-23.
- [11] Boswell GW, Bekersky I, Buell D, Hiles R, Walsh TJ. Toxicological profile and pharmacokinetics of a unilamellar liposomal vesicle formulation of amphotericin B in rats. *Antimicrobial Agents and Chemotherapy* 1998;42:263-8.
- [12] Walsh TJ, Teppler H, Donowitz GR, Maertens JA, Baden LR, Dmoszynska A, et al. Caspofungin versus liposomal amphotericin B for empirical antifungal therapy in patients with persistent fever and neutropenia. *New England Journal of Medicine* 2004;351:1391-402.
- [13] Vyas SP, Gupta S. Optimizing efficacy of amphotericin B through nanomodification. *International Journal of Nanomedicine* 2006;1:417-32.
- [14] Sedlak M, Pravda M, Kubicova L, Mikulcikova P, Ventura K. Synthesis and characterisation of a new pH-sensitive amphotericin B - poly(ethylene glycol)-b-poly(L-lysine) conjugate. *Bioorganic & Medicinal Chemistry Letters* 2007;17:2554-7.

- [15] Wang CH, Wang WT, Hsiue GH. Development of polyion complex micelles for encapsulating and delivering amphotericin B. *Biomaterials* 2009;30:3352-8.
- [16] Vakil R, Kwon GS. Poly(ethylene glycol)-b-poly(epsilon-caprolactone) and PEG-phospholipid form stable mixed micelles in aqueous media. *Langmuir* 2006;22:9723-9.
- [17] Vandermeulen G, Rouxhet L, Arien A, Brewster ME, Preat V. Encapsulation of amphotericin B in poly(ethylene glycol)-block-poly(epsilon-caprolactone-co-trimethylenecarbonate) polymeric micelles. *International Journal of Pharmaceutics* 2006;309:234-40.
- [18] Patel SK, Lavasanifar A, Choi P. Prediction of the solubility of cucurbitacin drugs in self-associating poly(ethylene oxide)-b-poly(alpha-benzyl carboxylate varepsilon-caprolactone) block copolymer with different tacticities using molecular dynamics simulation. *Biomaterials* 2009.
- [19] Adams ML, Kwon GS. Relative aggregation state and hemolytic activity of amphotericin B encapsulated by poly(ethylene oxide)-block-poly(N-hexyl-L-aspartamide)-acyl conjugate micelles: effects of acyl chain length. *J Control Release* 2003;87:23-32.
- [20] Aliabadi HM, Mahmud A, Sharifabadi AD, Lavasanifar A. Micelles of methoxy poly(ethylene oxide)-b-poly(epsilon-caprolactone) as vehicles for the solubilization and controlled delivery of cyclosporine A. *J Control Release* 2005;104:301-11.
- [21] Li Y, Kwon GS. Methotrexate esters of poly(ethylene oxide)-block-poly(2-hydroxyethyl-L-aspartamide). Part I: Effects of the level of methotrexate conjugation on the stability of micelles and on drug release. *Pharmaceutical Research* 2000;17:607-11.
- [22] Zhao CL, Winnik MA, Riess G, Croucher MD. Fluorescence Probe Techniques Used to Study Micelle Formation in Water-Soluble Block Copolymers. *Langmuir* 1990;6:514-6.
- [23] Elhasi S, Astaneh R, Lavasanifar A. Solubilization of an amphiphilic drug by poly(ethylene oxide)-block-poly(ester) micelles. *European Journal of Pharmaceutics and Biopharmaceutics* 2007;65:406-13.
- [24] Xiong XB, Uludag H, Lavasanifar A. Biodegradable amphiphilic poly(ethylene oxide)-block-polyesters with grafted polyamines as supramolecular nanocarriers for efficient siRNA delivery. *Biomaterials* 2009;30:242-53.
- [25] Molavi O, Ma ZS, Mahmud A, Alshamsan A, Samuel J, Lai R, et al. Polymeric micelles for the solubilization and delivery of STAT3 inhibitor cucurbitacins in solid tumors. *International Journal of Pharmaceutics* 2008;347:118-27.
- [26] Lee JY, Cho EC, Cho K. Incorporation and release behavior of hydrophobic drug in functionalized poly(D,L-lactide)-block-poly(ethylene oxide) micelles. *Journal of Controlled Release* 2004;94:323-35.
- [27] Nishiyama N, Kataoka K. Nanostructured devices based on block copolymer assemblies for drug delivery: Designing structures for enhanced drug function. *Polymer Therapeutics II: Polymers as Drugs, Conjugates and Gene Delivery Systems* 2006;193:67-101.
- [28] Lavasanifar A, Samuel J, Kwon GS. The effect of alkyl core structure on micellar properties of poly(ethylene oxide)-block-poly(L-aspartamide) derivatives. *Colloids Surf B Biointerfaces* 2001;22:115-26.

- [29] Patel SK, Lavasanifar A, Choi P. Roles of nonpolar and polar intermolecular interactions in the improvement of the drug loading capacity of PEO-b-PCL with increasing PCL content for two hydrophobic Cucurbitacin drugs. *Biomacromolecules* 2009;10:2584-91.
- [30] Adams ML, Andes DR, Kwon GS. Amphotericin B encapsulated in micelles based on poly(ethylene oxide)-block-poly(L-amino acid) derivatives exerts reduced in vitro hemolysis but maintains potent in vivo antifungal activity. *Biomacromolecules* 2003;4:750-7.
- [31] Vakil R, Kwon GS. Poly(ethylene glycol)-b-poly(epsilon-caprolactone) and PEG-phospholipid form stable mixed micelles in aqueous media. *Langmuir* 2006;22:9723-9.

## **CHAPTER THREE**

### **OPTIMIZATION OF THE HYDROPHOBIC DOMAIN IN POLY(ETHYLENE OXIDE)-POLY( $\epsilon$ -CAPROLACTONE) BASED NANOCARRIERS FOR THE SOLUBILIZATION AND DELIVERY OF AMPHOTERICIN B**

A version of this chapter has been published in

**Colloids and Surfaces B: Biointerfaces 81 (2010) 313–320**

**Arash Falamarzian<sup>1</sup>, Afsaneh Lavasanifar<sup>1,2</sup>**

<sup>1</sup>Faculty of Pharmacy and Pharmaceutical Sciences, University of Alberta, Edmonton, Alberta, Canada,

<sup>2</sup>Department of Chemical and Material Engineering, University of Alberta, Edmonton, Alberta, Canada.

### 3.1. Introduction

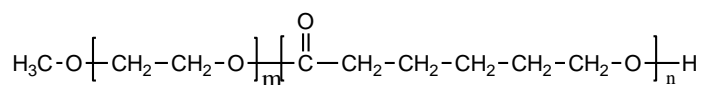
Amphotericin B (AmB) is the most potent, membrane active polyene macrolide antifungal agent used to treat systemic mycosis in clinical practice [1-3]. Poor water solubility and severe toxicity are major drawbacks for AmB application [4, 5]. Although current clinical formulations of AmB have been successful in increasing AmB solubility in water, they each have several limitations as detailed in previous chapters.

The long term objective of this study is to develop a polymer based nanocarrier that can overcome the limitations of current AmB formulations and enhance the therapeutic benefit of this potent anti-fungal agent in clinic [6-9],[10-13]. It is widely believed that AmB acts by interacting more explicitly with the ergosterol in fungal cell membrane, but it also interacts with cholesterol of the mammalian cell membrane [14, 15]. Success in the development of a better formulation for AmB will be defined by the ability of the drug carrier in the solubilization of AmB and controlling its release leading to a reduction in AmB interaction and toxicity towards mammalian cells. The level of AmB solubilization and release both will depend on the strength of interactions between drug and polymeric carrier. In the previous chapter we have reported on the chemical modification of polymeric nanocarriers based on methoxy-poly(ethylene oxide)-*block*-poly( $\epsilon$ -caprolactone) (MePEO-*b*-PCL) for AmB delivery. Our results showed better solubilization of AmB by nanocarriers containing hydrogen bond-forming carboxyl groups and/or stearyl modifications in their core structure compared to the original PCL core.

However, the introduction of free carboxyl in the core structure had a negative impact on the thermodynamic stability of nanocarriers and hemolytic activity of encapsulated AmB. When 40 % of carboxyl groups in the core were esterified with stearic acid, AmB solubility was still higher than what was achieved with original MePEO-*b*-PCL micelles. The hemolytic activity of encapsulated AmB; however, was higher than what observed with MePEO-*b*-PCL formulation and lower than that for micelles containing 100 % free carboxyls in the core [16]. The results of that study pointed to the potential of PCL modified MePEO-*b*-PCL nanocarriers in achieving an optimum formulation for AmB, but showed the necessity for further efforts in finding the right substituent on PCL.

In this chapter, a new member of MePEO-*b*-PCL copolymers family with palmitoyl substitutes at 100 % substitution level on the PCL block was synthesized, and the nanocarriers formed from this structure were compared to original MePEO-*b*-PCL, and those with benzyl or cholesteryl groups on the core structure (at 100 % substitution level), i.e., MePEO-*block*-poly( $\alpha$ -benzyl- $\epsilon$ -caprolactone) (MePEO-*b*-PBCL) and MePEO-*block*-poly( $\alpha$ -cholesteryl carboxylate- $\epsilon$ -caprolactone) (MePEO-*b*-PChCL), respectively (**Figure 3.1**) for the solubilization and delivery of AmB. In the biological system, AmB is carried by lipoproteins which are the carriers of cholesterol and fatty acid esters as well [17, 18]. Moreover, previous research has shown the interaction of AmB with cholesterol in MePEO-DSPE/cholesterol [1] micellar structures and with acyl chains in micelles composed of MePEO-*b*-poly(amino acid)s modified with fatty acid esters in the core [19]. Owing to favorable interactions between AmB and cholesteryl or fatty acid ester,

MePEO-*b*-PCL nanocarriers with these substituent structures in the core, were expected to provide better solubilization and reduced delivery of AmB to mammalian cell membrane leading to attenuated hemolytic activity when compared to original MePEO-*b*-PCL nanocarriers. The validity of this hypothesis was evaluated here.



PEO-*b*-PCL

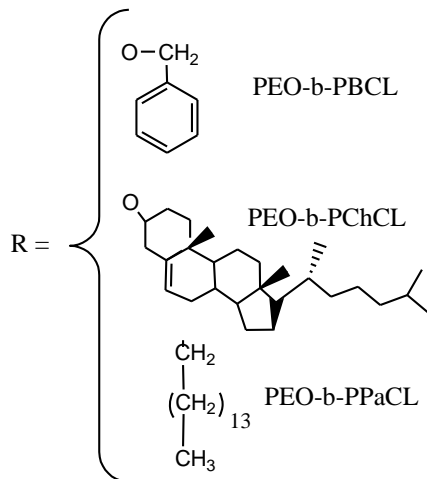
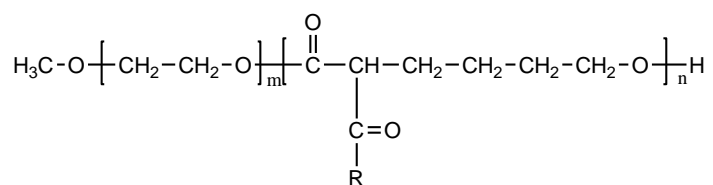


**Figure 3.1.** Chemical structure MePEO-*b*-poly(ester)s polymers used in this study.

## **3.2. Materials and methods**

### **3.2.1. Materials**

Amphotericin B (AmB), MePEO (average molecular weight of 5000 g.mol<sup>-1</sup>), diisopropylamine (99%), sodium (in kerosin), benzophenone, butyl lithium (Bu-Li) in hexane (2.5 M solution), palladium-coated charcoal, palmitoyl chloride, cholesteryl chloroformate, triton X 100 were purchased from Sigma, St. Louis, MO. Diisopropylamine was dried over calcium hydride at room temperature and freshly distilled before use.  $\epsilon$ -Caprolactone was purchased from Lancaster Synthesis, U.K., dried over calcium hydride for 48 h at room temperature, and freshly distilled before polymerization. Tetrahydrofuran (THF) was refluxed over sodium and benzophenone for several hours and distilled immediately before use. Stannous octoate was purchased from MP Biomedicals Inc., Germany, and used without further purification. Fluorescent probe 1,3-(1,1'-dipyrenyl)propane was purchased from Molecular Probes, U.S.A. 1,2-distearoyl-sn-glycero-3-phosphocholine was from Syngena Inc. (Cambridge, MA, USA). Phosphotungstic acid solution 10% v/v was purchased from Sigma-Aldrich (Oakville, ON, Canada). All other chemicals were reagent grade and were used as received.

### **3.2.2. Methods**

#### **3.2.2.1. Synthesis of block copolymers and their characterization**

Synthesis of MePEO-*b*-PCL, MePEO-*b*-PBCL and MePEO-*b*-PChCL have been described in detail in our previous publications [20-22]. In general, MePEO-*b*-PCL co-

polymer was synthesized by ring opening polymerization of  $\epsilon$ -caprolactone using MePEO (molecular weight of  $5000 \text{ g}\cdot\text{mol}^{-1}$ ) as initiator and stannous octoate as catalyst [20]. The molar feed ratio of monomer ( $\epsilon$ -caprolactone) to initiator (MePEO) was set at 44 to achieve MePEO-*b*-PCL block copolymers with PCL average molecular weights of  $5000 \text{ g/mol}$ .

MePEO-*b*-PBCL was synthesized, first, by preparing benzyl bearing monomer, i.e.,  $\alpha$ -benzyl carboxylate- $\epsilon$ -caprolactone. This procedure was followed by the synthesis of MePEO-*b*-PBCL co-polymer by ring opening polymerization of  $\alpha$ -benzylcarboxylate- $\epsilon$ -caprolactone using MePEO as initiator and stannous octoate as catalyst [22]. Similar procedure using cholesteryl bearing monomer i.e.,  $\alpha$ -cholesteryl carboxylate- $\epsilon$ -caprolactone was used to prepare MePEO-*b*-PChCL [21].

Palmitoyl bearing monomer, i.e.,  $\alpha$ -palmitoyl- $\epsilon$ -caprolactone, was synthesized as shown in **Figure 3.2** [21, 22]. Briefly, Bu-Li (24 mL) in hexane was slowly added to dry diisopropylamine (8.4 mL) in 60 mL of dry tetrahydrofuran (THF) in a three-neck round-bottomed flask at  $-30 \text{ }^\circ\text{C}$  under vigorous stirring with continuous argon supply. The solution was cooled to  $-78 \text{ }^\circ\text{C}$ .  $\epsilon$ -Caprolactone (3.42 g) was dissolved in 8 mL of dry THF and added to the above-mentioned mixture slowly. The temperature was allowed to rise to  $0 \text{ }^\circ\text{C}$  followed by the addition of palmitoyl chloride (8.246 g). The reaction was quenched with 5 mL of saturated ammonium chloride solution. The reaction mixture was diluted with water and extracted with ethyl acetate. The combined extracts were dried over  $\text{Na}_2\text{SO}_4$  and evaporated. The yellowish semisolid crude mixture was purified twice

over a silica gel column using hexane:ethyl acetate at 4:1 ratio as eluent. The purity of the compound was confirmed with thin-layer chromatography (TLC). The chemical structure of product was analyzed by  $^1\text{H}$  NMR spectroscopy (Bruker 300 AM; Billerica MA) using  $\text{CDCl}_3$  as solvent. Corresponding proton peaks were observed at  $\delta$  (ppm): 0.85 (t, 3H); 1.25 (s, 26H); 1.6-2.1 (m, 6H); 2.6 (m, 2H); 3.65 (dd, 1H); 4.3 (m, 2H). Palmitoyl group bearing block copolymer, i.e., MePEO-*b*-PPaCL, was synthesized by ring opening polymerization of  $\alpha$ -palmitoyl- $\epsilon$ -caprolactone using MePEO as initiator and stannous octoate as catalyst according to the procedure reported by our group in a previous publication [22]. Briefly, MePEO (MW: 5000  $\text{g}\cdot\text{mol}^{-1}$ ) (300 mg),  $\alpha$ -palmitoyl- $\epsilon$ -caprolactone (300 mg), and stannous octoate (0.002 equiv of monomer) were added to a 10 mL previously flamed ampule, nitrogen purged and sealed under vacuum. The polymerization reaction was allowed to proceed for 4 h at 160  $^\circ\text{C}$  in oven, by vortexing the mixture every 30 minutes. The reaction was terminated by cooling the product to room temperature.  $^1\text{H}$  NMR spectrum of MePEO-*b*-PPaCL in  $\text{CDCl}_3$  at 300 MHz was used to assess the conversion of  $\alpha$ -palmitoyl  $\epsilon$ -caprolactone monomer to PPaCL comparing the peak intensities of methylene protons ( $-\text{O}-\text{CH}_2-$ ,  $\delta$  4.28 ppm) of  $\alpha$ -palmitoyl- $\epsilon$ -caprolactone monomer to the intensity of the same proton of PPaCL ( $-\text{O}-\text{CH}_2$ ,  $\delta$  4.10 ppm). In  $^1\text{H}$  NMR spectroscopy in  $\text{CDCl}_3$  for MePEO-*b*-PPaCL corresponding proton peaks were observed at  $\delta$  (ppm): 0.85 (t, 3H); 1.25 (s, 26H); 1.6-2.1 (m, 6H); 2.4 (m, 2H); 3.4 (m, 4H); 3.65 (s, 4H); 4.10 (t, 2H). The number of protons in the parentheses represents the corresponding number of protons in one ethylene oxide versus one palmitoyl caprolactone unit in the MePEO-*b*-PPaCL block copolymer.

### 3.2.2.2. Characterization of block copolymers

The number average molecular weight ( $M_n$ ) of prepared co-polymers were determined from  $^1\text{H}$  NMR spectrum comparing the peak intensity of MePEO (- $\text{CH}_2\text{CH}_2\text{O}$ -,  $\delta$  3.65 ppm) to that of PCL (- $\text{O}-\text{CH}_2$ -,  $\delta$  4.10 ppm), considering a 5000 g/mol molecular weight for MePEO. The  $M_n$  and weight average molecular weight ( $M_w$ ) as well as polydispersity ( $M_w/M_n$ ) of the prepared block copolymers were assessed by gel permeation chromatography (GPC). Briefly, samples (20  $\mu\text{L}$  from 10 mg/mL polymer stock solutions in THF) were injected into a  $4.6 \times 300$  mm Waters Styragel HT4 column (Waters Inc., Milford, MA). The elution pattern was detected at 35  $^\circ\text{C}$  by refractive index (PD2000, Percision Detectors, Inc.)/light scattering detectors (Model 410, Waters Inc.). THF was used as eluent at a flow rate of 1.0 mL/min. The column was calibrated with a series of polystyrene standards of varying molecular weights ( $M_w$ : from 5900 g/mol to 13700 g/mol).

### 3.2.2.3. Assembly of block copolymers and characterization of self-assembled structures

Assembly of prepared block copolymers was achieved by dissolving prepared block copolymers (15 mg) in THF (1 mL) and dropwise addition ( $\sim$ 1 drop/15 s) of polymer solution to doubly distilled water (5 mL) under moderate stirring at 25  $^\circ\text{C}$  for 4 h. The resultant solution was dialyzed against doubly distilled water for 24 h. Average diameter (Z average) and size distribution of prepared particles were estimated by dynamic light scattering (DLS) using a Malvern Zetasizer 3000 at a polymer

concentration of 2.5 mg/mL in water at 25 °C after centrifuging the nanoparticle solution at 11,600×g for 5 min [23]. Morphology of the self-assembled structures was investigated by transmission electron microscopy (TEM). For TEM an aqueous droplet of nanoparticulate solution (20 μL) with a polymer concentration of 1-1.5 mg/mL was placed on a copper coated grid. The grid was held horizontally for 20 s to allow the colloidal aggregates to settle. A drop of 2% solution of phosphotungstic acid (PTA) in PBS (pH 7.0) was then added to provide the negative stain. After 1 min, the excess fluid was removed by filter paper. The samples were then air-dried and loaded into a Hitachi H 700 transmission electron microscope (TEM). Images were obtained at a magnification of ×36000 at 75 KV. The diameter of individual particles ( $n=50$ ) from micrographs was measured manually to obtain their average size. The viscosity of the hydrophobic domain in the nanoparticulate structure was estimated by measuring excimer to monomer intensity ratio ( $I_e/I_m$ ) from the emission spectra of 1,3-(1,1'-dipyrenyl) propane at 373 and 480 nm, respectively, as described in detail previously [24].

#### **3.2.2.4. Encapsulation of AmB in polymeric nanocarriers**

Encapsulation of AmB in MePEO-*b*-PCL, MePEO-*b*-PBCL, MePEO-*b*-PChCL, and MePEO-*b*-PPaCL nano-carriers was achieved by dialysis method. Briefly, prepared block copolymers (15 mg) and AmB (4 or 10 mg) were dissolved in THF (0.5 mL) and DMSO (0.5 mL), respectively, and mixed. This solution was added to 5 mL of doubly distilled water in a drop-wise manner. After 4 h stirring at room temperature, the resultant solution was dialyzed against doubly distilled water for 24 h. The aqueous solution of the

nanocarrier formulation was then centrifuged at  $11,600 \times g$  for 5 min to remove possible AmB precipitants. The hydrodynamic diameter of AmB loaded nanocarriers in the supernatant was measured by DLS as described above. Samples were frozen in dry ice/acetone and then freeze-dried (Virtis BenchTop Freeze Dryer). AmB loading level and encapsulation efficiency was determined using UV spectroscopy. To determine the level of encapsulated AmB, 100  $\mu\text{L}$  aliquot of the supernatant solution was diluted with 6900  $\mu\text{L}$  or 3900  $\mu\text{L}$  of DMSO to disrupt the nanocarrier structure and release incorporated drug. The level of AmB was determined from its UV absorbance at 415 nm. AmB loading and encapsulation efficiency were calculated by **equations (3.1)** and **(3.2)**, respectively. The amount of copolymer (in mg) in 1 mL of nanoparticle solution in **equation (3.1)** was determined by subtracting the amount of AmB (mg) in 1 mL of solution from the total weight of the dry powder in freeze dried sample:

**(3.1)**

$$\text{Amphotericin B loading (w/w)(\%)} = \frac{\text{Amount of loaded AmB in mg}}{\text{Amount of copolymer in mg}} \times 100$$

**(3.2)**

$$\text{Encapsulation efficiency (\%)} = \frac{\text{Amount of loaded AmB in mg}}{\text{Amount of added AmB in mg}} \times 100$$

### **3.2.2.5. Assessing the hemolytic activity of AmB formulations against rat red blood cells (RBCs)**

Blood was collected from Sprague-Dawley rats (250-350 g) by cardiac puncture under anesthesia and centrifuged. Supernatant and buffy coat were removed. RBCs were

washed and diluted with isotonic PBS, pH 7.4. The proper dilution factor was estimated from UV/VIS absorbance of hemoglobin at 576 nm in the supernatant after RBCs were lysed by 0.1 % triton X 100. Different empty polymeric nanocarriers, nanocarrier formulations of AmB and commercial formulation of AmB (Fungizone<sup>®</sup>) were incubated with diluted RBCs at 37 °C for 30 min and placed in ice afterwards to stop hemolysis. The unlysed RBCs were removed by centrifugation (11,600 × g for 30 s), and the supernatant was analyzed for hemoglobin at 576 nm using a microplate reader. The percent of hemolysis was determined using the following **equation (3.3)**:

$$(3.3) \quad \text{Hemolysis (\%)} = \frac{(\text{Abs} - \text{Abs}_0)}{(\text{Abs}_{100} - \text{Abs}_0)} \times 100$$

where Abs, Abs<sub>0</sub>, and Abs<sub>100</sub> are the absorbances for the sample, control with no drug and control in the presence of hemolytic dose of 0.1 % triton X 100, respectively [25, 26].

### 3.2.2.6. Statistical Analysis

Compiled data were presented as means ± SE. Where feasible, the data were analyzed for statistical significance by unpaired Student's test. The level of significance was set at  $P \leq 0.5$ .

## 3.3. Results

### 3.3.1. Preparation and characterization of Block Copolymers

The structures of MePEO-*b*-PCL, MePEO-*b*-PBCL, and MePEO-*b*-PChCL block copolymers were confirmed by the analysis of their  $^1\text{H}$  NMR spectra [21, 27]. Their calculated number average molecular weights ( $M_n$ ) determined from their  $^1\text{H}$  NMR spectra were found to be 10001, 9526 and 12400 g/mol, respectively, which were close to their molecular weight determined by GPC ( $M_n=9874$ , 10428 and 11800 g/mol, respectively) (**Table 3.1**). The structure of monomer,  $\alpha$ -palmitoyl- $\epsilon$ -caprolactone (**Figure 3.2**), was confirmed by  $^1\text{H}$  NMR spectroscopy (**Figure 3.3**). In the  $^1\text{H}$  NMR spectrum the peak at  $\delta$  3.65 ppm for  $\alpha$ -palmitoyl  $\epsilon$ -caprolactone, which corresponds to a single proton instead of two protons of  $\epsilon$ -caprolactone monomer, indicates the successful substitution of the palmitoyl on  $\epsilon$ -caprolactone monomer at the  $\alpha$ -position. The structure of MePEO-*b*-PPaCL block copolymer was confirmed with  $^1\text{H}$  NMR spectrum in  $\text{CDCl}_3$  (**Figure 3.5**). The presence of characteristic peaks for palmitoyl moiety at  $\delta$  0.85 ( $-\text{CH}_3$  protons),  $\delta$  1.25 ( $-(\text{CH}_2)_{13}$  protons) and  $\delta$  2.4 ( $-\text{O}=\text{C}-\text{CH}_2$ ) confirm the presence of pendant palmitoyl group in the structure of block copolymer. Furthermore, the characteristic downfield shift of  $-\text{OCH}_2-$  protons (from  $\delta$  4.25 to 4.10 ppm) and  $\text{O}=\text{C}-\text{CH}-$  proton (from  $\delta$  3.65 to 3.4 ppm) of caprolactone backbone in the  $^1\text{H}$  NMR spectra (**Figure 3.3 and 3.5**) strongly indicates the ring opening polymerization of the monomer and formation of block copolymer. The calculated molecular weight of PPaCL block, determined by comparing the peak intensity of MePEO ( $-\text{CH}_2-\text{CH}_2-$ ) at  $\delta$  3.65 ppm to that of PPaCL ( $-\text{CH}_2-\text{O}-$ ) at  $\delta$  4.10 ppm (**Figure 3.5**) was found to be 3063 g/mol (indicates degree of polymerization of 14). Therefore, total molecular weight of the synthesized MePEO-*b*-PPaCL block copolymer obtained from  $^1\text{H}$  NMR was calculated to be 8063 g/mol.

**Table 3.1.** Characteristics of synthesized block copolymers.

<b>Polymer<sup>a</sup></b>	<b>Theoretical M.Wt. (g/mol)</b>	<b>M<sub>n</sub> (g/mol)<sup>b</sup></b>	<b>M<sub>n</sub> (g/mol)<sup>c</sup></b>	<b>PDI<sup>d</sup></b>
PEO <sub>114</sub> - <i>b</i> -PCL <sub>44</sub>	10000	10001	9874	1.41
PEO <sub>114</sub> - <i>b</i> -PBCL <sub>20</sub>	9962	9526	10428	1.25
PEO <sub>114</sub> - <i>b</i> -PChCL <sub>18</sub>	14500	12400	11800	1.53
PEO <sub>114</sub> - <i>b</i> -PPaCL <sub>14</sub>	9928	8063	N/A	N/A

<sup>a</sup>The number showed as subscript indicates the polymerization degree of each block.

<sup>b</sup>Number average molecular weight of block copolymer measured by <sup>1</sup>H NMR.

<sup>c</sup>Number average molecular weight of block copolymer measured by GPC.

<sup>d</sup>Polydispersity index (*M<sub>w</sub>/M<sub>n</sub>*) measured by GPC.

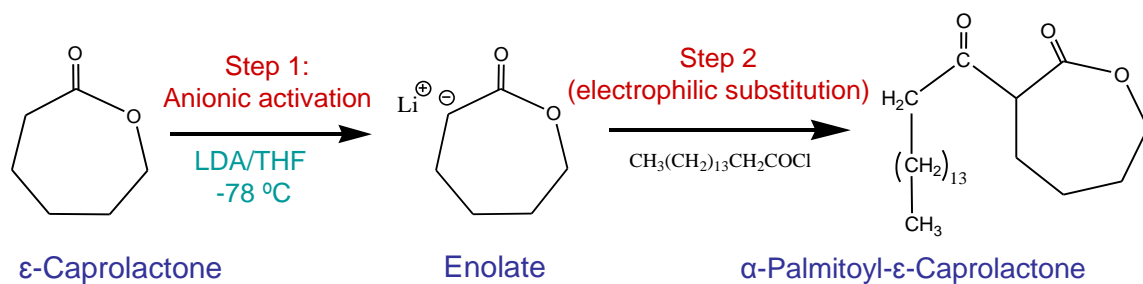


**Figure 3.2.** Synthetic scheme for the preparation of  $\alpha$ -palmitoyl  $\epsilon$ -caprolactone.

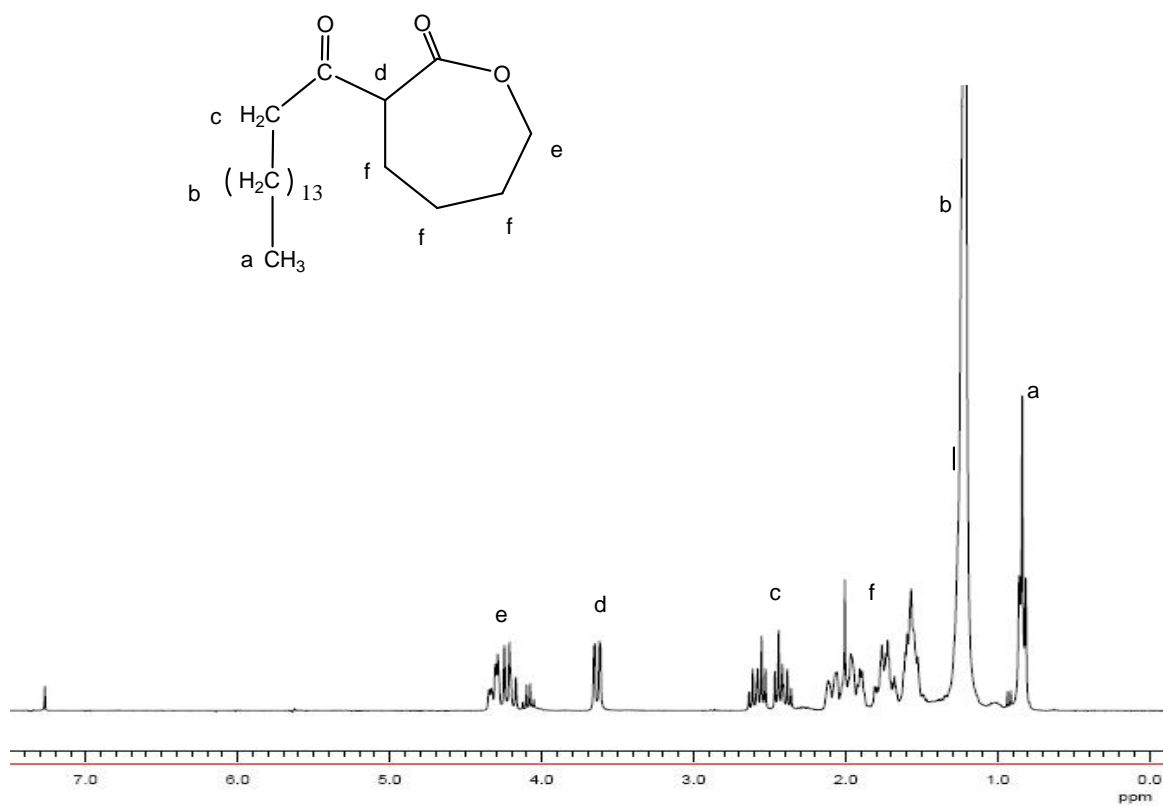


**Figure 3.3.** <sup>1</sup>H NMR spectra of  $\alpha$ -palmitoyl  $\epsilon$ -caprolactone (substituted monomer) in CDCl<sub>3</sub> and peak assignments.

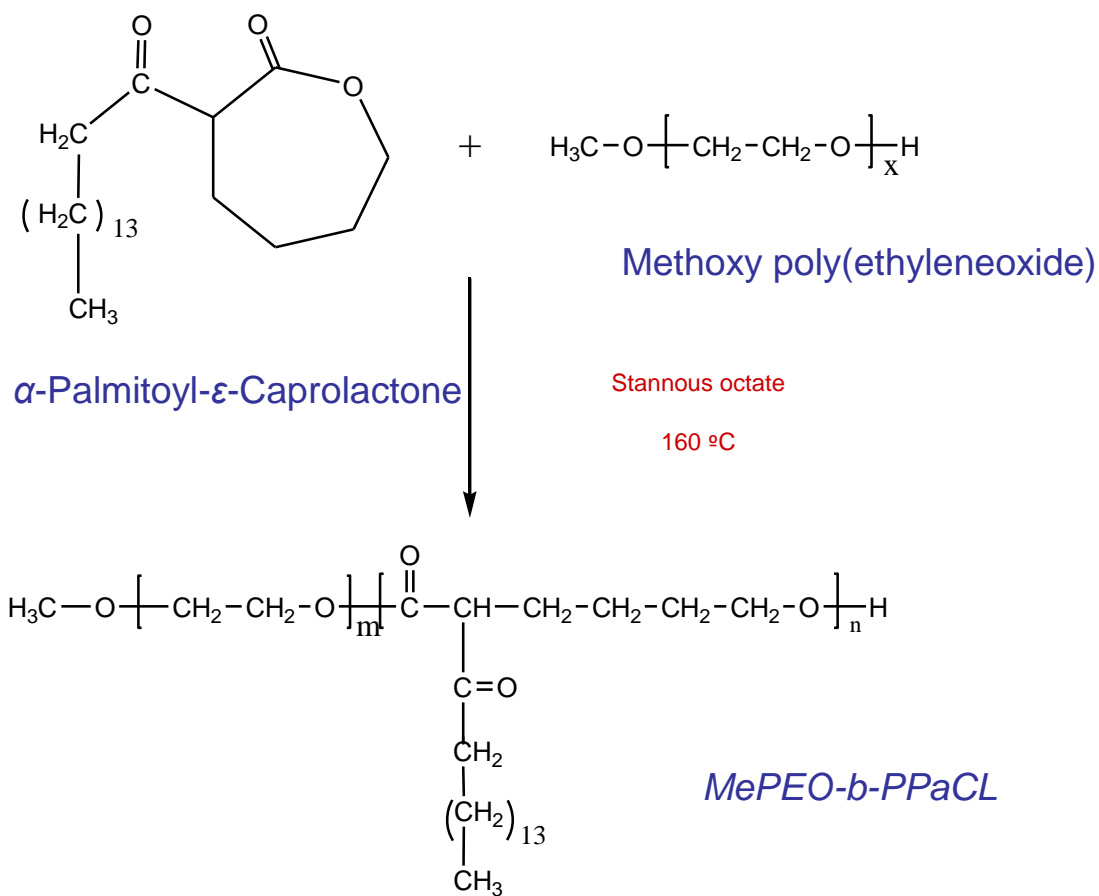


**Figure 3.4.** Synthetic scheme for the preparation of MePEO-*b*-PPaCL.

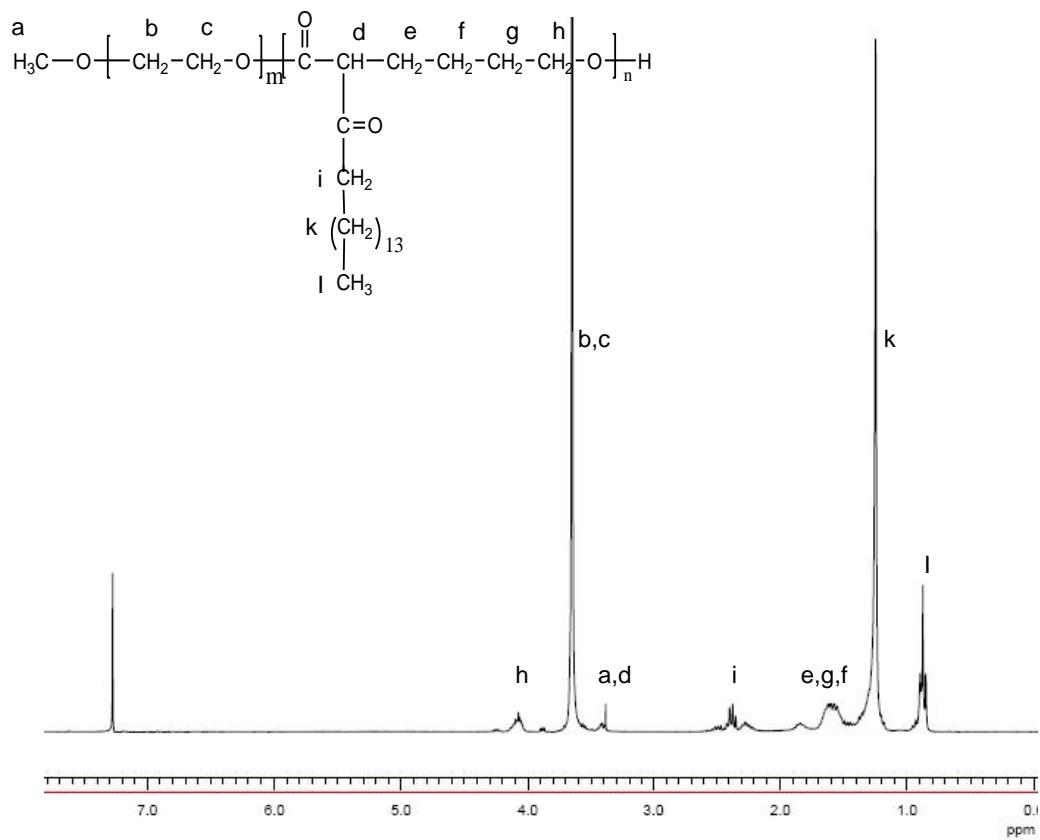


**Figure 3.5.** <sup>1</sup>H NMR spectra of MePEO-*b*-PPaCL in CDCl<sub>3</sub> and peak assignments.

### 3.3.2. Assembly of block co-polymers and characterization of self-assembled structures

The average diameter for MePEO-*b*-PPaCL particles determined by the DLS technique was  $214\pm 1$  nm. On the other hand, particles formed from MePEO-*b*-PCL, MePEO-*b*-PBCL and MePEO-*b*-PChCL were found to be smaller showing average diameters of 43, 65 and 167 nm, respectively. The TEM picture of MePEO-*b*-PPaCL particles shows the formation of true spherical carriers having a clear boundary, and the average diameter was  $231\pm 20$  nm (**Figure 3.6**), which is close to the size obtained from DLS measurement. A tendency for particle aggregation is also evident from the TEM results. The MePEO-*b*-PPaCL nanoparticles possessed viscous hydrophobic domains, as evidenced by the  $I_e/I_m$  ratios for the dipyrrene probe ( $0.49\pm 0.04$ ). However, the  $I_e/I_m$  values for MePEO-*b*-PPaCL particles was higher than the  $I_e/I_m$  values obtained for MePEO-*b*-PCL, MePEO-*b*-PBCL and MePEO-*b*-PChCL particles, which indicates lower viscosity of palmitoyl containing structures compared to unfunctionalized, benzyl or cholesteryl containing PCL domains (**Table 3.2**).

**Table 3.2.** Characteristics of empty nanocarriers (n=3).

Polymer <sup>a</sup>	Size±SE (nm) <sup>b</sup>	PD±SE <sup>c</sup>	CMC±SE (μM) <sup>d</sup>	Ie/Im±SE <sup>e</sup>
PEO <sub>114</sub> - <i>b</i> -PCL <sub>44</sub>	43±1	0.22±0.01	0.182±0.01 <sup>f</sup>	0.08±0.00
PEO <sub>114</sub> - <i>b</i> -PBCL <sub>20</sub>	65±2	0.32±0.03	0.098±0.01 <sup>f*</sup>	0.05±0.00 <sup>*</sup>
PEO <sub>114</sub> - <i>b</i> -PChCL <sub>18</sub>	167±5 <sup>*†</sup>	0.20±0.02	0.075±0.01 <sup>f*†</sup>	0.21±0.01 <sup>*†</sup>
PEO <sub>114</sub> - <i>b</i> -PPaCL <sub>14</sub>	214±1 <sup>*†#</sup>	0.17±0.02	N/A	0.49±0.04 <sup>*†#</sup>

<sup>a</sup> The number showed as subscript indicates the polymerization degree of each block.

<sup>b</sup> Z average mean estimated by DLS.

<sup>c</sup> Polydispersity (PD) of size distribution estimated by DLS technique.

<sup>d</sup> Measured from the onset of a rise in the intensity ratio of peaks at 339 nm to peaks at 334 nm in the fluorescence excitation spectra of pyrene plotted versus logarithm of polymer concentration.

<sup>e</sup> Intensity ratio (excimer/monomer) from emission spectrum of 1,3-(1,1' dipyrenyl) propane in presence of polymeric micelles.

<sup>f</sup> Data are reproduced from our previous publications for comparison.

<sup>\*</sup> Significantly different from MePEO-*b*-PCL (P<0.05, unpaired student's test).

<sup>†</sup> Significantly different from MePEO-*b*-PBCL (P<0.05, unpaired student's test).

<sup>#</sup> Significantly different from MePEO-*b*-PChCL (P<0.05, unpaired student's test).

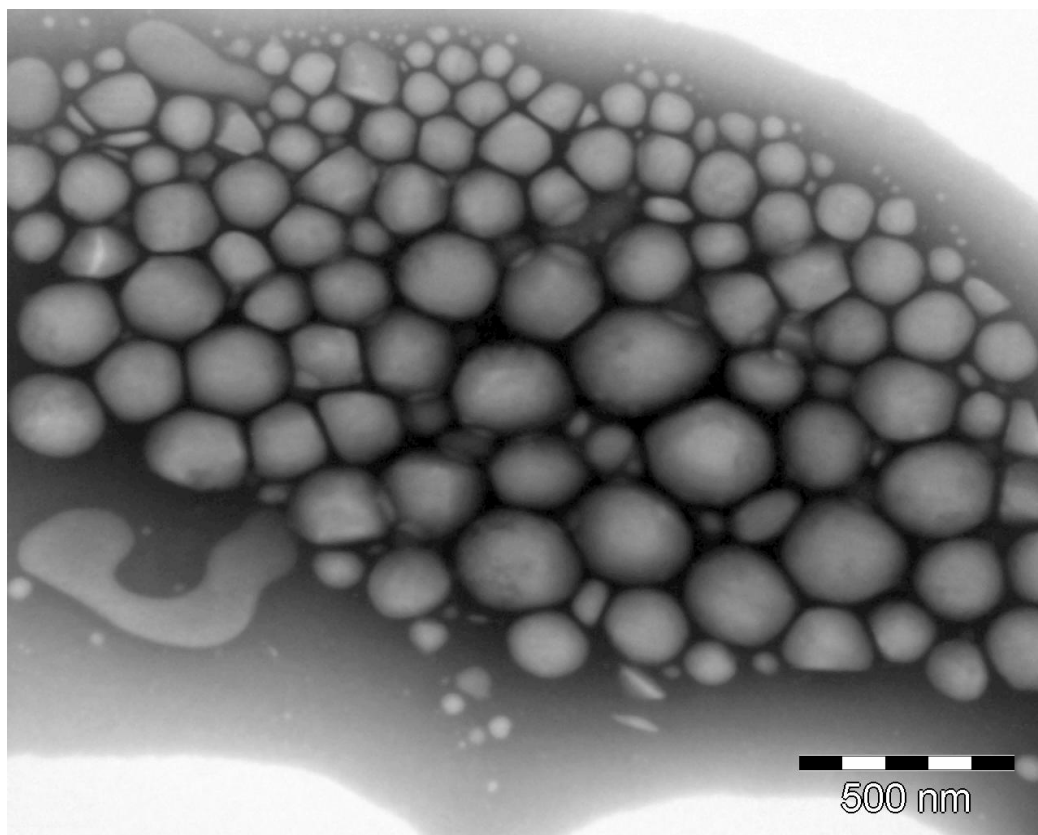


**Figure 3.6.** TEM picture of nano-carriers prepared from MePEO-*b*-PPaCL block copolymer (magnification 36000). The bar on the images represents 500 nm.

### 3.3.3. Encapsulation of AmB in polymeric nanocarriers

The average water soluble concentration of AmB in the presence of MePEO-*b*-PCL, MePEO-*b*-PBCL, MePEO-*b*-PChCL and MePEO-*b*-PPaCL nanocarriers was 222, 296, 355 and 436 µg/mL, respectively, when using an initial amount of 10 mg AmB in the encapsulation process. Compared to PCL core, the water solubility of AmB was increased by 1.5- and 2.0- fold in MePEO-*b*-PChCL and MePEO-*b*-PPaCL nanocarriers, respectively (**Table 3.3**). The average size of the AmB-loaded particles measured by DLS technique was between 173 and 229 nm (**Table 3.3**). A significant difference between the average diameters of unloaded and loaded carriers were observed for particles containing PCL and PBCL structures ( $P < 0.05$ , unpaired student's t test), but no significant difference for particles with PChCL and PPaCL structures was seen ( $P > 0.05$ , unpaired student's t test).

**Table 3.3.** Characteristic of AmB-loaded block copolymer nanocarriers (n=3)

Polymer <sup>a,b</sup>	AmB conc. (µg/mL) ±SE <sup>c</sup>	Encapsulation efficiency %±SE	Loading level % (w/w)±SE	Size (nm) ±SE <sup>d</sup>	PD ±SE <sup>e</sup>
PEO <sub>114</sub> - <i>b</i> -PCL <sub>44</sub>	222±34	13.9±2.2	10.5±1.7	196±6	0.37±0.03
PEO <sub>114</sub> - <i>b</i> -PBCL <sub>20</sub>	296±7	18.3±0.3	15.5±1.3	207±2	0.32±0.04
PEO <sub>114</sub> - <i>b</i> -PChCL <sub>18</sub>	355±20 <sup>*†</sup>	25.2±1.4 <sup>*†</sup>	46.4±5.3 <sup>*†</sup>	173±6 <sup>*†</sup>	0.22±0.01
PEO <sub>114</sub> - <i>b</i> -PPaCL <sub>14</sub>	436±35 <sup>*†</sup>	32.6±4.2 <sup>*†</sup>	28.6±3.9 <sup>*†</sup>	229±5 <sup>*†#</sup>	0.3±0.01

<sup>a</sup> The number showed as subscript the degree of conjugation calculated based on the <sup>1</sup>H NMR.

<sup>b</sup> Polymer concentration used in this study was 2.5 mg/mL.

<sup>c</sup> Initial amount of AmB used for encapsulation was 10 mg.

<sup>d</sup> Z average mean estimated by DLS technique.

<sup>e</sup> Polydispersity (PD) of size distribution estimated by DLS technique.

<sup>\*</sup> Significantly different from MePEO-*b*-PCL (P<0.05, unpaired student's test).

<sup>†</sup> Significantly different from MePEO-*b*-PBCL (P<0.05, unpaired student's test).

<sup>#</sup> Significantly different from MePEO-*b*-PChCL (P<0.05, unpaired student's test).

### 3.3.4. Hemolytic activity of AmB encapsulated nanocarriers

The MePEO-*b*-poly(ester)s did not display a significant hemolytic activity at highest polymer concentration of 2.5 mg/mL (**Figure 3.7**). The results of hemolysis experiment for AmB formulations and the specification of the formulations under hemolysis study is shown in **Figure 3.8** and **3.9**. The commercial formulation of AmB, Fungizone<sup>®</sup> caused > 90 % hemolysis against rat RBCs at AmB concentration of 30 µg/mL. When using an initial amount of 4 mg AmB for encapsulation, at a similar encapsulated AmB concentration of 30 µg/mL, MePEO-*b*-PCL and MePEO-*b*-PBCL formulations showed approximately 10 and 60 % hemolysis, respectively. The least hemolysis was shown by AmB encapsulated in MePEO-*b*-PChCL nano-carriers which only caused 6 % hemolysis at this concentration. At AmB concentration of 40-50 µg/mL, the MePEO-*b*-PCL, MePEO-*b*-PBCL and MePEO-*b*-PChCL formulations showed 10, 79 and 7 % hemolysis, respectively (**Figure 3.8**). At higher AmB concentrations, MePEO-*b*-PChCL formulation caused less hemolysis than MePEO-*b*-PCL. The equivalent concentration of MePEO-*b*-PCL, MePEO-*b*-PBCL and MePEO-*b*-PChCL block copolymers in the hemolysis study was between 0.03-0.28, 0.03-0.25 and 0.05-0.28 mg/mL, respectively. This level was above the corresponding CACs for MePEO-*b*-PCL, MePEO-*b*-PBCL and MePEO-*b*-PChCL block copolymers [21]. Because of the high hemolysis observed for AmB in MePEO-*b*-PBCL nano-carriers, this formulation was eliminated from further evaluations.

In further studies, we raised the initial amount of AmB in the encapsulation process from 4 to 10 mg (**Figure 3.9**). In this case, at a similar concentration of 30  $\mu\text{g/mL}$  for encapsulated AmB, MePEO-*b*-PCL and MePEO-*b*-PPaCL formulations showed approximately 15 and 40 % hemolysis, respectively. Again, the least hemolysis was shown by MePEO-*b*-PChCL nano-carriers of AmB which only caused 7 % hemolysis at this concentration (**Figure 3.9**). The MePEO-*b*-PChCL formulation of AmB caused 10.6 % hemolysis at AmB concentrations as high as 85  $\mu\text{g/mL}$ . The equivalent level of MePEO-*b*-PCL, MePEO-*b*-PChCL and MePEO-*b*-PPaCL block copolymers in the hemolysis study was between 0.04-0.50, 0.03-0.18 and 0.02-0.20 mg/mL, respectively. This level was above the corresponding CACs for MePEO-*b*-PCL and MePEO-*b*-PChCL block copolymers [21].

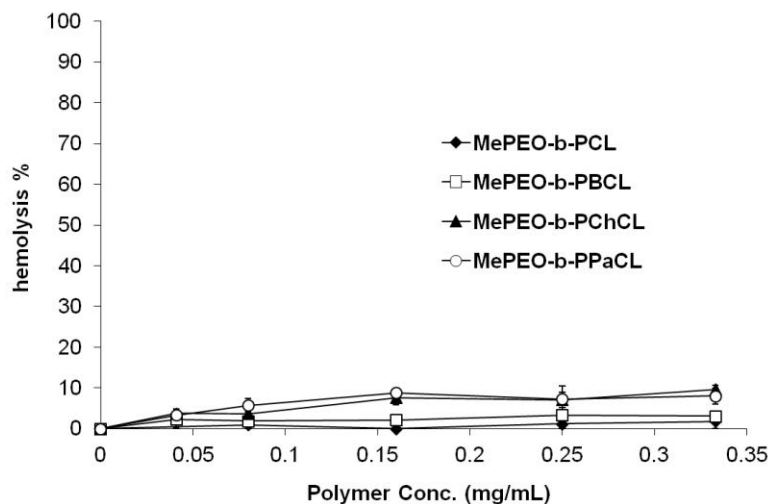
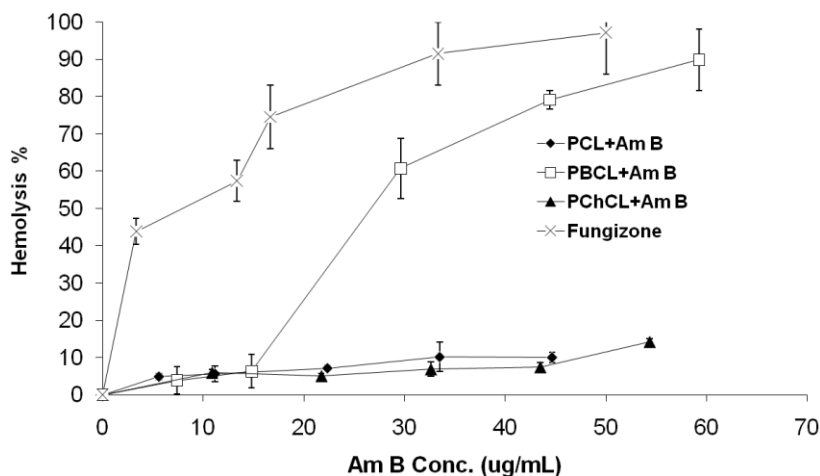


**Figure 3.7.** Hemolytic activity of synthesized MePEO-*b*-poly(esters). Each point represents average  $\pm$  standard error ( $n = 3$ ).



Polymer <sup>a,b</sup>	AmB conc. (μg/mL) <sup>c</sup>	Encapsulation efficiency %	Loading level % (w/w)	Size (nm) <sup>d</sup>	PD <sup>e</sup>
PEO <sub>114</sub> - <i>b</i> -PCL <sub>44</sub>	295	48.1	15.9	187	0.46
PEO <sub>114</sub> - <i>b</i> -PBCL <sub>20</sub>	444	64.0	23.4	164	0.35
PEO <sub>114</sub> - <i>b</i> -PChCL <sub>18</sub>	326	50.5	19.1	149	0.36

<sup>a</sup> The number showed as subscript the degree of conjugation calculated based on the <sup>1</sup>H NMR.

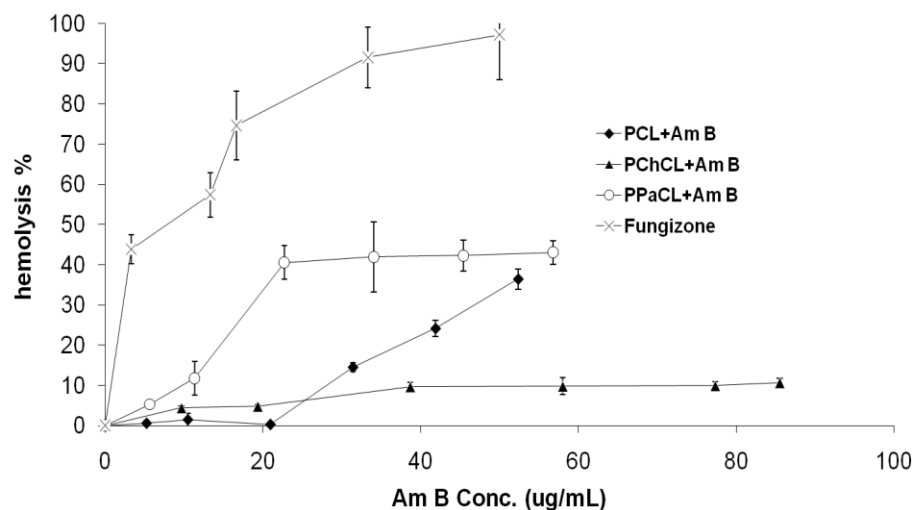
<sup>b</sup> Polymer concentration used in this study was 2.5 mg/mL.

<sup>c</sup> Initial amount of AmB used for encapsulation was 4 mg.

<sup>d</sup> Z average mean estimated by DLS technique.

<sup>e</sup> Polydispersity (PD) of size distribution estimated by DLS technique.

**Figure 3.8.** Hemolytic activity of AmB (4 mg initial amount) nanocarrier formulations in comparison to its commercial formulation (Fungizone<sup>®</sup>) against rat red blood cells. Each point represents average ± standard error (n = 3). Characteristic of the different batches used in the experiment are stated in the table below the figure.



Polymer <sup>a,b</sup>	AmB conc. (µg/mL) <sup>c</sup>	Encapsulation efficiency %	Loading level % (w/w)	Size (nm) <sup>d</sup>	PD <sup>e</sup>
PEO <sub>114</sub> - <i>b</i> -PCL <sub>44</sub>	314	51.0	13.6	188	0.43
PEO <sub>114</sub> - <i>b</i> -PChCL <sub>18</sub>	513	32.8	30.4	160	0.32
PEO <sub>114</sub> - <i>b</i> -PPaCL <sub>14</sub>	367	24.2	25.6	227	0.36

<sup>a</sup> The number showed as subscript the degree of conjugation calculated based on the <sup>1</sup>H NMR.

<sup>b</sup> Polymer concentration used in this study was 2.5 mg/mL.

<sup>c</sup> Initial amount of AmB used for encapsulation was 10 mg.

<sup>d</sup> Z average mean estimated by DLS technique.

<sup>e</sup> Polydispersity (PD) of size distribution estimated by DLS technique.

**Figure 3.9.** Hemolytic activity of AmB (10 mg initial amount) nanocarrier formulations in comparison to its commercial formulation (Fungizone<sup>®</sup>) against rat red blood cells. Each point represents average ± standard error (n = 3). Characteristic of the different batches used in the experiment are stated in the table below the figure.

### 3.4. Discussion

The long term objective of this study was to develop polymeric nanodelivery systems for the solubilization and controlled delivery of AmB. We previously reported on the preparation of self associating MePEO-*b*-poly( $\alpha$ -stearyl carboxylate- $\epsilon$ -caprolactone) (MePEO-*b*-PStCL) block copolymers bearing aliphatic stearyl and free carboxyl groups at respective 41 and 59 % substitution level on the  $\epsilon$  carbon of caprolactone unit in the PCL block [16]. Nanocarriers formed from this structure were compared to original MePEO-*b*-PCL and MePEO-*b*-PCCL with 100 % free carboxyl substitution on PCL block for the encapsulation and controlling the delivery of AmB to RBC membrane. MePEO-*b*-PCCL nano-carriers showed the highest efficacy in increasing AmB solubility followed by MePEO-*b*-PStCL and then original MePEO-*b*-PCL nanocarriers. Minimum hemolytic activity for encapsulated AmB was observed for the MePEO-*b*-PCL formulation followed by MePEO-*b*-PStCL, MePEO-*b*-PCCL formulations and then Fungizone<sup>®</sup>.

In order to find an optimum formulation that can increase AmB solubility and decrease its hemolytic activity simultaneously, we synthesized a new member of this family of block copolymers, i.e, MePEO-*b*-PCL copolymers bearing aliphatic palmitoyl side groups at 100 % substitution level on the PCL block. The potential of nanocarriers formed from this structure in the solubilization and controlled delivery of AmB was assessed and compared to original MePEO-*b*-PCL nano-carriers, those with benzyl (MePEO-*b*-PBCL) and cholesteryl groups (MePEO-*b*-PChCL), at 100 % substitution level on the PCL segment. Increasing the fatty acid substitution level has proven to be

successful in the solubilization and controlling the delivery of AmB from poly(ethylene oxide)-*block*-poly(*N*-hexyl stearate-*L*-aspartamide) based micellar carriers [24]. Previous studies also suggest an interaction between AmB and sterols containing membranes [28, 29].

Ring opening polymerization of palmitoyl bearing monomer,  $\alpha$ -palmitoyl- $\epsilon$ -caprolactone was used to prepare MePEO-*b*-PPaCL block copolymer (**Figure 3.2**). Conversion of  $\alpha$ -palmitoyl- $\epsilon$ -caprolactone to PPaCL occurred at a reaction temperature of 160 and a reaction time of 4 h (**Figure 3.4**). The synthesized MePEO-*b*-PPaCL block copolymers self assembled to spherical nanocarriers with larger average diameter than that of MePEO-*b*-PCL, MePEO-*b*-PBCL or MePEO-*b*-PChCL (**Figure 3.6, Table 3.2**). MePEO-*b*-PPaCL (DP=14) nanocarriers showed lower viscosity in their hydrophobic domain compared to MePEO-*b*-PCL, MePEO-*b*-PBCL or MePEO-*b*-PChCL nanocarriers. Large size of palmitoyl substituent in PPaCL cores might have induced steric hindrance restricting the intraparticulate interactions of hydrophobic chains leading to lower viscosities. The reduction in viscosity of the hydrophobic domain has also been observed for the block copolymer containing the bulky cholesteryl substituent on the hydrophobic block [21].

In general, the extent of AmB solubilization achieved by polymeric nanocarriers in this study appears to be higher than AmB water solubility levels achieved by previously reported polymeric nanocarriers [11, 30]. Among different structures in this study, under identical conditions, MePEO-*b*-PPaCL nanocarriers showed the most

efficient solubilization of AmB increasing AmB water solubility to 436  $\mu\text{g/mL}$  on average (**Table 3.3**), perhaps due to the formation of non-polar interactions between AmB and palmitoyl groups of the nanocarriers. Previous studies have reported the interaction of AmB with aliphatic chains [31, 32]. MePEO-*b*-PChCL copolymer showed higher encapsulation efficiency compared to MePEO-*b*-PCL and MePEO-*b*-PBCL, despite a shorter PCL backbone, but was less effective than MePEO-*b*-PPaCL nanocarriers in AmB solubilization. This can be attributed to hydrophobic interaction of AmB with cholesteryl groups of the nano-carriers [1, 33]. MePEO-*b*-PBCL copolymer showed similar encapsulation efficiency compared to MePEO-*b*-PCL [22].

The lowest hemolytic activity for encapsulated AmB was observed for MePEO-*b*-PChCL followed by MePEO-*b*-PCL, then MePEO-*b*-PPaCL and MePEO-*b*-PBCL nanocarriers. Since the equivalent concentrations of all the above polymers under hemolysis study were above their corresponding CACs, the dissociation of nanoparticles in the hemolysis experiment was unlikely. Therefore, the lower hemolysis observed for AmB as part of MePEO-*b*-PChCL nanocarrier, perhaps reflects a better control over the rate of AmB diffusion from these vehicles over other polymers rather than nanocarrier dissociation under the experimental condition (**Figure 3.8 and 3.9**) [4, 24].

High affinity of AmB to the cholesteryl side chains in MePEO-*b*-PChCL nanocarrier compared to that of nonfunctional PCL might have contributed to a more gradual or sustained release profile for the encapsulated AmB, causing less hemolysis for the MePEO-*b*-PChCL compared to MePEO-*b*-PCL formulation [1, 33]. The higher

viscosity of hydrophobic domain in PCL structure compared to that of PPaCL might be the cause of lower AmB release from the MePEO-*b*-PCL carriers leading to less hemolysis. These results indicate a reduced mobility of AmB in the nanocarrier core and a slower release from MePEO-*b*-PCL nanocarriers compared to MePEO-*b*-PPaCL. The lower core viscosity and lower degree of polymerization of the PPaCL may have contributed to this observation. In case of MePEO-*b*-PBCL, high degree of hemolysis might be a reflection of rapid drug release from this carrier. Given the higher level of drug loading in MePEO-*b*-PBCL compared to MePEO-*b*-PCL and high viscosity of the PBCL core, rapid AmB release might have resulted from AmB localization in micellar core/shell interface (rather than the micellar core) in MePEO-*b*-PBCL nanocarriers. In general, modification of the hydrophobic domain in MePEO-*b*-PCL carriers with AmB compatible structures (e.g., cholesterol and fatty acid esters) provided viable means for the development of polymeric nanocarriers that can afford efficient solubilization and control over the rate of AmB release.

### **3.5. Conclusion**

A new member of the family of functionalized MePEO-*b*-PCL block copolymers bearing pendant palmitoyl groups on the PCL block, i.e., MePEO-*b*-PPaCL, was successfully synthesized. A comparison between characteristics of nanoparticles formed from this structure and those from unmodified MePEO-*b*-PCL, MePEO-*b*-PBCL (bearing benzyl groups on PCL) or MePEO-*b*-PChCL (bearing cholesteryl groups on PCL) on AmB solubilization and delivery to red blood cell membrane was made. The results

showed a reduced hemolytic activity for all polymeric nanoformulations of AmB under study over Fungizone<sup>®</sup>. Among polymeric nano-carriers, MePEO-*b*-PPaCL showed the largest capacity for AmB encapsulation followed by MePEO-*b*-PChCL, MePEO-*b*-PBCL and MePEO-*b*-PCL nanocarriers. However, minimum hemolytic activity was observed for AmB in MePEO-*b*-PChCL nano-formulations. Thus, MePEO-*b*-PChCL carrier was the most effective among other nanocarriers under study, and might prove to be a valuable tool to both increase AmB solubility and reduce AmB delivery to RBC membranes.

### 3.6. References

- [1] Vakil R, Kwon GS. Effect of cholesterol on the release of amphotericin B from PEG-Phospholipid micelles. *Molecular Pharmaceutics* 2008;5:98-104.
- [2] Gupta S, Vyas SP. Development and characterization of amphotericin B bearing emulsomes for passive and active macrophage targeting. *J Drug Target* 2007;15:206-17.
- [3] Vakil R, Kwon GS. Effect of cholesterol on the release of amphotericin B from PEG-phospholipid micelles. *Mol Pharm* 2008;5:98-104.
- [4] Bang JY, Song CE, Kim C, Park WD, Cho KR, Kim PI, et al. Cytotoxicity of Amphotericin B-incorporated Polymeric Micelles Composed of Poly(DL-lactide-co-glycolide)/dextran Graft Copolymer. *Archives of Pharmacal Research* 2008;31:1463-9.
- [5] Brajtburg J, Bolard J. Carrier effects on biological activity of amphotericin B. *Clinical Microbiology Reviews* 1996;9:512-&.
- [6] Torrado JJ, Espada R, Ballesteros MP, Torrado-Santiago S. Amphotericin B formulations and drug targeting. *Journal of Pharmaceutical Sciences* 2008;97:2405-25.
- [7] Vyas SP, Gupta S. Optimizing efficacy of amphotericin B through nanomodification. *International Journal of Nanomedicine* 2006;1:417-32.
- [8] Sedlak M, Pravda M, Kubicova L, Mikulcikova P, Ventura K. Synthesis and characterisation of a new pH-sensitive amphotericin B - poly(ethylene glycol)-b-poly(L-lysine) conjugate. *Bioorganic & Medicinal Chemistry Letters* 2007;17:2554-7.
- [9] Moribe K, Maruyama K, Iwatsuru M. Molecular localization and state of amphotericin B in PEG liposomes. *Int J Pharm* 1999;193:97-106.
- [10] Wang CH, Wang WT, Hsiue GH. Development of polyion complex micelles for encapsulating and delivering amphotericin B. *Biomaterials* 2009;30:3352-8.
- [11] Vakil R, Kwon GS. Poly(ethylene glycol)-b-poly(epsilon-caprolactone) and PEG-phospholipid form stable mixed micelles in aqueous media. *Langmuir* 2006;22:9723-9.
- [12] Vandermeulen G, Rouxhet L, Arien A, Brewster ME, Preat V. Encapsulation of amphotericin B in poly(ethylene glycol)-block-poly(epsilon-caprolactone-co-trimethylenecarbonate) polymeric micelles. *International Journal of Pharmaceutics* 2006;309:234-40.
- [13] Adams M, Kwon GS. Spectroscopic investigation of the aggregation state of amphotericin B during loading, freeze-drying, and reconstitution of polymeric micelles. *J Pharm Pharm Sci* 2004;7:1-6.
- [14] Barwicz J, Dumont I, Ouellet C, Gruda I. Amphotericin B toxicity as related to the formation of oxidatively modified low-density lipoproteins. *Biospectroscopy* 1998;4:135-44.
- [15] Lemke A, Kiderlen AF, Kayser O. Amphotericin B. *Appl Microbiol Biotechnol* 2005;68:151-62.
- [16] Falamarzian A, Lavasanifar A. Chemical Modification of Hydrophobic Block in Poly(Ethylene Oxide) Poly(Caprolactone) Based Nanocarriers: Effect on the Solubilization and Hemolytic Activity of Amphotericin B. *Macromol Biosci*.
- [17] Wasan KM, Kennedy AL, Cassidy SM, Ramaswamy M, Holtorf L, Chou JW, et al. Pharmacokinetics, distribution in serum lipoproteins and tissues, and renal toxicities of

amphotericin B and amphotericin B lipid complex in a hypercholesterolemic rabbit model: single-dose studies. *Antimicrob Agents Chemother* 1998;42:3146-52.

[18] Ramaswamy M, Peteherych KD, Kennedy AL, Wasan KM. Amphotericin B lipid complex or amphotericin B multiple-dose administration to rabbits with elevated plasma cholesterol levels: pharmacokinetics in plasma and blood, plasma lipoprotein levels, distribution in tissues, and renal toxicities. *Antimicrob Agents Chemother* 2001;45:1184-91.

[19] Lavasanifar A, Samuel J, Kwon GS. The effect of alkyl core structure on micellar properties of poly(ethylene oxide)-block-poly(L-aspartamide) derivatives. *Colloids Surf B Biointerfaces* 2001;22:115-26.

[20] Aliabadi HM, Mahmud A, Sharifabadi AD, Lavasanifar A. Micelles of methoxy poly(ethylene oxide)-b-poly(epsilon-caprolactone) as vehicles for the solubilization and controlled delivery of cyclosporine A. *J Control Release* 2005;104:301-11.

[21] Mahmud A, Patel S, Molavi O, Choi P, Samuel J, Lavasanifar A. Self-associating poly(ethylene oxide)-b-poly(alpha-cholesteryl carboxylate-epsilon-caprolactone) block copolymer for the solubilization of STAT-3 inhibitor cucurbitacin I. *Biomacromolecules* 2009;10:471-8.

[22] Mahmud A, Xiong XB, Lavasanifar A. Novel self-associating poly(ethylene oxide)-block-poly(epsilon-caprolactone) block copolymers with functional side groups on the polyester block for drug delivery. *Macromolecules* 2006;39:9419-28.

[23] Mahmud A, Xiong XB, Lavasanifar A. Development of novel polymeric micellar drug conjugates and nano-containers with hydrolyzable core structure for doxorubicin delivery. *European Journal of Pharmaceutics and Biopharmaceutics* 2008;69:923-34.

[24] Lavasanifar A, Samuel J, Kwon GS. Micelles self-assembled from poly(ethylene oxide)-block-poly(N-hexyl stearate L-aspartamide) by a solvent evaporation method: effect on the solubilization and haemolytic activity of amphotericin B. *J Control Release* 2001;77:155-60.

[25] Elhasi S, Astaneh R, Lavasanifar A. Solubilization of an amphiphilic drug by poly(ethylene oxide)-block-poly(ester) micelles. *European Journal of Pharmaceutics and Biopharmaceutics* 2007;65:406-13.

[26] Xiong XB, Uludag H, Lavasanifar A. Biodegradable amphiphilic poly(ethylene oxide)-block-polyesters with grafted polyamines as supramolecular nanocarriers for efficient siRNA delivery. *Biomaterials* 2009;30:242-53.

[27] Abdullah Mahmud X-BX, and Afsaneh Lavasanifar. Novel Self-Associating Poly(ethylene oxide)-block-poly(caprolactone) Block Copolymers with Functional Side Groups on the Polyester Block for Drug Delivery. *Macromolecules* 2006;39:9419-28.

[28] Czub J, Neumann A, Borowski E, Baginski M. Influence of a lipid bilayer on the conformational behavior of amphotericin B derivatives - A molecular dynamics study. *Biophys Chem* 2009;141:105-16.

[29] Romero EA, Valdivieso E, Cohen BE. Formation of two different types of ion channels by amphotericin B in human erythrocyte membranes. *J Membr Biol* 2009;230:69-81.

[30] Adams ML, Andes DR, Kwon GS. Amphotericin B encapsulated in micelles based on poly(ethylene oxide)-block-poly(L-amino acid) derivatives exerts reduced in vitro

hemolysis but maintains potent in vivo antifungal activity. *Biomacromolecules* 2003;4:750-7.

[31] Adams ML, Kwon GS. Relative aggregation state and hemolytic activity of amphotericin B encapsulated by poly(ethylene oxide)-block-poly(N-hexyl-L-aspartamide)-acyl conjugate micelles: effects of acyl chain length. *J Control Release* 2003;87:23-32.

[32] Balakrishnan AR, Easwaran KR. Lipid-amphotericin B complex structure in solution: a possible first step in the aggregation process in cell membranes. *Biochemistry* 1993;32:4139-44.

[33] Charbonneau C, Fournier I, Dufresne S, Barwicz J, Tancrede P. The interactions of amphotericin B with various sterols in relation to its possible use in anticancer therapy. *Biophys Chem* 2001;91:125-33.

## CHAPTER FOUR

### LIPID-SUBSTITUTED POLYETHYLENEIMINE POLYPLEXES OF STAT3 siRNA FOR SENSITIZATION OF BREAST TUMOR CELLS TO CONVENTIONAL CHEMOTHERAPY

A version of this chapter has been submitted for publication to

**Acta Biomaterialia**

**Arash Falamarzian<sup>1</sup>, Hamidreza Montazeri Aliabadi<sup>2</sup>, Ommoleila Molavi<sup>4</sup>, John M. Seubert<sup>1,3</sup>, Raymond Lai<sup>4</sup>, Hasan Uludağ<sup>1,2</sup> and Afsaneh Lavasanifar<sup>1,2</sup>**

<sup>1</sup>Faculty of Pharmacy and Pharmaceutical Sciences, <sup>2</sup>Department of Chemical & Materials Engineering, Faculty of Engineering, <sup>3</sup>Department of Pharmacology, Faculty of Medicine, <sup>4</sup>Department of Laboratory Medicine and Pathology, Cross Cancer Institute, University of Alberta, Edmonton, Alberta, Canada.

All experiments for this chapter were completed by A. Falamarzian, except for synthesis of lipid modified PEI and development of MDA-MB-435 DOX/RES cells which has been accomplished by Dr. H.M. Aliabadi from Dr. H. Uludağ's lab. Dr. O. Molavi from Dr. R. Lai's lab has provided assistance in conduction of western blot studies and Dr. J.M. Seubert has provided assistance with fluorescence microscopy and RT-PCR studies.

#### **4.1. Introduction**

Signal transducers and activator of transcriptions (STATs) are a family of cytoplasmic proteins that convey signals from cell membrane to the nucleus [1]. STAT3 is an important member of this family that is constitutively activated in different malignancies including breast, head and neck, and prostate cancers [2-4]. STAT3 transduces signals from various oncogenic proteins and pathways. It can be activated by different kinds of cytokines and growth factors including interleukin (IL) 6, interferon (IFN)  $\beta$ , IFN  $\gamma$ , fibroblast growth factor (FGF), epidermal growth factor (EGF), insulin-like growth factor (IGF), hepatocyte growth factor (HGF) and vascular endothelial growth factor (VEGF) [5-10]. Following activation, STAT3 monomers dimerize through reciprocal phosphotyrosine-SH2 interactions, translocate to the nucleus and bind to STAT3-specific sites on the promoters of target genes to induce gene transcription [11]. Many proteins that are important for tumor-cell proliferation and survival are regulated by STAT3, including BCL-X<sub>L</sub>, MCL1, Survivin, MYC and Cyclin D1[12]. Pro-angiogenic factors including hepatocyte growth factor (HGF), basic fibroblast growth factor (bFGF) and matrix metalloproteinase 2 (MMP2) are also shown to be up-regulated by STAT3 [13, 14]. The capability of STAT3 to participate in many features of oncogenesis including cell proliferation, survival, angiogenesis, invasion, and tumor induced immune-suppression has made it a desirable target in cancer therapy [15]. Several small-molecule drugs have been tested to inhibit STAT3 and provoke apoptosis in cancer cells. Their mechanism of action includes upstream inhibition of growth factors and cytokines, disruption of STAT3 dimerization, blocking of STAT3 nuclear

translocation, and inhibition of STAT3 DNA-binding and transcriptional activity [1, 16-21]. Clinical use of many of these compounds, however, has been halted because of poor solubility, low bioavailability, limited biological stability and undesirable side effects caused by their non-specific activity.

An alternative approach for anti-STAT3 therapy would be to use small interfering RNA (siRNA) that inhibit the expression of STAT3 [11, 22, 23]. The purpose of such therapy is to specifically induce the cleavage of STAT3 mRNA for efficient gene silencing. RNA interference (RNAi) is a sequence specific, evolutionary mechanism that can be employed to suppress any specific gene, giving it an edge over classic low molecular weight drugs that may cause broad spectrum of side effects as a result of activity on undesired molecular targets [24]. However, advancement of this technology as a ground-breaking therapy with a high degree of specificity for disease related genes has been relatively slow, mainly due to problems associated with its safe and effective delivery in a clinical setting [25]. Delivering siRNA to the desired site of action constitutes a major challenge due to its rapid degradation by nucleases, uptake by the reticuloendothelial system and speedy renal excretion, all of which can lead to early elimination of the siRNA from biological system [26, 27]. In addition, the polyanionic nature of siRNA and its large molecular weight causes poor cellular uptake, restricting its access to intracellular siRNA target [28].

In order to alleviate these obstacles, different delivery materials including viral vectors, lipids and polymeric nano-carriers have been examined for siRNA delivery as

reviewed in chapter one. High immunogenicity and unsatisfactory safety profile of viral vectors has limited the application of such delivery systems in clinical settings [29, 30]. Cationic lipids and polymers can be used to electrostatically bind and form effective complexes with negatively charged siRNA. Polymeric systems have the advantage of structural flexibility over their lipid counterparts and can be chemically tailored in order to obtain desirable physiochemical properties [31]. Among cationic polymers, high molecular weight-PEIs (MW > 25 kDa) have shown to be efficient in protection and siRNA delivery [32, 33]. These polymers have high cationic charge density and are able to non-covalently bind siRNA and protect it against enzymatic degradation [34]. Unprotonated amines of the PEI generate a so-called “proton-sponge effect” causing enhanced influx of protons and water, endosomal rupture and release of complexes to the cytoplasm [35]. The toxicity of high molecular weight PEIs has been a major hurdle for their clinical use. Lower molecular weight PEIs might be more suitable due to better safety profiles, but these polymers have shown low transfection efficiency [36]. Hydrophobic modifications of low MW PEIs have been tried in order to develop more effective delivery systems for siRNA. These hydrophobic moieties are expected to increase the interaction of polymers with lipophilic membrane of cells and ease the uptake of complexed siRNA [37]. In previous studies, aliphatic lipid-substituted 2 kDa PEIs with an array of fatty acids with different chain lengths (from C8 to C18) have been explored for plasmid DNA delivery. An equivalent transfection ability to that of 25 kDa PEI was observed for lipid substituted 2 kDa PEIs, without the toxic effect associated with the former polymer [36]. In separate studies, the lipid-substituted 2 kDa PEIs have

been utilized for siRNA delivery and shown to improve the cellular uptake of siRNA compared to unmodified 2 kDa PEIs while demonstrating negligible toxicity. Effective silencing of target P-gp and BCRP by relevant siRNAs complexes of lipid modified PEI 2 kDa in P-gp transfected MDA-MB-435/MDR cells and BCRP-transfected MDCK cells have also been demonstrated, respectively [37, 38]. BCRP silencing caused a reversal in resistance to an anticancer agent, mitoxantrone, and a 14-fold reduction of its IC<sub>50</sub> value in drug resistant cells.

In the current study, we utilized a library of lipid-substituted 2 kDa PEIs polymers for efficient siRNA delivery and silencing of STAT3 in a triple negative breast cancer cell line, i.e., MDA-MB-435, and investigated the potential benefit of this approach in sensitization of wild type (WT) and resistant (RES) phenotypes to cytotoxic effects of conventional anti-cancer drugs, doxorubicin (DOX) and paclitaxel (PTX).

## **4.2. Experimental Section**

### **4.2.1. Materials**

The 2 kDa PEI (PEI2) (Mn: 1.8 kDa, Mw: 2 kDa), 25 kDa PEI (PEI25K), anhydrous dimethylsulfoxide (DMSO), Caproyl chloride (C8; >99%), Octanoyl chloride (C18:1 9Z, 12Z; 99%), Linoleyl chloride (C18:2 9Z,12Z; 99%), Hanks' Balanced Salt Solution (HBSS), and 3-(4,5-Dimethylthiazol-2 yl)-2,5-diphenyltetrazolium bromide (MTT) were obtained from SIGMA (St. Louis, MO). Stearoyl chloride (C18; >98.5%) was purchased from Fluka (St. Louis, MO). Cell culture media RPMI 1640, DMEM, penicillin–streptomycin, fetal bovine serum, HEPES buffer solution (1 M) and

trypsin/ethylenediaminetetraacetate were purchased from GIBCO, Invitrogen Corp (USA). The scrambled siRNA used as control and Silencer<sup>®</sup> FAM<sup>™</sup> labeled Negative siRNA were supplied from Ambion (catalog numbers: AM4636). The Silencer siRNAs against STAT3 was purchased from Qiagen (catalog numbers: SI02662338, sequence: CAGCCTCTCTGCAGAATTCAA). Doxorubicin and Paclitaxel were purchased from Ontario chemicals Inc. and LC laboratories, respectively.

#### **4.2.2. Cell Line**

The wild-type MDA-MB-435 (MDA-MB-435/WT) cells were originally obtained as a gift from the laboratory of Dr. Robert Clark (Georgetown University, USA). The MDA-MB-435 resistant cells (referred to as DOX/RES) were developed through exposure of MDA-MB-435/WT cells to DOX with a gradual dose increase, starting from 0.2 µg/mL (~20% of IC<sub>50</sub>; i.e., concentration for 50% cell death), and continuing with 0.5, 0.75, 1.0, 1.5 and 2 µg/mL. Cells were exposed to each dose for 3 passages or one week (whichever longer), and frozen at the end of each stage. MDA-MB-435 WT and DOX/RES cells were cultured in RPMI 1640 media with 10% FBS, 100 U/mL penicillin, and 100 mg/mL streptomycin in 37 °C and 5% CO<sub>2</sub>. DOX/RES cells were cultured in the presence of 2 µg/mL of DOX in culture media at all times. Cell cultures were considered confluent when a monolayer of cells covered more than 80% of the flask surface. To propagate the cells, a monolayer was washed with HBSS, and subsequently incubated with 0.05% trypsin/EDTA for 3 min at room temperature. The suspended cells were centrifuged at 650 rpm for 5 min, and were re-suspended in the medium after removal of

the supernatant. The suspended cells were either sub-cultured at 10% of the original count or seeded in multi-well plates for testing.

#### 4.2.3. Synthesis of Lipid-Substituted Polymers

Lipid-substituted polymers were synthesised according to the process which has been described elsewhere.[36, 39] Briefly, a 50% PEI2 solution (in water) was purified by freeze-drying, and substitution was performed by N-acylation of PEI with commercially available lipid chlorides. Acid chlorides were typically added to 100 mg of PEI in anhydrous DMSO. The lipid:PEI molar ratios were systemically varied between [0.066 to 0.2]. The mixture was allowed to react for 24 h at room temperature under nitrogen, after which excess ethyl ether was added to precipitate and wash the polymers. The substituted polymers were dried under vacuum at ambient temperature overnight. Polymers were analyzed by  $^1\text{H}$  NMR (Bruker 300 MHz; Billerica, MA) in  $\text{D}_2\text{O}$ . The characteristic proton shift of lipids ( $\delta \approx 0.8$ ;  $-\text{CH}_3$ ) and PEI ( $\delta \approx 2.5\text{--}2.8$ ;  $\text{NH}-\underline{\text{CH}_2}-\underline{\text{CH}_2}-\text{NH}-$ ) were integrated, normalized for the number of protons in each peak, and used to determine the extent of lipid substitutions on polymers (**Table 4.1**). PEI-SA0.5 and PEI-SA3.6 refer to stearic acid substitution at 0.5 and 3.6 lipids/PEI2. PEI-OA1, PEI-OA1.7 and PEI-OA2.5 refer to oleic acid substitution at 1, 1.7 and 2.5 lipids/PEI2. PEI-CA6.9 refers to caprylic acid substitution at 6.9 lipids/PEI2. PEI-LA1.5 and PEI-LA2.1 refer to linoleic acid substitution at 1.5 and 2.1 lipids/PEI2 accordingly.

#### 4.2.4. Assessing the cellular association of siRNA polyplexes by flow cytometry

To assess the ability of polymers to transfer siRNA into WT and DOX/RES cells, complexes were prepared using 5-carboxyfluorescein (FAM)-labeled scrambled siRNA at polymer:siRNA ratios of 8:1 (w/w) by incubation in water (corresponding 36 nM siRNA and 4  $\mu\text{g/mL}$  polymer in culture medium). Confluent cell cultures were trypsinized, re-suspended as described before and seeded in 24 well plates (0.6 mL in each well) at 50% confluence. After 24 h, 400 mL fresh medium was added to each well, followed by the addition of siRNA polyplexes. The prepared polyplexes were added to wells in triplicates and were incubated in 37 °C for 24 h. After the incubation period, cells were washed with HBSS and trypsinized. A 3.7% formaldehyde solution was added to suspend the cells and the siRNA uptake was quantified by a Beckman Coulter QUANTA flowcytometer using the FL1 channel to detect cell-associated fluorescence. The percentage of cells showing FAM fluorescence and the mean fluorescence in the total cell population was determined.

#### **4.2.5. Assessing the cellular uptake and distribution of selected siRNA polyplexes by fluorescence microscopy**

Fluorescent microscopy was used to assess the intracellular trafficking of siRNA in WT cells. FAM-labeled siRNA was complexed with PEI-LA1.5, PEI-LA2.1, PEI25K at polymer:siRNA ratio of 8:1 (w/w) and were added to the wells (final polymer and siRNA concentration of 6  $\mu\text{g/mL}$  and 54 nM per well). Cells grown on the glass-bottom Petri dishes were incubated with the polyplexes for 3 and 24 h, respectively. At the end of incubation period, the cells were washed three times with PBS. For nucleus labeling, cells

were incubated with DAPI (Molecular Probes, Invitrogen Co., OR, USA) for 15 min. Localization of complexes in cells was visualized by an epifluorescence microscope (Carl Zeiss Microscope systems, Jena, Germany) with identical settings for each study.

#### **4.2.6. *In vitro* cytotoxicity studies**

The cytotoxicity of STAT3 and scrambled siRNA complexed with different polymers within the PEI library was evaluated in MDA-MB-435 WT and DOX/RES cells using MTT assay. Confluent cell cultures were trypsinized and re-suspended as described before, and seeded in 24 well plates (0.6 mL in each well) at 50% confluency. After 24 h, 400  $\mu$ L fresh media was added to each well. siRNA polyplexes were prepared using the scrambled and STAT3-siRNA at polymer:siRNA ratio of 8:1 (w/w) and were added to the wells (final polymer and siRNA concentration of 6  $\mu$ g/mL and 54 nM per well in triplicate wells). Cells were incubated for 72 h in their normal maintenance conditions and then 60  $\mu$ L of MTT solution (5 mg/mL in HBSS) was added to each well. After 2 h of incubation in 37 °C, the medium was removed, and 300  $\mu$ L of DMSO was added to each well to dissolve the crystals formed. The optical density of the wells was measured with an ELx800 Universal Microplate Reader (BioTek Instruments; Winooski, VT, USA) with cell-less medium as blank. The absorbance of polyplex-treated cells was compared to untreated cells and % cell viability was calculated using the following equation.

% cell viability = (absorbance of siRNA polyplex treated cells/absorbance of untreated cells)  $\times$  100

To determine the optimum polymer:siRNA ratio, confluent cell cultures of WT and DOX/RES cells were trypsinized and seeded in 24 well plates (600 mL in each well) at 50% confluence. After 24 h, 400 mL fresh medium was added to each well. The PEI-LA/siRNA polyplexes were prepared at different ratios of polymer:siRNA in sterile tubes using the STAT3-siRNA and scrambled siRNA with polymer:siRNA ratios of 2:1, 4:1, and 8:1 (w/w) (corresponding to 54 nM siRNA and 1.5, 3 and 6 µg/mL polymer in cell culture medium), and were added to the wells in triplicates. Cells were incubated for 72 h in their normal maintenance conditions, followed by MTT assay as described earlier.

Furthermore, in order to evaluate the siRNA dose response as part for PEI-LA based polyplexes, confluent cell cultures of WT and DOX/RES cells were trypsinized and seeded in 24 well plates (600 mL in each well) at 50% confluence. After 24 h, 400 mL fresh medium was added to each well. The PEI-LA2.1/siRNA polyplexes were prepared using the scrambled and STAT3-siRNA at the ratio of 8:1 (w/w) and were added to the wells to give final siRNA concentrations of 9, 18, 27, 45, 54 and 72 nM per well in triplicate. Cells were incubated for 72 h in their normal maintenance conditions, followed by MTT assay as described earlier.

#### **4.2.7. Assessing the silencing activity of STAT3-siRNA polyplexes by real-time PCR**

Real-time (RT) PCR was carried out to determine STAT3 knock-down at the mRNA level. Confluent cell cultures were trypsinized and re-suspended as described before, and seeded in 6 well plates (2.4 mL in each well) at 50% confluency. After 24 h, 1.8 mL fresh medium was added to each well. siRNA polyplexes were prepared using

scrambled and STAT3-siRNA at polymer:siRNA ratio of 8:1 (w/w) and were added to the wells (final polymer and siRNA concentration of 6 µg/mL and 54 nM per well) in triplicate. After 48 h, total RNA was extracted using RNeasy spin columns (Qiagen, Mississauga, ON, Canada) according to the manufacturer's recommendations. cDNA was synthesised following Invitrogen's protocol, briefly adding 2 µL master mix 1 (0.5 µL Oligo(dT)<sub>12-18</sub> Primer, ), 0.5 µL random primer and 1 µL (10 mM MdNTP's per sample) to 10 µL of RNA (5000 ng) and then heated to 65 °C for 5 min. 7 µL of Master Mix 2 (4 µL 5 × Synthesis Buffer, 2 µL DTT (0.1 M) and 1 µL RNAout RNase inhibitor (1.8 U/µL)) was then added and the samples heated at 37 °C for 2 min. 1 µL of M-MLV RT enzyme was then added per sample and they were heated at 25 °C for 10 min, 37 °C for 50 min and 70 °C for 15 min. Real time PCR was performed on a StepOnePlus™ RT-PCR system (ABI) with GAPDH (Forward: 5'-CAC ATG GCC TCC AAG GAG TAA-3') and (Reverse: 5'-TGA GGG TCT CTC TCT TCC TCT TGT-3') as the endogenous housekeeping gene and the specific STAT3 primers (Forward: 5'-AAG TTT ATC TGT GTG ACA CCA ACG A-3') and (Reverse: 5'-CTT CAC CAT TAT TTC CAA ACT GCA T-3'). 7.5 µL of master mix containing 5 µL of SYBR® Green ROX™ qPCR Mastermix (Qiagen, Mississauga, ON, Canada) and 2.5 µL primer (3.2 µM; per sample) was added to each well. Then 2.5 µL of template of each sample was added in triplicate. Levels of mRNA were measured as CT threshold levels and normalized with the individual GAPDH control CT values. Altered mRNA levels in cells are indicated as a 'fold change' compared with control cells. Each sample was measured at least three times.

#### **4.2.8. Assessing the silencing activity of STAT3-siRNA polyplexes by Western blot**

Western blot was carried out to determine STAT3 knock-down at the protein level. Confluent cell cultures were trypsinized and re-suspended as described before, and seeded in 6 well plates (2.4 mL in each well) at 50% confluence. After 24 h, 1.8 mL fresh medium was added to each well. siRNA polyplexes were prepared using the scrambled and STAT3-siRNA at polymer:siRNA ratio of 8:1 and were added to the wells (final polymer and siRNA concentration of 6  $\mu\text{g}/\text{mL}$  and 54 nM per well) in triplicate wells. After 48 h incubation, the cells were washed with cold phosphate buffered saline (PBS) and lysed using RIPA cell lytic buffer supplemented with 0.1 mM phenylmethylsulfonylfluoride (PMSF) (Sigma Aldrich), a protease inhibitor cocktail (Nacalai Inc, San Diego, CA, USA) and a phosphatase inhibitor cocktail (Calbiochem, EMD Biosciences, Darmstadt, Germany). The lysate was then incubated on ice for 30 minutes which was followed by centrifugation at 17000  $g$  for 15 minutes to remove genomic DNA. Protein quantification was determined by the BCA protein assay kit (Pierce, Rockford, IL, USA) and equal amounts of protein (50  $\mu\text{g}$ ) were loaded in 4-20% Tris-HCl precast gel (Bio-Rad, Mississauga, Ontario). After gel electrophoresis the proteins were transferred to a nitrocellulose membrane and stained with 0.05% Ponceau S (Sigma-Aldrich) to ensure equivalent protein loading per lane. The membrane was probed with antibodies against STAT3 and p-STAT3 (Santa Cruz Biotechnology, Santa Cruz, CA). The proteins were then detected using peroxidase-conjugated anti-mouse IgG and visualized by enhanced chemiluminescence (Pierce ECL Western Blotting Substrate,

Thermo Scientific, Rockford, IL, USA). Optical intensity of STAT3 and p-STAT3 band was quantified and normalized to actin protein band using Adobe Photoshop software.

#### **4.2.9. Assessing the effect of STAT3-siRNA/PEI-LA pre-treatment on the cytotoxicity of doxorubicin and paclitaxel in WT and DOX/RES breast cancer cells**

The cytotoxicity of free DOX and PTX against WT and DOX/RES cells were evaluated. Confluent cell cultures of WT and DOX/RES cells were trypsinized and seeded in 24 well plates (600 mL in each well) at 50% confluence. After 24 h, 400 mL fresh medium was added to each well. DOX and PTX solutions were prepared at different concentrations in sterile tubes and added to the wells in triplicates. Cells were incubated for 24 h in their normal maintenance conditions, followed by MTT assay as described earlier. These experiments were followed by evaluating the effect of STAT3 silencing on cytotoxicity of these anticancer drugs against WT and DOX/RES cells. Confluent cell cultures of WT and DOX/RES cells were trypsinized and seeded in 24 well plates (600 mL in each well) at 50% confluence. After 24 h, 400 mL fresh medium was added to each well. The siRNA polyplexes were prepared in sterile tubes using STAT3 or scrambled siRNA with PEI-LA2.1 at polymer:siRNA ratios of 8:1 (w/w) (corresponding to 54 nM siRNA and 6 µg/mL polymer in cell culture medium), and were added to the wells in triplicates and kept for 24 h. DOX or PTX were added separately to the cells in different amount. Cells were incubated for another 24 h in their normal maintenance conditions followed by MTT assay as described earlier.

#### **4.2.10. Statistics**

Compiled data were presented as means  $\pm$  standard deviation (SD). Where feasible, the data were analyzed for statistical significance using unpaired Student's t-test, one-way analysis of variance followed by post hoc Tukey test as noted in the results section. The level of significance was set at  $\alpha \leq 0.05$ .

### **4.3. Results**

#### **4.3.1. Characterization of Lipid-Substituted Polymers**

A library of lipid substituted PEI2 polymers (with lipid:PEI2 ratios varying between 0.066 to 0.2) with SA, OA, CA and LA have been synthesized for siRNA delivery, based on method described elsewhere.[36] The characteristics of prepared polymers are shown in **Table 4.1**. Among the synthesized polymers, PEI-CA6.9 contained the highest number of lipid substitution (corresponding to CA substitution at 6.9 lipids/PEI2 [37]).

**Table 4.1.** Lipid-substituted PEI 2K library.

<b>Polymer</b>	<b>Substituted lipid</b>	<b>Lipid:PEI Ratio<sup>a)</sup></b>	<b>Lipid/PEI<sup>b)</sup></b>	<b>Methylene/PEI<sup>c)</sup></b>
PEI-SA0.5	stearic acid	0.066	0.5	8.4
PEI-SA3.6		0.1	3.6	66.6
PEI-OA1	oleic acid	0.066	1.0	18.1
PEI-OA1.7		0.1	1.7	30.0
PEI-OA2.5		0.2	2.5	44.1
PEI-CA6.9	caprylic acid	0.2	6.9	56.8
PEI-LA1.5	linoleic acid	0.2	1.5	27.2
PEI-LA2.1		0.2	2.1	37.9

<sup>a)</sup>Molar ratios used for synthesis; <sup>b)</sup>Extent of lipid substitution per PEI calculated from <sup>1</sup>H NMR analysis; <sup>c)</sup>Extent of methylene substitution per PEI, calculated based on the extent of substitution (from <sup>1</sup>H NMR) and number of methylene groups in each lipid.

### 4.3.2. Cellular association and uptake studies

The uptake of polymer/siRNA polyplexes was determined in WT and DOX/RES cells at 8:1 polymer:siRNA ratio (w/w). Based on these results PEI25 was the most effective polymer for siRNA delivery, while PEI2 had the least efficacy in both cell lines (**Figure 4.1**). Overall, substitution of lipids on PEI2 increased the association of siRNA complexes with breast cancer cells (**Figure 4.1**). PEI-LA/siRNA polyplexes achieved the highest percentage of siRNA positive cells (~80%) among lipid substituted polymers in both WT and DOX/RES cells (**Figure 4.1A and B**). This level was close to the number of siRNA positive cells achieved by PEI25 in both WT and DOX/RES cells. Lipid substituted polymers showed a higher percentage of cells with siRNA in WT cells compared to DOX/RES cells. Among lipid substituted siRNA polyplexes, PEI-LA polymers showed the highest siRNA delivery (mean fluorescence intensity) in both cell lines while PEI-OA and PEI-SA polymers showed the least uptake, respectively (**Figure 4.1C and D**). Among different lipid substituted PEI2s, PEI-LA2.1, PEI-LA1.5 and PEI-OA2.5 exhibited the highest uptake in WT cells. In DOX/RES cells PEI-LA1.5 showed the highest uptake which was significantly higher than other lipid substituted polymers under study (one way ANOVA followed by post hoc Tukey test,  $P < 0.05$ ).

Furthermore, the cellular distribution of selected polymer/siRNA complexes was investigated in WT cells by fluorescence microscopy (**Figure 4.2**). Very lucid fluorescence was observed in cytoplasm for PEI-LA2.1/siRNA polyplex compared to PEI-LA1.5/siRNA polyplex at both 3 and 24 h. Surprisingly PEI25/siRNA polyplex

exhibited less fluorescence compared to PEI-LA2.1/siRNA polyplex. siRNA delivered with PEI25 appeared to remain in more distinct punctuate (particle) shape, whereas a more disperse pattern was observed for siRNA delivered with PEI-LA polymers.

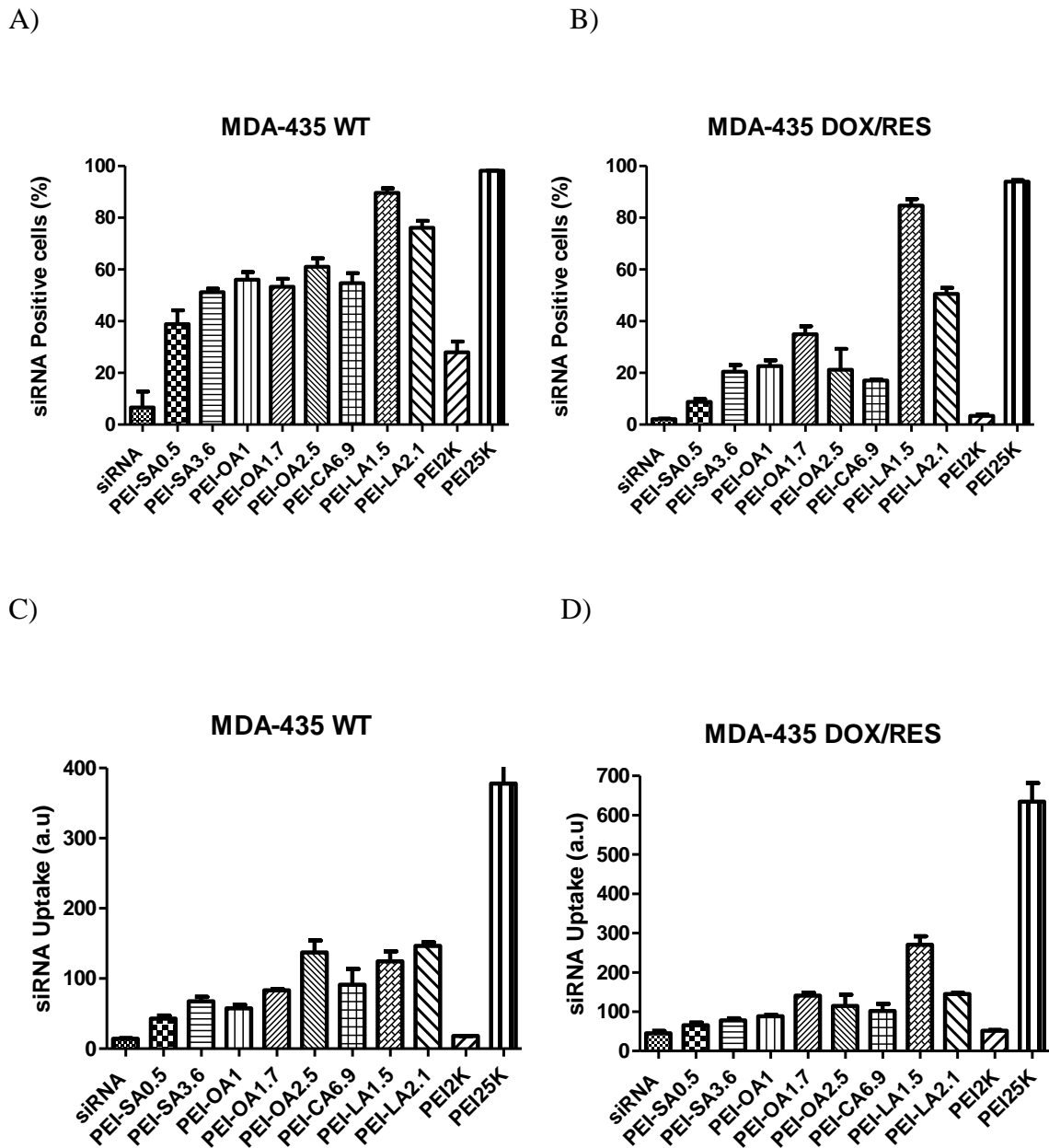
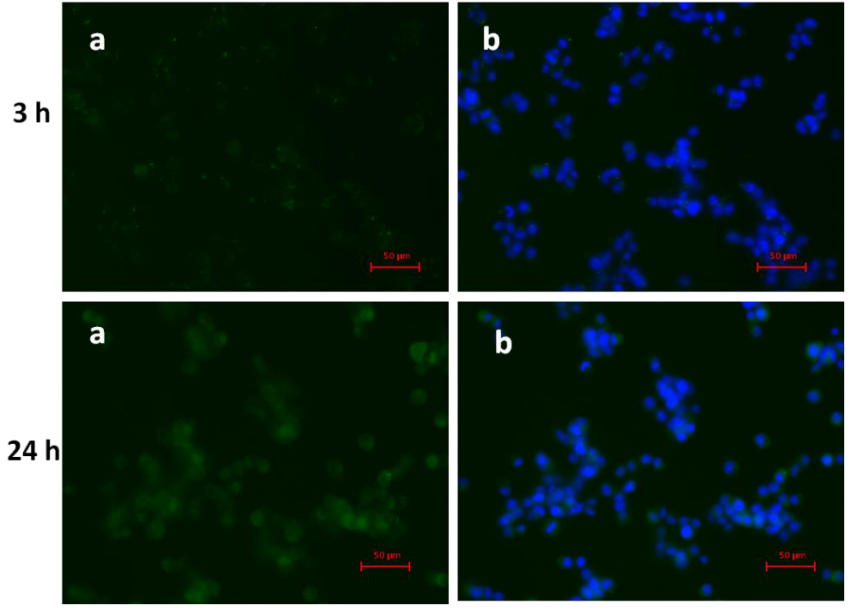


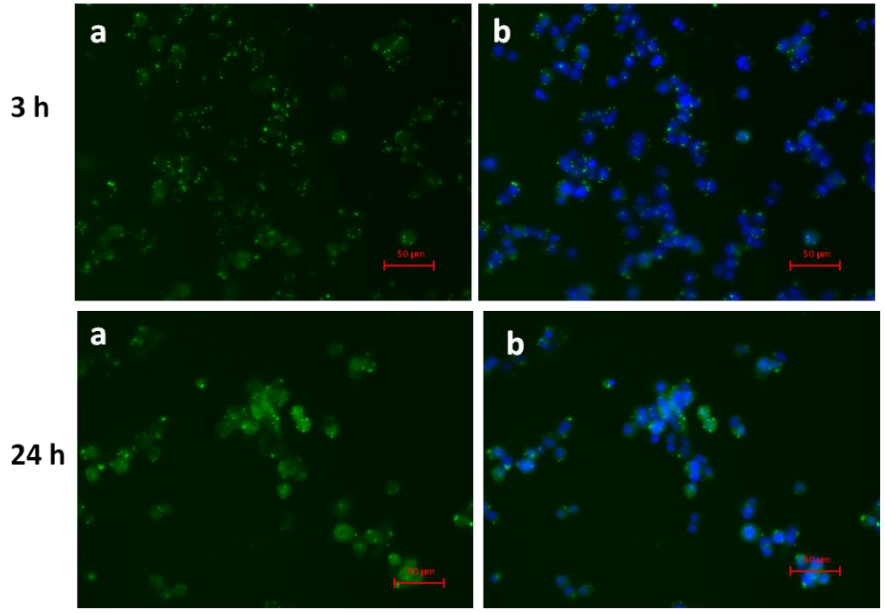
**Figure 4.1.** Cellular uptake of siRNA polyplexes by flow cytometry

Cellular uptake of polymer/FAM-siRNA complexes by MDA-MB-435 WT and DOX/RES cells. A and B) The percentage of cells positive for FAM-siRNA after 24 h exposure to siRNA complexes at polymer:siRNA ratios of 8:1 (weight/weight). C and D) The mean fluorescence of the cells after 24 h exposure to complexes. The complexes were added to the wells to give final polymer and siRNA concentration of 4  $\mu\text{g/mL}$  and 36 nM per well. The data are the mean  $\pm$  SD for n=3.

PEI-LA1.5



PEI-LA2.1



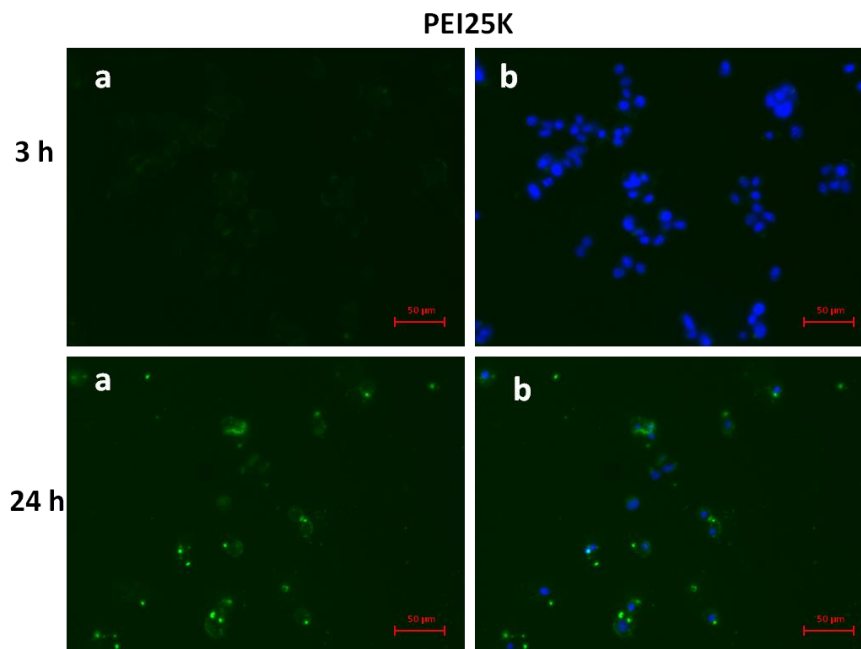


**Figure 4.2.** Cellular distribution of selected siRNA polyplexes by fluorescence microscopy

Uptake and intracellular distribution of FAM-siRNA formulated in polymer by MDA-MB-435 WT cells using fluorescence microscopy. The observation was done after 3 and 24 h exposure to siRNA complexes at polymer:siRNA ratios of 8:1 (weight/weight). The complexes were added to the wells to give final polymer and siRNA concentration of 6  $\mu\text{g}/\text{mL}$  and 54 nM per well. The nucleus was stained with DAPI (blue). a) Images represent FAM-siRNA (green) alone b) Images represent both FAM-siRNA (green) and nucleus (blue).

### 4.3.3. Cytotoxicity of STAT3 and scrambled siRNA polyplexes

The cytotoxic effect of STAT3-siRNA complexed with different polymers within the PEI library was investigated 72 h after treatment with MDA-MB-435 cells using MTT (**Figure 4.3**). Scrambled siRNA containing polyplexes did not cause any considerable non-specific cell death in both cell lines except when complexed with PEI-LA polymers. PEI-LA1.5 and PEI-LA2.1 complexed with scrambled siRNA caused ~50% and 35% cell death in MDA-435 WT cells, respectively. PEI-LA polymers complexed with STAT3-siRNA exhibited a higher level of cell death in WT cells compared to non-specific siRNA complexes, while other polymers in the library did not show any cell death associated with STAT3-siRNA. PEI-LA2.1/STAT3-siRNA polyplex caused ~72% cell death, while PEI-LA1.5/STAT3-siRNA polyplex caused ~68% which were significantly different compared to the same polymer complexes with scrambled siRNA (unpaired Students' t-test,  $P < 0.05$ ). PEI-LA2.1 was the most efficient in terms of STAT3 associated cell death in WT cells. In DOX/RES cells, PEI-CA6.9 and PEI-LA2.1 complexed with STAT3-siRNA showed ~30 and ~40% cell deaths which were significantly higher ( $P < 0.05$ ) compared to cell deaths caused by scrambled siRNA polyplexes. Overall, these results showed the superiority of PEI-LA2.1 polymer in terms of STAT3 associated toxicity over other polymers under study in both cell lines.

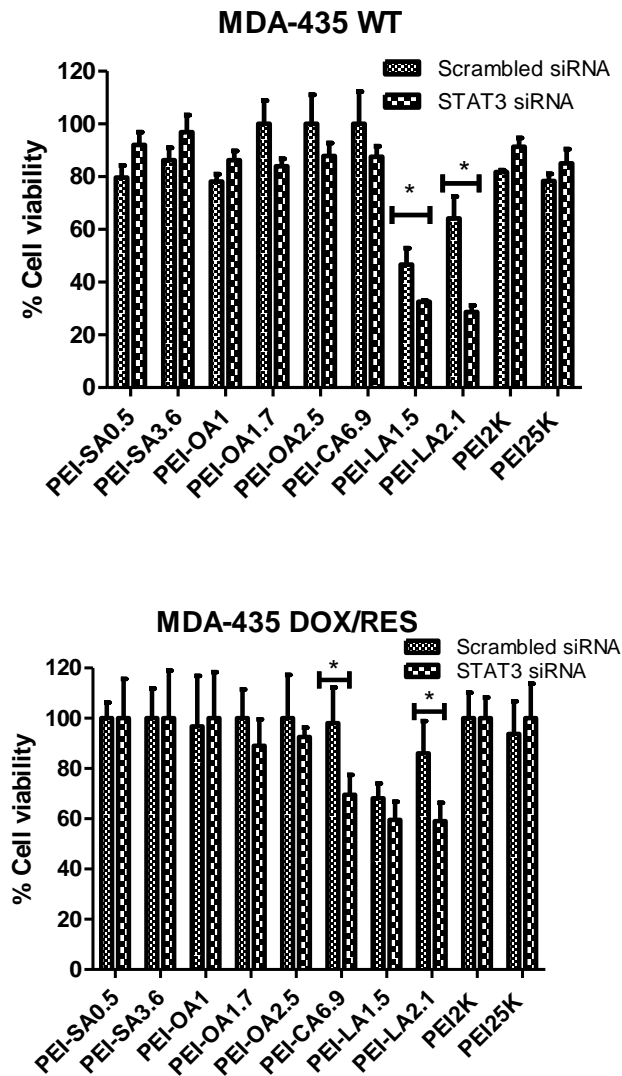


**Figure 4.3.** Cytotoxicity of STAT3-siRNA versus scrambled siRNA polyplexes.

The viability of the MDA-MB-435 WT and DOX/RES cells after 72 h exposure to polymer/siRNA polyplexes prepared using the scrambled and STAT3-siRNA at polymer:siRNA ratio of 8:1 (weight/weight). The complexes were added to the wells to give final polymer and siRNA concentration of 6  $\mu\text{g}/\text{mL}$  and 54 nM per well, respectively. The data are the mean  $\pm$  SD for n=3. \*Significantly different (unpaired student's t-test,  $P < 0.05$ ).

#### 4.3.4. Cytotoxicity at different PEI-LA:siRNA ratios

In order to find the optimum PEI-LA polymer:siRNA ratio, cytotoxicity of STAT3 and scrambled siRNA complexed with PEI-LA polymers at different polymer:siRNA ratios were investigated 72 h after treatment (**Figure 4.4**). The polymer:siRNA ratios were set at 2:1, 4:1 and 8:1 (w/w). Scrambled siRNA containing complexes did not cause considerable non-specific cell death in both cell lines except for PEI-LA polymer/siRNA complexes at polymer:siRNA ratio of 8:1 (w/w). PEI-LA1.5 and PEI-LA2.1 complexed with STAT3-siRNA exhibited the highest STAT3 associated cell death at 8:1 polymer:siRNA (w/w) ratio in WT cells showing ~68% and ~74% cell death, respectively, compared to 27 and 34 % cell death for same polymer polyplexes with scrambled siRNA. In DOX/RES cells, PEI-LA2.1/STAT3-siRNA polyplex at 8:1 polymer:siRNA (w/w) ratio was the only effective polyplex in exhibiting STAT3 associated cell death (at ~28%). The PEI-LA2.1/scrambled siRNA polyplexes did not cause cell death in RES/DOX cells. These results proved the superiority of PEI-LA2.1 polymer/siRNA complex at 8:1 (w/w) ratios in terms of STAT3 associated toxicity over other ratios under study in both cell lines.

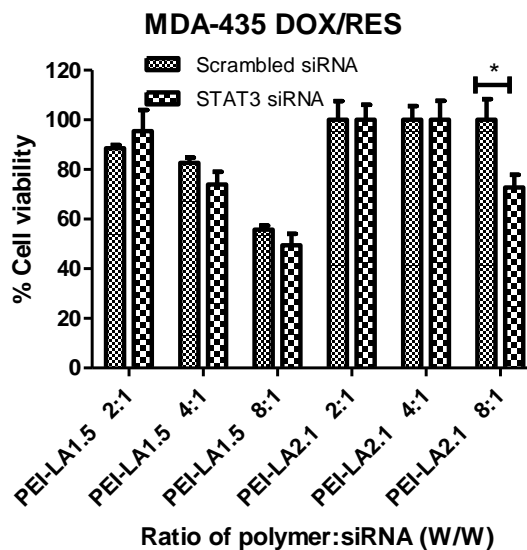
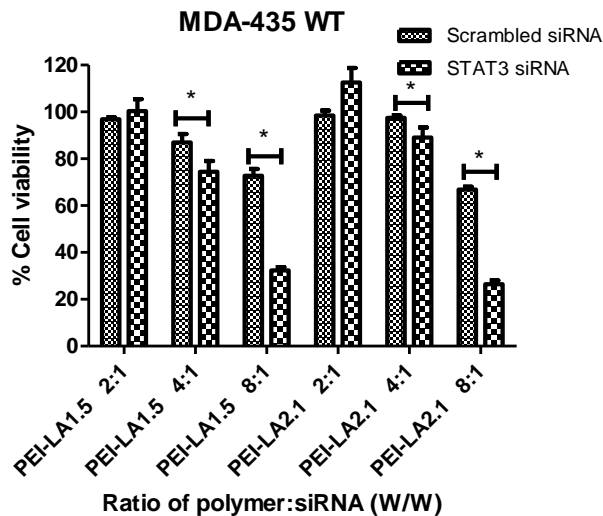


**Figure 4.4.** PEI-LA polymer efficiency

The viability of the MDA-MB-435 WT and DOX/RES cells after 72 h exposure to PEI-LA/siRNA complexes prepared using the scrambled and STAT3-siRNA at polymer:siRNA ratios of 2:1, 4:1 and 8:1 (weight/weight). The complexes were added to the wells to give final polymer concentrations of 1.5, 3 and 6  $\mu\text{g}/\text{mL}$  and siRNA concentration 54 nM per well. The data are the mean  $\pm$  SD for  $n=3$ . \*Significantly different (unpaired student's t-test,  $P<0.05$ ).

#### **4.3.5. siRNA dose response with PEI-LA2.1 polymer**

To evaluate the optimum siRNA dose for STAT3 specific cell death, WT and DOX/RES cells were treated with PEI-LA2.1/STAT3-siRNA polyplexes with varying siRNA doses ranging from 9 to 72 nM per well (**Figure 4.5**). PEI-LA2.1/STAT3-siRNA complexes with siRNA doses of 45, 54 and 72 nM exhibited STAT3 associated cell death which were significantly different from cell death observed by their identical scrambled siRNA polyplexes (unpaired students' t-test,  $P < 0.05$ ). The highest STAT3 associated cell death in WT cells was achieved with 54 nM siRNA/polymer complex, where STAT3-siRNA polyplexes caused ~58% cell compared to ~17 % cell death by scrambled siRNA polyplexes. In DOX/RES cells, STAT3 associated cell death was evident at doses of 18, 27, 45 and 54 (~19, 39, 40 and 60% cell death, respectively). This was significantly different from cell death caused by identical scrambled siRNA polyplex doses (~8, 14, 26 and 14% cell death, respectively). These results implied that PEI-LA2.1 polymer/siRNA complex with 54 nM siRNA dose to be the most effective in terms of STAT3 associated toxicity compared to other doses in both cell lines.

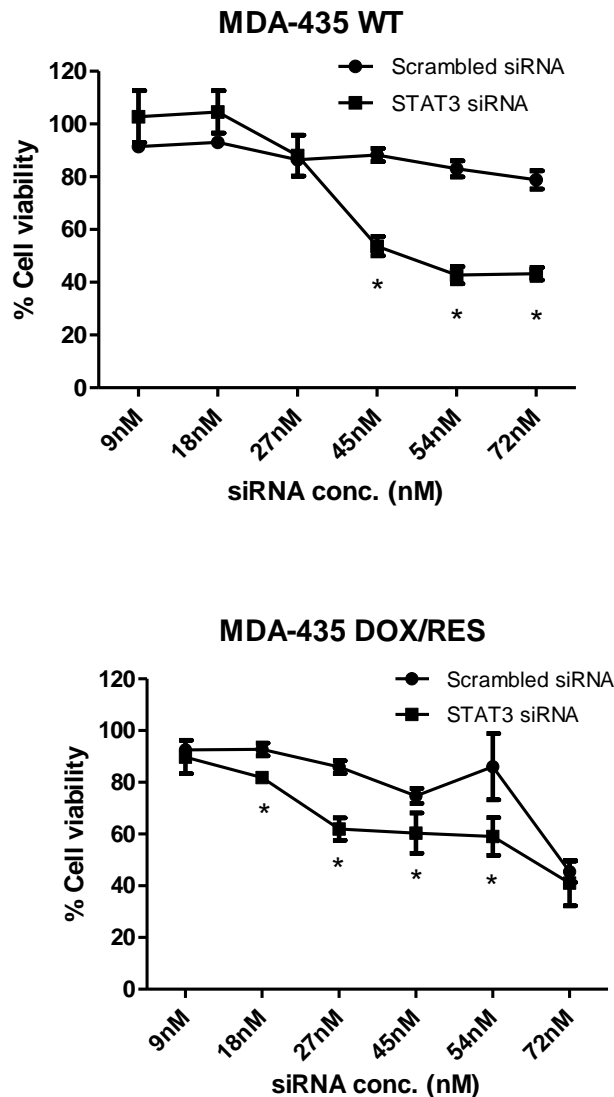


**Figure 4.5.** siRNA dose response with PEI-LA2.1 polymer

The viability of the MDA-MB-435 WT and MDA-435 DOX/RES cells after 72 h exposure to PEI-LA2.1/siRNA complexes prepared using the scrambled and STAT3-siRNA at polymer:siRNA ratios of 8:1 (weight/weight). The complexes were added to the wells to give final siRNA concentrations 9, 18, 27, 45, 54 and 72 nM per well. The data are the mean  $\pm$  SD for n=3. \*Significantly different from their identical scrambled siRNA polyplexes (unpaired student's t-test,  $P < 0.05$ ).

#### 4.3.6. STAT3 knockdown by siRNA complexes

To evaluate the ability of PEI-LA2.1/STAT3-siRNA polyplexes for STAT3 silencing at mRNA level, WT and DOX/RES were treated for 48 h with siRNA dose of 54 nM and polymer:siRNA ratio of 8:1 (w/w) (**Figure 4.6**). In WT cells, the level of STAT3 mRNA expression after incubation with STAT3-siRNA polyplex was reduced by ~70% compared to its corresponding non-treated (NT) control group. Identical polyplexes with scrambled siRNA did not decrease STAT3 mRNA expression. In DOX/RES cells, STAT3-siRNA polyplex caused a ~90% decrease in mRNA expression compared to its non-treated control group. STAT3-siRNA polyplex also caused a significant reduction (~85%) in STAT3 mRNA expression compared to identical scrambled siRNA polyplexes. Interestingly, the level of STAT3 mRNA expression has almost doubled in non-treated DOX/RES cells when compared to non-treated WT cells.

STAT3 and p-STAT3 protein levels were measured after 48 h treatment with PEI-LA2.1/siRNA polyplexes prepared at 8:1 ratio (w/w) and 54 nM siRNA dose (**Figure 4.7**). In WT cells, both STAT3 and p-STAT3 levels decreased significantly when treated with STAT3-siRNA polyplex compared to non-treated control group. Identical polyplexes with scrambled siRNA did not cause a reduction of STAT3 protein compared to non-treated group. In DOX/RES cells, the level of both STAT3 and p-STAT3 decreased significantly upon treatment with STAT3-siRNA when compared to their non-treated control groups. A non-specific reduction in STAT3 and p-STAT3 protein expression was observed with identical scrambled siRNA polyplexes in RES/DOX cells.

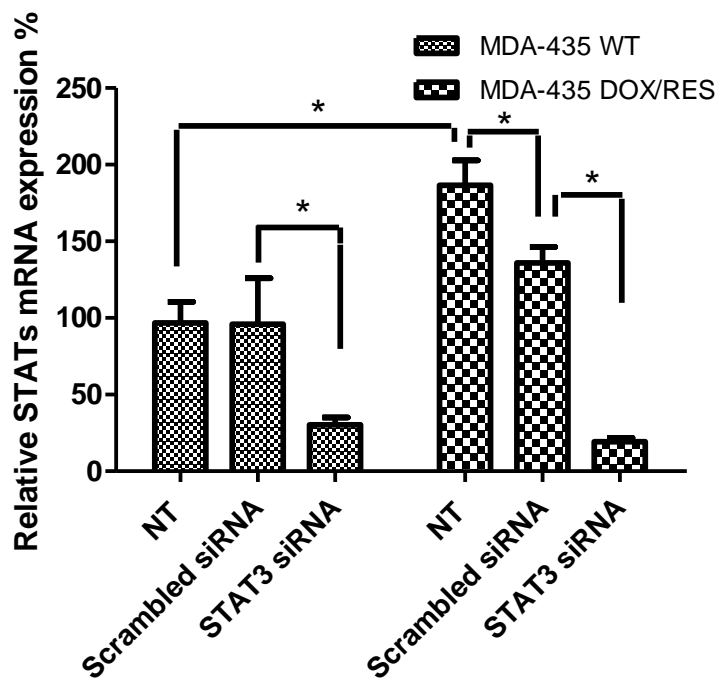


**Figure 4.6.** Silencing activity of STAT3-siRNA polyplexes by RT-PCR

STAT3 silencing activity of the STAT3-siRNA at mRNA level in MDA-MB-435 WT and DOX/RES cells after transfection with STAT3-siRNA formulated in PEI-LA2.1/siRNA polyplexes prepared using polymer:siRNA ratios of 8:1 (weight/weight). The complexes were added to the wells to give final polymer and siRNA concentrations 6  $\mu\text{g}/\text{mL}$  and 54 nM per well. Values are relative to non-treated controls (NT). The data are the mean  $\pm$  SD for  $n=3$ . \* Significantly different (one way ANOVA followed by Tukey test,  $P<0.05$ ).

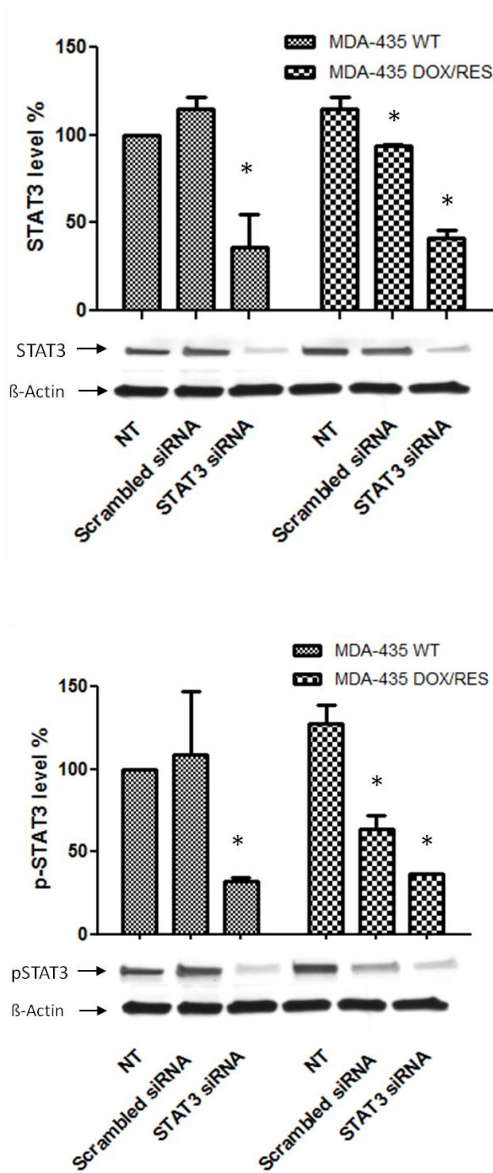


**Figure 4.7.** Silencing activity of STAT3-siRNA polyplexes by Western blot

STAT3 silencing activity of the STAT3-siRNA at protein level in MDA-MB-435 WT and DOX/RES cells after transfection with STAT3-siRNA formulated in PEI-LA2.1/siRNA polyplexes prepared using polymer:siRNA ratios of 8:1 (weight/weight). The complexes were added to the wells to give final polymer and siRNA concentrations 6  $\mu\text{g}/\text{mL}$  and 54 nM per well. Values are relative to non-treated controls (NT). \*Significantly different from its non-treated control (one way ANOVA followed by Tukey test,  $P < 0.05$ ).

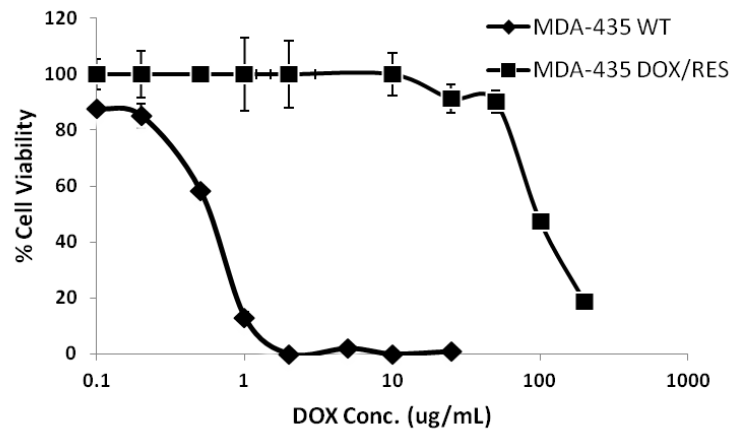
#### 4.3.7. Effect of STAT3 silencing on the cytotoxicity of DOX and PTX

The cytotoxicity of free DOX and PTX alone were evaluated in both WT and DOX/RES cells. A wide range of concentrations was used for DOX (0.1-200  $\mu\text{g}/\text{mL}$ ; **Figure 4.8A**) and PTX (0.2-1638  $\text{ng}/\text{mL}$ ; **Figure 4.8B**), respectively. As expected, the efficacy of both DOX and PTX in DOX/RES cells were significantly hampered. In light of previous results, we then examined the effect of STAT3 silencing on the cytotoxicity of DOX and PTX. As shown in **Figure 4.8C**, compared to WT cells treated with DOX alone (0.02-0.2  $\mu\text{g}/\text{mL}$ ), those pre-exposed to STAT3-siRNA/PEI-LA2.1 polyplexes and then treated with DOX at similar concentrations, showed significant increase in cell death (by ~25%). Pre-exposure of WT cells to scrambled siRNA polyplexes followed by DOX treatment did not cause changes in cytotoxic effect of drugs. A similar trend was observed in DOX/RES cells when pre-exposed to STAT3-siRNA polyplexes (**Figure 4.8D**). Treatment with STAT3-siRNA formulation, followed by 50  $\mu\text{g}/\text{mL}$  DOX treatment caused ~18% more cell death compared to identical dose of DOX alone.

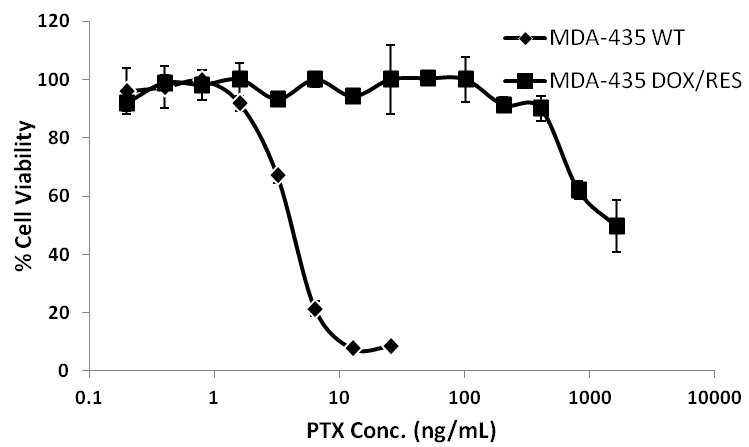
In the case of PTX, a ~25% reduction in cell viability was observed when WT cells were pre-exposed to STAT3-siRNA polyplexes, and then treated with PTX (0.1-1.6  $\text{ng}/\text{mL}$ ) compared to PTX treatment alone (**Figure 4.8E**). Non-specific toxicity was not observed when cells were treated with scrambled siRNA formulations. In DOX/RES cells, ~40% cell death was observed when cells were exposed to STAT3-siRNA formulation and PTX (25.6  $\text{ng}/\text{mL}$ ) combined (**Figure 4.8F**). This was in contrast to PTX

alone treatment at the same concentration that led to 2 % cell death in DOX/RES MDA-MB-435 cells upon 24 h incubation.

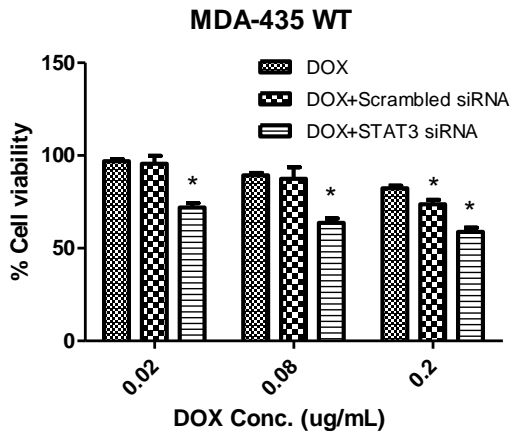
A)



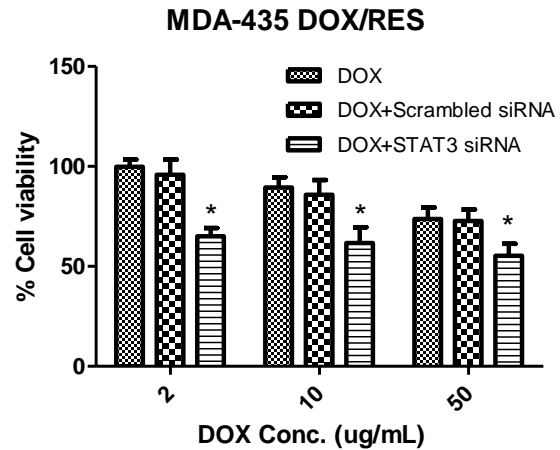
B)



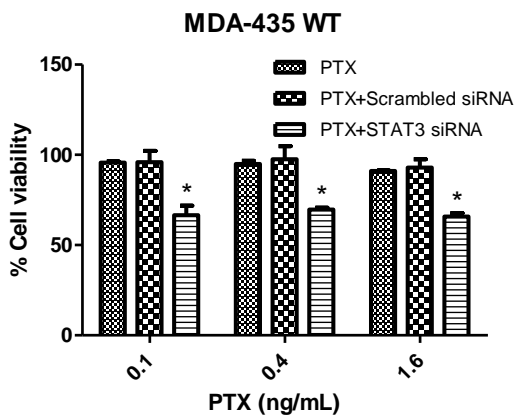
C)



D)



E)



F)

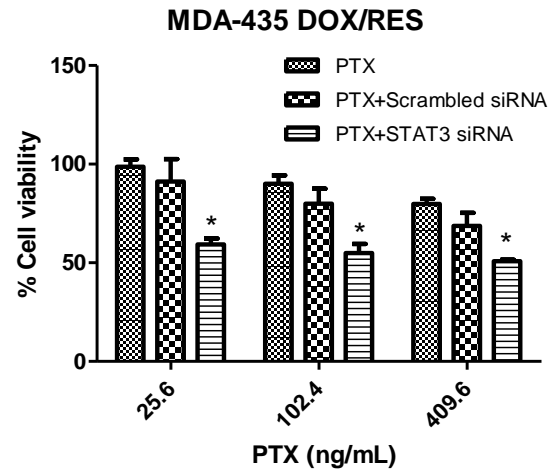


**Figure 4.8.** Effect of STAT3-siRNA/PEI-LA pre-treatment on the cytotoxicity of Doxorubicin and Paclitaxel in WT and resistant breast cancer cells. A) The viability of the MDA-MB-435 WT and DOX/RES cells after 48 h exposure to DOX alone B) The viability of the MDA-MB-435 WT and DOX/RES cells after 48 h exposure to PTX alone. The viability of the MDA-435 WT and MDA-435 DOX/RES cells after 48 h exposure to PEI-LA2.1/siRNA complexes and 24 h exposure to Doxorubicin (C and D) or Paclitaxel (E and F). The complexes were added to the wells to give final polymer concentrations of 6  $\mu\text{g/mL}$  and siRNA concentration 54 nM per well. The data are the mean  $\pm$  SD for  $n=3$ . \*Significantly different from DOX or PTX alone (one way ANOVA followed by Tukey test,  $P<0.05$ ).

#### 4.4. Discussion

STAT3 is persistently tyrosine-phosphorylated in 50% of primary breast carcinomas and tumor-derived cell lines [40, 41]. Clinical studies demonstrated that elevated levels of tyrosine-phosphorylated Stat3 (p-STAT3) to be a poor prognostic feature in breast cancer patients and correlates with an incomplete response to neoadjuvant chemotherapy [42, 43]. Recently, Marotta et al. discovered a network of 15 genes that are required for cell growth and proliferation in CD44<sup>+</sup>CD24<sup>-</sup> human stem cell-like breast cancer cells. STAT3 has been emphasized to have a critical role as key downstream transcriptional effector in this network. They found that inhibition of several of these genes such as IL6, PTGIS, HAS1, CXCL3, and PFKFB3 down-regulated STAT3 activation. It was proposed that a STAT3 inactivation treatment in combination with other chemotherapeutic drugs may circumvent therapeutic resistance and lower the side effects of cancer treatment [44]. Inhibition of STAT3 as a molecular target in breast cancer models has been mostly pursued through application of small molecule inhibitors. In this context, Turkson et al. identified ISS 610, a peptidomimetic analog of the tripeptide PY\*L, which binds to STAT3 SH2 domain. This molecule was shown to inhibit constitutively active STAT3 and caused selective growth blockage and initiation of apoptosis in MDAMB-231 and MDA-MB-435 human breast carcinoma cells that contain persistently active STAT3 [45]. A small molecule inhibitor of STAT3 dimerization, STA-21 has shown to inhibit growth and survival of MDA-MB-231, MDA-MB-435, and MDA-MB-468 breast cancer cells with constitutive STAT3 signaling [46]. In another study, platinum compounds CPA-1, CPA-7, and platinum (IV) tetrachloride

have been used to block STAT3 activity. These compounds inhibited STAT3 DNA binding, its mediated gene regulation and caused growth inhibition and apoptosis in MDA-MB-231 and MDA-MB-435 human breast cells [47]. Inhibition of STAT3 activation is shown to be an effective strategy in inhibition of breast cancer growth, however, many functions of STAT3 protein is regulated through its interaction with other transcription factors by mechanisms that are independent of phosphorylated status of STAT3 protein.

An alternative approach has sought inhibiting the expression of STAT3 protein (rather than inhibition of its activation) using oligonucleotides [48, 49] and siRNAs [50] for application in cancer therapy. RNAi has been investigated for targeting STAT3 expression as a more explicit modality. However, advancement of this technology has been relatively slow, mainly due to difficulties associated with its safe and effective delivery in a clinical setting [24]. Different non-viral delivery materials including lipids and polymeric nano-carriers have been examined for STAT3 siRNA delivery in different cancer models. For instance, inhibition of STAT3 by siRNA, inducing apoptosis in B16 melanoma tumor tissue has been achieved using nanoparticles based on polyethylenimine (PEI) 25KDa modified with stearic acid (STA) for siRNA delivery by our group. In that study, at 50 nM siRNA, PEI-StA complexes showed up to 60% reduction in p-STAT3 protein level compared to non-treated control. This has led to a significant regression in tumor growth after multi-dose treatments both *in vitro* and *in vivo* (upon intra-tumoral administration). Factors associated with STAT3 activity i.e. IL-6 level and caspase-3 activity were increased, while a reduction of VEGF level has been achieved [11]. In

another study, STAT3 down-regulation using siRNA-Lipofectamine™ 2000 complex has been demonstrated to hinder cell motility and invasion, as well as inducing cell death in human DU145 and PC3 prostate cancer cells *in vitro* [51]. Zhang et al. used targeted STAT3 with siRNA expressing plasmid in human hepatocellular carcinoma Bel-7402 cells. A siRNA and rapamycin combined treatment enhanced apoptosis and up-regulated cleaved caspase 3 in Bel-7402 cells [52].

In the current study, we investigated application of lipid-substituted (low molecular weight) PEI2 polymer-siRNA complexes for STAT3 down-regulation in a model triple negative human breast cancer (TNBC) cell line, MDA-MB-435 cells. The possible efficacy of this approach in reducing the viability of WT and DOX/RES phenotypes alone or in combination with common anticancer agents used in therapy of TNBC (i.e., DOX and PTX) was also investigated. Lipid modification of polymers has been pursued as a method to enhance the efficacy of polymeric complexes in delivering siRNA to cells. The lipid substitution of polymers is suggested to help the cellular uptake of siRNA complexes due to increased interaction of polyplexes with cell membrane [53]. Our results demonstrated that some of lipid-substituted polymers under study (not all) were quite effective for siRNA delivery into cells (**Figure 4.1**). Cellular association of siRNA was highest when complexed with PEI-LA polymer as compared to other lipid-substituted PEI2s. The results was in line with previous findings by Aliabadi et al. who also reported that LA-substituted PEI2 to be the most effective carrier for siRNA delivery among lipid-substituted PEI2s [37]. Fluorescence microscope images confirmed the results of flow cytometry revealing better intracellular uptake of siRNA by PEI-LA2.1

polyplexes (**Figure 4.2**). PEI-LA2.1 appeared to be successful in delivery of complexed siRNA into cytoplasm, whereas siRNA complexed by PEI 25K appeared as distinct particle in cytoplasm as well as in the nucleus. Accumulation of siRNA in released not particulate form and in the cytoplasm where its target mRNA locates (rather than nucleus) provides advantage for the lipid-substituted PEI 2K over PEI 25K for siRNA delivery. We have then screened the library of lipid-PEI2K forming polyplexes with scrambled and STAT3-siRNA for induction of non-specific and STAT3 associated cell death, respectively, in both WT and DOX/RES human breast cancer cells. STAT3 is known to regulate the expression of anti-apoptotic factors such as BCL-2, BCL-xL, MCL-1 and Survivin [54-58] in breast cancer cells, hence inhibition of STAT3 is expected to lead to cancer cell death. Among lipid-substituted polymers under study, PEI-LA2.1 exhibited the most effective results in causing a significantly higher level of cytotoxicity after delivery of STAT3-siRNA compared to scrambled siRNA polyplexes in both cell lines (**Figure 4.3**). We then tried to maximize the efficiency of the PEI2-LA polyplexes of STAT3-siRNA by assessing the effect of polymer:siRNA (w/w) ratio on the cytotoxicity against MDA-MB-435 WT and DOX/RES cells making comparisons with identical polyplexes of scrambled siRNA. The complexes prepared at the ratio of 8:1 generally showed better efficiency (more STAT3 associated cell cytotoxicity) compared to the 2:1 and 4:1 ratios (**Figure 4.4**). This can be explained by higher association of lipid-substituted polyplexes with the cell membrane at higher ratios of polymer to siRNA. A siRNA dose-response experiment showed a siRNA dose of 54 nM to be the most effective dose for STAT3 mediated cell cytotoxicity effect in both WT and DOX/RES

cells. At this dose, PEI-LA2.1/STAT3-siRNA polyplex also yielded significant silencing of STAT3 mRNA and protein in both WT and DOX/RES cell lines compared to untreated cells or cells treated with scrambled siRNA polyplexes (**Figure 4.6 and 4.7**). In DOX/RES cells an unspecific STAT3 mRNA silencing as well as STAT3 and p-STAT3 protein down-regulation for the polyplexes made from scrambled siRNA was seen (**Figure 4.6 and 4.7**). The reason for this observation is not clear. Interestingly, relative mRNA expression almost doubled in DOX/RES cells compared to WT cells (**Figure 4.6**). This may imply a possible role for up-regulation of STAT3 expression, as a mechanism of drug resistance in DOX/RES breast cancer cells. Conventional anti-neoplastic drugs, i.e., DOX and PTX, are included in the majority of chemotherapy regimens for breast cancer patients [59, 60]. However, nonspecific distribution leading to intolerable adverse effects, restricted access and accumulation of these anticancer agents to tumor site upon systemic administration and development of drug resistance have limited their clinical success specially in advanced stages of the disease. Inhibition of STAT3 expression and/or activity in breast tumors was hypothesized to reduce the threshold cytotoxic dose of standard anti-cancer agents in both WT and RES breast cancer phenotypes. In this study, this hypothesis was examined through STAT3 silencing by PEI-LA polyplexes in breast cancer cells. Then, cytotoxicity analysis was carried out combining STAT3-siRNA polyplexes with DOX and PTX treatment in WT and DOX/RES human breast cancer cells. As expected, the efficacy of both DOX and PTX in DOX/RES cells were significantly decreased compared to WT cells (**Figure 4.8A and 4.8B**). Over-expression of STAT3 might be responsible for this resistance, partly. Our

data showed an increase in the cytotoxic efficacy when STAT3-siRNA/PEI-LA polyplexes were combined with DOX and PTX. Overall, the results of our studies provides proof for the benefit of STAT3 silencing in enhancing the potency of chemotherapeutic drugs in breast tumors or their anti-cancer activity at given doses. A combination approach in therapy can take care of STAT3<sup>+</sup> RES cells in heterogenous breast tumor population and enhance the effect of standard chemotherapy in primary or reoccurring breast tumors. These observations point to the capability of silencing STAT3 expression as potential therapeutic modality and its ability to potentiate anti-cancer drug activity in both sensitive and resistant phenotype.

#### **4.5. Conclusion**

In this study, we reported on effective silencing of STAT3 that is involved in cancer proliferation and survival, angiogenesis and invasion, and tumor induced immune-suppression by lipid-substituted low molecular weight PEI polyplexes of specific siRNA. Effective delivery of STAT3-siRNA into MDA-MB-435 cell translated into efficient down-regulation of STAT3 mRNA and protein, and subsequent cell death. STAT3 down-regulation additionally increased the cytotoxic capability of model anti-cancer drugs, i.e. DOX and PTX, in WT and DOX/RES breast tumor phenotypes. The result of this study provided proof of concept for combination therapy approaches combining STAT3 silencing with conventional chemotherapy as means to improve the clinical benefit of breast cancer chemotherapy in both WT and RES breast tumor phenotypes.

#### 4.6. References

- [1] Schust J, Sperl B, Hollis A, Mayer TU, Berg T. Stattic: a small-molecule inhibitor of STAT3 activation and dimerization. *Chem Biol* 2006;13:1235-42.
- [2] Walker SR, Nelson EA, Zou L, Chaudhury M, Signoretti S, Richardson A, et al. Reciprocal effects of STAT5 and STAT3 in breast cancer. *Mol Cancer Res* 2009;7:966-76.
- [3] Lin TS, Mahajan S, Frank DA. STAT signaling in the pathogenesis and treatment of leukemias. *Oncogene* 2000;19:2496-504.
- [4] Turkson J, Jove R. STAT proteins: novel molecular targets for cancer drug discovery. *Oncogene* 2000;19:6613-26.
- [5] Zhong Z, Wen Z, Darnell JE, Jr. Stat3: a STAT family member activated by tyrosine phosphorylation in response to epidermal growth factor and interleukin-6. *Science* 1994;264:95-8.
- [6] Ruff-Jamison S, Zhong Z, Wen Z, Chen K, Darnell JE, Jr., Cohen S. Epidermal growth factor and lipopolysaccharide activate Stat3 transcription factor in mouse liver. *J Biol Chem* 1994;269:21933-5.
- [7] Darnell JE, Jr., Kerr IM, Stark GR. Jak-STAT pathways and transcriptional activation in response to IFNs and other extracellular signaling proteins. *Science* 1994;264:1415-21.
- [8] Heinrich PC, Horn F, Graeve L, Dittrich E, Kerr I, Muller-Newen G, et al. Interleukin-6 and related cytokines: effect on the acute phase reaction. *Z Ernahrungswiss* 1998;37 Suppl 1:43-9.
- [9] Sumimoto H, Imabayashi F, Iwata T, Kawakami Y. The BRAF-MAPK signaling pathway is essential for cancer-immune evasion in human melanoma cells. *J Exp Med* 2006;203:1651-6.
- [10] Burdelya L, Kujawski M, Niu GL, Zhong B, Wang TH, Zhang SM, et al. Stat3 activity in melanoma cells affects migration of immune effector cells and nitric oxide-mediated antitumor effects. *Journal of Immunology* 2005;174:3925-31.
- [11] Alshamsan A, Hamdy S, Samuel J, El-Kadi AO, Lavasanifar A, Uludag H. The induction of tumor apoptosis in B16 melanoma following STAT3 siRNA delivery with a lipid-substituted polyethylenimine. *Biomaterials* 2010;31:1420-8.
- [12] Yu H, Jove R. The STATs of cancer--new molecular targets come of age. *Nat Rev Cancer* 2004;4:97-105.
- [13] Wojcik EJ, Sharifpoor S, Miller NA, Wright TG, Watering R, Tremblay EA, et al. A novel activating function of c-Src and Stat3 on HGF transcription in mammary carcinoma cells. *Oncogene* 2006;25:2773-84.
- [14] Xie TX, Wei D, Liu M, Gao AC, Ali-Osman F, Sawaya R, et al. Stat3 activation regulates the expression of matrix metalloproteinase-2 and tumor invasion and metastasis. *Oncogene* 2004;23:3550-60.
- [15] Yu H, Kortylewski M, Pardoll D. Crosstalk between cancer and immune cells: role of STAT3 in the tumour microenvironment. *Nat Rev Immunol* 2007;7:41-51.
- [16] Blaskovich MA, Sun J, Cantor A, Turkson J, Jove R, Sefti SM. Discovery of JSI-124 (cucurbitacin I), a selective Janus kinase/signal transducer and activator of

transcription 3 signaling pathway inhibitor with potent antitumor activity against human and murine cancer cells in mice. *Cancer Res* 2003;63:1270-9.

[17] Bharti AC, Donato N, Aggarwal BB. Curcumin (diferuloylmethane) inhibits constitutive and IL-6-inducible STAT3 phosphorylation in human multiple myeloma cells. *J Immunol* 2003;171:3863-71.

[18] Catlett-Falcone R, Landowski TH, Oshiro MM, Turkson J, Levitzki A, Savino R, et al. Constitutive activation of Stat3 signaling confers resistance to apoptosis in human U266 myeloma cells. *Immunity* 1999;10:105-15.

[19] Turkson J, Ryan D, Kim JS, Zhang Y, Chen Z, Haura E, et al. Phosphotyrosyl peptides block Stat3-mediated DNA binding activity, gene regulation, and cell transformation. *J Biol Chem* 2001;276:45443-55.

[20] Turkson J, Zhang SM, Mora LB, Burns A, Sebt S, Jove R. A novel platinum compound inhibits constitutive Stat3 signaling and induces cell cycle arrest and apoptosis of malignant cells. *Journal of Biological Chemistry* 2005;280:32979-88.

[21] Liu X, Li J, Zhang J. STAT3-decoy ODN inhibits cytokine autocrine of murine tumor cells. *Cell Mol Immunol* 2007;4:309-13.

[22] Yue P, Turkson J. Targeting STAT3 in cancer: how successful are we? *Expert Opin Investig Drugs* 2009;18:45-56.

[23] Wang Z, Rao DD, Senzer N, Nemunaitis J. RNA interference and cancer therapy. *Pharm Res* 2011;28:2983-95.

[24] Falamarzian A, Xiong XB, Uludag H, Lavasanifar A. Polymeric micelles for siRNA delivery. *J Drug Deliv Sci Tec* 2012;22:43-54.

[25] Shim MS, Kwon YJ. Efficient and targeted delivery of siRNA in vivo. *FEBS J* 2010;277:4814-27.

[26] Kim SS, Garg H, Joshi A, Manjunath N. Strategies for targeted nonviral delivery of siRNAs in vivo. *Trends Mol Med* 2009;15:491-500.

[27] Dykxhoorn DM, Palliser D, Lieberman J. The silent treatment: siRNAs as small molecule drugs. *Gene Ther* 2006;13:541-52.

[28] Xiong XB, Uludag H, Lavasanifar A. Biodegradable amphiphilic poly(ethylene oxide)-block-polyesters with grafted polyamines as supramolecular nanocarriers for efficient siRNA delivery. *Biomaterials* 2009;30:242-53.

[29] Edelstein ML, Abedi MR, Wixon J. Gene therapy clinical trials worldwide to 2007--an update. *J Gene Med* 2007;9:833-42.

[30] Couto LB, High KA. Viral vector-mediated RNA interference. *Curr Opin Pharmacol* 2010;10:534-42.

[31] Putnam D. Polymers for gene delivery across length scales. *Nat Mater* 2006;5:439-51.

[32] Gunther M, Lipka J, Malek A, Gutsch D, Kreyling W, Aigner A. Polyethylenimines for RNAi-mediated gene targeting in vivo and siRNA delivery to the lung. *Eur J Pharm Biopharm* 2011;77:438-49.

[33] Grayson AC, Doody AM, Putnam D. Biophysical and structural characterization of polyethylenimine-mediated siRNA delivery in vitro. *Pharm Res* 2006;23:1868-76.

- [34] Boussif O, Lezoualc'h F, Zanta MA, Mergny MD, Scherman D, Demeneix B, et al. A versatile vector for gene and oligonucleotide transfer into cells in culture and in vivo: polyethylenimine. *Proc Natl Acad Sci U S A* 1995;92:7297-301.
- [35] Aigner A. Gene silencing through RNA interference (RNAi) in vivo: strategies based on the direct application of siRNAs. *J Biotechnol* 2006;124:12-25.
- [36] Neamnark A, Suwantong O, Bahadur RK, Hsu CY, Supaphol P, Uludag H. Aliphatic lipid substitution on 2 kDa polyethylenimine improves plasmid delivery and transgene expression. *Mol Pharm* 2009;6:1798-815.
- [37] Aliabadi HM, Landry B, Bahadur RK, Neamnark A, Suwantong O, Uludag H. Impact of lipid substitution on assembly and delivery of siRNA by cationic polymers. *Macromol Biosci* 2011;11:662-72.
- [38] Aliabadi HM, Landry B, Mahdipoor P, Hsu CY, Uludag H. Effective down-regulation of breast cancer resistance protein (BCRP) by siRNA delivery using lipid-substituted aliphatic polymers. *Eur J Pharm Biopharm* 2012;81:33-42.
- [39] Incani V, Tunis E, Clements BA, Olson C, Kucharski C, Lavasanifar A, et al. Palmitic acid substitution on cationic polymers for effective delivery of plasmid DNA to bone marrow stromal cells. *J Biomed Mater Res A* 2007;81:493-504.
- [40] Silva CM. Role of STATs as downstream signal transducers in Src family kinase-mediated tumorigenesis. *Oncogene* 2004;23:8017-23.
- [41] Darnell JE. Validating Stat3 in cancer therapy. *Nat Med* 2005;11:595-6.
- [42] Gariboldi MB, Ravizza R, Molteni R, Osella D, Gabano E, Monti E. Inhibition of Stat3 increases doxorubicin sensitivity in a human metastatic breast cancer cell line. *Cancer Lett* 2007;258:181-8.
- [43] Barre B, Vigneron A, Perkins N, Roninson IB, Gamelin E, Coqueret O. The STAT3 oncogene as a predictive marker of drug resistance. *Trends Mol Med* 2007;13:4-11.
- [44] Marotta LL, Almendro V, Marusyk A, Shipitsin M, Schemme J, Walker SR, et al. The JAK2/STAT3 signaling pathway is required for growth of CD44(+)CD24(-) stem cell-like breast cancer cells in human tumors. *J Clin Invest* 2011;121:2723-35.
- [45] Turkson J, Kim JS, Zhang S, Yuan J, Huang M, Glenn M, et al. Novel peptidomimetic inhibitors of signal transducer and activator of transcription 3 dimerization and biological activity. *Mol Cancer Ther* 2004;3:261-9.
- [46] Song H, Wang R, Wang S, Lin J. A low-molecular-weight compound discovered through virtual database screening inhibits Stat3 function in breast cancer cells. *Proc Natl Acad Sci U S A* 2005;102:4700-5.
- [47] Turkson J, Zhang S, Palmer J, Kay H, Stanko J, Mora LB, et al. Inhibition of constitutive signal transducer and activator of transcription 3 activation by novel platinum complexes with potent antitumor activity. *Mol Cancer Ther* 2004;3:1533-42.
- [48] Leong PL, Andrews GA, Johnson DE, Dyer KF, Xi S, Mai JC, et al. Targeted inhibition of Stat3 with a decoy oligonucleotide abrogates head and neck cancer cell growth. *Proc Natl Acad Sci U S A* 2003;100:4138-43.
- [49] Barton BE, Murphy TF, Shu P, Huang HF, Meyenhofer M, Barton A. Novel single-stranded oligonucleotides that inhibit signal transducer and activator of transcription 3 induce apoptosis in vitro and in vivo in prostate cancer cell lines. *Mol Cancer Ther* 2004;3:1183-91.

- [50] Ling X, Arlinghaus RB. Knockdown of STAT3 expression by RNA interference inhibits the induction of breast tumors in immunocompetent mice. *Cancer Res* 2005;65:2532-6.
- [51] Zhou W, Grandis JR, Wells A. STAT3 is required but not sufficient for EGF receptor-mediated migration and invasion of human prostate carcinoma cell lines. *Br J Cancer* 2006;95:164-71.
- [52] Zhang Y, Zhang JW, Lv GY, Xie SL, Wang GY. Effects of STAT3 gene silencing and rapamycin on apoptosis in hepatocarcinoma cells. *Int J Med Sci* 2012;9:216-24.
- [53] Incani V, Lavasanifar A, Uludag H. Lipid and hydrophobic modification of cationic carriers on route to superior gene vectors. *Soft Matter* 2010;6:2124-38.
- [54] Clevenger CV. Roles and regulation of stat family transcription factors in human breast cancer. *Am J Pathol* 2004;165:1449-60.
- [55] Real PJ, Sierra A, De Juan A, Segovia JC, Lopez-Vega JM, Fernandez-Luna JL. Resistance to chemotherapy via Stat3-dependent overexpression of Bcl-2 in metastatic breast cancer cells. *Oncogene* 2002;21:7611-8.
- [56] Kim J, Lee YJ, Shin DS, Jeon SH, Son KH, Han DC, et al. Cosmomycin C inhibits signal transducer and activator of transcription 3 (STAT3) pathways in MDA-MB-468 breast cancer cell. *Bioorg Med Chem* 2011;19:7582-9.
- [57] Liu H, Tekle C, Chen YW, Kristian A, Zhao Y, Zhou M, et al. B7-H3 silencing increases paclitaxel sensitivity by abrogating Jak2/Stat3 phosphorylation. *Mol Cancer Ther* 2011;10:960-71.
- [58] Kunigal S, Lakka SS, Sodadasu PK, Estes N, Rao JS. Stat3-siRNA induces Fas-mediated apoptosis in vitro and in vivo in breast cancer. *Int J Oncol* 2009;34:1209-20.
- [59] Octavia Y, Tocchetti CG, Gabrielson KL, Janssens S, Crijns HJ, Moens AL. Doxorubicin-induced cardiomyopathy: from molecular mechanisms to therapeutic strategies. *J Mol Cell Cardiol* 2012;52:1213-25.
- [60] Shahin M, Lavasanifar A. Novel self-associating poly(ethylene oxide)-b-poly(epsilon-caprolactone) based drug conjugates and nano-containers for paclitaxel delivery. *Int J Pharm* 2010;389:213-22.

## **CHAPTER FIVE**

**LIPID MODIFICATION OF THE CORE IN POLY(ETHYLENE OXIDE)-  
BLOCK-POLY( $\epsilon$ -CAPROLACTONE-GRAFTED SPERMINE) MICELLES FOR  
EFFICIENT siRNA DELIVERY TO CANCER CELLS:  
TOWARD DEVELOPMENT OF SYSTEMIC siRNA DELIVERY SYSTEMS**

## 5.1. Introduction

In the previous chapter, we investigated downregulation of signal transducer and activator of transcription 3 (STAT3) by lipid-substituted low molecular weight PEI polymer-siRNA complexes as a possible strategy for sensitization of breast cancer to conventional chemotherapeutic drugs; i.e. DOX and PTX. We have shown the superiority of lipid modified PEI 2 kDa over non-modified PEI 2 kDa in siRNA delivery *in vitro* leading to better downregulation of STAT3 mRNA and protein by lipid modified PEI. However, the use of PEI based carriers for systemic administration is questionable because of their non-specific interaction with normal cells and toxicity; immunogenicity and possibility for early removal from blood circulation [1].

The long term objective of our research is to develop an efficient delivery system for tumor targeted delivery of STAT3 siRNA following systemic administration. In this context, our research groups has previously reported on the development of a family of biodegradable self-associating block copolymers composed of methoxy poly(ethylene oxide)-*b*-poly( $\epsilon$ -caprolactone) grafted with polyamines on their PCL block (MePEO-PCL-*g*-polyamine), as potential carriers for systemic siRNA delivery. In previous studies, MePEO-*b*-PCL grafted spermine (MePEO-*b*-P(CL-*g*-SP)) micelles exhibited great promise for siRNA encapsulation and protection against degradation in serum. MePEO-*b*-P(CL-*g*-SP) micelles containing MDR-1-siRNA (300 nM) were able to silence P-gp expression by 50% in human MDA-MB-435/LCC6 resistant cancer cell line which was transfected with P-gp gene [2]. The results of our *in vivo* bio-distribution studies on

polymeric micelles composed of mixed micelles composed of acetal-PEO-*b*-P(CL-g-SP) and acetal-PEO-*b*-P(CL-Hyd-DOX) pointed to the suboptimal stability of this system upon iv administration in mice [3].

In this chapter, modification of the MePEO-*b*-P(CL-g-SP) micellar core by lipid substituents has been pursued, to enhance the properties of this delivery system for *in vivo* administration in terms of micellar stability and perhaps transfection efficiency. Lipid modification of MePEO-*b*-P(CL-SP) was expected to enhance the hydrophobicity of block copolymers leading to better thermodynamic stability for the polymeric micellar siRNA delivery systems [4, 5]. On the other hand, partial substitution of the primary amine group on SP may have a negative impact on the condensation and binding of siRNA with the micellar delivery system. Hydrophobic modifications of polymeric nanocarriers with fatty acids and cholesterol have been shown to promote the efficiency of siRNA transfection [6-8]. Here we conducted preliminary studies reporting on the synthesis of MePEO-*b*-P(CL-g-SP)) copolymers with stearyl and cholesteryl substitutions on SP. The effect of this lipid modification on micellar size and thermodynamic stability, siRNA binding and uptake by MDA-MB-435 breast cancer cells was further investigated to evaluate the overall impact of this modification on siRNA delivery and choose the best core structure for further studies.

## **5.2. Experimental Section**

### **5.2.1. Materials**

Diisopropyl amine (99%), benzyl chloroformate (tech. 95%), sodium (in kerosin), butyl lithium (Bu-Li) in hexane (2.5 M solution), 3,3-diethoxy-1-propanol (DEP), naphthalene, methoxy polyethylene oxide (Mw 5000 Da), N,N-dicyclohexyl carbodiimide (DCC), N-hydroxysuccinimide (NHS), pyrene, spermine, stearic acid, cholesteryl chloroformate, anhydrous dimethylsulfoxide (DMSO), Hank's Balanced Salt Solution (HBSS), and 3-(4,5-Dimethylthiazol-2-yl)-2,5-diphenyltetrazolium bromide (MTT) were obtained from Sigma Aldrich (St. Louis, MO).  $\epsilon$ -Caprolactone was purchased from Lancaster Synthesis (Heysham, UK) and distilled by calcium hydride before use. Stannous octoate was purchased from MP Biomedicals Inc. (Eschwege, Germany). Acetone, THF and DMF were obtained from Caledon Laboratories Ltd. (Ontario, Canada). All other chemicals were reagent grade. Cell culture media RPMI 1640, penicillin-streptomycin, fetal bovine serum, HEPES buffer solution (1M) and trypsin/ethylenediaminetetraacetate were purchased from GIBCO, Invitrogen Corp (USA). The scrambled siRNA used as control and Silencer<sup>®</sup> FAM<sup>™</sup> labeled Negative siRNA were supplied from Ambion (catalog numbers: AM4636). The silencer siRNAs against STAT3 was purchased from Qiagen (catalog numbers: SI02662338, sequence: CAGCCTCTCTGCAGAATTCAA).

### **5.2.2. Cell Line**

The wild-type MDA-MB-435 (MDA-MB-435/WT) cells were originally obtained as a gift from the laboratory of Dr. Robert Clark (Georgetown University, USA). MDA-MB-435/WT cells were cultured in RPMI 1640 media with 10% FBS, 100 U/mL

penicillin, and 100 mg/mL streptomycin in 37 °C and 5% CO<sub>2</sub>. Cell cultures were considered confluent when a monolayer of cells covered more than 80% of the flask surface. To propagate the cells, a monolayer was washed with HBSS, and subsequently incubated with 0.05% trypsin/EDTA for 3 min at room temperature. The suspended cells were centrifuged at 650 rpm for 5 min, and were re-suspended in the medium after removal of the supernatant. The suspended cells were either sub-cultured at 10% of the original count or seeded in multi-well plates for testing.

### 5.2.3. Synthesis of lipid substituted MePEO-*b*-P(CL-g-SP) block copolymers

Methoxy-poly(ethylene oxide)-*block*-poly( $\epsilon$ -caprolactone-g-N-(spermine)-stearamide) (MePEO-*b*-P(CL-g-SP-STA)) and methoxy-poly(ethylene oxide)-*block*-poly( $\epsilon$ -caprolactone-g-N-(spermine)-cholesteryl carboxylate) (MePEO-*b*-P(CL-g-SP-Chol)) were prepared from MePEO-*b*-P(CL-g-SP). The synthesis of MePEO-*b*-P(CL-g-SP) has been described in detail in previous publication from our lab [2]. Briefly, block copolymers of MePEO-*b*-PBCL was synthesized by ring opening polymerization of  $\alpha$ -benzyl carboxylate- $\epsilon$ -caprolactone using methoxy-PEO as initiator and stannous octoate as catalyst. Then, carboxyl group bearing block copolymer MePEO-*b*-PCCL was obtained by the catalytic debenzoylation of MePEO-*b*-PBCL in the presence of hydrogen gas. MePEO-*b*-PCCL was then dissolved in 10 mL of dry THF. After addition of DCC and NHS in THF, the solution was stirred for 2 h until a precipitate was formed. The precipitate was removed by filtration. Spermine was dissolved in THF and added dropwise to the polymer solution. The reaction proceeded for another 24 h under stirring at

room temperature. The resulting solution was centrifuged to remove the precipitate followed by evaporation under vacuum to remove the solvents. Methanol (10 mL) was introduced to dissolve the product. The resulting solution was then dialyzed (molecular weight cut-off of 3500 Da) extensively against water for 24h. The polymer solution was then freeze-dried for further use. After purification, the synthesis of MePEO-*b*-P(CL-*g*-SP) was confirmed by  $^1\text{H}$  NMR. The SP substitution level of the synthesized copolymer was estimated based on peak intensity ratio of the methylene protons from polyamine (-CH<sub>2</sub>-NH-) and PEO (-CH<sub>2</sub>CH<sub>2</sub>O-). The degree of polymerization was estimated based on peak intensity ratio of proton from PCL (-OCH<sub>2</sub>- proton,  $\delta = 4.1$  ppm) to the intensity of specific peak in PEO ((-CH<sub>2</sub>CH<sub>2</sub>O-) proton,  $\delta = 3.65$  ppm).

MePEO-*b*-P(CL-*g*-SP-STA) was synthesized by attaching pendant stearyl groups to the polyamine section of MePEO-*b*-P(CL-*g*-SP) (**Figure 5.1.A**). In a typical process, stearic acid (7.52 mg) was dissolved in 20 mL of dry THF. After addition of DCC and NHS in THF, the solution was stirred for 2 h until a precipitate was formed. The precipitate was removed by filtration. MePEO-*b*-P(CL-*g*-SP) was dissolved in THF and added drop-wise to the polymer solution. The reaction proceeded for another 24 h under stirring at room temperature. The resulting solution was centrifuged to remove the precipitate followed by dialysis (molecular weight cut-off of 3500 Da) against DMSO for 24 h to remove the free stearic acid. The resulting solution was then dialyzed extensively against water for 24 h and freeze-dried for further use. The composition of the reaction products in CDCl<sub>3</sub> was determined by a 300 MHz  $^1\text{H}$  NMR spectroscope (Bruker 300 AM; Billerica MA). The degree of polymerization of PCL backbone after reaction with

stearic acid was estimated as described for MePEO-*b*-P(CL-g-SP). The stearyl substitution level was estimated by comparing the peak intensities of (-CH<sub>3</sub> proton,  $\delta$  = 0.9 ppm) of stearyl moiety to the intensity of specific peak in PEO (-CH<sub>2</sub>CH<sub>2</sub>O-) proton,  $\delta$  = 3.65 ppm).

Similarly MePEO-*b*-P(CL-g-SP-Chol) was synthesized by attaching pendant cholesteryl groups to the polyamine section of MePEO-*b*-P(CL-g-SP) (**Figure 5.1.B**). Briefly, MePEO-*b*-P(CL-g-SP) copolymer (100 mg) was dissolved in 20 mL of dry THF. Cholesteryl chloroformate (2.46 and 6.15 mg, respectively) was dissolved in THF and added drop-wise to the polymer solution. The reaction proceeded for another 24 h under stirring at room temperature. The reaction mixture was condensed under reduced pressure, precipitated in diethyl ether, and washed repeatedly to remove impurities. The final product was collected and dried under vacuum at room temperature for 48 h. The degree of polymerization of PCL backbone after reaction with cholesteryl chloroformate was estimated as described for MePEO-*b*-P(CL-g-SP). Cholesteryl substitution levels was estimated by comparing the peak intensities of (-CH<sub>3</sub> proton,  $\delta$  = 0.9 ppm) of cholesteryl moiety to the intensity of specific peak in PEO (-CH<sub>2</sub>CH<sub>2</sub>O-) proton,  $\delta$  = 3.65 ppm).

For MePEO-*b*-P(CL-g-SP) copolymer, the polymerization degree of PCL block was 11 and the number of spermines on the PCL block has been determined to be 5. For the MePEO-*b*-P(CL-g-SP-STA), primary amine of spermine was substituted with stearyl groups. This polymer is shown as MePEO<sub>114</sub>-*b*-P(CL-g-SP-STA)<sub>10-5-2.5</sub>, where 10-5-2.5

subscript refers to the degree of CL polymerization, number of carboxyl groups on PCCL that were substituted with SP and number of primary amines in SP substituted with stearyl group, respectively. This polymer is abbreviated as SP-STA 50% to reflect the 50% substitution of stearyl group on spermine. For the MePEO-*b*-(CL-g-SP-Chol), two polymers with different cholesteryl substitution levels were synthesized. For these polymers, the primary amine of spermine was substituted with cholesteryl groups. These polymers are shown as MePEO<sub>114</sub>-*b*-P(CL-g-SP-chol)<sub>11-5-2.5</sub> and MePEO<sub>114</sub>-*b*-P(CL-g-SP-chol)<sub>11-5-1.25</sub> where 11-5-2.5 and 11-5-1.25 subscript refers to the degree of CL polymerization, number of free carboxyl groups on PCCL that were substituted with SP and number of primary amines in SP substituted with cholesteryl groups, respectively. These polymers are abbreviated as SP-Chol 50% and SP-Chol 25% to reflect the 50 and 25% substitution of cholesteryl groups on SP. Similarly for all polymers under study, for the purpose of simplification, an abbreviate is used as summarized in **Table 5.1**.



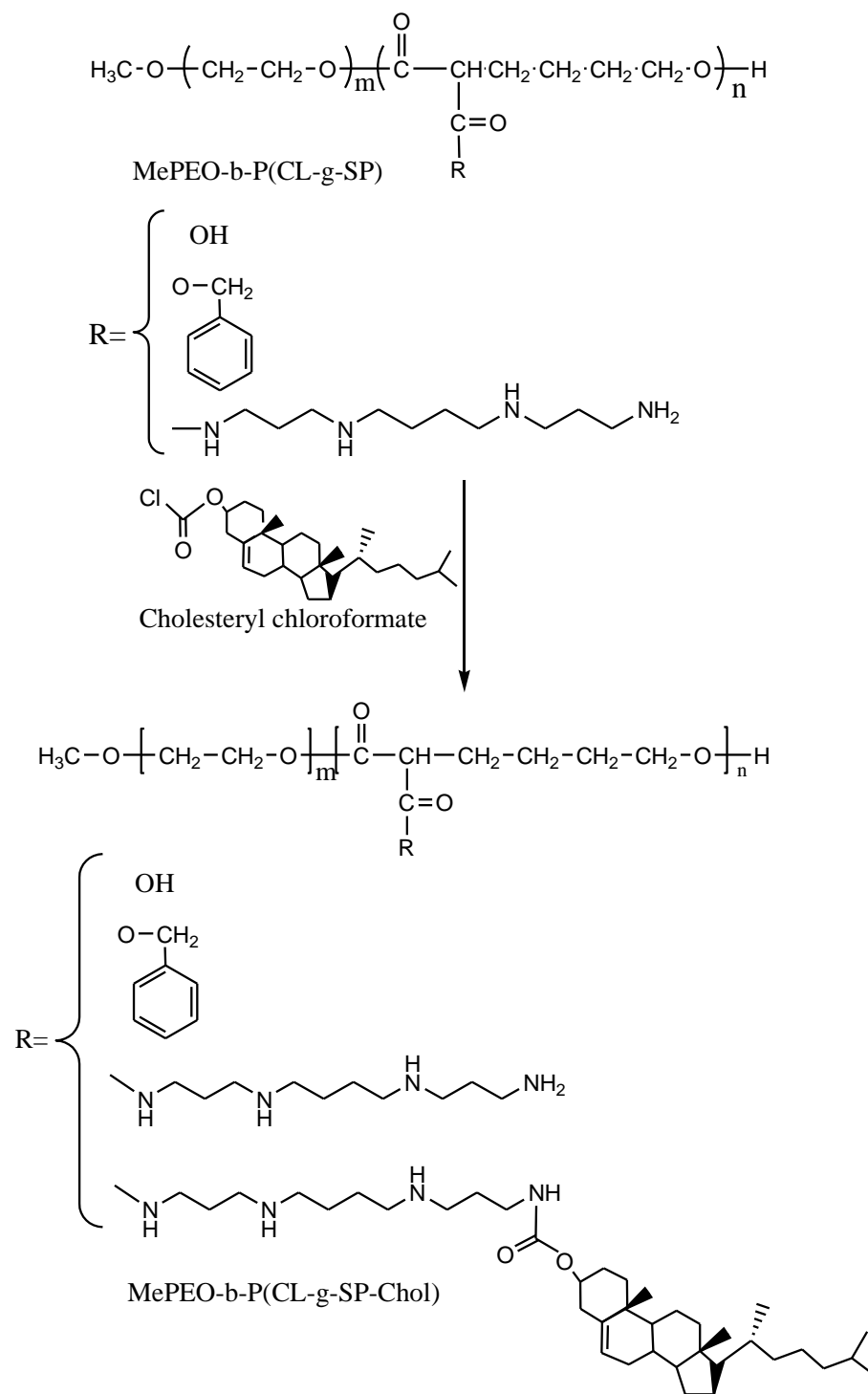


**Figure 5.1.B.** Synthetic scheme for the preparation of MePEO-*b*-P(CL-g-SP-Chol).

#### **5.2.4. Assembly of block copolymers and characterization of self-Assembled structures**

SP-STA 50%, SP-Chol 25% and SP-Chol 50% micelles were prepared using co-solvent evaporation method. Assembly of the prepared block copolymers were achieved by dissolving prepared block copolymers (4 mg) in acetone and dropwise addition (~1 drop/15 s) of polymer solution to doubly distilled water (1 mL) under moderate stirring at 25 °C for 4 h. For SP polymer, micelles were prepared simply by dissolving 4 mg of block copolymer in doubly distilled water (1 mL) under moderate stirring at 25 °C. Average diameter (Z average) and size distribution of prepared particles were estimated by dynamic light scattering (DLS) using a Malvern Zetasizer 3000 at a polymer concentration of 2 mg/mL in water at 25 °C. Morphology of the self-assembled structures was investigated by transmission electron microscopy (TEM). For TEM an aqueous droplet of micellar solution with a polymer concentration of 1–1.5 mg/mL was placed on a copper coated grid. The grid was held horizontally for 20 s to allow the colloidal aggregates to settle. A drop of 2% solution of phosphotungstic acid (PTA) in PBS (pH 7.0) was then added to provide the negative stain. After 1 min, the excess fluid was removed by filter paper. The samples were then air dried and loaded into a HitachiH700 TEM. Images were obtained at a magnification of 140000 at 75 kV. The diameter of individual particles (n = 50) from micrographs was measured manually to obtain their average size. A change in the fluorescence excitation spectra of pyrene in the presence of varied concentrations of different block copolymers were used to measure their critical aggregation concentration (CAC). Pyrene was dissolved in acetone and added to 5 mL

volumetric flasks to provide a concentration of  $6 \times 10^{-7}$  M in the final solutions. Acetone was then evaporated and replaced with aqueous polymeric micellar solutions with concentrations ranging from 0.05 to 1000  $\mu\text{g/mL}$ . Samples were heated at 65 °C for an hour, cooled to room temperature overnight, and deoxygenated with nitrogen gas prior to fluorescence measurements. The excitation spectrum of pyrene for each sample was obtained at room temperature using a Varian Cary Eclipse fluorescence spectrophotometer (Victoria, Australia). Emission wavelength and excitation/emission slit were set at 390 and 5 nm, respectively. The intensity ratio of peaks at 339 nm to those at 334 nm was plotted against the logarithm of copolymer concentration. The CAC was measured from a sharp rise in intensity ratios ( $I_{339}/I_{334}$ ) at the onset of micellization.

#### **5.2.5. Determination of siRNA binding by gel retardation assay**

The siRNA binding ability of the SP, SP-STA 50%, SP-Chol 25% and SP-Chol 50% copolymers was analyzed by agarose gel electrophoresis. The complexes were prepared by mixing 8  $\mu\text{L}$  of 0.1 M HEPES buffer (pH 6.5) with 4  $\mu\text{L}$  of negative siRNA (containing 1  $\mu\text{g}$  siRNA) and 8  $\mu\text{L}$  of serially-diluted concentrations of micellar solutions (containing polymers ranging from 0.5 to 64  $\mu\text{g}$ ) and incubated for 30 min at 37 °C. After that 4  $\mu\text{L}$  of 6 $\times$  sample buffer (50% glycerol, 1% bromophenol blue, and 1% cylene cyenol FF in TBE buffer) was added, and the samples were loaded onto 2% agarose gels containing 0.05 mg/mL ethidium bromide (EtBr). Electrophoresis was performed at 130 mV and 52 mA for 15 min, and the resulting gels were photographed under UV-illumination. The pictures were digitized and analyzed with Scion image analysis

software to determine the mean density of siRNA bands. The binding percentage was calculated based on the relative intensity of free siRNA band in each well with respect to wells with free siRNA (i.e., in the absence of any polymers).

#### **5.2.6. Assessing the cellular association of polymer/siRNA micelles by flow cytometry**

To assess the ability of polymeric micelles to transfer siRNA into MDA-MB-435/WT cells, complexes were prepared using 5-carboxyfluorescein (FAM)-labeled scrambled siRNA at polymer:siRNA ratios of 64:1 (w/w) by incubation in water (corresponding 200 nM siRNA and 224 µg/mL polymer in culture medium). Confluent cell cultures were trypsinized, re-suspended as described before and seeded in 24 well plates (0.6 mL in each well) at 50% confluence. After 24 h, 400 mL fresh medium was added to each well. The prepared micelles were added to wells in triplicates and were incubated in 37 °C for 3 and 24 h. After the incubation period, cells were washed with HBSS and trypsinized. A 3.7% formaldehyde solution was added to suspend the cells and the siRNA uptake was quantified by a Beckman Coulter QUANTA flowcytometer using the FL1 channel to detect cell-associated fluorescence. The percentage of cells showing FAM fluorescence and the mean fluorescence in the total cell population were determined.

#### **5.2.7. Assessing the cellular uptake and distribution of siRNA by confocal microscopy**

Confocal microscopy was used to assess the intracellular trafficking of siRNA in MDA-MB-435/WT cells. siRNA complexes were prepared using 200 nM per well (FAM)-labeled scrambled siRNA at polymer:siRNA ratios of 64:1 (w/w) by incubation in water (corresponding 224  $\mu\text{g/mL}$  polymer in culture medium) or with Trifectin<sup>®</sup> in 3:1 weight ratio. Cells grown on the glass-bottom petri dishes were incubated with the complexes for 24 h. At the end of incubation period, the cells were washed three times with PBS, fixed in paraformaldehyde in PBS for 10 min. For nucleus labeling, fixed cells were washed with PBS and then incubated with DAPI (Molecular Probes, Invitrogen Co., OR, USA) for 15 min. The cells were then washed three times with PBS and stored at 4 °C. Localization of complexes in cells was visualized by a Zeiss 510 LSMNLO confocal microscope (Carl Zeiss Microscope systems, Jena, Germany) with identical settings for each confocal study.

### **5.2.8. Statistics**

Compiled data were presented as means  $\pm$  standard deviation (SD). Where feasible, the data were analyzed for statistical significance using unpaired student's t-test, one-way analysis of variance followed by post hoc Tukey test. The level of significance was set at  $\alpha \leq 0.05$ .

### 5.3. Results

#### 5.3.1. Synthesis and characterization of MePEO-*b*-P(CL-g-SP-STA) and MePEO-*b*-P(CL-g-SP-Chol) polymers

The MePEO-*b*-P(CL-g-SP-STA) and MePEO-*b*-P(CL-g-SP-Chol) polymers were synthesized from MePEO-*b*-P(CL-g-SP) (**Figure 5.1.A and 5.1.B**). The final structures of copolymers were confirmed by  $^1\text{H}$  NMR (**Figure 5.2.A, B and C**). The characteristics of prepared block copolymers are shown in **Table 5.1**. Peaks corresponding to specific stearyl group of SP-STA polymer were observed at  $\delta = 0.9$  and 1.2-1.3 ppm in the  $^1\text{H}$  NMR spectra, indicating the successful conjugation of stearyl groups to block copolymer (**Figure 5.2.B**). Based on peak intensity ratio of proton from PCL (-OCH<sub>2</sub>- proton,  $\delta = 4.1$  ppm) to the intensity of specific peak in PEO ((-CH<sub>2</sub>CH<sub>2</sub>O-) proton,  $\delta = 3.65$  ppm), degree of polymerization was calculated to be 10. We observed a minimal chain cleavage of PCL block for SP-STA polymer. The stearyl substitution level was calculated to be 2.5 per CL chain which reflects 50% substitution of stearyl group on spermine.

Peaks corresponding to specific cholesteryl group of SP-Chol polymer were observed at  $\delta = 0.84-1.1$  and 5.35 ppm in the  $^1\text{H}$  NMR spectra, indicating the successful conjugation of cholesteryl groups to block copolymer (**Figure 5.2.C**). Based on peak intensity ratio of proton from PCL (-OCH<sub>2</sub>- proton,  $\delta = 4.1$  ppm) to the intensity of specific peak in PEO (-CH<sub>2</sub>CH<sub>2</sub>O-) proton,  $\delta = 3.65$  ppm), degree of polymerization was calculated to be 11. We did not observe chain cleavage of PCL block for SP-Chol polymers. For synthesized polymers, the cholesteryl substitution levels was calculated to

be 2.5 and 1.25 per CL chain which reflects 50% and 25% substitution of cholesteryl groups on spermine.

A closer assessment of  $^1\text{H}$  NMR spectra shows the existence of minimal benzyl carboxylate residues in all lipid substituted polymers under study. The number of benzyl carboxylate residues on the PCCL backbone varied between 1-2 per polymer chain. This was attributed to the incomplete removal of benzyl carboxylate substituent during the reduction procedure in catalytic debenzoylation of MePEO-*b*-PBCL. The peak corresponding to specific  $\text{CH}_2$  in benzyl group of polymers was observed at  $\delta = 5.1$  ppm in the  $^1\text{H}$  NMR spectra for both SP-STA and SP-Chol polymers, respectively. However this peak was not observed in spectra for SP polymer because the spectrum was obtained in  $\text{D}_2\text{O}$ , where the peaks related to hydrophobic moiety of the polymer is hidden in the rigid structure of the micellar core.

The average diameter of SP-STA 50% micelles determined by the DLS technique was  $105 \pm 5$  nm. On the other hand, micelles formed from SP-Chol 25% and SP-Chol 50% were found to show smaller trend exhibiting average diameters of  $66 \pm 3$  and  $52 \pm 5$  nm, respectively (**Table 5.1**). The TEM picture of SP-STA 50% and SP-Chol 50% micelles showed the formation of true spherical particles having a clear boundary with average diameters of  $40 \pm 20$  and  $18.5 \pm 5$  nm, respectively (**Figure 5.3**), which is much smaller than the size obtained from DLS measurement. A tendency for aggregation was also evident from the TEM pictures. Amphiphilic block copolymers are expected to self-assemble to micelles in aqueous solution when the concentration of the polymer is above

CAC. The CAC of SP-Chol 50% polymer (0.67  $\mu\text{M}$ ) was determined to be lowest among the synthesized block copolymers. It was significantly lower than that of SP and SP-STA 50% polymer (1.14 and 0.86  $\mu\text{M}$ , respectively). Conjugation of hydrophobic lipid groups to SP polymer has led to copolymers with lower CAC values (**Table 5.1**).

**Table 5.1.** Characteristics of empty micelles (n=3).

Polymer	Abbreviate	Polymer Mn (g.mol <sup>-1</sup> ) <sup>a</sup>	CAC $\pm$ SD ( $\mu\text{M}$ ) <sup>b</sup>	Average diameter $\pm$ SD (nm) <sup>c</sup>
MePEO <sub>114</sub> - <i>b</i> -P(CL-g-SP-) <sub>11-5</sub>	SP	7749	1.14 $\pm$ 0.2	42 $\pm$ 6
MePEO <sub>114</sub> - <i>b</i> -P(CL-g-SP-STA) <sub>10-5-2.5</sub>	SP-STA 50%	8300	0.86 $\pm$ 0.2	105 $\pm$ 5
MePEO <sub>114</sub> - <i>b</i> -P(CL-g-SP-chol) <sub>11-5-1.25</sub>	SP-Chol 25%	8591	0.72 $\pm$ 0.1	66 $\pm$ 3
MePEO <sub>114</sub> - <i>b</i> -P(CL-g-SP-chol) <sub>11-5-2.5</sub>	SP-Chol 50%	8713	0.67 $\pm$ 0.1	52 $\pm$ 5

<sup>a</sup>) Determined by <sup>1</sup>H NMR. <sup>b</sup>) Measured from the onset of a rise in the intensity ratio of peaks at 339nm to peaks at 334nm in the fluorescence excitation spectra of pyrene plotted versus logarithm of polymer concentration. <sup>c</sup>) Z average mean estimated by DLS technique.



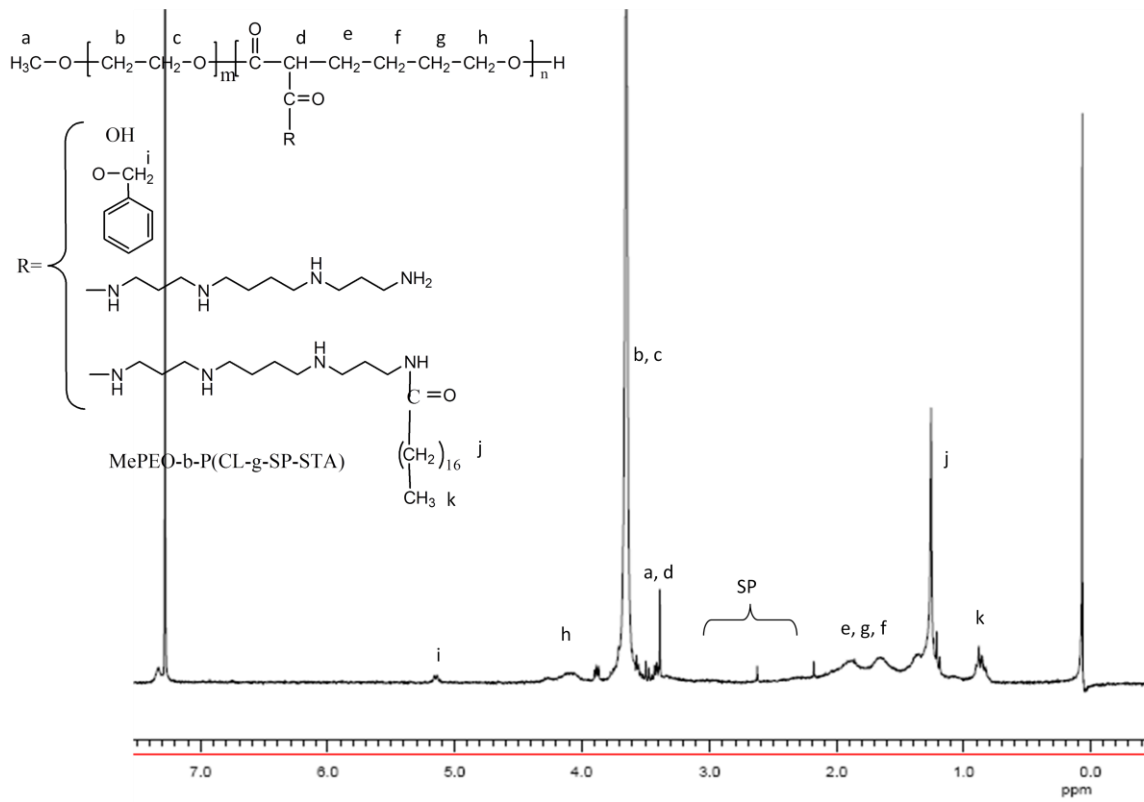
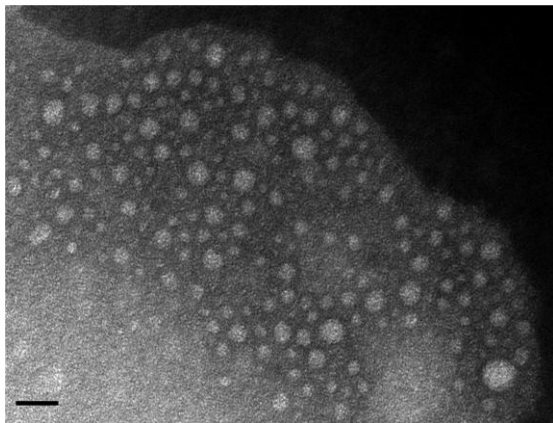


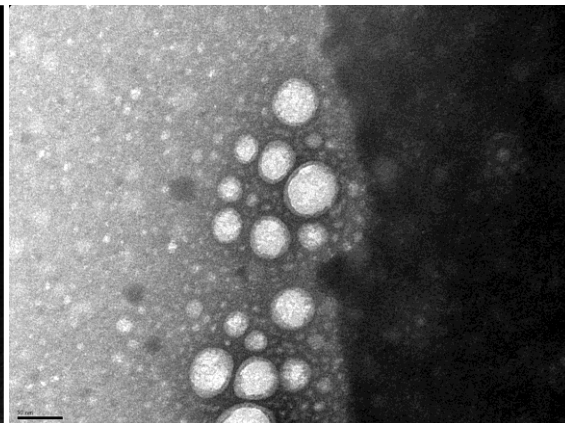
**Figure 5.2.B.**  $^1\text{H}$  NMR spectra of MePEO-*b*-P(CL-g-SP-STA) in  $\text{CDCl}_3$  and peak assignments.



A)



B)



C)

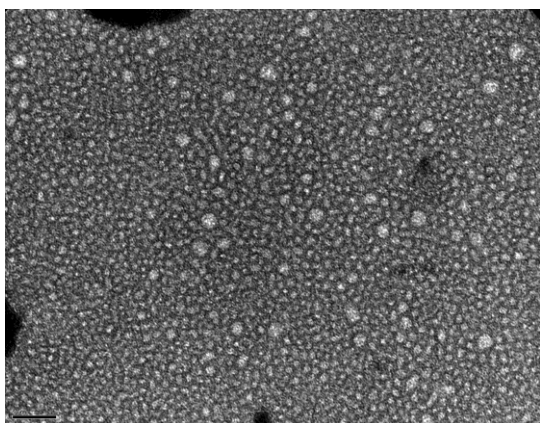
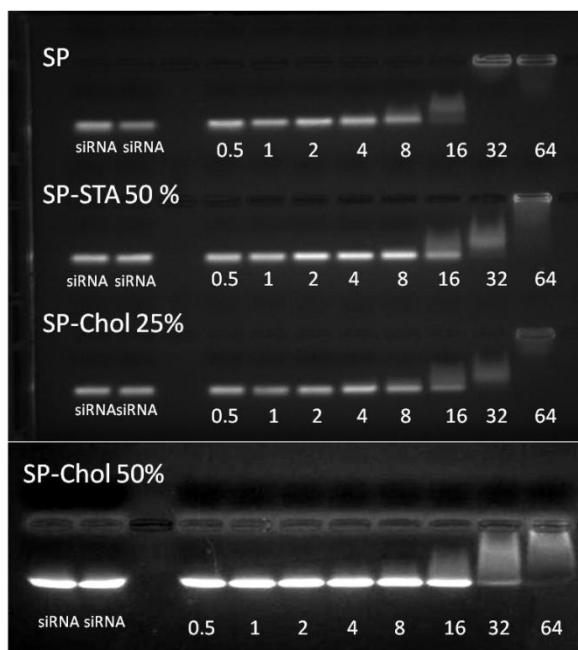


**Figure 5.3.** TEM picture of micelles prepared from A) MePEO-*b*-P(CL-g-SP), B) MePEO-*b*-P(CL-g-SP-STA) and C) MePEO-*b*-P(CL-g-SP-Chol) block copolymers (magnification 140000). The bar on the images represents 50 nm.

### 5.3.2. siRNA binding

Agarose gel electrophoresis was utilized to detect complex formation between the synthesized copolymers and the siRNA. This was based on the disappearance of free siRNA bands in the agarose gels. As expected, the synthesized SP-STA and SP-Chol copolymers were capable of effectively binding siRNA, resulting in retardation or disappearance of siRNA bands in agarose gel (**Figure 5.4.A**). When the polymer:siRNA weight ratios were higher than 64:1, the migration of siRNA was completely retarded for all the copolymers under study (**Figure 5.4.B**). The binding ability of the synthesized copolymers were not significantly different from each other, but less than that of SP polymer at lower polymer/siRNA weight ratios as indicated by a left shift in binding versus polymer/siRNA weight ratio plot (**Figure 5.4.B**).

A)



**B)**

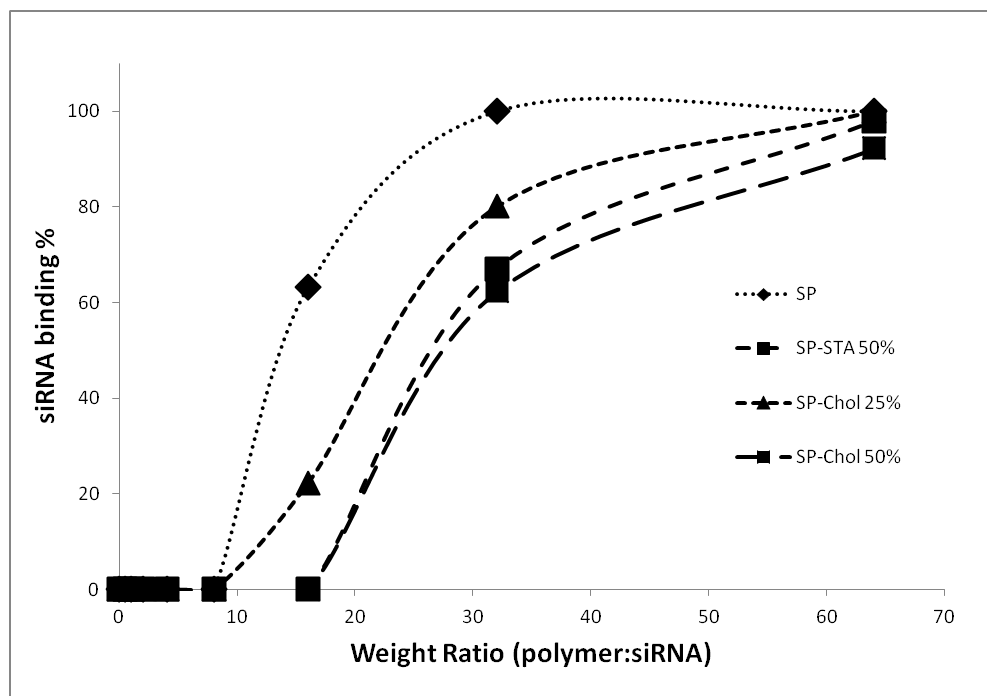


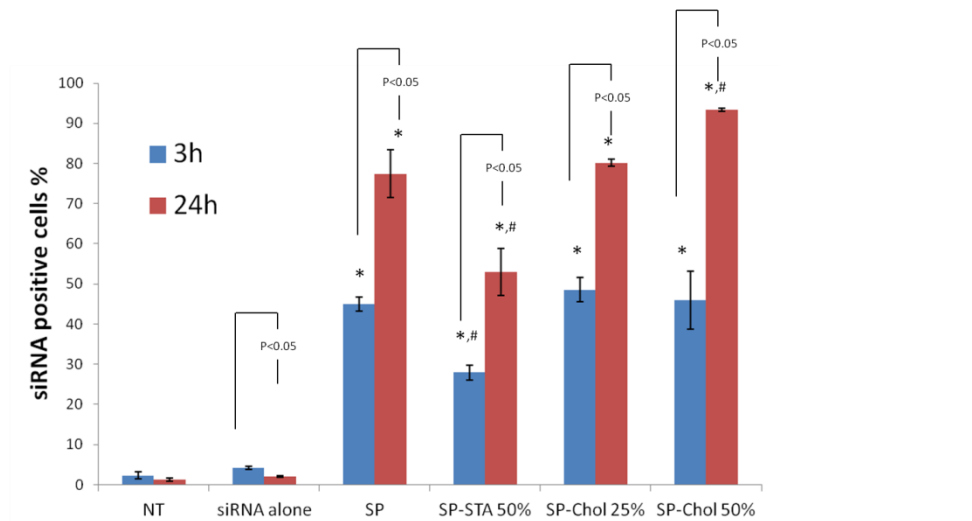
**Figure 5.4.** Electrophoretic retardation analysis of siRNA binding by different polymers. The gel results for the individual polymers are shown in (A). Lane numbers in (A) corresponds to different polymer/siRNA weight ratios for SP, SP-STA 50%, SP-Chol 25% and SP-Chol 50%. The numbers indicates the polymer:siRNA weight ratio. The densitometric analysis of the binding results is shown in (B). The inserted panel in (B) shows the percentage of siRNA binding versus polymer:siRNA weight ratio.

### 5.3.3. Cellular association and uptake studies

The uptake of polymer/siRNA micelles was determined in MDA-MB-435/WT cells. FAM-labeled negative siRNA was used to assess the uptake of polymer/siRNA micelles. Based on the flowcytometry, SP-Chol 50% was the most effective polymer for siRNA delivery to MDA-MB-435/WT cells at 24 h (mean fluorescence intensity) (**Figure 5.5.B**). SP-Chol 50% polymer also exhibited the highest percentage of siRNA positive cells among polymers under study at 24 h (**Figure 5.5.A**). Substitution of cholesteryl on SP polymer increased the association of siRNA micelles with breast cancer cells (as judged by the mean fluorescence intensity of siRNA in cells under study) (**Figure 5.5.B**). At 24 h, SP-Chol 25% also showed a significantly higher uptake compared to SP polymer (**Figure 5.5.B**). Surprisingly, SP-STA 50% exhibited less uptake compared to SP polymer both at 3 and 24 h.

Furthermore, the cellular distribution of selected polymer/siRNA micelles was investigated in MDA-MB-435/WT cells by confocal microscopy (**Figure 5.6**). Clear siRNA fluorescence was exclusively observed in cytoplasm when siRNA was formulated in SP-Chol 25% or SP-Chol 50% micelles (**Figure 5.6 (D) and (E)**, respectively). The highest siRNA fluorescence was observed when SP-Chol 50% micelles used for siRNA delivery. siRNA formulated in SP, SP-STA 50% and Trifectin (**Figure 5.6 (B), (C) and (F)**) gave less detectable fluorescence, while siRNA alone (**Figure 5.6 (A)**) exhibited no detectable fluorescence in the cells.

**A)**



**B)**

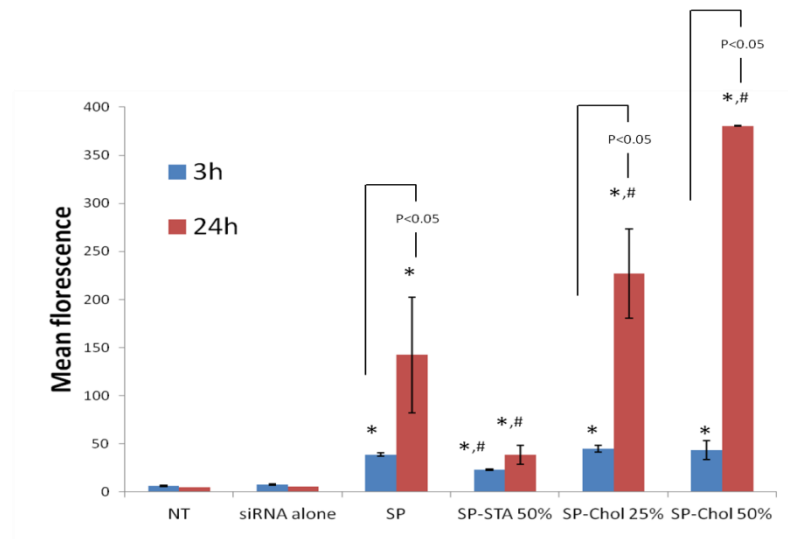


**Figure 5.5.** Cellular uptake of polymer/siRNA micelles by flow cytometry

Cellular uptake of polymer/FAM-siRNA complexes by MDA-MB-435/WT cells. **A)** The percentage of cells positive for FAM-siRNA after 3 and 24 h exposure to siRNA micelles at polymer:siRNA ratios of 64:1 (w/w). **B)** The mean fluorescence of the cells after 3 and 24 h exposure to micelles. The data are the mean  $\pm$  SD for  $n=3$ . \*Significantly different from siRNA alone ( $P<0.05$ ), #Significantly different from SP ( $P<0.05$ ). (One way anova followed by Tukey test,  $P<0.05$ ).

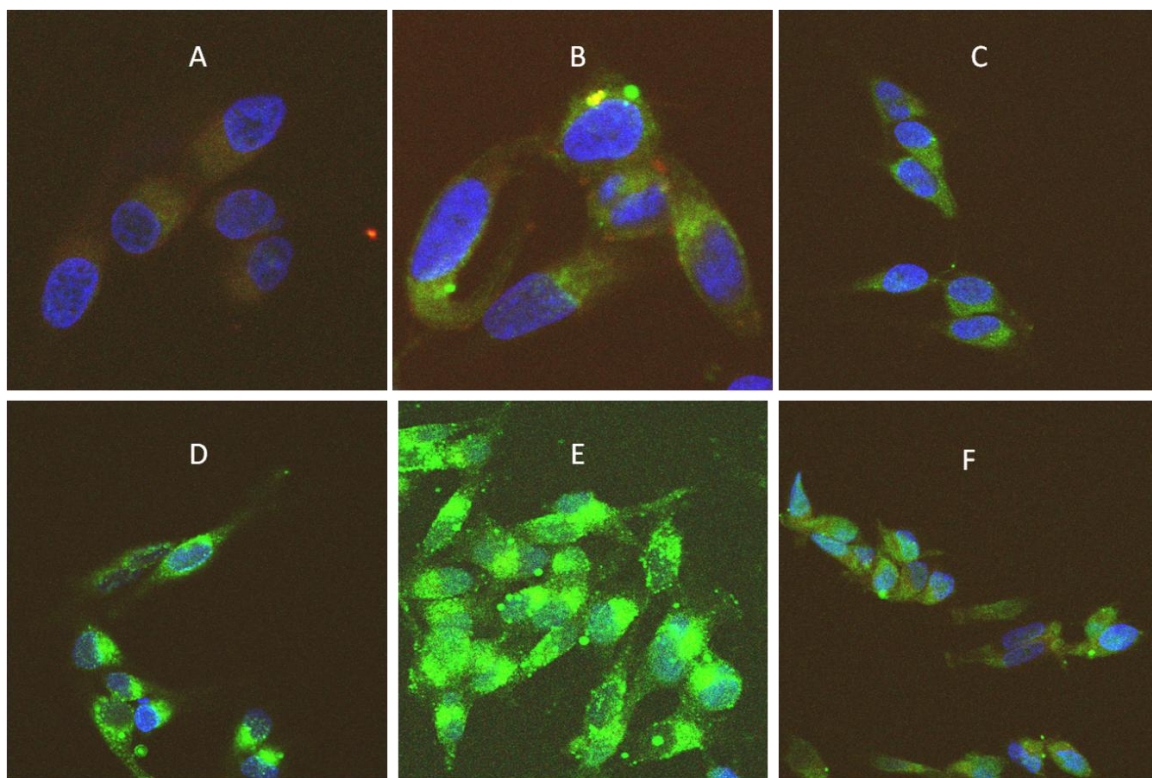


**Figure 5.6.** Confocal microscopy images of cells after treatment with FAM-siRNA formulated in (A) siRNA alone, (B) SP, (C) SP-STA 50%, (D) SP-Chol 25% (E) SP-Chol 50% and (F) Trifectin<sup>®</sup>. The nuclei are stained blue (DAPI) and the internalized siRNA appears as green (FAM).

#### 5.4. Discussion

The separated core-shell architecture of polymeric micelles affords ideal structural features to these carriers for efficient protection and delivery of genetic materials such as siRNA. Among different polymeric micellar structures those based on biodegradable and biocompatible PEO-poly(ester) block copolymers are the subject of most attention. The non-ionic polyester based micellar carriers were found not to be capable of interaction and protection of siRNA, however (data not shown). Therefore, modification of the polyester backbone i.e., PCL by biocompatible short polycationic side groups, i.e. spermine has been tried in our lab to provide efficient carriers for complexation and protection of siRNA [2]. MePEO-*b*-P(CL-g-SP) micelles prepared previously are expected to be safe carriers for siRNA delivery *in vivo* owing the biodegradability of PCL core and biocompatibility of MePEO shell which hides the polycationic SP structure within the micellar core. Besides, spermine is an endogenous polycation found in most eukaryote cells and associated with nucleic acids particularly in viruses [9].

The developed MePEO-*b*-P(CL-g-SP) block copolymers were able to self-assemble into micelles and effectively bind siRNA increasing the stability and cell association of complexed siRNA. In previous studies, the effective down-regulation of target gene by an MDR-1 siRNA complex of MePEO-*b*-P(CL-g-SP) was achieved at relatively high siRNA concentrations (300 nM) [2]. In a subsequent manuscript, we reported on the modification of MePEO-*b*-P(CL-g-SP) micellar shell with cancer targeting and cell penetrating peptides, i.e., RGD4C and TAT, respectively, and showed

the success of this approach in reducing the required dose of siRNA to 100 nM for efficient down regulation of P-gp at mRNA and protein level [10]. The RGD4C decorated micelles were also shown to enhance the localization of incorporated siRNA to tumor in an MDA-MB-435 xenograft model [3]. Tumor delivery by non-micelles (those not modified by RGD4C) was insignificant, however.

In our efforts towards development of more effective polymeric micelles for *in vivo* siRNA delivery, we pursued lipid modification of the P(CL-g-SP) core. Our primary aim was to enhance the stability of micellar structure against dissociation. In this chapter we assessed whether lipid modification of the P(CL-g-SP) core can enhance the thermodynamic stability of polymeric micelles. Meanwhile, the effect of this modification on other important properties of MePEO-*b*-P(CL-g-SP) for systemic siRNA delivery such as siRNA binding, cell association and transfection for was evaluated. During these studies, the effect of lipid structure and substitution degree on polymer backbone on such properties was assessed as well.

Our results showed lipid modified MePEO-P(CL-SP) block copolymers to form micelles with average particle sizes around  $\leq 100$  nm. In general, lipid modification increased the size of resulting micelles, but this size was much smaller and more desirable than PEI/siRNA complexes (with particle size of 570 nm) for *in vivo* delivery through intravenous application [2]. Large size of particles will enhance the chance of their uptake by the reticuloendothelial system upon systemic administration leading to quick removal of nanocarrier by reticuloendothelial system organs like liver and spleen.

Among two different lipids under study, cholesterol modification led to the formation of smaller micelles, leading to the formation of micelles with average diameters even more desirable for passive tumor targeting.

Stearyl and cholesteryl modification of polyamine section in MePEO-*b*-P(CL-g-SP) led to the formation more stable nanocarriers reflected by a decrease in the CAC of micelles (**Table 5.1**). The lower CAC values for newly synthesized polymeric micelles clearly shows that the introduction of hydrophobic stearyl and cholesteryl groups to the P(CL-g-SP) makes self-association of block copolymers, thermodynamically more favorable. These results are consistent with previous findings on the effect of core hydrophobicity on CAC value [11].

However, attachment of such lipids into SP decreased the number of protonated amines available for siRNA binding, reducing the ability of the polymers to bind siRNA to some extent (**Figure 5.4.A and B**). In further studies, to ensure complete binding of siRNA by polymer under study, micelles were prepared at high polymer:siRNA weight ratio of 64:1. The uptake of the micelles by the cells is presumed to be reliant on the micellar shell that directly interfaces the cells. Other factors such as nature of the cell, the core of micelles and particle size may also play important role in cellular uptake [12-15]. Hydrophobic modification of polymeric carriers has been reported to induce the efficacy of such carriers in nucleic acid delivery [6]. Hydrophobic moieties are presumed to increase the interaction between the carrier and the lipophilic cell membrane, therefore enhancing the cellular uptake of nucleic acid associated polymeric carriers. We found that

amphiphilic polycationic polymers with cholesteryl in their core particularly at higher level of cholesteryl substitution were more efficient for siRNA uptake compared to polymers without lipid attachment (**Figure 5.5**). Confocal images further revealed that the SP-Chol 50% polymer delivered the siRNA more effectively into the cells among all carriers under study (**Figure 5.6**). Overall, the results of our studies provide proof for the benefit of lipid modification of MePEO-*b*-P(CL-g-SP) micelles in increasing the stability of the carriers, as well as enhancing the siRNA uptake and delivery into MDA-MB-435/WT cells. Among different lipid substituents under study, the cholesteryl group at higher degree of substitution was found to be the more efficient structure in terms of micellar stability, average size and cellular siRNA delivery.

## 5.5. Conclusion

In conclusion, we report on the design, synthesis and evaluation of a novel family of stearyl and cholesteryl substituted MePEO-*b*-P(CL-g-SP) polycationic polymers and explored their potential for siRNA delivery. We showed that all of these amphiphilic copolymers are able to effectively bind siRNA and self-assemble into micelles. SP-Chol 50% micelles were in particular the most effective carrier for delivery of siRNA into MDA-MB-435 breast cancer cells. The results of this study provided proof of concept for lipid modification of MePEO-*b*-P(CL-g-SP) polymer as means to improve micellar stability and transfection efficiency of these siRNA carriers.

## 5.6. References

- [1] Wightman L, Kircheis R, Rossler V, Carotta S, Ruzicka R, Kursa M, et al. Different behavior of branched and linear polyethylenimine for gene delivery in vitro and in vivo. *J Gene Med* 2001;3:362-72.
- [2] Xiong XB, Uludag H, Lavasanifar A. Biodegradable amphiphilic poly(ethylene oxide)-block-polyesters with grafted polyamines as supramolecular nanocarriers for efficient siRNA delivery. *Biomaterials* 2009;30:242-53.
- [3] Xiong XB, Lavasanifar A. Traceable multifunctional micellar nanocarriers for cancer-targeted co-delivery of MDR-1 siRNA and doxorubicin. *ACS Nano* 2011;5:5202-13.
- [4] Falamarzian A, Lavasanifar A. Optimization of the hydrophobic domain in poly(ethylene oxide)-poly( $\epsilon$ -caprolactone) based nano-carriers for the solubilization and delivery of Amphotericin B. *Colloids Surf B Biointerfaces* 2010;81:313-20.
- [5] Falamarzian A, Lavasanifar A. Chemical modification of hydrophobic block in poly(ethylene oxide) poly( $\epsilon$ -caprolactone) based nanocarriers: effect on the solubilization and hemolytic activity of amphotericin B. *Macromol Biosci* 2010;10:648-56.
- [6] Aliabadi HM, Landry B, Bahadur RK, Neamnark A, Suwantong O, Uludag H. Impact of lipid substitution on assembly and delivery of siRNA by cationic polymers. *Macromol Biosci* 2011;11:662-72.
- [7] Aliabadi HM, Landry B, Mahdipoor P, Hsu CY, Uludag H. Effective down-regulation of breast cancer resistance protein (BCRP) by siRNA delivery using lipid-substituted aliphatic polymers. *Eur J Pharm Biopharm* 2012;81:33-42.
- [8] Gusachenko Simonova O, Kravchuk Y, Konevets D, Silnikov V, Vlassov VV, Zenkova MA. Transfection efficiency of 25-kDa PEI-cholesterol conjugates with different levels of modification. *J Biomater Sci Polym Ed* 2009;20:1091-110.
- [9] Du Z, Chen M, He Q, Zhou Y, Jin T. Polymerized spermine as a novel polycationic nucleic acid carrier system. *Int J Pharm* 2012;434:437-43.
- [10] Xiong XB, Uludag H, Lavasanifar A. Virus-mimetic polymeric micelles for targeted siRNA delivery. *Biomaterials* 2010;31:5886-93.
- [11] Lavasanifar A, Samuel J, Kwon GS. The effect of alkyl core structure on micellar properties of poly(ethylene oxide)-block-poly(L-aspartamide) derivatives. *Colloids Surf B Biointerfaces* 2001;22:115-26.
- [12] Maysinger D, Berezovska O, Savic R, Soo PL, Eisenberg A. Block copolymers modify the internalization of micelle-incorporated probes into neural cells. *Biochim Biophys Acta* 2001;1539:205-17.
- [13] Deshpande MC, Davies MC, Garnett MC, Williams PM, Armitage D, Bailey L, et al. The effect of poly(ethylene glycol) molecular architecture on cellular interaction and uptake of DNA complexes. *J Control Release* 2004;97:143-56.
- [14] Mahmud A, Lavasanifar A. The effect of block copolymer structure on the internalization of polymeric micelles by human breast cancer cells. *Colloids Surf B Biointerfaces* 2005;45:82-9.

[15] Miyata K, Fukushima S, Nishiyama N, Yamasaki Y, Kataoka K. PEG-based block cationomers possessing DNA anchoring and endosomal escaping functions to form polyplex micelles with improved stability and high transfection efficacy. *J Control Release* 2007;122:252-60.

## **CHAPTER SIX**

### **OPTIMIZATION OF HYDROPHOBIC DOMAIN IN POLY(ETHYLENE OXIDE)-BLOCK-POLY( $\epsilon$ -CAPROLACTONE-GRAFTED SPERMINE) FOR EFFICIENT siRNA DELIVERY**

The data presented in this chapter will be submitted as part of a manuscript to “Biomaterials”.

## 6.1. Introduction

Our research group has been working on the development of a polymeric micellar delivery system based on methoxy-poly(ethylene oxide)-*b*-poly( $\epsilon$ -caprolactone-*g*-spermine) (MePEO-*b*-P(CL-SP)) with potential application in tumor targeted delivery of siRNA upon systemic administration [1, 2]. In previous chapter, lipid modification of the P(CL-SP) core in these micelles was pursued as means to improve micellar properties in siRNA delivery. Here, we report on a new method of synthesis and purification for the preparation of MePEO-*b*-P(CL-SP). This modification was intended to address the lack of reproducibility in obtaining MePEO-*b*-P(CL-SP) with controlled degree of polymerization for the P(CL-SP) block. The modified method of synthesis and purification allowed reproducible preparation of MePEO-*b*-P(CL-SP) block copolymers with higher degrees of polymerization for the P(CL-SP) block and their lipid substituted derivatives. Based on the results of our studies provided in Chapter 5, for lipid modification of SP, the cholesteryl substituent was chosen as it has shown better properties in siRNA delivery in terms of micellar size, thermodynamic stability and siRNA cell uptake. In the current study, MePEO-*b*-P(CL-SP) with a degree of polymerization of 15 for PCL (versus 11 used in previous chapter) and complete reduction of benzyl carboxylate group to carboxyl groups on the backbone were prepared first. In the following step, two copolymers with different level of cholesteryl substitution on SP were prepared. The resulted co-polymers were then evaluated for their properties in siRNA delivery such as micellar stability and size, siRNA binding, siRNA release, cell uptake and intracellular distribution. In further studies, STAT3 silencing ability of

STAT3-siRNA complexed with developed polymers in a triple negative breast cancer cell line, i.e., MDA-MB-435, was examined at both mRNA and protein level. The effect of STAT3-siRNA treatment with its polymeric micellar formulations on the viability of MDA-MB-435 cells was assessed. In a separate study, myeloid cell leukemia sequence 1 (MCL-1) silencing ability of MCL-1 siRNA complexed with developed polymers was assessed at mRNA level and the effect of such treatment on the viability of MDA-MB-435 cells was examined.

## **6.2. Experimental Section**

### **6.2.1. Materials**

Diisopropyl amine (99%), benzyl chloroformate (tech. 95%), sodium (in kerosin), butyl lithium (Bu-Li) in hexane (2.5 M solution), 3,3-diethoxy-1-propanol (DEP), naphthalene, methoxy polyethylene oxide (Mw 5000 Da), N,N-dicyclohexyl carbodiimide (DCC), N-hydroxysuccinimide (NHS), pyrene, spermine, cholesteryl chloroformate, anhydrous dimethylsulfoxide (DMSO), Hank's Balanced Salt Solution (HBSS), and 3-(4,5-Dimethylthiazol-2-yl)-2,5-diphenyltetrazolium bromide (MTT) were obtained from Sigma (St. Louis, MO).  $\epsilon$ -Caprolactone was purchased from Lancaster Synthesis (Heysham, UK) and distilled by calcium hydride before use. Stannous octoate was purchased from MP Biomedicals Inc. (Eschwege, Germany). Acetone, THF and DMF were obtained from Caledon Laboratories Ltd. (Ontario, Canada). All other chemicals were reagent grade. Cell culture media RPMI 1640, penicillin–streptomycin, fetal bovine serum, HEPES buffer solution (1M) and trypsin/ethylenediaminetetraacetate

were purchased from GIBCO, Invitrogen Corp (USA). The scrambled siRNA used as control and Silencer<sup>®</sup> FAM<sup>™</sup> labeled Negative siRNA were supplied from Ambion (catalog numbers: AM4636). The Silencer siRNAs against STAT3 was purchased from Qiagen (catalog numbers: SI02662338, sequence: CAGCCTCTCTGCAGAATTCAA). The Silencer siRNAs against MCL-1 was purchased from Qiagen (catalog numbers: SI02781205, sequence: CGCCGAAUUCAUUAUUUATT).

### 6.2.2 Cell Line

The wild-type MDA-MB-435 (MDA-MB-435/WT) cells were originally obtained as a gift from the laboratory of Dr. Robert Clark (Georgetown University, USA). MDA-MB-435/WT cells were cultured in RPMI 1640 media with 10% FBS, 100 U/mL penicillin, and 100 mg/mL streptomycin in 37 °C and 5% CO<sub>2</sub>. Cell cultures were considered confluent when a monolayer of cells covered more than 80% of the flask surface. To propagate the cells, a monolayer was washed with HBSS, and subsequently incubated with 0.05% trypsin/EDTA for 3 min at room temperature. The suspended cells were centrifuged at 650 rpm for 5 min, and were re-suspended in the medium after removal of the supernatant. The suspended cells were either sub-cultured at 10% of the original count or seeded in multi-well plates for testing.

### 6.2.3 Synthesis of cholesteryl substituted MePEO-*b*-P(CL-g-SP) block copolymers

Methoxy-poly(ethylene oxide)-*block*-poly( $\epsilon$ -caprolactone-g-N-(spermine)-cholesteryl carboxylate) (MePEO-*b*-P(CL-g-SP-Chol)) were prepared in four steps. In the first step, MePEO-*b*-PBCL was synthesized by ring opening polymerization of  $\alpha$ -benzyl

carboxylate- $\epsilon$ -caprolactone using methoxy-PEO as initiator and stannous octoate as catalyst. In the second step MePEO-*b*-PBCL was reduced to MePEO-*b*-poly( $\alpha$ -carboxyl- $\epsilon$ -caprolactone) (MePEO-PCCL) using a modified method with constant stream of hydrogen gas to obtain a fully reduced polymer. In the third step SP was conjugated to MePEO-PCCL forming MePEO-*b*-P(CL-*g*-SP). Briefly, MePEO-*b*-PCCL was dissolved in 10 mL of dry THF. After addition of DCC and NHS in THF, the solution was stirred for 2 h until a precipitate was formed. The precipitate was removed by filtration. Spermine was dissolved in THF and added drop-wise to the polymer solution. The reaction proceeded for another 24 h under stirring at room temperature. The resulting solution was centrifuged to remove the precipitate followed by evaporation under vacuum to remove the solvents. The product was then purified using a modified method where DMF was introduced to dissolve the product and the resulting solution was then dialyzed (molecular weight cut-off of 3500 Da) extensively against DMF and then water (each for 24 h). The polymer solution was then freeze-dried for further use. After purification, the synthesis of MePEO-*b*-P(CL-*g*-SP) was confirmed by  $^1\text{H}$  NMR. The SP substitution level of the synthesized copolymer was estimated based on peak intensity ratio of the methylene protons from polyamine (-CH<sub>2</sub>-NH-) and PEO (-CH<sub>2</sub>CH<sub>2</sub>O-). The degree of polymerization was estimated based on peak intensity ratio of proton from PCL (-OCH<sub>2</sub>-proton,  $\delta = 4.1$  ppm) to the intensity of specific peak in PEO ((-CH<sub>2</sub>CH<sub>2</sub>O-) proton,  $\delta = 3.65$  ppm).

MePEO-*b*-P(CL-*g*-SP-Chol) was synthesized by attaching pendant cholesteryl groups to the polyamine section of MePEO-*b*-P(CL-*g*-SP) (**Figure 6.1**). Briefly, a

solution of 0.3 g of MePEO-*b*-P(CL-g-SP) in 6 mL dried DMF was placed in a round bottom flask under argon atmosphere. This flask was cooled down to 0° C by an ice-water bath. A solution of cholesteryl chloroformate (either 0.038 or 0.074 g) in 6 mL of dry DMF was added dropwise to previous solution over a period of 45 min. The reaction was left for 24 h at room temperature under argon atmosphere. Finally, the resulting solution was poured into a large amount of ether to precipitate the product. The separated solid product was completely washed by ether and dried under vacuum. The degree of polymerization of PCL backbone after reaction with cholesteryl chloroformate was estimated as described for MePEO-*b*-P(CL-g-SP). Cholesteryl substitution levels was estimated by comparing the peak intensities of (-CH<sub>3</sub> proton,  $\delta = 0.9$  ppm) cholesteryl moiety to the intensity of specific peak in PEO ((-CH<sub>2</sub>CH<sub>2</sub>O-) proton,  $\delta = 3.65$  ppm).

For MePEO-*b*-P(CL-g-SP) copolymer, the polymerization degree of PCL block was 15 and the number of SPs on the PCL block was determined to be 6. For the MePEO-*b*-P(CL-g-SP-Chol), two polymers with different cholesteryl substitution levels were synthesized. For these polymers, the primary amine of SP was substituted with cholesteryl groups. These polymers are shown as MePEO<sub>114</sub>-*b*-P(CL-g-SP-Chol)<sub>15-6-2.2</sub> and MePEO<sub>114</sub>-*b*-P(CL-g-SP-Chol)<sub>15-6-1.5</sub> where 15-6-2.2 and 15-6-1.5 subscript refers to the degree of CL polymerization, number of free carboxyl groups on PCCL that were substituted with SP and number of primary amines in SP substituted with cholesteryl groups, respectively. These polymers are abbreviated as SP-Chol 37% and SP-Chol 25% to reflect the 37 and 25% substitution of cholesteryl groups on spermine. Similarly for all

polymers under study, for the purpose of simplification, an abbreviate is used as summarized in **Table 6.1**.

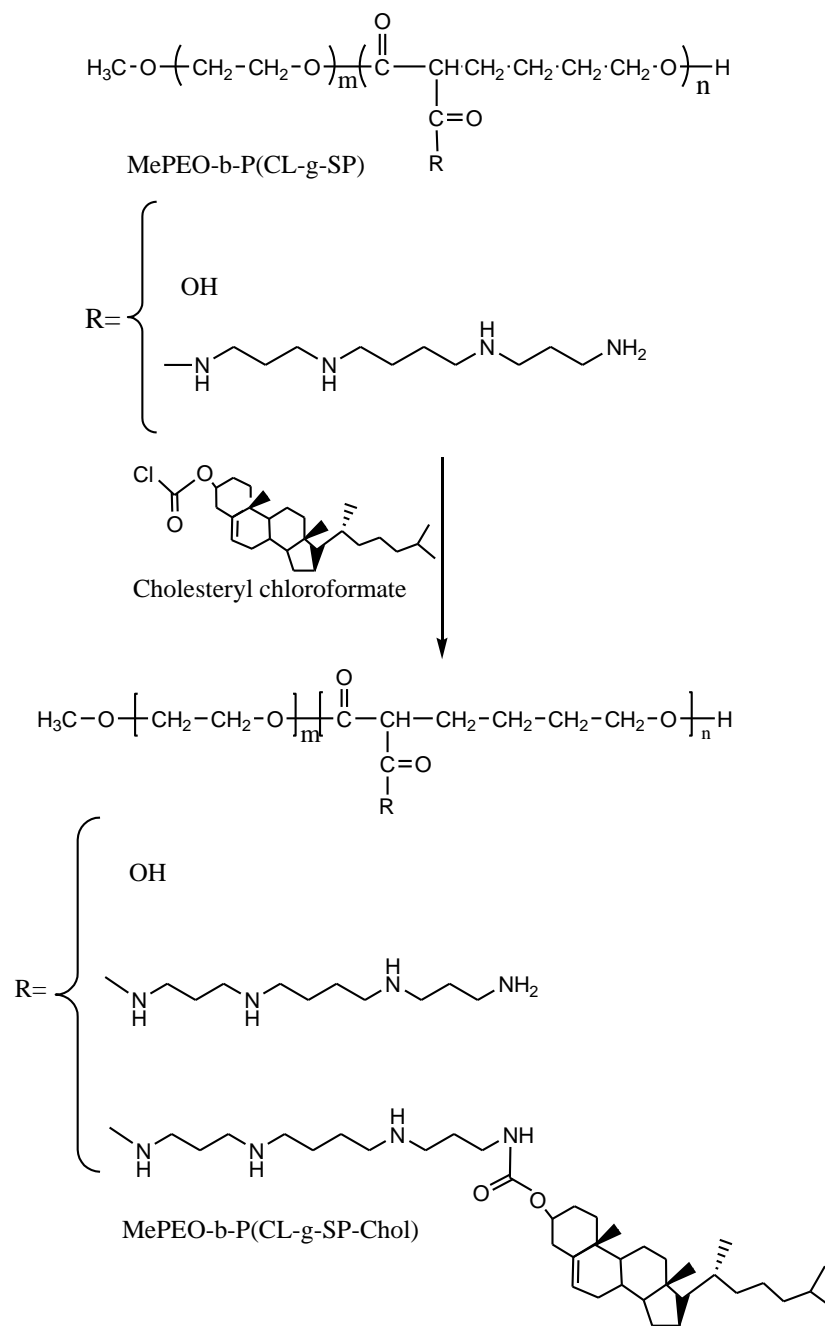


**Figure 6.1.** Synthetic scheme for the preparation of MePEO-*b*-P(CL-g-SP-Chol).

#### **6.2.4. Assembly of block copolymers and characterization of self-Assembled structures**

SP, SP-Chol 25% and SP-Chol 37% micelles were prepared simply by dissolving 4 mg of block copolymer in doubly distilled water (1 mL) under moderate stirring at 25 °C. Average diameter (Z average) and size distribution of prepared particles were estimated by dynamic light scattering (DLS) using a Malvern Zetasizer nano ZS at a polymer concentration of 2 mg/mL in water at 25 °C. A change in the fluorescence excitation spectra of pyrene in the presence of varied concentrations of different block copolymers were used to measure their critical aggregation concentration (CAC). Pyrene was dissolved in acetone and added to 5 mL volumetric flasks to provide a concentration of  $6 \times 10^{-7}$  M in the final solutions. Acetone was then evaporated and replaced with aqueous polymeric micellar solutions with concentrations ranging from 0.05 to 1000 µg/mL. Samples were heated at 65 °C for an hour, cooled to room temperature overnight, and deoxygenated with nitrogen gas prior to fluorescence measurements. The excitation spectrum of pyrene for each sample was obtained at room temperature using a Varian Cary Eclipse fluorescence spectrophotometer (Victoria, Australia). Emission wavelength and excitation/emission slit were set at 390 and 5 nm, respectively. The intensity ratio of peaks at 339 nm to those at 334 nm was plotted against the logarithm of copolymer concentration. The CAC was measured from a sharp rise in intensity ratios (I<sub>339</sub>/I<sub>334</sub>) at the onset of micellization.

#### **6.2.5. Determination of siRNA binding by SYBR Green Dye Exclusion Assay**

The ability of the polymers to bind siRNA was assessed by the SYBR Green II binding assay [3]. Briefly, complexes were prepared by mixing 8  $\mu\text{L}$  of 0.1 M HEPES buffer (pH 6.5) with 4  $\mu\text{L}$  of scrambled siRNA (containing 0.5  $\mu\text{g}$  siRNA) and 8  $\mu\text{L}$  of serially-diluted concentrations of polymeric micellar solutions (containing polymers ranging from 0.5 to 64  $\mu\text{g}$ ). After 30 min of incubation at 37  $^{\circ}\text{C}$ , 200  $\mu\text{L}$  of the SYBR Green II solution was added to the complexes and the fluorescence of the samples was measured in a 96-well plate ( $\lambda_{\text{ex}}$ : 485 nm,  $\lambda_{\text{em}}$ : 527 nm) to quantify the amount of free siRNA. The binding curves were generated by plotting the percentage of siRNA bound to the polymer vs. polymer to siRNA weight/weight (w/w) ratio. The binding for each polymer was tested at least in 2 independent experiments.

#### **6.2.6. siRNA release by polyanion competition**

As a measure of complex stability, the ability of micelles to release siRNA after a challenge with the competing polyanionic heparin was determined. Micelles were prepared at polymer:siRNA ratio of 32:1 (w/w) to ensure complete binding of siRNA by the polymers. After incubation of the mixtures for 30 min at 37  $^{\circ}\text{C}$ , the resulting complexes were incubated with 0.78, 1.52, 3.04, 6.08, 12.48, and 24.32  $\mu\text{g}$  of heparin sulfate at 37  $^{\circ}\text{C}$  for 1 h. Subsequently, 4  $\mu\text{L}$  of 6  $\times$  loading buffer (50% glycerol, 1% bromophenol blue, and 1% cylene FF in TBE buffer) was added, and the samples were loaded onto 2% agarose gels containing 0.05 mg/mL ethidium bromide (EtBr). Electrophoresis was performed at 130 mV and  $\sim$ 52 mA for 15 min, and the resulting gels were photographed under UV-illumination. The pictures were digitized and analyzed

with Scion image analysis software to determine the mean density of siRNA bands. The dissociation curve was generated by plotting the percentage of siRNA dissociated from the complex vs. heparin: polymer ratio ( $\mu\text{g}/\mu\text{g}$ ). Results were presented as average of at least 2 independent experiments.

#### **6.2.7. Assessing the cellular association of polymer/siRNA micelles by flow cytometry**

To assess the ability of polymeric micelles to transfer siRNA into MDA-MB-435/WT cells, complexes were prepared using 5-carboxyfluorescein (FAM)-labeled scrambled siRNA at polymer:siRNA ratios of 16:1 (w/w) by incubation in water (corresponding 100 nM siRNA and 22.4  $\mu\text{g}/\text{mL}$  polymer in culture medium) or with PEI25K in 1:1 weight ratio as positive control. Confluent cell cultures were trypsinized, re-suspended as described before and seeded in 24 well plates (0.6 mL in each well) at 50% confluence. After 24 h, 400 mL fresh medium was added to each well. The prepared micelles were added to wells in triplicates and were incubated in 37 °C for 3 and 24 h. After the incubation period, cells were washed with HBSS and trypsinized. A 3.7% formaldehyde solution was added to suspend the cells and the siRNA uptake was quantified by a Beckman Coulter QUANTA flowcytometer using the FL1 channel to detect cell-associated fluorescence. The percentage of cells showing FAM fluorescence and the mean fluorescence in the total cell population were determined.

#### **6.2.8. Assessing the cellular uptake and distribution of siRNA by confocal microscopy**

Confocal microscopy was used to assess the intracellular trafficking of siRNA in MDA-MB-435/WT cells. Micelles were prepared using (FAM)-labeled scrambled siRNA at polymer:siRNA ratios of 16:1 (w/w) by incubation in water (corresponding 100 nM siRNA and 22.4 µg/mL polymer in culture medium). Cells grown on the glass-bottom Petri dishes were incubated with the complexes for 24 h. At the end of incubation period, the cells were washed three times with PBS, fixed in paraformaldehyde in PBS for 10 min. For nucleus labeling, fixed cells were washed with PBS and then incubated with DAPI (Molecular Probes, Invitrogen Co., OR, USA) for 15 min. To observe the intracellular distribution of the micelles, cells were incubated with LysoTracker Red (50 nM, Molecular Probe, Invitrogen Co., OR, USA) for 0.5 h at the end of uptake study for endosome/lysosome labeling. The cells were then washed three times with PBS and stored at 4 °C. Localization of complexes in cells was visualized by a Zeiss 510 LSMNLO confocal microscope (Carl Zeiss Microscope systems, Jena, Germany) with identical settings for each confocal study.

#### **6.2.9. Cytotoxicity evaluation by MTT Assay**

The cytotoxicity of various polymeric micelles were evaluated in MDA-MB-435/WT cells using the MTT assay. Confluent cell cultures were trypsinized, seeded in 24 well plates with 0.4 mL medium in each well, and allowed to reach ~80% confluence (24 h). Polymer/siRNA micelles were prepared using the scrambled siRNA at the ratio of 8:1 and 16:1 (w/w). They were added to the wells to give final polymer concentrations of 11.2, 22.4 and 44.8 µg/mL in triplicate. Cells were incubated for 24 h in their normal

maintenance conditions and then 60 mL of MTT solution (5 mg/mL in HBSS) was added to each well. After 2 h of incubation in 37 °C, the medium was removed, and 300 mL of DMSO was added to each well to dissolve the crystals formed. The optical density of the wells was measured with an ELx800 Universal Microplate Reader (BioTek Instruments; Winooski, VT, USA) with cell-less medium as a blank. The absorbance of micelle-treated cells was compared to untreated cells and % cell viability was calculated using the following equation.

$$\% \text{ cell viability} = (\text{absorbance of siRNA polyplex treated cells} / \text{absorbance of untreated cells}) \times 100$$

#### **6.2.10. Assessing the silencing activity of STAT3-siRNA micelles by Real time PCR**

Real time (RT) PCR was carried out to determine STAT3 knock-down at the mRNA level measured at 48 and 72 h. Confluent cell cultures were trypsinized and re-suspended as described before, and seeded in 6 well plates (2.4 mL in each well) at 50% confluency. After 24 h, 1.8 mL fresh medium was added to each well. Micelles were prepared using scrambled and STAT3 siRNA at polymer:siRNA ratio of 8:1 (w/w) and were added to the wells (final polymer and siRNA concentration of 22.4 µg/mL and 200 nM per well) in triplicate. PEI-LA1.6 complexed with scrambled and STAT3 siRNA at polymer:siRNA ratio of 8:1 (w/w) (final polymer and siRNA concentration of 6.05 µg/mL and 54 nM per well) was used as positive control. After 48 or 72 h, total RNA was extracted using RNeasy spin columns (Qiagen, Mississauga, ON, Canada) according to the manufacturer's recommendations. cDNA was synthesised following Invitrogen's

protocol, briefly adding 2  $\mu\text{L}$  master mix 1 (0.5  $\mu\text{L}$  Oligo(dT)<sub>12-18</sub> Primer), 0.5  $\mu\text{L}$  random primer and 1  $\mu\text{L}$  (10 mM MdNTP's per sample) to 10  $\mu\text{L}$  of RNA (5000 ng) and then heated to 65 °C for 5 min. 7  $\mu\text{L}$  of Master Mix 2 (4  $\mu\text{L}$  5 × Synthesis Buffer, 2  $\mu\text{L}$  DTT (0.1 M) and 1  $\mu\text{L}$  RNAout RNase inhibitor (1.8 U/ $\mu\text{L}$ )) was then added and the samples heated at 37 °C for 2 min. 1  $\mu\text{L}$  of M-MLV RT enzyme was then added per sample and they were heated at 25 °C for 10 min, 37 °C for 50 min and 70 °C for 15 min. Real time PCR was performed on a StepOnePlus™ RT-PCR system (ABI) with GAPDH (Forward: 5'-CAC ATG GCC TCC AAG GAG TAA-3') and (Reverse: 5'-TGA GGG TCT CTC TCT TCC TCT TGT-3') as the endogenous housekeeping gene and the specific STAT3 primers (Forward: 5'-AAG TTT ATC TGT GTG ACA CCA ACG A-3') and (Reverse: 5'-CTT CAC CAT TAT TTC CAA ACT GCA T-3'). 7.5  $\mu\text{L}$  of master mix containing 5  $\mu\text{L}$  of SYBR® Green ROX™ qPCR Mastermix (Qiagen, Mississauga, ON, Canada) and 2.5  $\mu\text{L}$  primer (3.2  $\mu\text{M}$ ; per sample) was added to each well. Then 2.5  $\mu\text{L}$  of template of each sample was added in triplicate. Levels of mRNA were measured as CT threshold levels and normalized with the individual GAPDH control CT values. Altered mRNA levels in cells are indicated as a 'fold change' compared with control cells. Each sample was measured at least three times.

#### **6.2.11. Assessing the silencing activity of STAT3-siRNA micelles by Western blot**

Western blot was carried out to determine STAT3 knock-down at the protein level measured at 48 h. Confluent cell cultures were trypsinized and re-suspended as described before, and seeded in 6 well plates (2.4 mL in each well) at 50% confluence. After 24 h,

1.8 mL fresh medium was added to each well. Micelles were prepared using the scrambled and STAT3 siRNA at polymer:siRNA ratio of 8:1 and were added to the wells (final polymer and siRNA concentration of 22.4 µg/mL and 200 nM per well) in triplicate wells. PEI-LA1.6 complexed with scrambled and STAT3 siRNA at polymer:siRNA ratio of 8:1 (w/w) (final polymer and siRNA concentration of 6.05 µg/mL and 54 nM per well) was used as positive control. After 48 h incubation, the cells were washed with cold phosphate buffered saline (PBS) and lysed using RIPA cell lytic buffer supplemented with 0.1 mM phenylmethylsulfonylfluoride (PMSF) (Sigma Aldrich), a protease inhibitor cocktail (Nacalai Inc, San Diego, CA, USA) and a phosphatase inhibitor cocktail (Calbiochem, EMD Biosciences, Darmstadt, Germany). The lysate was then incubated on ice for 30 minutes which was followed by centrifugation at 17000 g for 15 minutes to remove genomic DNA. Protein quantification was determined by the BCA protein assay kit (Pierce, Rockford, IL, USA) and equal amounts of protein (50 µg) were loaded in 4-20% Tris-HCl precast gel (Bio-Rad, Mississauga, Ontario). After gel electrophoresis the proteins were transferred to a nitrocellulose membrane and stained with 0.05% Ponceau S (Sigma-Aldrich) to ensure equivalent protein loading per lane. The membrane was probed with antibodies against STAT3, p-STAT3 and BCL-2 (Santa Cruz Biotechnology, Santa Cruz, CA). The proteins were then detected using peroxidase-conjugated anti-mouse IgG and visualized by enhanced chemiluminescence (Pierce ECL Western Blotting Substrate, Thermo Scientific, Rockford, IL, USA). Optical intensity of STAT3, p-STAT3 and BCL-2 band was quantified and normalized to actin protein band using Adobe Photoshop software.

### **6.2.12. In vitro cytotoxicity of STAT3-siRNA micelles**

The cytotoxicity of STAT3 and scrambled siRNA complexed with different polymers was evaluated in MDA-MB-435/WT cells using MTT assay. Confluent cell cultures were trypsinized and re-suspended as described before, and seeded in 24 well plates (0.6 mL in each well) at 50% confluency. After 24 h, 400 mL fresh media was added to each well. siRNA micelles were prepared using the scrambled and STAT3 siRNA at polymer:siRNA ratios of 8:1, 16:1 and 32:1 (w/w) and were added to the wells (final polymer concentrations of 11.2, 22.4 and 44.8  $\mu\text{g}/\text{mL}$  and siRNA concentrations 100 and 200 nM per well in triplicate wells). Cells were incubated for 72 h in their normal maintenance conditions and then 60  $\mu\text{L}$  of MTT solution (5 mg/mL in HBSS) was added to each well. After 2 h of incubation in 37 °C, the medium was removed, and 300  $\mu\text{L}$  of DMSO was added to each well to dissolve the crystals formed. The optical density of the wells was measured with an ELx800 Universal Microplate Reader (BioTek Instruments; Winooski, VT, USA) with cell-less medium as blank. The absorbance of micelle-treated cells was compared to untreated cells and % cell viability was calculated using the above mentioned equation.

### **6.2.13. Assessing the silencing activity of MCL-1 siRNA micelles by real time PCR**

Real time (RT) PCR was carried out to determine MCL-1 knock-down at the mRNA level measured at 48 following the procedure as described earlier. Micelles were prepared using scrambled and MCL-1 siRNA at polymer:siRNA ratio of 16:1 (w/w) and were added to the wells (final polymer and siRNA concentration of 11.2  $\mu\text{g}/\text{mL}$  and 50

nM per well) in triplicate. Specific MCL-1 primers were used (Forward: 5'-CCTTTGTGGCTAAACACTTGAAG-3') and (Reverse: 5'-CGAGAACGTCTGTGATACTTTCTG-3'). Levels of mRNA were measured as CT threshold levels and normalized with the individual GAPDH control CT values. Altered mRNA levels in cells are indicated as a 'fold change' compared with control cells. Each sample was measured at least three times.

#### **6.2.14. In vitro cytotoxicity of MCL-1 siRNA micelles**

The cytotoxicity of MCL-1 and scrambled siRNA complexed with different polymers was evaluated in MDA-MB-435/WT cells using MTT assay as describe above. siRNA micelles were prepared using the scrambled and MCL-1 siRNA at polymer:siRNA ratios of 16:1 and 32:1 (w/w) and were added to the wells (final polymer concentrations of 11.2 and 22.4 µg/mL and siRNA concentrations 50 and 100 nM per well in triplicate wells). Cells were incubated for 72 h in their normal maintenance conditions and then 60 µL of MTT solution (5 mg/mL in HBSS) was added to each well. After 2 h of incubation in 37 °C, the medium was removed, and 300 µL of DMSO was added to each well to dissolve the crystals formed. The optical density of the wells was measured with an ELx800 Universal Microplate Reader (BioTek Instruments; Winooski, VT, USA) with cell-less medium as blank. The absorbance of micelle-treated cells was compared to untreated cells and % cell viability was calculated using the above mentioned equation.

#### **6.2.15. Statistics**

Compiled data were presented as means  $\pm$  standard deviation (SD). Where feasible, the data were analyzed for statistical significance using unpaired student's t-test, One-way analysis of variance followed by post hoc Tukey test as noted in the results section. The level of significance was set at  $\alpha \leq 0.05$ .

### 6.3. Results

#### 6.3.1. Synthesis and characterization of MePEO-*b*-P(CL-g-SP-Chol) polymer

The MePEO-*b*-P(CL-g-SP-Chol) with two different cholesteryl substitution levels were synthesized from MePEO-*b*-P(CL-g-SP) (**Figure 6.1**). The final structure of copolymers was confirmed by  $^1\text{H}$  NMR (**Figure 6.2.A and B**). The characteristics of prepared block copolymers are shown in **Table 6.1**. Peaks corresponding to specific cholesteryl group of SP-Chol polymer were observed at  $\delta = 0.84\text{-}1.1$  and  $5.35$  ppm in the  $^1\text{H}$  NMR spectra, indicating the successful conjugation of cholesteryl groups to block copolymer (**Figure 6.2.B**). Based on peak intensity ratio of proton from PCL ( $-\text{OCH}_2-$  proton,  $\delta = 4.1$  ppm) to the intensity of specific peak in PEO ( $-\text{CH}_2\text{CH}_2\text{O}-$  proton,  $\delta = 3.65$  ppm), degree of polymerization was calculated to be 15. We did not observe chain cleavage of PCL block for SP-Chol polymers. For synthesized polymers, the cholesteryl substitution levels was calculated to be 2.2 and 1.5 per CL chain which reflects 37% and 25% substitution of cholesteryl groups on SP.

A closer assessment of  $^1\text{H}$  NMR spectra shows complete removal of benzyl carboxylate residues in both SP and SP-Chol polymers under study. This was attributed to

the complete removal of benzyl carboxylate substituent during the modified reduction procedure in catalytic debenylation of MePEO-*b*-PBCL.

The amphiphilic block copolymers are known to self-assemble into micelles in aqueous solution at polymer concentrations above CAC. The formation of the micelles was investigated by DLS measurements. The average diameter of SP micelles determined by the DLS technique was  $40 \pm 10$  nm. On the other hand, micelles formed from SP-Chol 25% and SP-Chol 37% exhibited smaller size trend, showing average diameters of  $23 \pm 1$  and  $28 \pm 5$  nm, respectively (**Table 6.1**). The CAC of SP-Chol 25% and SP-Chol 37% (0.097 and 0.092  $\mu$ M, respectively) was determined to be significantly lower than that of SP (0.67  $\mu$ M) ( $P \leq 0.05$ ) (**Table 6.1**).

**Table 6.1.** Characteristics of prepared copolymers and empty micelles (n=3).

Polymer	Abbreviate	Cholesteryl substitution on SP % <sup>a)</sup>	Mn <sup>b)</sup> g/mol	CAC <sup>c)</sup> $\pm$ SD ( $\mu$ M)	Size <sup>d)</sup> $\pm$ SD (nm)
MePEO <sub>114</sub> - <i>b</i> -P(CL-g-SP-Chol) <sub>15-6-1.5</sub>	SP-Chol 25%	25	9131	0.097 $\pm$ 0.1	23 $\pm$ 1
MePEO <sub>114</sub> - <i>b</i> -P(CL-g-SP-Chol) <sub>15-6-2.2</sub>	SP-Chol 37%	37	9400	0.092 $\pm$ 0.1	28 $\pm$ 5
MePEO <sub>114</sub> - <i>b</i> -P(CL-g-SP) <sub>15-6</sub>	SP	NA	8552	0.67 $\pm$ 0.5	40 $\pm$ 10

<sup>a)</sup> Mole percent <sup>a,b)</sup> Determined by <sup>1</sup>H NMR. <sup>c)</sup> Measured from the onset of a rise in the intensity ratio of peaks at 339nm to peaks at 334nm in the fluorescence excitation spectra of pyrene plotted versus logarithm of polymer concentration. <sup>d)</sup> Z average mean estimated by DLS technique. NA, not applicable.

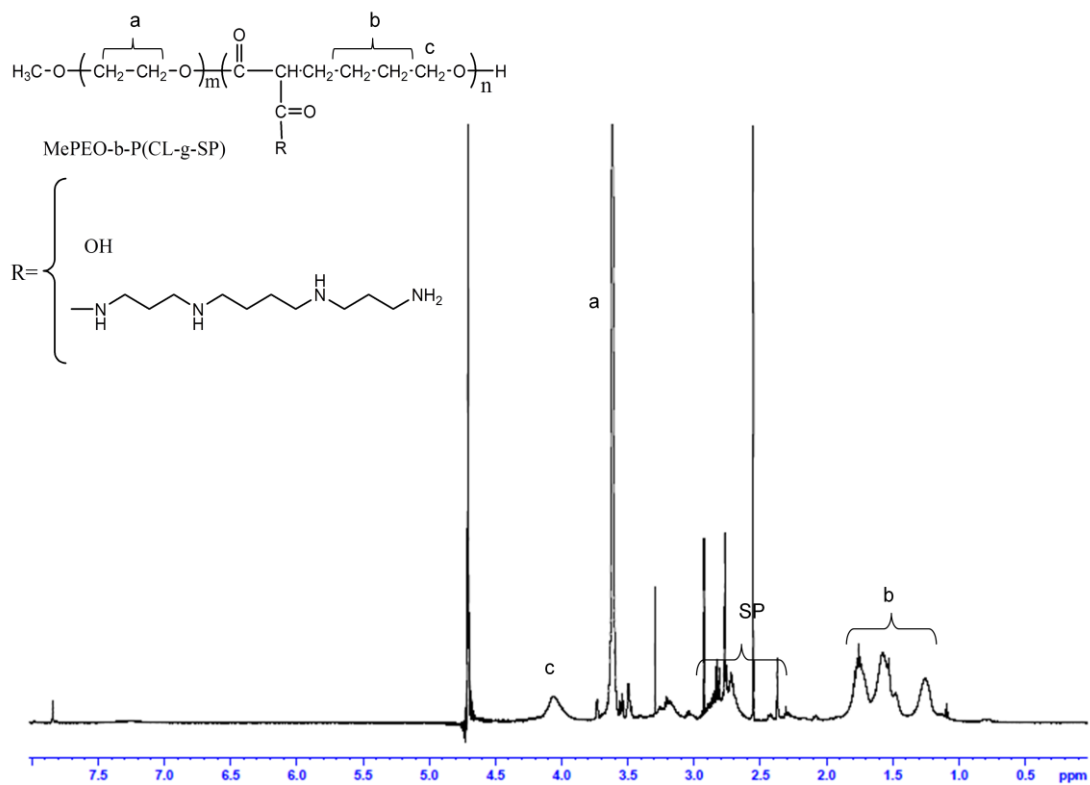


**Figure 6.2.A.** <sup>1</sup>H NMR spectra of MePEO-*b*-P(CL-g-SP) in D<sub>2</sub>O and peak assignments.

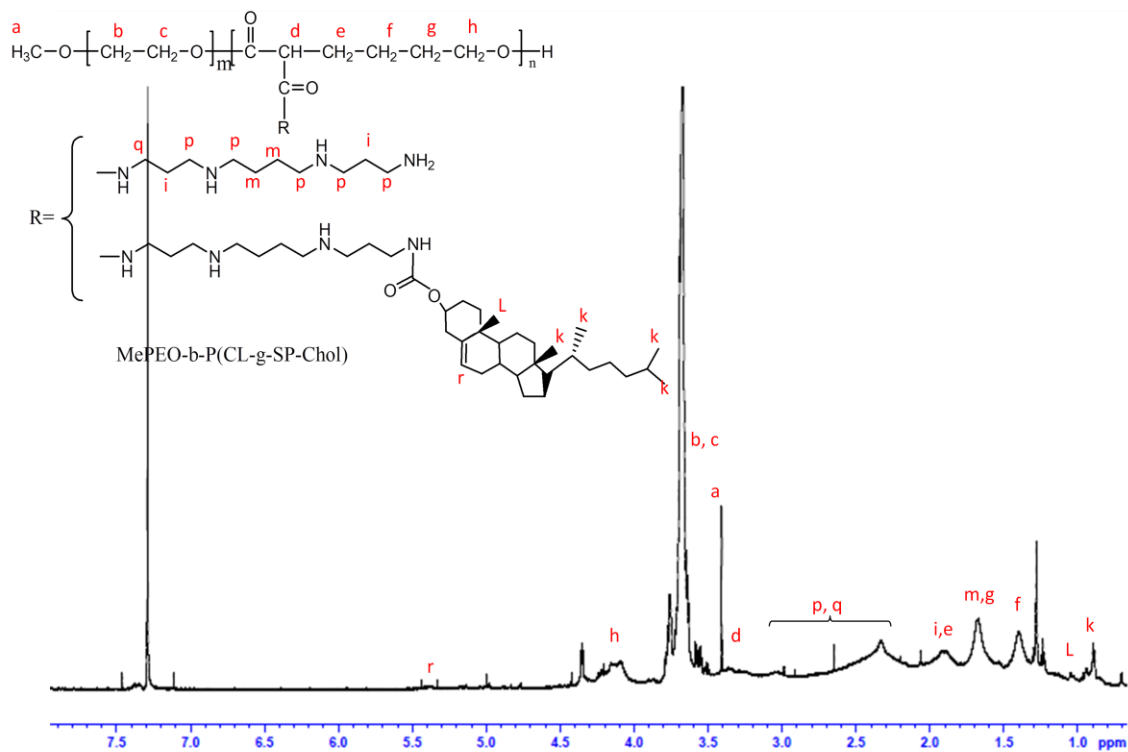


**Figure 6.2.B** <sup>1</sup>H NMR spectrum of MePEO-*b*-P(CL-g-SP-Chol) in CDCl<sub>3</sub> and peak assignments.

### 6.3.2 siRNA binding

SYBR Green II binding assay was used to detect complex formation between the synthesized copolymers and the siRNA. This was determined by affinity of the SYBR Green to free siRNA in polymer/siRNA micelles prepared with different polymer:siRNA (w/w) ratios. As expected, the synthesized SP and SP-Chol copolymers were capable of effectively binding siRNA (**Figure 6.3**). When the polymer:siRNA ratios (w/w) were higher than 16:1, all the copolymers were capable of 100% siRNA binding. There was not any obvious difference in siRNA binding ability among the copolymers, except that of SP-Chol 25% which showed slightly higher siRNA binding at 8:1 and 4:1 polymer:siRNA ratios (w/w).

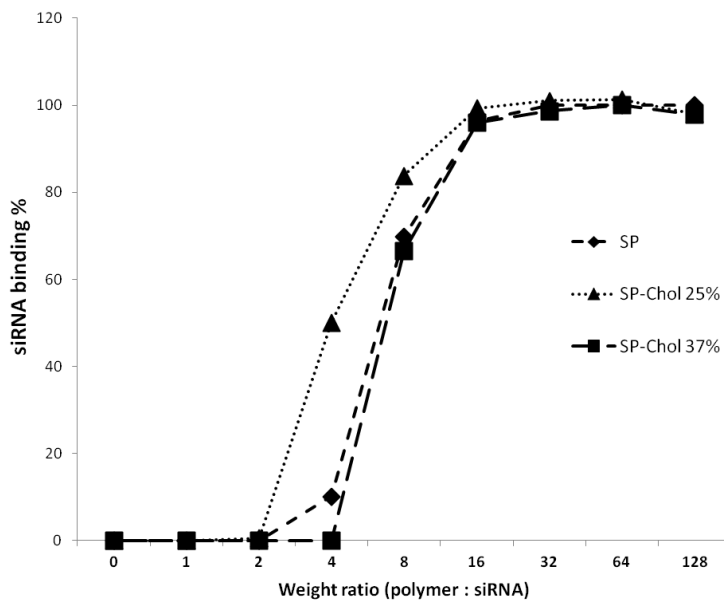


**Figure 6.3.** The binding affinity of different polymers to scrambled siRNA. Percentage of siRNA binding versus polymer:siRNA weight ratios is shown (n=2).

### 6.3.3. Release of siRNA from polymer/siRNA micelles with polyanion heparin

The release of siRNA from various polymer/siRNA micelles in the presence of heparin is shown in **Figure 6.4**. The siRNA release was dependent on heparin concentration. The heparin: polymer ratio ( $\mu\text{g}/\mu\text{g}$ ) which led to 50% siRNA release ( $\text{RR}_{50}$ ) from the complexes was used as measure of propensity for dissociation. SP polymer exhibited slightly slower release of siRNA compared to SP-Chol 25% and SP-Chol 37%, based on the higher  $\text{RR}_{50}$  values for the former polymer (0.2  $\mu\text{g}/\mu\text{g}$  heparin:polymer) as compared to the  $\text{RR}_{50}$  value of 0.1  $\mu\text{g}/\mu\text{g}$  for both SP-Chol 25% and SP-Chol 37%. All polymer/siRNA complexes exhibited higher siRNA release compared to PEI25K/siRNA complex ( $\text{RR}_{50} = 4.12 \mu\text{g}/\mu\text{g}$ , heparin:polymer), even though the latter was prepared at a low 1:1 polymer:siRNA ratio (w/w).

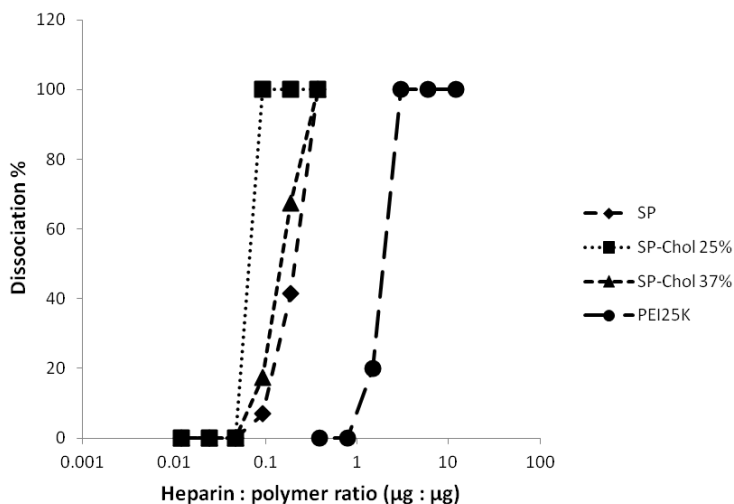


**Figure 6.4.** siRNA release from different micelles by heparin competition. Scrambled siRNA was complexed with various polymers at 32:1 polymer:siRNA ratio (w/w) and with PEI25K at 1:1 ratio (w/w). Amount of complex dissociation was determined with assessing free siRNA by agarose gel electrophoresis (n=2).

#### 6.3.4. Cellular association and uptake studies

The uptake of polymer/siRNA micelles was determined in MDA-MB-435/WT cells. FAM-labeled negative siRNA was used to uptake of polymer/siRNA micelles or PEI/siRNA complexes. In general, complexation of siRNA with all polymers under study was found to be effective in increasing the association of siRNA with cells as the percent of siRNA positive cells reached its maximum level within 24 h following complexation with either PEI25K or polymeric micellar formulations (**Figure 6.5 A and B**). Based on the mean fluorescent intensity data, PEI25K was the most effective polymer for siRNA delivery to MDA-MB-435/WT cells at both 3 and 24 h (**Figure 6.5**). Overall, substitution of cholesteryl on SP polymer increased the association of siRNA micelles with breast cancer cells (**Figure 6.5**). Among polymer/siRNA micelles, SP-Chol 37% showed the highest siRNA delivery (maximum mean fluorescence intensity) at both 3 and 24 h (**Figure 6.5 C and D**). At 24h, SP-Chol 25% also showed a significantly higher uptake compared to SP polymer (**Figure 6.5 D**).

Furthermore, the cellular distribution of selected polymer/siRNA micelles was investigated in MDA-MB-435/WT cells by confocal microscopy (**Figure 6.6**). Clear green colored siRNA fluorescence was observed in cytoplasm when siRNA was formulated in SP-Chol micelles (**Figure 6.6 (2) and (3)**), respectively). siRNA formulated in SP micelles (**Figure 6.6 (1)**) gave less detectable fluorescence while siRNA alone (**Figure 6.6 (4)**) exhibited no detectable fluorescence in the cells. The observation of yellow color in the merged fluorescence images of the FAM-labeled siRNA (green, Panel

a) and LysoTracker (red, Panel c) for SP-Chol siRNA complexes implies internalization of these micelles into cells by endocytosis.

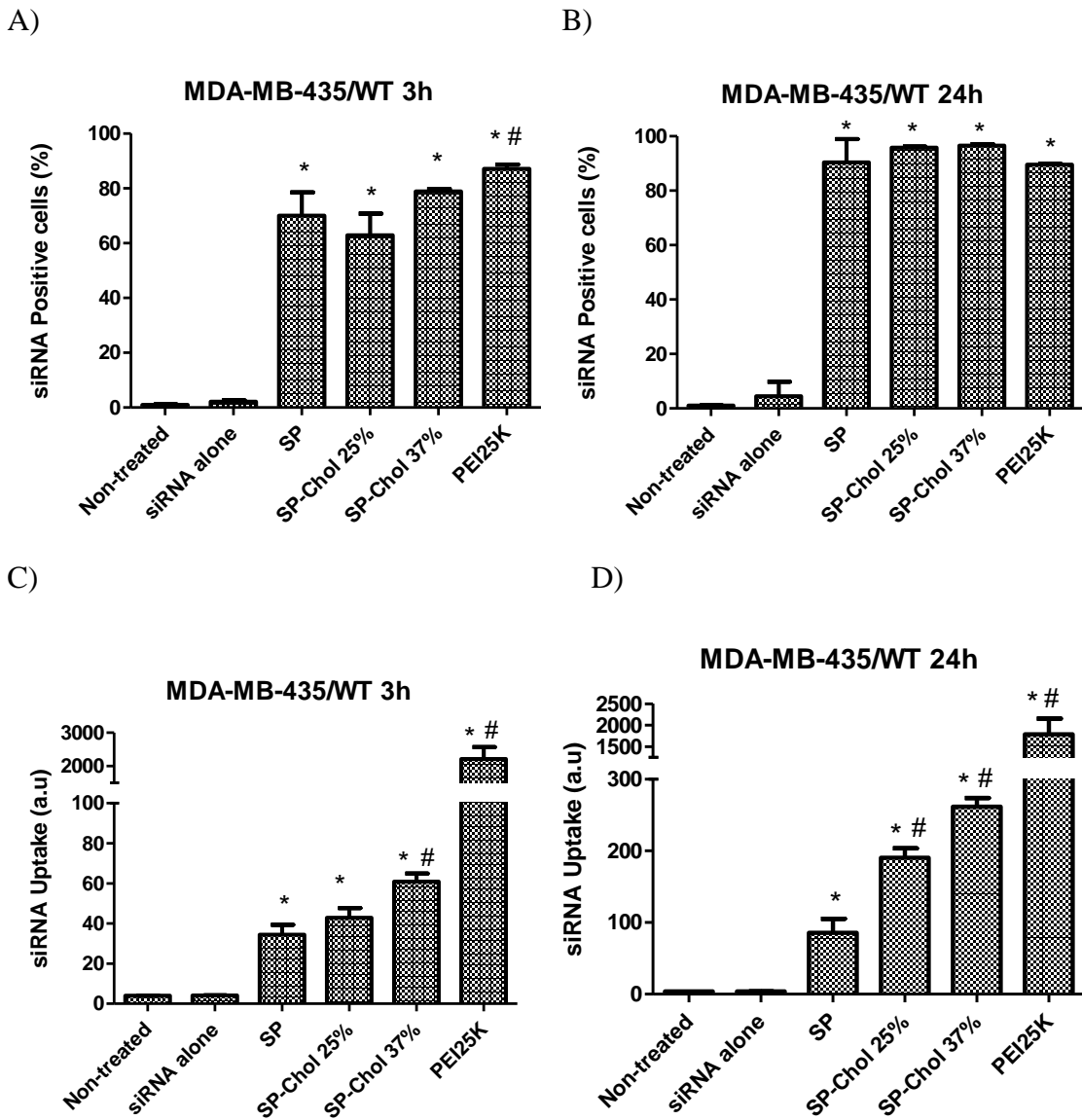


**Figure 6.5.** Cellular uptake of polymer/FAM-siRNA complexes by MDA-MB-435/WT cells. A and B) The percentage of cells positive for FAM-siRNA after 3 and 24 h exposure to siRNA micelles at polymer:siRNA ratios of 16:1 (w/w) and PEI25K:siRNA ratio of 1:1 (w/w). C and D) The mean fluorescence of the cells after 3 and 24 h exposure to micelles. The data are the mean  $\pm$  SD for n=3. \*Significantly different from siRNA alone ( $P < 0.05$ ), #Significantly different from SP ( $P < 0.05$ ). (One way ANOVA followed by Tukey test,  $P < 0.05$ ).

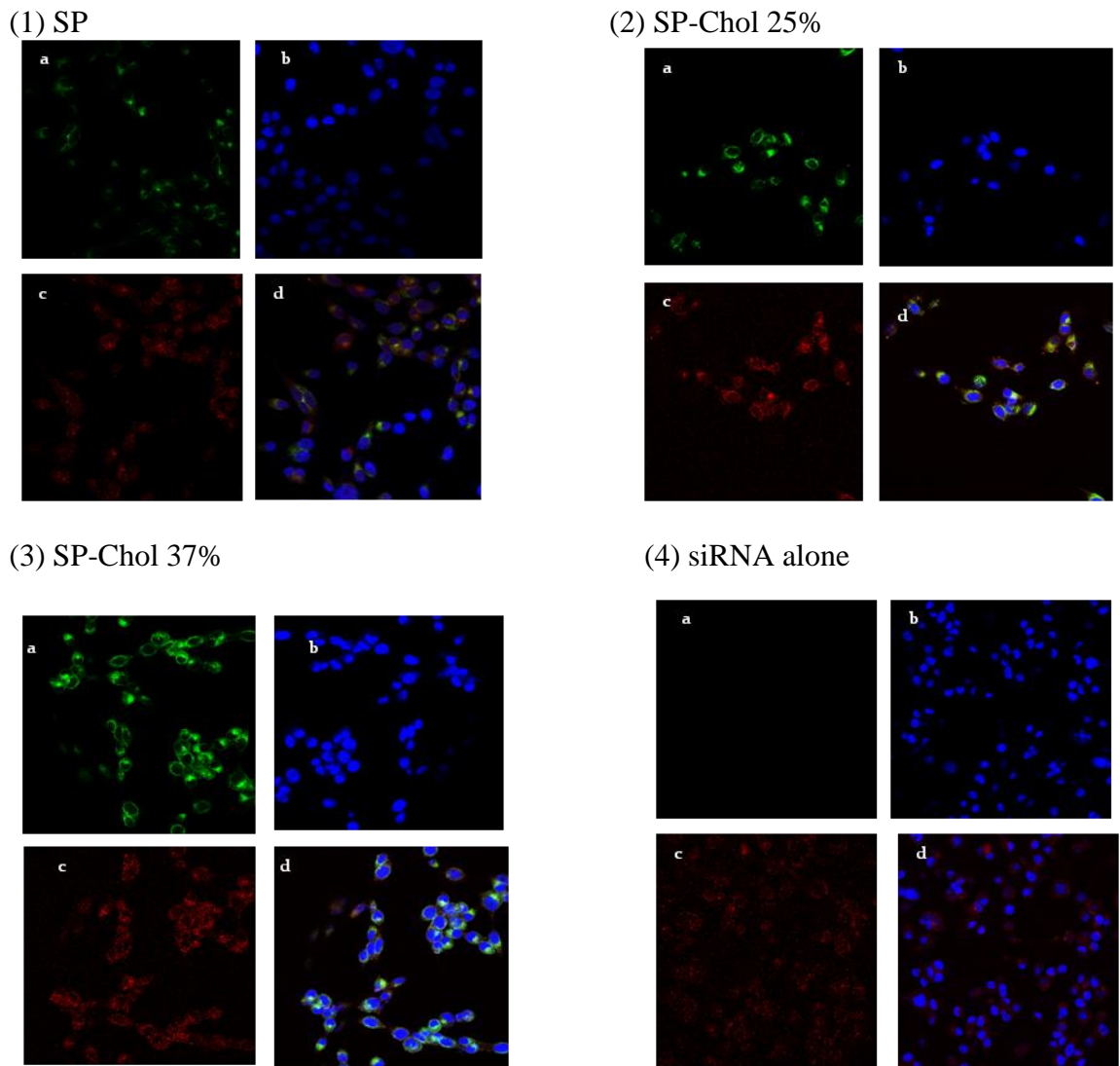


**Figure 6.6.** Cellular distribution of polymer/siRNA micelles by confocal microscopy

Uptake and intracellular distribution of FAM-siRNA formulated in micelles by MDA-MB-435/WT cells using confocal microscopy. The observation was done 24 h exposure to FAM-siRNA formulated (1) SP, (2) SP-Chol 25%, (3) SP-Chol 37%, (4) siRNA alone at polymer:siRNA ratios of 16:1 (weight/weight). a) Images represent FAM-siRNA (green) alone, b) Images represent nucleus stained with DAPI (blue), c) Images represent lysosomes stained with lysoTracker (red) and d) the images were merged together.

### 6.3.5. Cytotoxicity study

Cytotoxicity of the synthesized polymers upon complexation with siRNA was evaluated in MDA-MB-435/WT cells using MTT assay (**Figure 6.7**). All polymeric micellar siRNAs under study exhibited minimal cytotoxicity at polymer:siRNA 8:1 (w/w) ratio with 100 nM of siRNA. SP and SP-Chol 25% micelles caused ~40% toxicity at polymer:siRNA 16:1 ratio (w/w) and 100 nM siRNA, while SP-Chol 37% caused only ~20% toxicity at this concentration. This was significantly different from cytotoxicity caused by SP polymer siRNA complexes (one way ANOVA followed by Tukey test,  $P \leq 0.05$ ). At polymer:siRNA 8:1 (w/w) ratio and 200 nM siRNA, SP-Chol 37% micelles exhibited minimal toxicity and were significantly less cytotoxic than SP micelles.

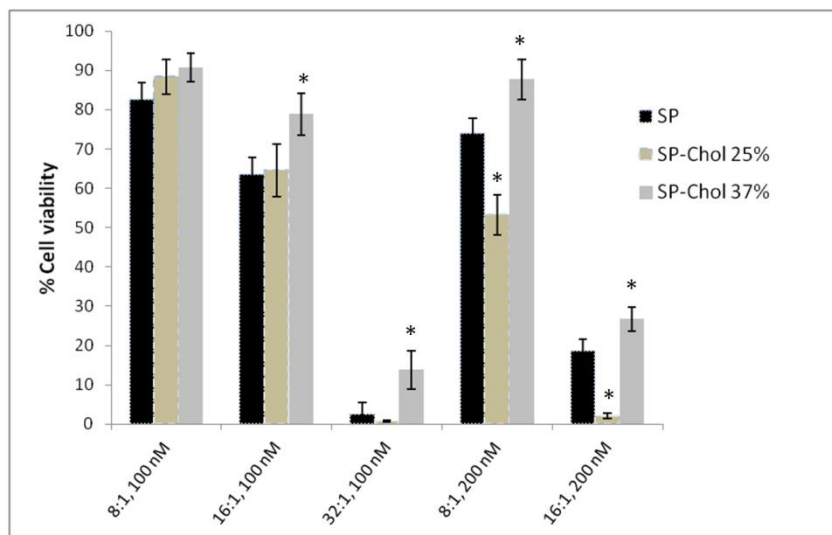


**Figure 6.7.** Cytotoxicity of the synthesized block copolymers/scrambled siRNA complexes against MDA-MB-435/WT cells. Incubation time was 72 h. 8:1, 16:1 and 32:1 ratios represent polymer:siRNA ratio (w/w). 100 and 200 nM indicate the dose of siRNA used in each well. The data are the mean  $\pm$  SD for  $n=3$ . \*Significantly different from SP (one way ANOVA followed by Tukey test,  $P < 0.05$ ).

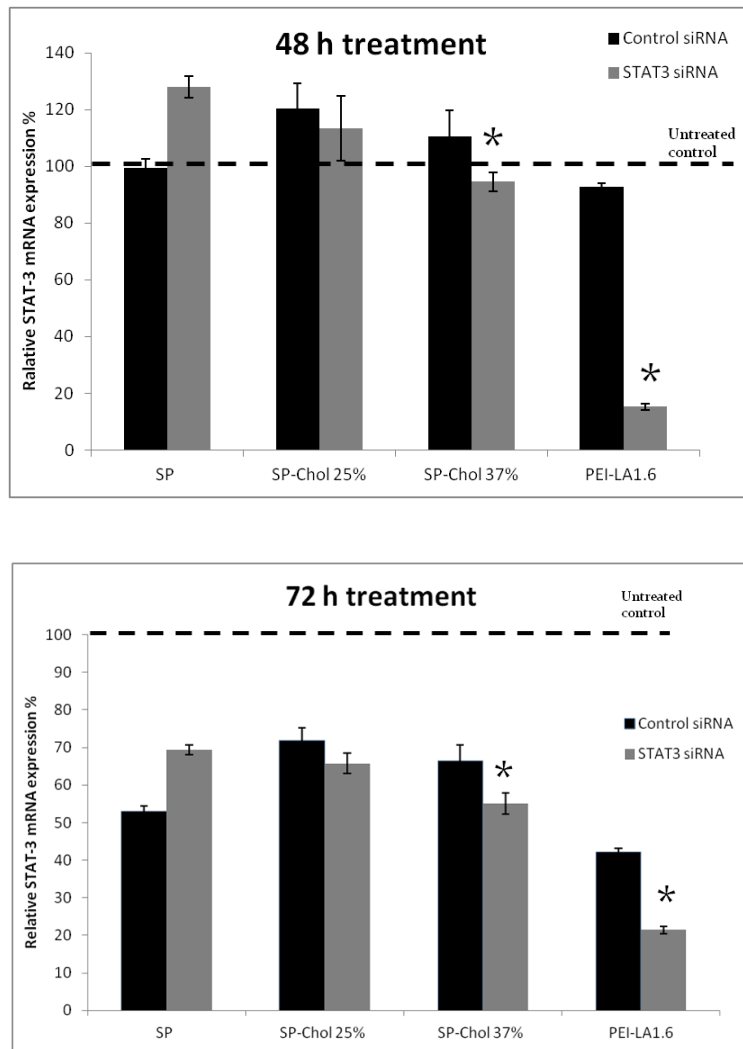
Based on these results, a 37% cholesteryl substitution of SP polymer has significantly decreased the cytotoxicity. A polymer:siRNA ratio of 8:1 at a siRNA dose of 200 nM was chosen for further studies.

### **6.3.6. STAT3 knockdown by polymer/siRNA micelles**

To evaluate the ability of STAT3-siRNA micelles for STAT3 silencing at mRNA level, MDA-MB-435/WT were treated for 48 and 72 h with siRNA dose of 200 nM and polymer:siRNA ratio of 8:1 (w/w) (**Figure 6.8**). At 48 h, the level of STAT3 mRNA expression after incubation with STAT3-siRNA/SP-Chol 37% micelles was reduced by ~6 % compared to non-treated (NT) control group. This level of STAT3 mRNA knockdown was significantly different from identical scrambled-siRNA/SP-Chol 37% micelles which did not decrease STAT3 mRNA expression (unpaired student's t-test,  $P < 0.05$ ). At 72 h, STAT3-siRNA/SP-Chol 37% micelles caused a ~45% decrease in STAT3 mRNA expression compared to non-treated control group. This level of down-regulation was also significantly different from its identical scrambled-siRNA micelles which caused (~33%) reduction in STAT3 mRNA expression. No change has been detected in STAT3 mRNA expression level using SP and SP-Chol 25% micelles. STAT3-siRNA/PEI-LA1.6 polyplexes, which were used as positive controls in the study, caused a significant decrease (~80%) in STAT3 mRNA expression both at 48 and 72 h compared to non-treated control group.

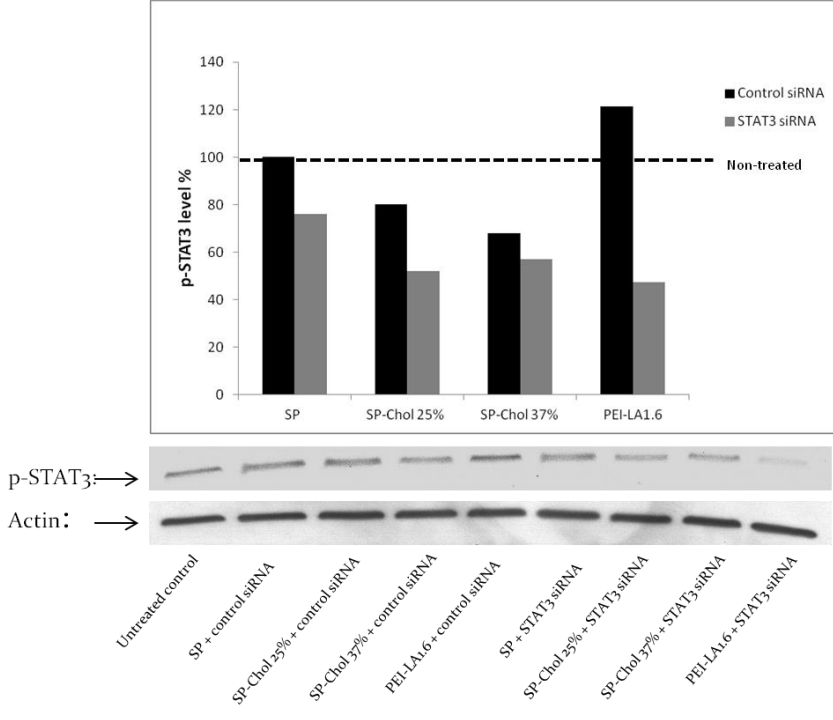
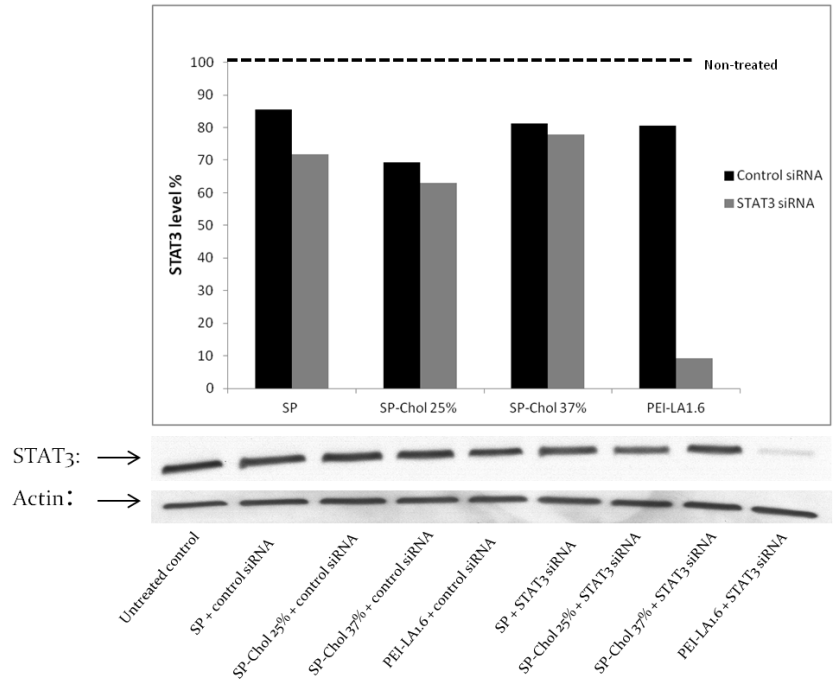
STAT3, p-STAT3 and BCL-2 protein levels were measured after 48 h treatment with polymer/siRNA micelles prepared at 8:1 ratio (w/w) and 200 nM siRNA dose

**(Figure 6.9).** The expression of STAT3 protein using complexes of STAT3-siRNA with SP, SP-Chol 25 %, SP-Chol 37 % and PEI-LA1.6 (positive control) was decreased by approximately ~29, 38, 23 and 90 % compared to the untreated cells, respectively. However, silencing of proteins was less specific for polymeric micellar STAT3 siRNA complexes compared to PEI-LA1.5 complexes as ~14, 30 and 19 % STAT3 protein downregulation was also observed for scrambled siRNA micellar complexes of SP, SP-Chol 25 %, SP-Chol 37 %, respectively. This was in contrast to PEI-LA1.6 complexes of STAT3 siRNA that showed 20 % silencing of STAT3 protein with scrambled siRNA. In case of p-STAT3 protein, treatment of cells with complexes of STAT3-siRNA and SP, SP-Chol 25 %, SP-Chol 37 % and PEI-LA1.6, led to 24, 48, 42 and 53 % protein downregulation compared to untreated control, respectively. Similar to previous observation, this silencing effect was not as specific for polymeric micellar siRNA complexes as it was for PEI-LA1.6/STAT3-siRNA complexes (20 and 33 % non-specific downregulation of p-STAT3 was observed for scrambled siRNA complexes of SP-Chol 25 %, SP-Chol 37 %, respectively). For SP and PEI-LA1.6 no non-specific downregulation of p-STAT3 was observed. Treatment of cells with STAT3-siRNA complexes of SP, SP-Chol 25 %, SP-Chol 37 % led to reduced expression of BCL-2, a downstream product of STAT3 activation, by 30, 44 and 15 %. For comparison, 17, 20, and 2 % downregulation for complexes of scrambled siRNA was observed, respectively. Interestingly, despite better downregulation of STAT3 and p-STAT3 by STAT3-siRNA complexes of PEI-LA1.6, this complex did not affect BCL-2 expression.



**Figure 6.8.** Silencing activity of STAT3-siRNA micelles by RT-PCR

STAT3 silencing activity of the STAT3-siRNA at mRNA level in MDA-MB-435/WT after 48 and 72 h. The cells were transfected with STAT3-siRNA formulated in various micelles prepared using polymer:siRNA ratios of 8:1 (w/w) and 200 nM siRNA. PEI-LA1.6 at polymer:siRNA ratios of 8:1 (w/w) complexed with 54 nM siRNA was used as positive control. Values are relative to non-treated controls (NT). The data are the mean  $\pm$  SD for n=3. \*Significantly different from its corresponding control siRNA group (unpaired student's t-test,  $P < 0.05$ ).



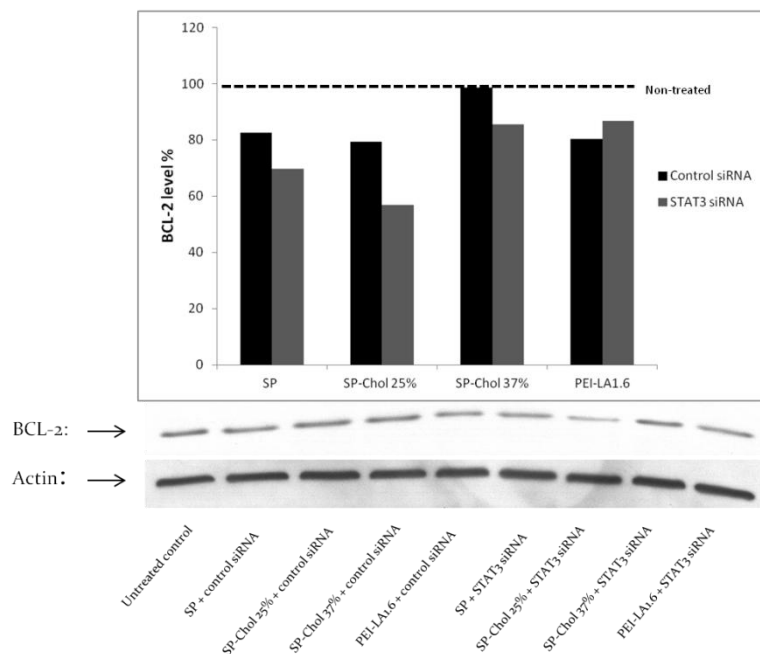
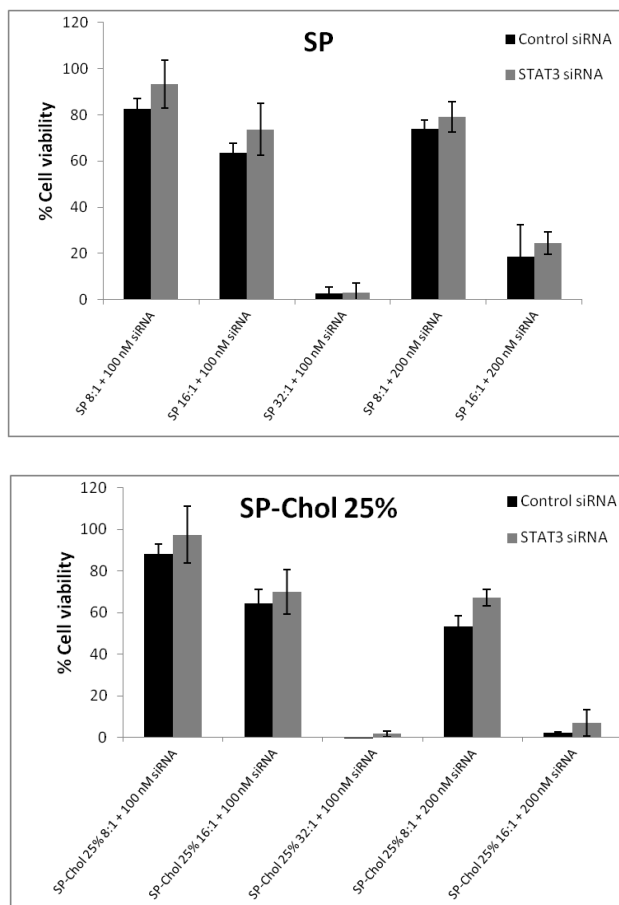


**Figure 6.9.** Silencing activity of STAT3-siRNA micelles by Western blot.

STAT3, p-STAT3 and BCL-2 silencing activity of the STAT3-siRNA at protein level in MDA-MB-435/WT after 48 h. The cells were transfected with STAT3-siRNA formulated in various micelles prepared using polymer:siRNA ratios of 8:1 (w/w) and 200 nM siRNA. PEI-LA1.6 at polymer:siRNA ratios of 8:1 (w/w) complexed with 54 nM siRNA was used as positive control. Values are relative to non-treated controls (NT). The bar graph represents the mean of two identical experiments.

### 6.3.7. In vitro cytotoxicity of STAT3-siRNA micelles

The cytotoxic effect of STAT3-siRNA complexed with different polymers was investigated 72 h after treatment with MDA-MB-435/WT cells using MTT (**Figure 6.10**). None of the STAT3-siRNA polymeric micelles caused STAT3 associated cell death. In other words, cytotoxicity induced by STAT3 siRNA polymeric micellar formulations were similar to that induced by their scrambled siRNA counterparts.



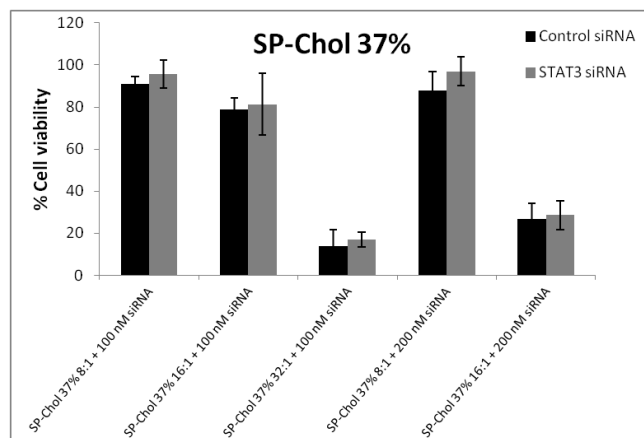


**Figure 6.10.** Cytotoxicity of STAT3-siRNA versus scrambled siRNA micelles.

The viability of the MDA-MB-435/WT after 72 h exposure to polymer/siRNA micelles prepared using the scrambled and STAT3-siRNA at polymer:siRNA ratios of 8:1, 16:1 and 32:1 (w/w). 100 and 200 nM indicate the dose of siRNA used in each well. The data are the mean  $\pm$  SD (n=3).

### 6.3.8. MCL-1 knockdown by polymer/siRNA micelles

To evaluate the ability of MCL-1 siRNA micelles for MCL-1 silencing at mRNA level, MDA-MB-435/WT were treated for 48 h with siRNA doses of 50 nM siRNA and polymer:siRNA ratio of 16:1 (w/w) (**Figure 6.11**). At 48 h, the level of MCL-1 mRNA expression after incubation with MCL-1 siRNA/SP-Chol 37% micelles was reduced by ~98 % compared to non-treated (NT) control group. This level of MCL-1 mRNA knockdown was significantly different from identical scrambled-siRNA/SP-Chol 37% micelles which decreased MCL-1 mRNA expression by 55 % (unpaired student's t-test,  $P < 0.05$ ). MCL-1 siRNA/SP micelles were also effective in reducing MCL-1 mRNA expression by ~90 % compared to non-treated (NT) control group. This level of MCL-1

mRNA knockdown was significantly different from identical scrambled-siRNA/SP micelles which decreased MCL-1 mRNA expression by 42 % (unpaired student's t-test,  $P < 0.05$ ).

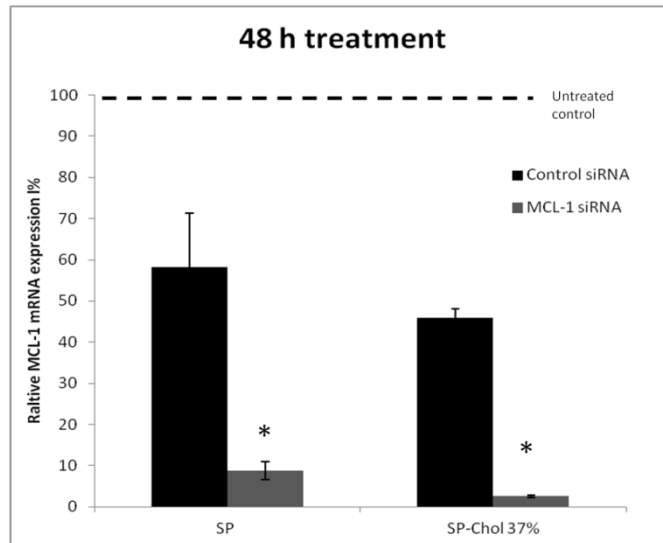


**Figure 6.11.** Silencing activity of MCL-1 siRNA micelles by RT-PCR

MCL-1 silencing activity of the MCL-1 siRNA at mRNA level in MDA-MB-435/WT after 48 h. The cells were transfected with MCL-1 siRNA formulated in various micelles prepared using polymer:siRNA ratios of 16:1 (w/w) and 50 nM siRNA. Values are relative to non-treated controls (NT). The data are the mean  $\pm$  SD for  $n=3$ . \*Significantly different from its corresponding control siRNA group (unpaired student's t-test,  $P < 0.05$ ).

### 6.3.9. In vitro cytotoxicity of MCL-1 siRNA micelles

The cytotoxic effect of MCL-1 siRNA complexed with SP and SP-Chol 37% polymers was investigated 72 h after treatment with MDA-MB-435 cells using MTT (**Figure 6.12**). MCL-1 siRNA/SP-Chol 37% polymeric micelles with 50 nM siRNA dose and polymer:siRNA ratio of 16:1 (w/w) caused 47 % MCL-1 associated cell death. This

level of cell death was significantly different from identical control-siRNA/SP-Chol 37% micelles which caused 20% non-specific cell death (unpaired student's t-test,  $P < 0.05$ ). MCL-1 siRNA/SP polymeric micelles with the same siRNA dose and polymer: siRNA ratio did not exhibit any specific MCL-1 associated cell death. Both siRNA dose of 100 nM/well and polymer:siRNA ratio of 32:1 proved to be not effective and caused considerable non-specific cell death.

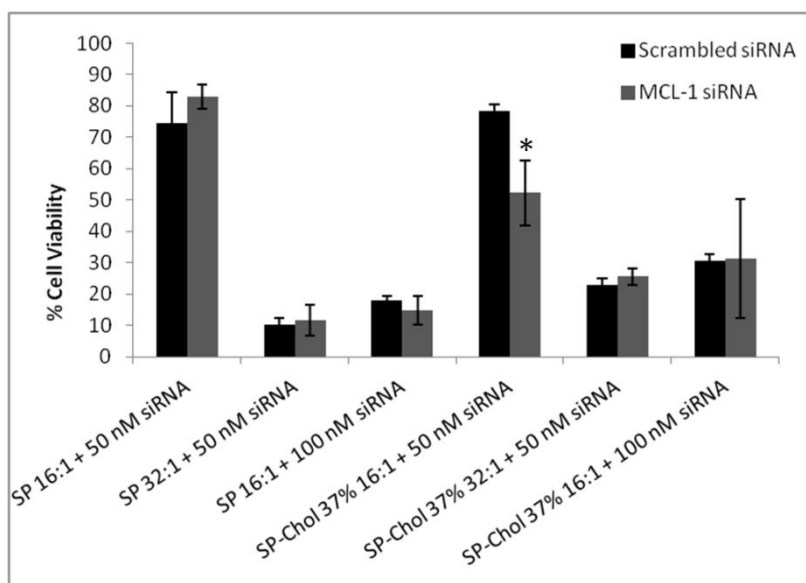


**Figure 6.12.** Cytotoxicity of MCL-1siRNA versus scrambled siRNA micelles.

The viability of the MDA-MB-435/WT after 72 h exposure to polymer/siRNA micelles prepared using the scrambled and MCL-1 siRNA at polymer:siRNA ratios of 16:1 and 32:1 (w/w). 50 and 100 nM indicate the dose of siRNA used in each well. The data are the mean  $\pm$  SD (n=3).

#### 6.4. Discussion

The aim of this study was twofold; first to employ an optimized synthetic method that can lead to the preparation of MePEO-*b*-P(CL-SP) and its cholesterol modified analogue in a reproducible and controlled manner. Our second aim was to assess the effect of cholesteryl substitution on the synthesized MePEO-*b*-P(CL-SP) on the properties of their polymeric micellar siRNA complexes in siRNA delivery. We hypothesized that the lipid modification of the polycation can enhance the stability, cellular association and silencing activity of polymeric micellar complexes of siRNA.

The modified method of synthesis and purification allowed preparation of MePEO-*b*-PCCL with higher degree of polymerization (DP = 15). This modified method of debenylation of MePEO-*b*-PBCL has led to less cleavage of PBCL chain as well as complete removal of benzyl group from the polymer. A higher degree of polymerization for MePEO-*b*-PCCL has led to successful synthesis of MePEO-*b*-P(CL-SP) block copolymers with higher degrees of polymerization (DP = 15) for the P(CL-SP) block and their cholesterol substituted derivatives compared to DP = 11 for polymers from previous chapter. A modified purification step in MePEO-*b*-P(CL-SP) synthetic procedure resulted in more successful removal of unconjugated free spermine from polymeric solution, reduced the possibility of chain cleavage for the P(CL-SP) block and enhanced the reproducibility of synthetic method in obtaining MePEO-*b*-P(CL-SP) polymer with controlled degree of polymerization.

The prepared SP, SP-Chol 25% and SP-Chol 37% were shown to form micelles of < 50 nm (**Table 6.1**). Lipid modification of SP in PEO-P(CL-SP) provided a more stable nanocarrier reflected by a decrease in the CAC of cholesteryl modified polymer compared to parent MePEO-P(CL-SP) (**Table 6.1**). The trend is similar to our observation in the previous chapter. The lower CAC values for cholesteryl substituted polymeric micelles clearly shows that the introduction of hydrophobic cholesteryl groups to the P(CL-g-SP) makes self-association of block copolymers, thermodynamically, more favorable. These results are consistent with previous findings on the effect of core hydrophobicity on CAC value [4].

Substitution of cholesteryl on SP was expected to reduce the protonation of polyamine side chain compared to the original SP polymer, but our results showed this modification not to have significant negative impact on siRNA binding (**Figure 6.3**). This is in contrast to the results of previous chapter where lipid modification of the SP group in MePEO-P(CL-SP) block copolymer led to a significant reduction in siRNA binding by polymeric micelles. This observation might be due to differences in the sensitivity of the assay methods used assessing the complexation of siRNA in Chapter 5 (gel electrophoresis) and Chapter 6 (syber green assay). Another possible explanation is the better binding of current polymers to siRNA because of the higher number of free COOH groups on the parent and cholesteryl modified MePEO-P(CL-SP) leading to better ionization of amine groups of SP forming Zwitterions in the current polymers. The more efficient binding of original MePEO-P(CL-SP) of this chapter with siRNA (100% siRNA binding at polymer: siRNA ratio of 16:1) compared to the one prepared in previous

chapter (100% siRNA binding at polymer: siRNA ratio of 64:1) points to the validity of the latter explanation.

We then evaluated the effect of lipid substitution on siRNA release in the presence of different heparin concentrations at a polymer:siRNA ratio of 32:1, where 100 % siRNA binding was achieved (**Figure 6.4**). All polymers under study showed significantly higher siRNA release compared to PEI/siRNA complex. In general, cholesteryl modification of MePEO-P(CL-SP) did not impact the release of complexed siRNA in the presence of heparin to a great extent. Among synthesized polymers, SP showed slightly lower release of siRNA in the presence of heparin perhaps due to strong electrostatic interaction between protonated amines on SP and negatively charged siRNA.

Cholesterol substitution of MePEO-P(CL-SP) significantly enhanced cellular delivery of incorporated siRNA (**Figure 6.5**). Cellular association of siRNA was highest when complexed with SP-Chol 37% as compared to other polymers under study. The results were in line with our previous findings reported in chapter 5 that SP-Chol 50% was the most effective carrier for siRNA delivery. Confocal microscope images confirmed the results of flow cytometry revealing better intracellular uptake of siRNA by SP-Chol 37% micelles (**Figure 6.6**). SP-Chol 37% also appeared to be successful in delivery of complexed siRNA into cytoplasm to some extent. Hydrophobic moieties are presumed to increase the interaction between the carrier and the lipophilic cell membrane, therefore enhancing the cellular uptake of nucleic acid associated polymeric carriers. In general, cellular uptake of siRNA incorporated in polymeric micelles under study were

much lower than the control PEI/siRNA complexes. This is due to the shielding effect of PEG that reduces the interaction of polymeric micelles with cell membranes or other hydrophobic surfaces in a non-specific manner.

Since cytotoxicity is a major concern for polycations employed for siRNA delivery, the MTT assay was performed with MDA-MB-435/WT to determine the toxicity of the synthesized polymers under study (**Figure 6.7**). Cholesterol modification of SP, particularly at higher level of substitution decreased the cytotoxicity of polymeric micellar siRNA complexes, perhaps by masking the positive charge of polycation due to primary amine substitution.

In line with the results of cellular uptake study, cholesterol substitution at higher levels was shown to significantly enhance the silencing activity of complexed siRNA at the mRNA level. At a dose of 200 nM siRNA per well, only SP-Chol 37% STAT3-siRNA micelles yielded significant silencing of STAT3 mRNA in MDA-MB-435/WT cells compared to cells treated with scrambled siRNA micelles of the same polymer at both 48 and 72 h (**Figure 6.8**). The mRNA downregulation did not translate to significant downregulation of STAT3 protein or its activated form, i.e., p-STAT3, at a 48h incubation period and an siRNA dose of 200 nM, however. STAT3 is known to regulate the expression of anti-apoptotic factors such as BCL-2, BCL-xL, MCL-1 and Survivin [5-9] in breast cancer cells, hence inhibition of STAT3 is expected to decrease the level of aforementioned factors in cells [8, 10, 11]. In line with the results obtained for STAT3 protein and its phosphorylated form, BCL-2 downregulation in cancer cells treated with

all polymeric micellar STAT3-siRNA treatments was small. Interestingly PEI-LA1.6 polyplex of STAT3 siRNA that had effectively downregulated STAT3 and p-STAT3 expression did not cause significant BCL-2 silencing in this cell line at 48h incubation period. The reason for this observation is not clear and needs further clarification. In line with our observation on the insignificant downregulation of STAT3 and its activation products by polymeric micellar STAT3-siRNA complexes under study, no significant cell death as a result of this treatment in MDA-MB-435 cells was observed at a dose of 200 nM siRNA (**Figure 6.10**).

MCL-1 is key regulator of apoptosis and has been shown to be essential for survival of a variety of cell types, therefore its suppression is expected to cause cell death [12]. Similar to the results of STAT3 silencing, SP-Chol 37% was shown to significantly enhance the silencing activity of complexed MCL-1 siRNA at the mRNA level. At a low dose of 50 nM siRNA per well, both SP and SP-Chol 37% STAT3-siRNA micelles resulted in significant silencing of MCL-1 mRNA in MDA-MB-435/WT cells compared to cells treated with scrambled siRNA micelles of the same polymer at 48 h (**Figure 6.11**). However, only SP-Chol 37% exhibited effective results in causing a significantly higher level of cytotoxicity after delivery of MCL-1 siRNA compared to identical scrambled siRNA micelles (**Figure 6.12**).

The lower overall silencing activity of polymeric micellar siRNA compared to PEI-LA complexes was expected due to the shielding effect of PEG and condensation of siRNA within the micellar core in polymeric micelles that can limit the cellular delivery

and intracellular release of incorporated siRNA, respectively. Although both structural features (the presence of PEG shell and higher nanoparticle/siRNA complex stability) are desired for success in systemic in vivo administration of siRNA with the aim of site specific siRNA delivery.

## 6.5. Conclusion

Successful synthesis of cholesteryl substituted MePEO-*b*-P(CL-g-SP) at a controlled and reproducible manner led to the formation of more stable and compact micelles capable of efficient siRNA binding. Lipid substitution of SP moiety in MePEO-*b*-P(CL-g-SP), particularly at higher levels of cholesteryl substitution, was successful in enhancing the stability of micellar siRNA carrier, improving the safety of siRNA delivery system and enhancing the cellular uptake leading to better silencing activity of incorporated siRNA at mRNA level. However, under current experimental conditions, cholesterol modification of the P(CL-SP) core, was found to be insufficient in causing significant improvements in the silencing activity of siRNA in terms of STAT3 protein expression leading to cancer cell death. Future strategies may focus on simultaneous engineering of the micellar core and shell to achieve improved siRNA silencing activity in cancer cells.

## 6.6. References

- [1] Xiong XB, Uludag H, Lavasanifar A. Biodegradable amphiphilic poly(ethylene oxide)-block-polyesters with grafted polyamines as supramolecular nanocarriers for efficient siRNA delivery. *Biomaterials* 2009;30:242-53.
- [2] Xiong XB, Uludag H, Lavasanifar A. Virus-mimetic polymeric micelles for targeted siRNA delivery. *Biomaterials* 2010;31:5886-93.
- [3] Aliabadi HM, Landry B, Bahadur RK, Neamnark A, Suwanton O, Uludag H. Impact of lipid substitution on assembly and delivery of siRNA by cationic polymers. *Macromol Biosci* 2011;11:662-72.
- [4] Lavasanifar A, Samuel J, Kwon GS. The effect of alkyl core structure on micellar properties of poly(ethylene oxide)-block-poly(L-aspartamide) derivatives. *Colloids Surf B Biointerfaces* 2001;22:115-26.
- [5] Clevenger CV. Roles and regulation of stat family transcription factors in human breast cancer. *Am J Pathol* 2004;165:1449-60.
- [6] Real PJ, Sierra A, De Juan A, Segovia JC, Lopez-Vega JM, Fernandez-Luna JL. Resistance to chemotherapy via Stat3-dependent overexpression of Bcl-2 in metastatic breast cancer cells. *Oncogene* 2002;21:7611-8.
- [7] Kim J, Lee YJ, Shin DS, Jeon SH, Son KH, Han DC, et al. Cosmomycin C inhibits signal transducer and activator of transcription 3 (STAT3) pathways in MDA-MB-468 breast cancer cell. *Bioorg Med Chem* 2011;19:7582-9.
- [8] Liu H, Tekle C, Chen YW, Kristian A, Zhao Y, Zhou M, et al. B7-H3 silencing increases paclitaxel sensitivity by abrogating Jak2/Stat3 phosphorylation. *Mol Cancer Ther* 2011;10:960-71.
- [9] Kunigal S, Lakka SS, Sodadasu PK, Estes N, Rao JS. Stat3-siRNA induces Fas-mediated apoptosis in vitro and in vivo in breast cancer. *Int J Oncol* 2009;34:1209-20.
- [10] Zhao SH, Zhao F, Zheng JY, Gao LF, Zhao XJ, Cui MH. Knockdown of stat3 expression by RNAi inhibits in vitro growth of human ovarian cancer. *Radiol Oncol* 2011;45:196-203.
- [11] Huang C, Yang G, Jiang T, Cao J, Huang KJ, Qiu ZJ. Down-regulation of STAT3 expression by vector-based small interfering RNA inhibits pancreatic cancer growth. *World J Gastroenterol* 2011;17:2992-3001.
- [12] Mandelin AM, 2nd, Pope RM. Myeloid cell leukemia-1 as a therapeutic target. *Expert Opin Ther Targets* 2007;11:363-73.

## **CHAPTER SEVEN**

**TOWARDS DEVELOPMENT OF PEPTIDE MODIFIED POLYMERIC  
MICELLES FOR TUMOR TARGETED siRNA DELIVERY**

## 7.1. Introduction

The aim of this study was to construct an optimum mixed micellar structure for targeted delivery of siRNA to breast tumor cells. For this purpose, two sets of mixed micellar systems have been prepared. At first, in order to optimize the structure of the core in mixed micelles, MePEO-*b*-P(CL-g-SP) copolymer was combined with various lipid-conjugated MePEO-*b*-PCL copolymers. This strategy was used based on the results of our previous chapters, where hydrophobic modifications of polymeric nanocarriers with fatty acids and cholesterol have been shown to promote the efficiency of siRNA transfection [1-3]. Secondly, peptide modified mixed micelles were prepared by mixing of MePEO-*b*-P(CL-g-SP) with acetal-PEO-*b*-PCL copolymer to which cancer targeting peptide were attached. Two different cancer targeting peptides i.e. RGDfK and P160 were used for this purpose. Peptides with Arg-Gly-Asp (RGD) sequence are known to target and bind to  $\alpha\beta3$  and  $\alpha\beta5$  integrins which are up-regulated during the process of angiogenesis [4, 5]. The peptide P160 (VPWMEPAYQRFL) is a linear peptide with high binding affinity and specificity to the breast cancer cell (MDA-MB-435) and neuroblastoma cell (WAC-2) [6]. In previous studies, polymeric micelles with functional peptides on their shell have led to effective siRNA delivery and down-regulation of target mRNA [7]. Here we carried out preliminary studies, reporting on synthesis of mixed micellar systems of MePEO-*b*-P(CL-g-SP) copolymer which has been shell or core modified. The effect of these modifications on siRNA binding and uptake by MDA-MB-435 breast cancer cells was investigated.

## **7.2. Experimental Section**

### **7.2.1. Materials**

Diisopropyl amine (99%), benzyl chloroformate (tech. 95%), sodium (in kerosin), butyl lithium (Bu-Li) in hexane (2.5 M solution), 3,3-diethoxy-1-propanol (DEP), naphthalene, ethylene oxide (EO), methoxy PEO (Mw = 5000), N,N-dicyclohexyl carbodiimide (DCC), N-hydroxysuccinimide (NHS), pyrene, spermine, anhydrous dimethylsulfoxide (DMSO), palladium-coated charcoal, stearic acid, palmitoyl chloride, cholesteryl chloroformate Hank's Balanced Salt Solution (HBSS) were obtained from SIGMA (St. Louis, MO).  $\epsilon$ -Caprolactone was purchased from Lancaster Synthesis (Heysham, UK) and distilled by calcium hydride before use. Stannous octoate was purchased from MP Biomedicals Inc. (Eschwege, Germany). Acetone, THF and DMF were obtained from Caledon Laboratories Ltd. (Ontario, Canada). All other chemicals were reagent grade. Cell culture media RPMI 1640, penicillin–streptomycin, fetal bovine serum, HEPES buffer solution (1M) and trypsin/ethylenediaminetetraacetate were purchased from GIBCO, Invitrogen Corp (USA). The scrambled siRNA used as control and Silencer<sup>®</sup> FAM<sup>™</sup> labeled Negative siRNA were supplied from Ambion (catalog numbers: AM4636).

### **7.2.2. Cell Line**

The wild-type MDA-MB-435 (MDA-MB-435/WT) cells were originally obtained as a gift from the laboratory of Dr. Robert Clark (Georgetown University, USA). MDA-MB-435/WT cells were cultured in RPMI 1640 media with 10% FBS, 100 U/mL

penicillin, and 100 mg/mL streptomycin in 37 °C and 5% CO<sub>2</sub>. Cell cultures were considered confluent when a monolayer of cells covered more than 80% of the flask surface. To propagate the cells, a monolayer was washed with HBSS, and subsequently incubated with 0.05% trypsin/EDTA for 3 min at room temperature. The suspended cells were centrifuged at 650 rpm for 5 min, and were re-suspended in the medium after removal of the supernatant. The suspended cells were either sub-cultured at 10% of the original count or seeded in multi-well plates for testing.

### 7.2.3. Synthesis of block copolymers

Synthesis of MePEO-*b*-PCL, MePEO-*b*-PStCL, MePEO-*b*-PPaCL, MePEO-*b*-PChCL and MePEO-*b*-P(CL-*g*-SP) copolymers have been described in detail in previous chapters and publications (**Chapter 2, 3 and 5**) (**Figure 7.1**) [8-11]. Synthesis of Acetal PEO-*b*-PCL block copolymer has been described in detail in our previous publication [12]. Briefly, 1 mmol (0.15 mL) of initiator (3,3-diethoxy-1-propanol) and 1 mmol (3.5 mL) of potassium naphthalene were added to 20 mL of dry THF. After 10 min of vigorous stirring, 114 mmol (5.7 mL) of condensed ethylene oxide (EO) was added via a cooled syringe to the mixture. The polymerization of EO proceeded for 2 days at room temperature under argon resulting in a highly viscous solution. A part of the reaction product was sampled to follow the progression of EO polymerization. Potassium naphthalene (about 0.1 mmol) was then added to stabilize the living chain end until the reaction solution turned pale green. At this point, the reaction was stopped by the addition of 1-2 mL of acidified ethanol to neutralize excess potassium, and the polymer was

precipitated by the addition of the reaction mixture to a large amount of cold diethyl ether. Acetal-PEO was then centrifuged for 15 min at  $1800 \times g$ . For the synthesis of Acetal-PEO-*b*-PCL, Acetal-PEO (0.5 g),  $\epsilon$ -caprolactone (0.5 g) and stannous octoate (0.002 eq. of monomer) were added to a 10 mL previously flamed ampoule and sealed. The polymerization reaction was allowed to proceed for 4 h at  $140^\circ\text{C}$  in the oven. For the purpose of simplification, MePEO-*b*-PCL, MePEO-*b*-PStCL, MePEO-*b*-PPaCL, MePEO-*b*-PChCL, MePEO-*b*-P(CL-g-SP) and Acetal-PEO-*b*-PCL are abbreviated as PCL, PStCL, PPaCL, PChCL, SP and Acetal-PCL, respectively.

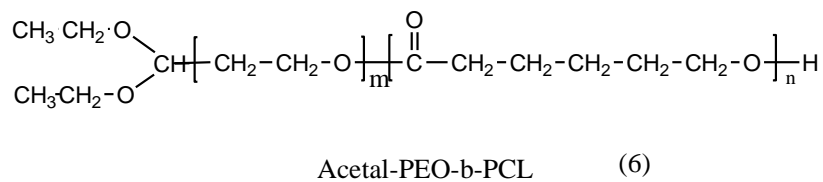
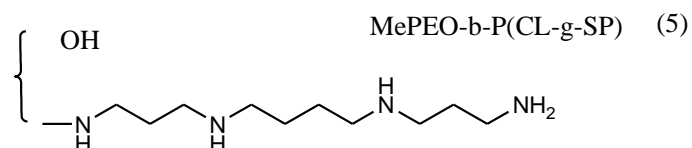
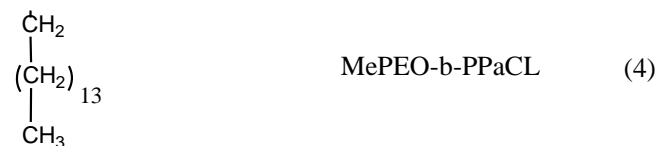
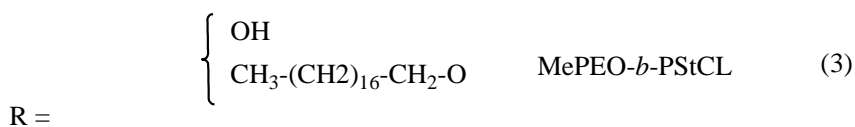
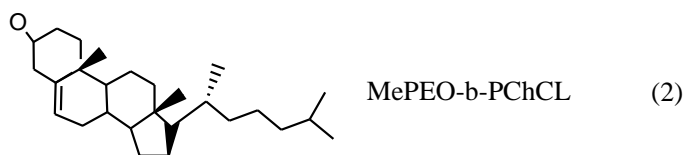
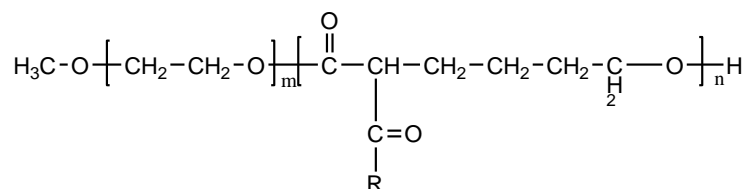
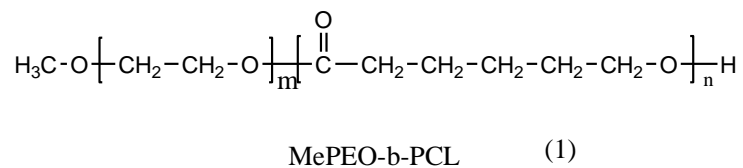


**Figure 7.1.** Chemical structure PEO-*b*-poly(ester) polymers used in this study.

#### 7.2.4. Preparation of peptide decorated micelles

P160 peptide was obtained from laboratory of Dr. Kamaljit Kaur (University of Alberta, Canada). RGDfK peptide was purchased from Ana Spec (Fremont, USA). These peptides were conjugated to the micellar shell through reaction with the functional acetal groups on the micellar shell as reported previously (**Figure 7.2**) [12]. Briefly, Acetal-PEO-*b*-PCL copolymer was dissolved in acetone to provide a 20 mg/mL polymer concentration. The solution was then added dropwise to doubly distilled water under moderate stirring at 25 °C, followed by evaporation of acetone under vacuum. Conversion of acetal to aldehyde group under acidic condition was carried out on Acetal-PEO-*b*-PCL micelles to protect PCL from hydrolysis under acidic condition. The acetal groups on the surface of PEO-*b*-PCL micelles were converted to aldehyde groups by dropwise addition of 0.5 mol/L HCl at room temperature adjusting the pH of the medium to 2. After stirring for 2 h, the mixture was neutralized with NaOH (0.5 mol/L) to stop the reaction. The resulting micellar solution was first concentrated by ultracentrifugation with MILLIPORE Centrifugal Filter Device (Mw cutoff of 100 000 Da). Finally, the micellar solution was extensively dialyzed (molecular weight cut off of 3500 Da) against water to remove the salt and was freeze-dried for further use. For conjugation of the peptides, a sodium phosphate buffer (pH 7.0, ionic strength 0.1 M) solution was added to aldehyde-PEO-*b*-PCL micelles to obtain 4 mg/mL polymer concentration. RGDfK was added and incubated with the polymeric micelles at 1:2 molar ratio (GRGDS:aldehyde-PEO-*b*-PCL) at room temperature under moderate stirring. After 2 h, NaBH<sub>3</sub>CN (10 equiv) was added to the polymer to reduce the Schiff base. After 4 days of reaction, the micellar solution

was purified by dialysis against water (Mw cut off of 3000 Da). The resulting RGDfK attached polymeric micelles were lyophilized and stored at -20 °C until use. P160 decorated micelles were also prepared using an identical protocol.

### 7.2.5. Preparation of mixed micelles

Mixed micelles were prepared by mixing of SP copolymer (4 mg/mL) with PCL or PStCL, or PPaCL or PChCL copolymer (4 mg/mL) (**Table 7.1**). Peptide decorated mixed micelles were prepared by mixing of SP copolymer (4 mg/mL) with RGDfK or P160 decorated Acetal-PCL polymeric micelles (4 mg/mL) at different weight/weight ratios (**Table 7.1**).

**Table 7.1.** Preparation of mixed micelles.

Micelles	Composition
SP:PCL	I:V
SP:PChCL	II:V
SP:PStCL	III:V
SP:PPaCL	IV:V
SP:P160-PCL	VI:V
SP:RGDfK-PCL	VII:V

Chemical structure of polymers shown in the table: (I) MePEO-*b*-PCL, (II) MePEO-*b*-PChCL, (III) MePEO-*b*-PStCL, (IV) MePEO-*b*-PPaCL, (V) MePEO-*b*-P(CL-g-SP), (VI) P160-PEO-*b*-PCL, (VII) RGDfK-PEO-*b*-PCL

### **7.2.6. Determination of siRNA binding by gel retardation assay**

The siRNA binding abilities of the mixed micelles were analyzed by agarose gel electrophoresis. The complexes were prepared by mixing negative siRNA (1  $\mu\text{g}$  siRNA), serially-diluted concentrations of micellar solutions and 0.1 M HEPES buffer (pH 6.5) and were incubated for 30 min at 37 °C. The ratio of SP polymer to siRNA was kept constant at 32:1 polymer:siRNA (w/w) ratio to ensure complete binding of siRNA. Different ratios of 1:0.5, 1:1, 1:2, 1:4 (w/w) of SP micellar solution to PStCL, or PPaCL or PChCL or RGDfK-Acetal-PCL or P160-Acetal-PCL micellar solution has been utilized. After that 4  $\mu\text{L}$  of 6 $\times$  sample buffer (50% glycerol, 1% bromophenol blue, and 1% cylene cyenol FF in TBE buffer) was added, and the samples were loaded onto 2% agarose gels containing 0.05 mg/mL ethidium bromide (EtBr). Electrophoresis was performed at 130 mV and 52 mA for 15 min, and the resulting gels were photographed under UV-illumination. The pictures were digitized and analyzed with Scion image analysis software to determine the mean density of siRNA bands. The binding percentage was calculated based on the relative intensity of free siRNA band in each well with respect to wells with free siRNA (i.e., in the absence of any polymers).

### **7.2.7. Assessing the cellular association of polymer/siRNA micelles by flow cytometry**

To assess the ability of polymeric micelles to transfer siRNA into MDA-MB-435/WT cells, complexes were prepared using 5-carboxyfluorescein (FAM)-labeled scrambled siRNA and mixed micelles by incubation in water (corresponding 100 nM

siRNA). First set of mixed micelles used in this study were prepared by mixing SP micellar solution with PCL or PStCL or PPaCL or PChCL micellar solutions at a ratio of 1:0.5 (w/w). Second set of mixed micelles were prepared by mixing SP micellar solution with Acetal-PCL or RGDfK-Acetal-PCL or P160-Acetal-PCL micellar solutions at a ratio of 1:1 (w/w). The ratio of SP polymer to siRNA in mixed micellar solution was kept at 32:1 (w/w) in all mixed micelles. Confluent cell cultures were trypsinized, re-suspended as described before and seeded in 24 well plates (0.6 mL in each well) at 50% confluence. After 24 h, 400 mL fresh medium was added to each well. The prepared micelles were added to wells in triplicates and incubated in 37 °C for 3 and 24 h. After the incubation period, cells were washed with HBSS and trypsinized. A 3.7% formaldehyde solution was added to suspend the cells and the siRNA uptake was quantified by a Beckman Coulter QUANTA flowcytometer using the FL1 channel to detect cell-associated fluorescence. The percentage of cells showing FAM fluorescence in the total cell population and mean fluorescence were determined.

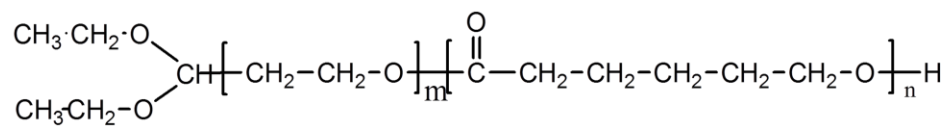
#### **7.2.8. Statistics**

Compiled data were presented as means  $\pm$  standard deviation (SD). Where feasible, the data were analyzed for statistical significance using unpaired student's t-test, one-way analysis of variance followed by post hoc Tukey test. The level of significance was set at  $\alpha \leq 0.05$ .

### **7.3. Results**

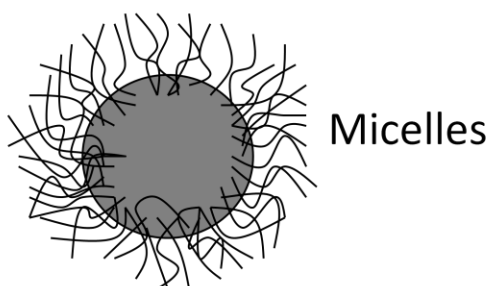
#### **7.3.1. Preparation and characterization of block copolymers**

The structures of MePEO-*b*-PCL, MePEO-*b*-PStCL, MePEO-*b*-PPaCL, MePEO-*b*-PChCL and MePEO-*b*-P(CL-g-SP) and Acetal-PEO-*b*-PCL block copolymers were confirmed by the analysis of their <sup>1</sup>H NMR spectra (not shown). Their calculated number average molecular weights ( $M_n$ ) determined from their <sup>1</sup>H NMR spectra were found to be 10001, 8762, 8063, 12400, 7749 and 7693 g/mol, respectively. Acetal-PEO-*b*-PCL assembled to polymeric micelles through a cosolvent evaporation method using acetone as the organic cosolvent. RGDfK and P160 were conjugated separately at the PEO end of micelles through a reaction between the aldehyde group on the micelle with the terminal amino group of the peptide (**Figure 7.2**). Based on the HPLC results from previous experiments in our lab, a 100% conjugation efficiency was assumed for the conjugated peptide:aldehyde-PEO-*b*-PCL at a molar peptide:polymer feed ratio of 1:2 [12].



Acetal PEO-b-PCL

Micellization ↓ Dialysis



1) pH 2, 2h  
2) pH 7, peptide solution  
3) NaBH<sub>3</sub>CN, 96 h

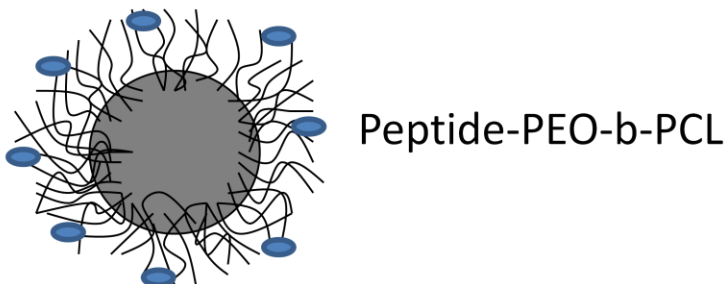
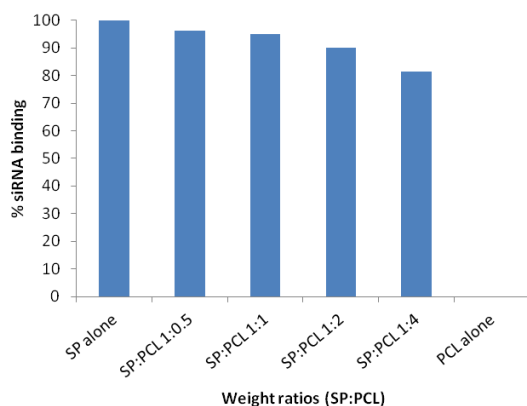


**Figure 7.2.** Model for the preparation of RGDfK and P160-decorated PEO-*b*-PCL micelles.

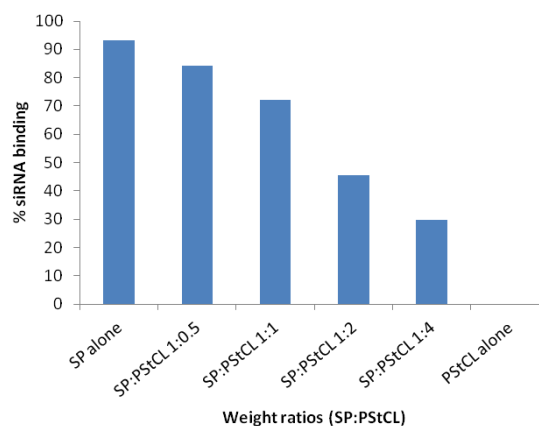
### 7.3.2. siRNA binding

Agarose gel electrophoresis was utilized to detect complex formation between the mixed micelles and the siRNA. This was based on the disappearance of free siRNA bands in the agarose gels. As expected, SP polymer alone was capable of effectively binding siRNA, resulting in the retardation or disappearance of siRNA bands in agarose gel (**Figure 7.3**). For SP:PCL, SP:PPaCL and SP:PChCL mixed micelles, when the SP:other polymer weight ratios were at 1:0.5, 1:1 and 1:2, the binding of siRNA was ~ 90 %. The binding declined for mixed micelles of SP:PCL and SP:PChCL at 1:4 ratio (w/w). For SP:PStCL mixed micelles the binding of siRNA decreased as the ratio of SP:PStCL (w/w) decreased. Peptide decorated mixed micelles achieved ~ 90 % siRNA binding at SP:peptide-PCL ratio of 1:0.5 (w/w); however, when the ratio of SP:peptide-PCL was 1:1, 1:2 and 1:4 (w/w), the siRNA binding abilities of the mixed polymeric micelles were declined.

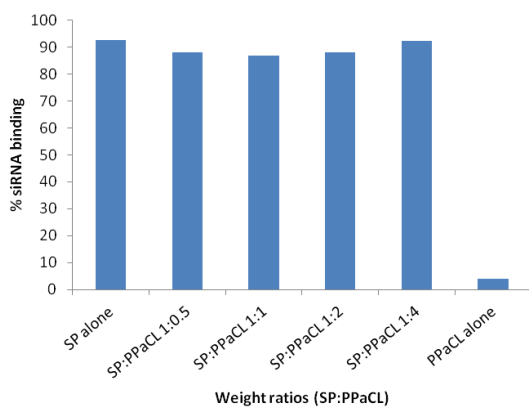
A) SP:PCL



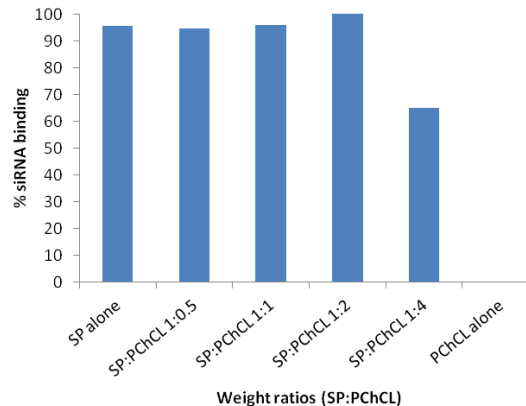
B) SP:PStCL



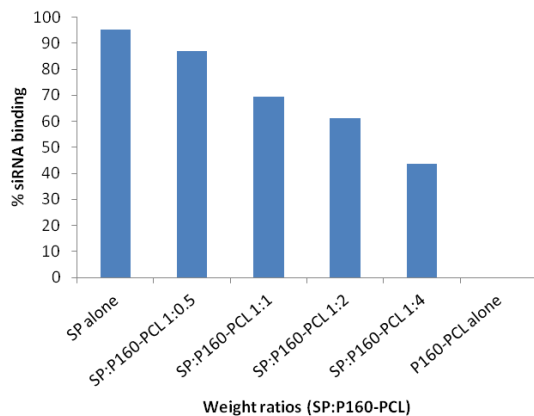
C) SP:PPaCL



D) SP:PChCL



E) SP:P160-PCL



F) SP:RGDfK-PCL

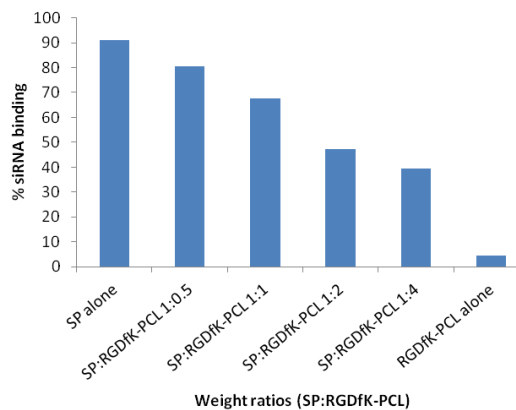
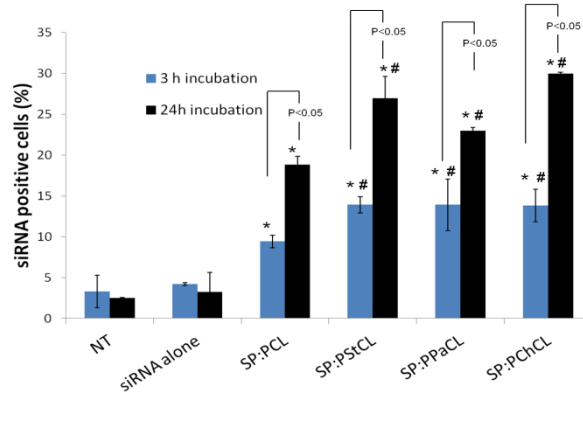


**Figure 7.3.** Electrophoretic retardation analysis of siRNA binding by different mixed polymeric micelles. The densitometric analysis of the binding results for different mixed micelles (A) SP: PCL; (B) SP:PStCL; (C) SP:PPaCL; (D) SP:PChCL; (E) SP:P160-PCL and (F) SP:RGDfK-PCL. The inserted panel in shows the percentage of siRNA binding versus mixed SP polymer: PEO-*b*-poly(ester)s weight ratio.

### 7.3.3. Cellular association studies

The uptake of mixed micelles/siRNA was determined in MDA-MB-435/WT cells. Two sets of experiments were conducted using FAM-labeled negative siRNA for uptake of mixed micelles. Based on the flowcytometry results for the first set of experiments, SP:PChCL and SP:PStCL mixed micelles were the most effective polymers for siRNA delivery to MDA-MB-435/WT cells at 24 h (mean fluorescence intensity) (**Figure 7.4.B**). SP:PChCL mixed micelles also exhibited the highest percentage of siRNA positive cells among mixed micelles under study at 24 h (**Figure 7.4.A**). Among peptide modified mixed micelles, SP:P160-PCL was the most effective mixed polymeric micelle for siRNA delivery to MDA-MB-435/WT cells at 24 h (both mean fluorescence and siRNA positive cells %) (**Figure 7.5**). SP:RGDfK-PCL did not exhibit a significant increase in siRNA uptake when compared to SP:Acetal-PCL. Overall, presence of lipids in the core of mixed micelles or decoration of PEO-*b*-PCL polymer with P160 peptide increased the association of siRNA micelles with breast cancer cells.

A)



B)

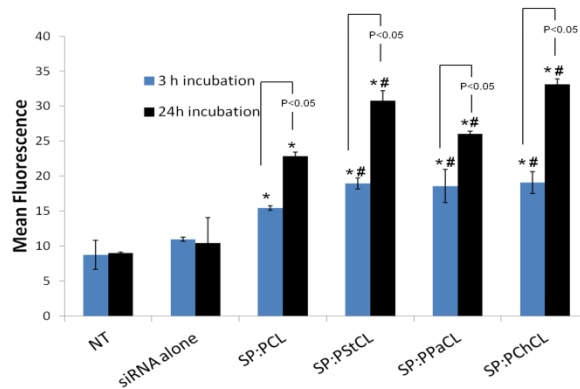
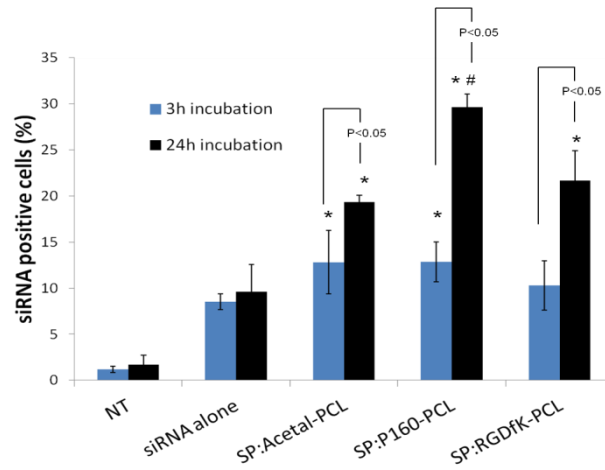


**Figure 7.4.** Cellular uptake of core modified mixed micelles/siRNA by MDA-MB-435/WT cells. A) The percentage of cells positive for FAM-siRNA after 3 and 24 h exposure to siRNA/mixed micelles. B) The mean fluorescence of the cells after 3 and 24 h exposure to micelles. The data are the mean  $\pm$  SD for n=3. \*Significantly different from siRNA alone ( $P<0.05$ ), #Significantly different from SP:PCL ( $P<0.05$ ). (One way ANOVA followed by Tukey test,  $P<0.05$ ).

A)



B)

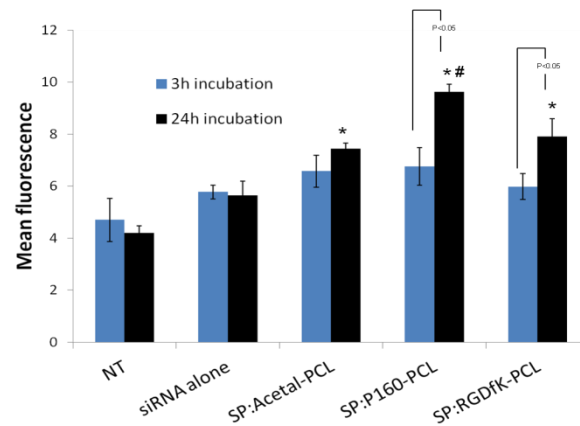


**Figure 7.5.** Cellular uptake of peptide decorated mixed micelles/siRNA by flowcytometry by MDA-MB-435/WT cells. A) The percentage of cells positive for FAM-siRNA after 3 and 24 h exposure to siRNA/mixed micelles. B) The mean fluorescence of the cells after 3 and 24 h exposure to micelles. The data are the mean  $\pm$  SD for n=3. \*Significantly different from siRNA alone ( $P < 0.05$ ), #Significantly different from SP:Acetal-PCL ( $P < 0.05$ ). (One way ANOVA followed by Tukey test,  $P < 0.05$ ).

#### 7.4. Discussion

An effective and safe siRNA delivery carrier which is appropriate for systemic administration will fast-forward the clinical use of siRNA. Polymeric carriers with functionalized core and shell have been extensively utilized for delivery of drugs and siRNA [13-15]. Hydrophobic modification of polycationic polymeric carriers has been reported to induce the efficacy of such carriers in nucleic acid delivery [1]. As mentioned before, hydrophobic moieties are presumed to increase the interaction between the carrier and the lipophilic cell membrane; therefore, enhancing the cellular uptake of nucleic acid associated polymeric carriers. Also shell modification of polymeric carriers has been reported to increase the efficacy of gene delivery systems. Oba et al. reported on the conjugation of the cyclic RGD (cRGDfK) to PEO-b-P(L-lysine) to construct  $\alpha_v\beta_3$ -targeted micelles for effective gene delivery [16, 17]. These targeted micelles exhibited increased transfection efficiency and a preferential accumulation in the perinuclear region compared to non-targeted micelles for HeLa cells. Xiong et al. synthesized a PEO-*b*-polyester based virus-like micelle containing a biodegradable polycationic core and a RGD/TAT-functionalized shell for targeted siRNA delivery. Targeted micelles exhibited increased cellular uptake of siRNA, effective silencing P-gp expression as well as increased DOX intracellular uptake. These micelles enhanced DOX cytotoxicity in MDA435/LCC6 DOX resistant cells [7].

In our efforts towards development of more effective polymeric micelles for in vivo siRNA delivery, we pursued both shell or core modification of the SP polymeric

micelles thorough construction of a series of mixed micelles. In this chapter, we assessed whether shell decoration of micelles with cancer targeting peptides or lipid modification of micelles core can enhance the delivery of siRNA. The effect of these modifications on properties of mixed micelles for siRNA delivery such as siRNA binding, cell association was evaluated.

Mixing of lipid modified PCL with SP micelles did not hamper the ability of the polymeric micelles to bind siRNA in general (**Figure 7.3**). However, among different lipid modified mixed micelles, SP:PStCL did reduce the ability of the polymers to bind siRNA to some extent, perhaps because of presence of carboxyl groups in the core of the mixed micelles which may repel negatively charged siRNA and decrease the binding. The binding of peptide-decorated mixed micelles to siRNA was also decreased as the amount of peptide-PCL to SP polymer increased in mixed micelles.

The uptake of the micelles by the cells is presumed to be reliant on both the micellar shell that directly interfaces the cells and also to a lesser extent core of the micelles [18-21]. We found that amphiphilic mixed micelles with cholesteryl and stearyl in their core were more efficient for siRNA uptake compared to polymers without lipid moieties in the core (**Figure 7.4**). Also, amphiphilic mixed polycationic polymeric micelles with P160 attached to their shell were more efficient for siRNA uptake compared to mixed micelles with RGDfK or micelles without peptide decoration (**Figure 7.5**). Askoxylakis et al. demonstrated that radio-labeled P160 can achieve a better tumor targeting in vivo compared to RGD4C peptide [22]. This is in line with previous data

from our lab in which polymeric micelles based on PEO-*b*-PCL or PEO-*b*-PBCL block copolymers were decorated with c(RGDfK) or P160. P160-decorated micelles exhibited better binding and internalization compared to c(RGDfK) micelles. Peptide decoration enhanced the cytotoxicity of PTX against MDA-MB-435 cancer cells [23]. In another study, our lab developed stealth liposomes bearing an engineered ligand, p18-4 peptide (an analogue of P160 peptide) that can target the breast cancer MDA-MB-435 cells. Liposomal DOX formulations bearing p18-4 peptide exhibited promising in vitro selective cytotoxicity as well in vivo therapeutic efficacy [24, 25]. Among different mixed micelles under study, the core cholesteryl modification and P160 shell modification were found to be more efficient structures in terms of cellular siRNA delivery. Such modification can be harnessed for future design of polymeric micelles capable of in vivo siRNA delivery.

## **7.5. Conclusion**

We have described the design, synthesis and evaluation of the mixed PEO-*b*-polyester based micelles containing either a biodegradable polycationic and hydrophobic core and a peptide-functionalized shell for targeted siRNA delivery. We demonstrated that such modification increased cellular uptake of siRNA formulated mixed micelles. The results of this study demonstrated a promise for core and shell modified PEO-*b*-P(CL-polyamine) micelles as non-viral vehicle for efficient siRNA delivery to its cellular and molecular targets.

## 7.6. References

- [1] Aliabadi HM, Landry B, Bahadur RK, Neamark A, Suwantong O, Uludag H. Impact of lipid substitution on assembly and delivery of siRNA by cationic polymers. *Macromol Biosci* 2011;11:662-72.
- [2] Aliabadi HM, Landry B, Mahdipoor P, Hsu CY, Uludag H. Effective down-regulation of breast cancer resistance protein (BCRP) by siRNA delivery using lipid-substituted aliphatic polymers. *Eur J Pharm Biopharm* 2012;81:33-42.
- [3] Gusachenko Simonova O, Kravchuk Y, Konevets D, Silnikov V, Vlassov VV, Zenkova MA. Transfection efficiency of 25-kDa PEI-cholesterol conjugates with different levels of modification. *J Biomater Sci Polym Ed* 2009;20:1091-110.
- [4] Enback J, Laakkonen P. Tumour-homing peptides: tools for targeting, imaging and destruction. *Biochem Soc Trans* 2007;35:780-3.
- [5] Maubant S, Saint-Dizier D, Boutillon M, Perron-Sierra F, Casara PJ, Hickman JA, et al. Blockade of alpha v beta3 and alpha v beta5 integrins by RGD mimetics induces anoikis and not integrin-mediated death in human endothelial cells. *Blood* 2006;108:3035-44.
- [6] Zhang J, Spring H, Schwab M. Neuroblastoma tumor cell-binding peptides identified through random peptide phage display. *Cancer Lett* 2001;171:153-64.
- [7] Xiong XB, Uludag H, Lavasanifar A. Virus-mimetic polymeric micelles for targeted siRNA delivery. *Biomaterials* 2010;31:5886-93.
- [8] Falamarzian A, Lavasanifar A. Chemical Modification of Hydrophobic Block in Poly(Ethylene Oxide) Poly(Caprolactone) Based Nanocarriers: Effect on the Solubilization and Hemolytic Activity of Amphotericin B. *Macromolecular Bioscience* 2010;10:648-56.
- [9] Falamarzian A, Lavasanifar A. Optimization of the hydrophobic domain in poly(ethylene oxide)-poly(varepsilon-caprolactone) based nano-carriers for the solubilization and delivery of Amphotericin B. *Colloids Surf B Biointerfaces* 2010;81:313-20.
- [10] Mahmud A, Patel S, Molavi O, Choi P, Samuel J, Lavasanifar A. Self-associating poly(ethylene oxide)-b-poly(alpha-cholesteryl carboxylate-epsilon-caprolactone) block copolymer for the solubilization of STAT-3 inhibitor cucurbitacin I. *Biomacromolecules* 2009;10:471-8.
- [11] Xiong XB, Uludag H, Lavasanifar A. Biodegradable amphiphilic poly(ethylene oxide)-block-polyesters with grafted polyamines as supramolecular nanocarriers for efficient siRNA delivery. *Biomaterials* 2009;30:242-53.
- [12] Xiong XB, Mahmud A, Uludag H, Lavasanifar A. Conjugation of arginine-glycine-aspartic acid peptides to poly(ethylene oxide)-b-poly(epsilon-caprolactone) micelles for enhanced intracellular drug delivery to metastatic tumor cells. *Biomacromolecules* 2007;8:874-84.
- [13] Itaka K, Kanayama N, Nishiyama N, Jang WD, Yamasaki Y, Nakamura K, et al. Supramolecular nanocarrier of siRNA from PEG-based block cationic polymer carrying diamine side chain with distinctive pKa directed to enhance intracellular gene silencing. *J Am Chem Soc* 2004;126:13612-3.

- [14] Hwa Kim S, Hoon Jeong J, Chul Cho K, Wan Kim S, Gwan Park T. Target-specific gene silencing by siRNA plasmid DNA complexed with folate-modified poly(ethylenimine). *J Control Release* 2005;104:223-32.
- [15] Nishiyama N, Kataoka K. Current state, achievements, and future prospects of polymeric micelles as nanocarriers for drug and gene delivery. *Pharmacol Ther* 2006;112:630-48.
- [16] Oba M, Aoyagi K, Miyata K, Matsumoto Y, Itaka K, Nishiyama N, et al. Polyplex micelles with cyclic RGD peptide ligands and disulfide cross-links directing to the enhanced transfection via controlled intracellular trafficking. *Mol Pharm* 2008;5:1080-92.
- [17] Oba M, Fukushima S, Kanayama N, Aoyagi K, Nishiyama N, Koyama H, et al. Cyclic RGD peptide-conjugated polyplex micelles as a targetable gene delivery system directed to cells possessing alphavbeta3 and alphavbeta5 integrins. *Bioconjug Chem* 2007;18:1415-23.
- [18] Maysinger D, Berezovska O, Savic R, Soo PL, Eisenberg A. Block copolymers modify the internalization of micelle-incorporated probes into neural cells. *Biochim Biophys Acta* 2001;1539:205-17.
- [19] Deshpande MC, Davies MC, Garnett MC, Williams PM, Armitage D, Bailey L, et al. The effect of poly(ethylene glycol) molecular architecture on cellular interaction and uptake of DNA complexes. *J Control Release* 2004;97:143-56.
- [20] Mahmud A, Lavasanifar A. The effect of block copolymer structure on the internalization of polymeric micelles by human breast cancer cells. *Colloids Surf B Biointerfaces* 2005;45:82-9.
- [21] Miyata K, Fukushima S, Nishiyama N, Yamasaki Y, Kataoka K. PEG-based block cationomers possessing DNA anchoring and endosomal escaping functions to form polyplex micelles with improved stability and high transfection efficacy. *J Control Release* 2007;122:252-60.
- [22] Askoxylakis V, Zitzmann S, Mier W, Graham K, Kramer S, von Wegner F, et al. Preclinical evaluation of the breast cancer cell-binding peptide, p160. *Clin Cancer Res* 2005;11:6705-12.
- [23] Shahin M, Ahmed S, Kaur K, Lavasanifar A. Decoration of polymeric micelles with cancer-specific peptide ligands for active targeting of paclitaxel. *Biomaterials* 2011;32:5123-33.
- [24] Shahin M, Soudy R, El-Sikhry H, Seubert JM, Kaur K, Lavasanifar A. Engineered peptides for the development of actively tumor targeted liposomal carriers of doxorubicin. *Cancer Lett* 2012.
- [25] Shahin M, Soudy R, Aliabadi HM, Kneteman N, Kaur K, Lavasanifar A. Engineered breast tumor targeting peptide ligand modified liposomal doxorubicin and the effect of peptide density on anticancer activity. *Biomaterials* 2013;34:4089-97.

## **CHAPTER EIGHT**

### **GENERAL DISCUSSION, CONCLUSION AND FUTURE DIRECTION**

## 8.1. General discussion

Nanotechnology has been utilized in pharmaceutical research and proven to be a useful approach to enhance drug delivery in several fronts. Nanotechnology has shown promise as a tool to increase the solubility and/or stability of drugs, reduce their side effects, improve their bioavailability and provide targeted drug delivery. Lipid-based nanocarriers offer several outstanding biochemical properties, including biodegradability, biocompatibility, protection of drug cargo from surrounding environment, and the capability to encapsulate both hydrophobic and hydrophilic drugs. New applications such as gene therapy have made these nanocarriers even more attractive [1]. Among various lipid-based delivery systems, liposomes are in the front line of development and already have several formulations available on the market [2]. Liposomes are particularly shown to be effective carriers for hydrophilic or amphiphilic drugs, but lack chemical flexibility in their structure. As a result, development of costume made formulations for therapeutic entities with versatile physicochemical properties is somewhat limited using liposomes. Besides, the process of liposomes production in large scale is problematic. This has enforced shortage in the availability of liposomal formulations to pharmaceutical market from time to time [3, 4]. Lipid modified polymeric nanocarriers may provide a chemically flexible and more reliable alternative to liposomes for the delivery of small molecule drugs and genetic materials. Lipid-based polymeric nanocarriers have also been utilized for the delivery of certain drugs with a proven tendency for interaction with lipids, such as AmB and CuI [5-7]. The miscibility and interaction between such lipid

modified polymer and drugs plays a crucial role in drug loading efficiency as well as the release profile of drugs from such nanocarriers.

Our goal in the first section of this thesis (**Chapters 2 & 3**) was to design and develop lipid substituted polymeric nanocarriers based on MePEO-*b*-PCL and explore the effect of this structural modification in micellar core on AmB delivery by the prepared nanocarriers. AmB is a poorly soluble drug which is available in form of a solution for intravenous injection for use in systemic fungal infections. The most commonly used water soluble formulation of AmB on the market, Fungizone<sup>®</sup>, uses sodium deoxycholate as a solubilizing agent for AmB. Fungizone<sup>®</sup> use in the clinic has been associated with extensive nephrotoxicity in patients, however. Many hydrophobic drugs including AmB are transported by plasma proteins such as  $\beta$ -lipoprotein, albumin and  $\alpha_1$  acid glycoprotein in the biological system [8, 9]. For improved encapsulation and delivery of AmB in biological system, lipid-based nanocarriers that can imitate plasma proteins in terms of their capacity for AmB loading but show altered AmB distribution in the biological system have been proposed [10]. AmB is known to be compatible with acyl chains (found at the site of drug action, i.e. lipid bilayer membrane); therefore a good encapsulation efficiency for AmB in lipid based nanocarriers is expected. In reality the three lipid-based AmB formulations have been able to achieve clinically relevant concentrations of loaded AmB and were shown less nephrotoxic effects compared to Fungizone<sup>®</sup>. Despite such advantages over Fungizone<sup>®</sup>, possible disadvantages such as unpredictable pharmacokinetics, toxic effects at higher AmB doses, emergence of infusion related

reactions and high cost, have limited the benefit lipid based formulations of AmB in the clinical settings.

We have synthesized two new members of the family of functionalized MePEO-*b*-PCL block copolymers bearing pendant stearyl (at 41 % substitution level) or palmitoyl groups (at 100 % substitution level) on the PCL block, i.e., MePEO-*b*-PStCL and MePEO-*b*-PPaCL, respectively. The above mentioned block copolymers were used to prepare nano-formulations of AmB. These nanocarriers were compared to other nanocarriers, i.e., MePEO-*b*-PCL (with no substitution of PCL); MePEO-*b*-PCCL (bearing carboxyl groups on PCL); MePEO-*b*-PBCL (bearing benzyl carboxylate groups on PCL) and MePEO-*b*-PChCL (bearing cholesteryl carboxylate on PCL) as carriers for delivery AmB. Overall, within the first set of polymeric nanocarriers we tried (**Chapter 2**), nanocarriers composed of MePEO-*b*-PCCL and MePEO-*b*-PStCL exhibited the most efficiency in the solubilization of AmB (**Table 2.3**), respectively, perhaps due to formation of hydrogen bonds and hydrophobic interactions between the core of the micelles and functional groups of AmB. Remarkably the extent of AmB solubilisation by above mentioned nanocarriers appears to be higher than AmB water solubility levels achieved by previously reported polymeric nanocarriers [11, 12]. Within this group; however, the lowest hemolytic activity (as a measure of toxicity) for encapsulated AmB was observed for unsubstituted MePEO-*b*-PCL followed by MePEO-*b*-PstCL and then MePEO-*b*-PCCL nanocarriers (**Figure 2.5B**). Lower hemolysis observed for AmB as part of MePEO-*b*-PCL nanocarrier, perhaps reflects a better control over the rate of AmB diffusion from these vehicles over the other two vehicles. It can be concluded that

although the presence of hydrogen bond forming groups was efficient in increasing the solubility of AmB, but it could not restrict the partitioning of solubilized AmB from the carrier to cell membrane. Therefore, such design in the polymeric micellar structure can be employed where solubilisation along with rapid release of drugs with hydrogen bond forming groups is desired.

On the other hand, among different nanocarriers formed from polymers with 100 % substitution of lipids on the MePEO-*b*-PCL backbone (**Chapter 3**), MePEO-*b*-PPaCL and then MePEO-*b*-PChCL nanocarriers showed the most efficient solubilization of AmB, respectively (**Table 3.3**), perhaps due to the formation of non-polar interactions between AmB and lipid groups of the nanocarriers. Increasing the fatty acid substitution level has proven to be successful in the solubilization and controlling the delivery of AmB from poly(ethylene oxide)-block-poly(N-hexyl stearate-L-aspartamide) based micellar carriers [5]. The lowest hemolytic activity for encapsulated AmB was observed for MePEO-*b*-PChCL followed by MePEO-*b*-PCL, then MePEO-*b*-PPaCL and MePEO-*b*-PBCL nanocarriers; however (**Figure 3.8 and 3.9**). It is worth mentioning that all the above mentioned polymeric nanoformulations of AmB exhibited reduced hemolytic activity compared to Fungizone<sup>®</sup>.

Based on the improved solubility and reduced hemolytic activity, the MePEO-*b*-PChCL nanocarriers was considered as optimum structures for AmB delivery. This is not surprising, considering high affinity of AmB to cholesterol [13]. Even among the commercial lipid AmB formulations mentioned before, cholesterol containing

AmBisome<sup>®</sup> exhibited the highest plasma concentrations after administration than those obtained with Fungizone<sup>®</sup> [14].

In the second section of this thesis (**Chapters 4-7**), our efforts were shifted toward development of lipid-based polymeric nanocarriers for localized or systemic siRNA delivery. siRNA can be employed to silence any specific gene at will, and reduce the expression of disease causing proteins [15, 16]. Free siRNA is negatively charged and cannot cross the cell membrane for access to intracellular targets [17]. Other challenges for the delivery of siRNA to the site of action include its large molecular weight [18], short half-life, uptake by RES and rapid renal excretion [19]. In order to circumvent these problems, chemical modification of siRNA with molecules such as cholesterol [20],  $\alpha$ -tocopherol [21] and lipid [22] has been examined. These modifications have slightly improved the pharmacokinetic behavior and cellular uptake of siRNA. However, such modifications have been demonstrated to alter the potency of siRNA to some extent [23]. An alternative approach is to use nanocarriers made from lipids [24-26] or cationic polymers [27-29] for siRNA delivery. We have tried to take advantage of the benefits of both entities (cationic polymers for siRNA binding and condensation as well as lipids for interaction with cell membrane) and explore development of two different lipid-based polymeric nanocarriers for either local (**Chapter 4**) or systemic delivery of siRNA (**Chapter 5-7**). Attachment of lipids to cationic polymers is desirable in siRNA carriers since lipids are an abundant component of cell membrane and such carriers have enhanced interaction with cell membrane and higher cellular uptake. To further pursue a therapeutic approach for application of our polymers, we assessed the efficiency of such

carriers in siRNA delivery for silencing of STAT3 in breast cancer cells. STAT3 is a transcription factor that plays a key role in expression of many oncogenic factors leading to several hall marks of cancer such as cell proliferation, survival, angiogenesis, invasion, and tumor induced immune-suppression [30]. Therefore, STAT3 knockdown can be beneficial to induce tumor killing effect and possibly increase the efficiency of chemotherapy in the treatment of cancer.

**Chapter 4** of this thesis presents a study on capability of STAT3 knockdown by lipid substituted low molecular weight (2 kDa) polyethyleneimine (PEI2) complexes of STAT3-siRNA. Among different lipid substituted PEI2 for siRNA delivery (**Table 4.1**), linoleic acid-substituted (PEI-LA) polymer was the most efficient carrier, leading to most STAT3 associated loss of cell viability in MDA-MB-435 cells (**Figure 4.3**). STAT3 down-regulation additionally increased the cytotoxic capability of model anti-cancer drugs, i.e. DOX and PTX, in WT and DOX/RES breast tumor phenotypes (**Figure 4.8**). The result of this study provided proof of concept for therapeutic approaches combining STAT3 silencing with conventional chemotherapy as means to improve the clinical benefit of breast cancer chemotherapy in both WT and RES breast tumor phenotypes. The success of this combinational approach in both WT and RES phenotypes implies a potential benefit for STAT3 siRNA + chemo combination therapy in the prevention as well as treatment of chemo-resistance in breast tumors.

We have then shifted our research towards development of safer carriers for systemic siRNA delivery due to reported limitation associated with the systemic

administration of PEI based carriers such as toxicity and immunogenicity. A novel family of lipid functionalized MePEO-*b*-P(CL-g-SP) polymers with potential for in vivo administration have been developed in our lab. In previous studies, MePEO-*b*-P(CL-g-SP) micelles exhibited great promise for siRNA encapsulation, protection against degradation in serum and successful silencing of P-gp gene and protein expression [17]. In this thesis (**Chapter 5 and 6**) modification of the MePEO-*b*-P(CL-g-SP) micellar core by stearyl and cholesteryl substituents was pursued to enhance the properties of this carrier for systemic siRNA delivery. Lipid modification of MePEO-*b*-P(CL-g-SP), particularly with cholesterol has provided thermodynamically stable nanocarriers reflected by a decrease in the CAC of lipid modified polymers compared to the parent MePEO-*b*-P(CL-g-SP) (**Table 5.1 and 6.1**). Thermodynamic stability of delivery system is a key factor in design of successful carriers for systemic delivery of siRNA as it insures preservation of the integrity of the carrier upon dilution in blood following intravenous administration. In addition to better stability, MePEO-*b*-P(CL-g-SP-Chol) was found to significantly enhance the cellular delivery of incorporated siRNA (**Figure 6.5 and 6.6**) and decreased the cytotoxicity of polymeric micellar siRNA complexes when compared to parent MePEO-*b*-P(CL-g-SP). MePEO-*b*-P(CL-g-SP-Chol) successfully enhanced the silencing activity of complexed STAT3 and MCL-1 siRNA at the mRNA in level MDA-MB-435 cells. Under current experimental conditions, we did not observe a significant improvement in the silencing activity of STAT3-siRNA at protein level by its MePEO-*b*-P(CL-g-SP-Chol) leading to cancer cell death. Finally, MePEO-*b*-P(CL-g-SP-Chol)

polymer proved to be an efficient carrier, leading to MCL-1 associated loss of cell viability in MDA-MB-435/WT cells (**Figure 6.12**).

We then pursued modification of the micellar structure with peptide targeting ligands to as means to improve tumor cell targeted delivery of siRNA upon systemic administration (**Chapter 7**). Modification of the micellar surface with peptide ligands has been accomplished through schiff base reaction between primary amine on the peptide moiety and the aldehyde groups on the functionalized micellar surface. However, this method is not appropriate for attachment of peptide ligands to the surface of functionalized MePEO-*b*-P(CL-SP) micelles as the primary amine in the SP group may compete with the primary amine of peptide ligands for reaction with the aldehyde groups on micellar shell. For this reason, and in order to develop ligand guided polymeric micelles for tumor targeted siRNA delivery, we have pursued formation of mixed micelles composed of peptide modified PEO-*b*-PCL and MePEO-*b*-P(CL-g-SP). We showed the superiority of P160 peptide decorated mixed micelles for siRNA uptake in MDA-MB-435 cancer cells over mixed micelles with RGDfK or micelles without peptide decoration (**Figure 7.5**). The peptide P160 (VPWMEPAYQRFL) is a linear peptide with high binding affinity and specificity to the breast cancer cell (MDA-MB-435) and neuroblastoma cell (WAC-2) [31]. These results were in line with previous findings from our group and others which demonstrated that P160 peptide can achieve a better tumor targeting compared to RGD4C peptide [32] and can enhance the cytotoxicity of polymeric micelles containing PTX against MDA-MB-435 cancer cells [33]. Liposomal

DOX formulations bearing p18-4 peptide (an analogue of P160 peptide) exhibited promising in vitro selective cytotoxicity as well in vivo therapeutic efficacy [34, 35].

We then investigated the effect of core structure in the mixture on siRNA complexation and binding to choose the best core modified polymer within the library of substituted PEO-*b*-PCLs. A series of mixed micelles were investigated for the latter purpose. Our results showed, mixed micelles composed of MePEO-*b*-P(CL-g-SP) and MePEO-*b*-PChCL or MePEO-*b*-PStCL to be more efficient carriers providing higher cellular siRNA uptake compared to micelles without lipid moieties in the core (**Figure 7.4**). These results indicate the importance fatty acid modification of core in siRNA delivery systems once again. The results also provided the proof of concept research for possibility of simultaneous shell and core modification for MePEO-*b*-P(CL-g-SP) based polymeric micelles for active targeting to human cancers.

## 8.2. Conclusions

The flexibility in the chemical structure of the functionalized PEO-*b*-PCL platform provides opportunities for the incorporation of various lipids, hydrogen bond forming groups and/or charged moieties in the core of micelles formed from these polymers. The feasibility of this strategy for the development of custom made and optimized structures for the delivery of various therapeutic agents with versatile physicochemical properties has been shown in this thesis. In this context, two new members in the family of functionalized MePEO-*b*-PCL block copolymers bearing pendant stearyl (MePEO-*b*-PStCL) or palmitoyl groups (MePEO-*b*-PPaCL) were

synthesized for the delivery of AmB. Although incorporation of hydrogen bond forming groups served as an effective strategy to enhance the solubility of poorly soluble AmB in water, it was not effective in reducing the rate of AmB partition out of the micellar structure. As a result, micelles with hydrogen bond forming groups in the PCL were not efficient in reducing the hemolytic activity of AmB. Among different core substituted MePEO-*b*-PCL nanocarriers, incorporation of cholesteryl group in the core (MePEO-*b*-PChCL) provided the optimum structures for AmB delivery leading to maximum level of loaded drug in micellar carrier and minimum hemolytic activity for encapsulated AmB.

For siRNA delivery, substitution of linoleic acid on low molecular weight polycations (i.e., PEI2K) was found to lead to better efficiency for STAT3-siRNA delivery, leading to most STAT3 associated loss of cell viability in MDA-MB-435 cells and enhanced the sensitivity of WT and RES breast tumor cells to the effect of conventional cancer chemotherapy. A similar approach using substitution of cholesteryl groups on the polycation section of MePEO-*b*-P(CL-*g*-SP) micelles was successful in increasing the stability of micellar siRNA carrier, improving the safety of siRNA delivery system and enhancing the cellular uptake leading to better silencing activity of incorporated siRNA at the mRNA level. Our efforts towards development of a tumor targeted micellar delivery system for siRNA delivery pointed to the superiority of a mixed PEO-*b*-polyester based micellar system containing a peptide-functionalized shell for targeted siRNA delivery and lipid substituents in the core.

Overall, the results of our studies pointed to the benefit of lipid modification of polymeric nanocarriers as a strategy to enhance their properties for the delivery of specific drugs and/or siRNA such as carrier stability, cell interaction, level of binding and encapsulation and/or release. It also showed that the type of lipid substituent, level and location of substitution will impact the final behavior of the nanocarrier with respect to its properties in drug and siRNA delivery. Nevertheless, the chemical flexibility of polymer structure can be used as a valuable advantage in this regard for the development of optimum nanocarriers for individual drug and/or siRNA of interest.

### **8.3. Future directions**

In this thesis work, we explored lipid-based polymeric nanocarriers for AmB and siRNA delivery. Future development these carriers may constitute several paths. For AmB MePEO-*b*-PChCL nanocarriers, we might think about evaluating these lipid-based nanocarriers in terms of level of antifungal activity of encapsulated AmB and the rate of AmB release from the formulation. Assays can be used to determine the minimum inhibitory concentration of AmB formulations against the growth of different pathogenic fungi at various time points. The efficacy of our formulation can be compared to in vitro antifungal activity of commercially available AmB formulations and free AmB. Other possible avenues include further investigation of efficacy of AmB polymeric nanocarriers by measurement of nephrotoxicity and activity in animal models of systemic fungal disease. A dose escalation study to determine the most effective dose of AmB MePEO-*b*-PChCL nanocarriers can be considered. Also we anticipate a prolonged circulation

behavior for MePEO-*b*-PChCL nanocarriers due to their nanoscopic size and PEO shell. Investigation of pharmacokinetic and biodistribution profile of encapsulated nanocarriers in comparison to free AmB is needed to assess this hypothesis. These studies would let to proper optimization the lipid-based carrier for achieving the best therapeutic outcome [11, 36].

Our in vitro experiments with lipid-substituted low molecular weight (2 kDa) PEI exhibited a high efficiency in siRNA delivery against STAT3 gene for linoleic acid-substituted PEI. The next study in this path would be the use of PEI-LA for siRNA delivery against STAT3 in vivo. Continuous siRNA formulation injection via intratumoral or intraperitoneal routes over defined period for sustained STAT3 knockdown and detection of its effect on tumor suppression can be investigated. Furthermore, simultaneous injection of siRNA formulation and anticancer drugs such as DOX and PTX can be carried out. For this purpose, PEI-LA/STAT3 siRNA complexes should be injected intratumorally (or intraperitoneally) and DOX or PTX injection should be performed systemically. The efficacy of combinational therapy in terms of tumor suppression can be assessed.

Our current study has pointed to the superiority of MePEO-P(CL-g-SP-Chol) over parent Me-PEO-P(CL-SP) in siRNA delivery. A systematic study on the effect of shell and core forming block lengths, as well as nature of the lipid substituent on MePEO-P(CL-g-SP) polymers may be conducted to draw structure activity relationships in this

class of delivery system towards successful STAT3 knockdown and STAT3-specific cell death in vitro and/or enhanced stability leading to tumor accumulation in vivo [37].

A complimentary approach should seek development of tumor targeted polymeric micelles for siRNA delivery. Based on our current results, the best formulation for this purpose is mixed micelles composed of MePEO-*b*-P(CL-g-SP-Chol) and P160-PEO-PChCL. The efficacy of this siRNA delivery system, in combination with STAT3 siRNA for down-regulation of STAT3 gene should be tested in vitro and in vivo (following intravenous administration). Our groups has also reported on the development of derivatives of P160 that are more stable in biological system and show better affinity and interaction for cancer versus normal cells. The efficacy of these peptides for active targeting and enhanced delivery of nano-formulations has been shown in several in vitro and in vivo studies [32, 33, 35]. Further investigations should assess the efficacy of P160 derivatives as ligands for active targeting siRNA nano-complexes. Inclusion of a membrane active agent in this construct may be considered to enhance its siRNA transfection efficiency if necessary. Finally, once the siRNA delivery system is optimized its combination with several different siRNA against key oncogenes in breast tumor and combination therapy with different chemotherapeutics in different therapeutics schedules should be tested.

#### 8.4. References

- [1] Zasadzinski JA. Novel approaches to lipid based drug delivery. *Curr Opin Solid St M* 1997;2:345-9.
- [2] Torchilin VP. Recent advances with liposomes as pharmaceutical carriers. *Nat Rev Drug Discov* 2005;4:145-60.
- [3] McBride A, Holle LM, Westendorf C, Sidebottom M, Griffith N, Muller RJ, et al. National survey on the effect of oncology drug shortages on cancer care. *Am J Health Syst Pharm* 2013;70:609-17.
- [4] FDA Approves Generic Version of Doxil to Address Shortage.
- [5] Lavasanifar A, Samuel J, Kwon GS. Micelles self-assembled from poly(ethylene oxide)-block-poly(N-hexyl stearate L-aspartamide) by a solvent evaporation method: effect on the solubilization and haemolytic activity of amphotericin B. *J Control Release* 2001;77:155-60.
- [6] Lavasanifar A, Samuel J, Kwon GS. The effect of alkyl core structure on micellar properties of poly(ethylene oxide)-block-poly(L-aspartamide) derivatives. *Colloids Surf B Biointerfaces* 2001;22:115-26.
- [7] Mahmud A, Patel S, Molavi O, Choi P, Samuel J, Lavasanifar A. Self-associating poly(ethylene oxide)-b-poly(alpha-cholesteryl carboxylate-epsilon-caprolactone) block copolymer for the solubilization of STAT-3 inhibitor cucurbitacin I. *Biomacromolecules* 2009;10:471-8.
- [8] Ayestaran A, Lopez RM, Montoro JB, Estibalez A, Pou L, Julia A, et al. Pharmacokinetics of conventional formulation versus fat emulsion formulation of amphotericin B in a group of patients with neutropenia. *Antimicrob Agents Chemother* 1996;40:609-12.
- [9] Bekersky I, Fielding RM, Dressler DE, Lee JW, Buell DN, Walsh TJ. Plasma protein binding of amphotericin B and pharmacokinetics of bound versus unbound amphotericin B after administration of intravenous liposomal amphotericin B (AmBisome) and amphotericin B deoxycholate. *Antimicrob Agents Chemother* 2002;46:834-40.
- [10] Lavasanifar A, Samuel J, Kwon GS. Micelles of poly(ethylene oxide)-block-poly(N-alkyl stearate L-aspartamide): synthetic analogues of lipoproteins for drug delivery. *J Biomed Mater Res* 2000;52:831-5.
- [11] Adams ML, Andes DR, Kwon GS. Amphotericin B encapsulated in micelles based on poly(ethylene oxide)-block-poly(L-amino acid) derivatives exerts reduced in vitro hemolysis but maintains potent in vivo antifungal activity. *Biomacromolecules* 2003;4:750-7.
- [12] Vakil R, Kwon GS. Poly(ethylene glycol)-b-poly(epsilon-caprolactone) and PEG-phospholipid form stable mixed micelles in aqueous media. *Langmuir* 2006;22:9723-9.
- [13] Kirby C, Gregoriadis G. The effect of the cholesterol content of small unilamellar liposomes on the fate of their lipid components in vitro. *Life Sci* 1980;27:2223-30.
- [14] Torrado JJ, Espada R, Ballesteros MP, Torrado-Santiago S. Amphotericin B formulations and drug targeting. *J Pharm Sci* 2008;97:2405-25.
- [15] Lenz G. The RNA interference revolution. *Braz J Med Biol Res* 2005;38:1749-57.

- [16] Kim DH, Rossi JJ. Strategies for silencing human disease using RNA interference. *Nat Rev Genet* 2007;8:173-84.
- [17] Xiong XB, Uludag H, Lavasanifar A. Biodegradable amphiphilic poly(ethylene oxide)-block-polyesters with grafted polyamines as supramolecular nanocarriers for efficient siRNA delivery. *Biomaterials* 2009;30:242-53.
- [18] Kim SS, Garg H, Joshi A, Manjunath N. Strategies for targeted nonviral delivery of siRNAs in vivo. *Trends Mol Med* 2009;15:491-500.
- [19] Dykxhoorn DM, Palliser D, Lieberman J. The silent treatment: siRNAs as small molecule drugs. *Gene Ther* 2006;13:541-52.
- [20] Lorenz C, Hadwiger P, John M, Vornlocher HP, Unverzagt C. Steroid and lipid conjugates of siRNAs to enhance cellular uptake and gene silencing in liver cells. *Bioorg Med Chem Lett* 2004;14:4975-7.
- [21] Nishina K, Unno T, Uno Y, Kubodera T, Kanouchi T, Mizusawa H, et al. Efficient in vivo delivery of siRNA to the liver by conjugation of alpha-tocopherol. *Mol Ther* 2008;16:734-40.
- [22] Wolfrum C, Shi S, Jayaprakash KN, Jayaraman M, Wang G, Pandey RK, et al. Mechanisms and optimization of in vivo delivery of lipophilic siRNAs. *Nat Biotechnol* 2007;25:1149-57.
- [23] Behlke MA. Chemical modification of siRNAs for in vivo use. *Oligonucleotides* 2008;18:305-19.
- [24] Santel A, Aleku M, Keil O, Endruschat J, Esche V, Fisch G, et al. A novel siRNA-lipoplex technology for RNA interference in the mouse vascular endothelium. *Gene Ther* 2006;13:1222-34.
- [25] Kim HK, Davaa E, Myung CS, Park JS. Enhanced siRNA delivery using cationic liposomes with new polyarginine-conjugated PEG-lipid. *Int J Pharm* 2010;392:141-7.
- [26] Palliser D, Chowdhury D, Wang QY, Lee SJ, Bronson RT, Knipe DM, et al. An siRNA-based microbicide protects mice from lethal herpes simplex virus 2 infection. *Nature* 2006;439:89-94.
- [27] Urban-Klein B, Werth S, Abuharbeid S, Czubayko F, Aigner A. RNAi-mediated gene-targeting through systemic application of polyethylenimine (PEI)-complexed siRNA in vivo. *Gene Ther* 2005;12:461-6.
- [28] Grzelinski M, Urban-Klein B, Martens T, Lamszus K, Bakowsky U, Hobel S, et al. RNA interference-mediated gene silencing of pleiotrophin through polyethylenimine-complexed small interfering RNAs in vivo exerts antitumoral effects in glioblastoma xenografts. *Hum Gene Ther* 2006;17:751-66.
- [29] Kim SH, Jeong JH, Lee SH, Kim SW, Park TG. Local and systemic delivery of VEGF siRNA using polyelectrolyte complex micelles for effective treatment of cancer. *J Control Release* 2008;129:107-16.
- [30] Yu H, Kortylewski M, Pardoll D. Crosstalk between cancer and immune cells: role of STAT3 in the tumour microenvironment. *Nat Rev Immunol* 2007;7:41-51.
- [31] Zhang J, Spring H, Schwab M. Neuroblastoma tumor cell-binding peptides identified through random peptide phage display. *Cancer Lett* 2001;171:153-64.

- [32] Askoxylakis V, Zitzmann S, Mier W, Graham K, Kramer S, von Wegner F, et al. Preclinical evaluation of the breast cancer cell-binding peptide, p160. *Clin Cancer Res* 2005;11:6705-12.
- [33] Shahin M, Ahmed S, Kaur K, Lavasanifar A. Decoration of polymeric micelles with cancer-specific peptide ligands for active targeting of paclitaxel. *Biomaterials* 2011;32:5123-33.
- [34] Shahin M, Soudy R, El-Sikhry H, Seubert JM, Kaur K, Lavasanifar A. Engineered peptides for the development of actively tumor targeted liposomal carriers of doxorubicin. *Cancer Lett* 2012.
- [35] Shahin M, Soudy R, Aliabadi HM, Kneteman N, Kaur K, Lavasanifar A. Engineered breast tumor targeting peptide ligand modified liposomal doxorubicin and the effect of peptide density on anticancer activity. *Biomaterials* 2013;34:4089-97.
- [36] Echevarria I, Barturen C, Renedo MJ, Troconiz IF, Dios-Vieitez MC. Comparative pharmacokinetics, tissue distributions, and effects on renal function of novel polymeric formulations of amphotericin B and amphotericin B-deoxycholate in rats. *Antimicrob Agents Chemother* 2000;44:898-904.
- [37] Xiong XB, Lavasanifar A. Traceable multifunctional micellar nanocarriers for cancer-targeted co-delivery of MDR-1 siRNA and doxorubicin. *ACS Nano* 2011;5:5202-13.